Alma Mater Studiorum – Università di Bologna

DOTTORATO DI RICERCA IN

CHIMICA

Ciclo 35

Settore Concorsuale: 03/C2 – CHIMICA INDUSTRIALE

Settore Scientifico Disciplinare: CHIM/04 – CHIMICA INDUSTRIALE

DESIGN, SYNTHESIS AND PHOTOVOLTAIC PROPERTIES OF SOME THIOPHENE-BASED CONJUGATED POLYMERS FOR ORGANIC SOLAR CELLS

Presentata da: Debora Quadretti

Coordinatore Dottorato

Prof. Luca Prodi

Supervisore

Prof. Massimiliano Lanzi

Co-Supervisore

Prof.ssa Elisabetta Salatelli

Prof.ssa Elisabetta Venuti

Esame finale anno 2023

Abstract

The current issue of the resource of energy combined with the tendency to give a green footprint to our lifestyle have prompted the research to focus the attention on alternative sources with great strides in the optimization of polymeric photovoltaic devices.

The research work described in this dissertation consists in the study of different semiconducting π-conjugated materials based on polythiophenes (Chapter I). In detail, the GRIM polymerization was deepened defining the synthetic conditions to obtain regioregular poly(3-alkylthiophene) (Chapter II). Since the use of symmetrical monomers functionalized with oxygen atom(s) allows to adopt easy synthesis leading to performing materials, disubstituted poly(3,4-dialkoxythiophene)s were successfully prepared, characterized and tested as photoactive materials in solar cells (Chapter III).

A "green" resource of energy should be employed through sustainable devices and, for this purpose, the research work was continued on the synthesis of thiophene derivatives soluble in eco-friendly solvents. To make this possible, the photoactive layer was completely tailored starting from the electron-acceptor material. A fullerene derivative soluble in alcohols was successfully synthetized and adopted for the realization of the new devices (Chapter IV).

New water/alcohol soluble electron-donor materials with different functional groups were prepared and their properties were compared (Chapter V).

Once found the best ionic functional group, a new double-cable material was synthetized optimizing the surface area between the different materials (Chapter VI).

Finally, other water/alcohol soluble materials were synthetized, characterized and used as cathode interlayers in eco-friendly devices (Chapter VII).

In this work, all prepared materials were characterized by spectroscopy analyses, gel permeation chromatography and thermal analyses. Cyclic voltammetry, X-ray diffraction, atomic force microscopy and external quantum efficiency were used to investigate some peculiar aspects.

Table of contents

CHAPTER I: INTRODUCTION

1. Conductive polymers……..……...1

1.1. Main overview……...1

1.2. Conductivity...……...2

1.3. Doping…….....3

2. Polythiophenes and poly-alkylthiophenes……..……4

2.1. Synthetic routes for polythiophenes……..6

2.2. Oxidative polymerization with ferric chloride……..6

2.3. Grignard Metathesis Polymerization (GRIM Method)…….7

3. Final applications……..10

3.1. Organic photovoltaic solar cells (OSCs)……...…….10

3.2. Solar cell parameters……..11

3.3. Device optimization……13

4. Fullerene and its applications……...13

4.1. Main characteristics of fullerene……13

4.2. Fullerene derivatives……..14

4.3. C_{60} in photovoltaic solar cells……15

References……..17

CHAPTER II: STUDY OF GRIGNARD METATHESIS POLYMERIZATION (GRIM)

1. Introduction

1.1 Overview……..19

1.2. Aim of the chapter……...19

2. Results and discussion

2.1. Synthesis……..20

2.2. NMR characterization……23

2.3. Conclusions……28

3. Experimental section

3.1. Materials……29
3.2. Synthesis……..29
3.2.1. Synthesis of 1-bromo-6-(p-methoxyphenoxy)hexane (B6P)……29
3.2.2. Synthesis of 3-[6-(p-methoxyphenoxy)hexyl]thiophene (T6P)……30
3.2.3. Synthesis of 3-(6-bromohexyl)thiophene (T6Br)……..30
3.2.4. Synthesis of 2,5-dibromo-3-(6-bromohexyl)thiophene (2,5BT6Br)…….31
3.2.5. Synthesis of poly[3-(6-bromohexyl)thiophene] (PT6Br)…….32
3.3. Methods……...32

References……..33

CHAPTER III: STUDY OF PHOTOACTIVE LAYERS IN BHJ SOLAR CELLS

1. Introduction
1.1 Overview……..35
1.2. Aim of the chapter……...35
2. Results and discussion
2.1. Synthesis……..36
2.2. NMR characterization…….38
2.3. FT-IR characterization……...41
2.4. Thermal properties……41
2.5. Optical properties (UV-Vis characterization)……43
2.6. Electrochemical properties (CV)……45
2.7. Photovoltaic properties……...47
2.8. Conclusions……49
3. Experimental section
3.1. Materials……50
3.2. Synthesis……..50
3.2.1. Synthesis of 3,4-bis[6-(4-methoxyphenoxy)hexyl]thiophene (3,4T6P)……50
3.2.2. Generic procedure for the synthesis of n-bromohexyl-1-oxy ($B(CH_2)_nOH$)……...51
3.2.2.1. Synthesis of 6-bromo-1-hexanol (B6OH)……51
3.2.2.2. Synthesis of 10-bromo-1-decanol (B10OH)……51
3.2.3. Synthesis of monomeric precursors……52

3.2.3.1. Synthesis of 3,4-bis(6-dibromohexyl)thiophene (3,4T6Br)……...52
3.2.3.2. Generic procedure for synthesis of 3,4-dialkoxythiophenes…….52
3.2.3.2.1. Synthesis of 3,4-bis(6-dibromohexyl-1-oxy)thiophene (3,4TO6Br)……...52
3.2.3.2.2. Synthesis of 3,4-bis(10-dibromodecyl-1-oxy)thiophene (3,4TO10Br)……...53
3.2.4. Synthesis of monomer by functionalization with sodium methoxide……53
3.2.4.1. Synthesis of 3,4-bis(6-dimethoxyhexyl)thiophene (3,4T6OMe)……53
3.2.4.2. Synthesis of 3,4-bis(6-dimethoxyhexyl-1-oxy)thiophene (3,4TO6OMe)……...54
3.2.4.3. Synthesis of 3,4-bis(10-dimethoxydecyl-1-oxy)thiophene (3,4TO10OMe)……...54
3.2.5. Oxidative polymerization of monomers with $FeCl_3$…….54
3.2.5.1. Synthesis of poly[3,4-bis(6-dimethoxyhexyl)thiophene] [P(3,4T6OMe)]……55
3.2.5.2. Synthesis of poly[3,4-bis(6-dimethoxyhexyl-1-oxy)thiophene] [P(3,4TO6OMe)]……..55
3.2.5.3. Synthesis of poly[3,4-bis(10-dimethoxydecyl-1-oxy)thiophene] [P(3,4TO10OMe)].....55
3.2.6. Synthesis of poly[3-(6-methoxyhexyl)thiophene] (PT6OMe)……..56
3.3. NMR spectra……...57
3.4. FT-IR assignments……..60
3.5. Methods……...62
3.5.1. Solar cells……62

References……..64

CHAPTER IV: SYNTHESIS OF A WATER-SOLUBLE FULLERENE DERIVATIVE

1. Introduction
1.1 Overview……..65
1.2. Aim of the chapter……...65
2. Results and discussion
2.1. Synthesis……..66
2.2. NMR characterization……66
2.3. FT-IR characterization……...70
2.4. Optical properties (UV-Vis characterization)……71
2.5. Electrochemical properties (CV)……72
2.6. Conclusions……73

3. Experimental section

3.1. Materials……74

3.2. Synthesis……..74

3.2.1. Synthesis of N,N'-Bis{2-(acetyloxy)-1-[(acetyloxy)methyl]ethyl}-malonamide (P-Ser)....74

3.2.2. Synthesis of protected malonodiserinolamide fullerene (PC_{60}-Ser)……74

3.2.3. Synthesis of the malonodiserinolamide fullerene (C_{60}-Ser)……75

3.3. Methods……...76

References……..77

CHAPTER V: SYNTHESIS OF ALCOHOL-SOLUBLE POLYTHIOPHENES AS ELECTRO-DONOR MATERIALS FOR BHJ SOLAR CELLS

1. Introduction

1.1 Overview……..79

1.2. Aim of the chapter……...79

2. Results and discussion

2.1. Synthesis……..80

2.2. NMR Characterization……83

2.3. FT-IR characterization……...87

2.4. Thermal properties……90

2.5. Optical properties (UV-Vis characterization)……92

2.6. Electrochemical properties (CV)……94

2.7. Photovoltaic properties……...96

2.8. Conclusions……97

3. Experimental section

3.1. Materials……98

3.2. Synthesis of ionic electron-donor materials……...98

3.2.1. Synthesis of poly{3-[6-(1-methyl-1H-imidazol-3-ium)-hexyl]-thiophene}bromide (PT6I) ……98

3.2.2. Synthesis of poly{3-[6-(tributylphosphonium)-hexyl]-thiophene}bromide ($PT6buP^+Br^-$)……99

3.2.3. Synthesis of 6-bromo-1-hexanol (B6OH)……..100
3.2.4. Synthesis of 3,4-bis(6-bromohexyl-1-oxy)thiophene (3,4TO6Br)……..100
3.2.5. Synthesis of poly[3,4-bis(6-bromohexyl-1-oxy)thiophene] [P(3,4TO6Br)]……..101
3.2.6. Synthesis of poly[3,4-bis(6-bromohexyl-1-tributylphosphonium)thiophene]dibromide [P(3,4TO6buP^{+}Br^{-})]……101
3.3. Synthesis of non-ionic electron-donor materials……..102
3.3.1. Synthesis of poly[3-(6-diethylphosphonate)hexylthiophene] [PT6PO(OEt)$_2$]……102
3.3.2. Synthesis of poly[3-(6-phosphonic acid)hexylthiophene] [PT6PO(OH)$_2$]……102
3.4. Synthesis of non-ionic electron-donor materials polyethereal……102
3.4.1. Synthesis of 2-(2-(2-(2-hydroxyehoxy)ethox)ethoxy)ethyl-4-methylbenzenesulfonate…..102
3.4.2. Synthesis of 2-(2-(2-(2-thiophene-3-yloxy)ethox)ethoxy)ethyl-4-methylbenzenesulfonate……...103
3.5. NMR spectra……104
3.6. Methods……106
3.6.1. Solar cells……..106

References……108

CHAPTER VI: SYNTHESIS OF A DOUBLE-CABLE WATER-SOLUBLE COPOLYMER

1. Introduction
1.1 Overview……109
1.2. Aim of the chapter……109
2. Results and discussion
2.1. Synthesis……110
2.2. NMR Characterization……..111
2.3. FT-IR characterization……114
2.4. Thermal properties……...116
2.5. Optical properties (UV-Vis characterization) ……118
2.6. X-ray diffraction……...119
2.7. Photovoltaic properties……120
2.8. Morphological analysis……121
2.9. Conclusion……122

3. Experimental section

3.1. Materials……...123

3.2. Synthesis of water-soluble double-cable copolymer……123

3.2.1. Synthesis of poly [3-(6-bromohexyl)thiophene-co-3-(6-fullerenylhexyl)thiophene] (P[(T6Br)-co-(T6F)]) by post-functionalization of PT6Br……..123

3.2.2. Synthesis of poly{[3-(6-tributylphosphonium)thiophene]bromide-co-3-(6-fullerenylhexyl)thiophene} (P[(T6buP^{+}Br^{-})-co-(T6F)]) by post-functionalization of P[(T6Br)-co-(T6F)])……124

3.3. Methods……125

3.3.1. Solar cells……..126

References……127

CHAPTER VII: DEVICE OPTIMIZATION THROUGH THE USE OF INTERLAYERS

1. Introduction

1.1 Overview……129

1.2. Aim of the chapter……129

2. Results and discussion

2.1. Synthesis……130

2.2. NMR characterization……...132

2.3. FT-IR characterization……133

2.4. Thermal properties……...137

2.5. Optical properties (UV-Vis characterization)……..139

2.6. Electrochemical properties (CV)……..142

2.7. XRD diffraction……145

2.8. Photovoltaic properties……145

2.9. EQE measurements……...148

2.10. Morphology characterization……148

2.11. Conclusions……149

3. Experimental section

3.1. Materials……..151

3.2. Synthesis of non-ionic electron-donor material poly[3-(6-diethanolamino)-hexylthiophene] [PT6N(EtOH)$_2$]……151
3.3. Synthesis of monomers……..152
3.3.1. Synthesis of 3-(6-bromohexyl-1-oxy)thiophene (TO6Br)……..152
3.3.2. Synthesis of 6-bromohexyl-1-oxymethyl-EDOT (EDOT-MeO6Br)……...152
3.4. Synthesis of cationic polythiophene interlayers……153
3.4.1. General procedure for oxidative polymerization with $FeCl_3$……153
3.4.1.1. Poly[3-(6-bromo-hexyl)thiophene] (PT6Br)……..153
3.4.1.2. Poly[3-(6-bromo-hexyl-1-oxy)thiophene] (PTO6Br)……154
3.4.1.3. Poly(6-bromohexyl-1-oxymethyl-EDOT) [P(EDOT-MeO6Br)]……154
3.4.2. General procedure for the post-functionalization with tributylphosphine……155
3.4.2.1. Poly[3-(6-tributylphosponium-hexyl)thiophene]bromide (PT6buP$^+$Br$^-$)……...155
3.4.2.2. Poly[3-(6-tributylphosphonium-hexyl-1-oxy)thiophene]bromide (PTO6buP$^+$Br$^-$)……155
3.4.2.3. Poly(6-tributylphosphinehexyl-1-oxymethyl-EDOT)bromide [P(EDOT-MeO6buP$^+$Br$^-$)]……..156
3.5. NMR spectra……157
3.6. FT-IR assignments……162
3.7. Methods……163
3.7.1. Solar cells……..164

References……165

CHAPTER I: INTRODUCTION

1. Conductive polymers

1.1. Main overview

The family of electro-active polymers includes semi-conductive polymers, which are materials that allow the passage of the electric current. The two main subclasses are based on the obtainment of conductivity:

- extrinsically conductive polymers (ECPs), i.e. polymer composites filled with an element that promotes electrical conduction;
- intrinsically conductive polymers (ICPs),[1,2] i.e. materials whose conductive properties are due to their molecular structure and to the possibility to be doped.

The latter materials aroused great interest due to their ability to combine electrical properties of metals with the main characteristics of polymeric materials such as flexibility, workability, light weight and processability.[3] Moreover, ICPs exhibit an improved conductivity and require small amounts of doping than ECPs and this constitutes an important parameter to be taken into account for the sustainability of production process.

In 1977 Heeger, McDiarmid e Shirakawa found out the possibility to achieve high values of conductivity with a properly doped polyacetylene (PAc).[4] The values obtained were in a range between metals and semiconductor materials. This peculiarity is due to the structure of polymer which ensures a high extended conjugated system.

Polyacetylene was widely studied and used as a model for the development of several cycle and heterocycles conjugated polymers such as poly-*p*-phenylene (PPP), polypyrrole (PPy), poly-*p*-phenylene sulfide (PPS), poly-*p*-phenylene vinylene (PPV), polythiophene (PT), polyisothianaphthene (PITN), polyaniline (PANI) and polyethylenedioxythiophene (PEDOT) (Figure 1).

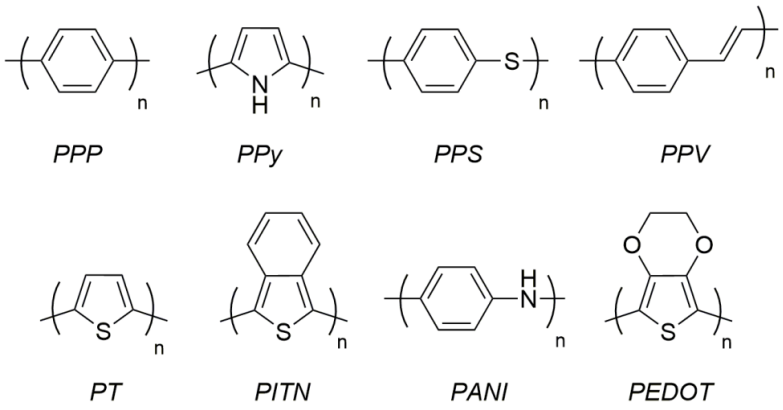

Figure 1. Structures of the main conductive conjugated polymers.

The free rotation around C-C bonds of polymeric backbone leads the conjugated polymers to assume several conformations. The most favoured is the planar one as it allows the best overlap of p_z orbitals of single units and thus extends the conjugation length of polymer.

1.2. Conductivity

In order to explain the electrical conduction mechanism, it's possible to use the "band model" developed for inorganic semiconductors. While in metallic materials the charge transport takes place thanks to the electrons, in polymeric materials the species responsible of conductivity are charged solitons, called polarons and bipolarons.[5]

The phenomenon of electrical conductivity in intrinsically conductive polymers usually depends on their electronic structure, especially the electrons in valence band (VB) play an important role. The bonding (π) and anti-bonding (π^*) energy levels are separated by an amount of energy, namely energy gap (Eg), that determines the conduction in material. By increasing the number of double conjugated bonds, this energy difference between valence and conduction (CB) bands consequently decreases up to the formation of quasi-isoenergetic electronic levels with each other.

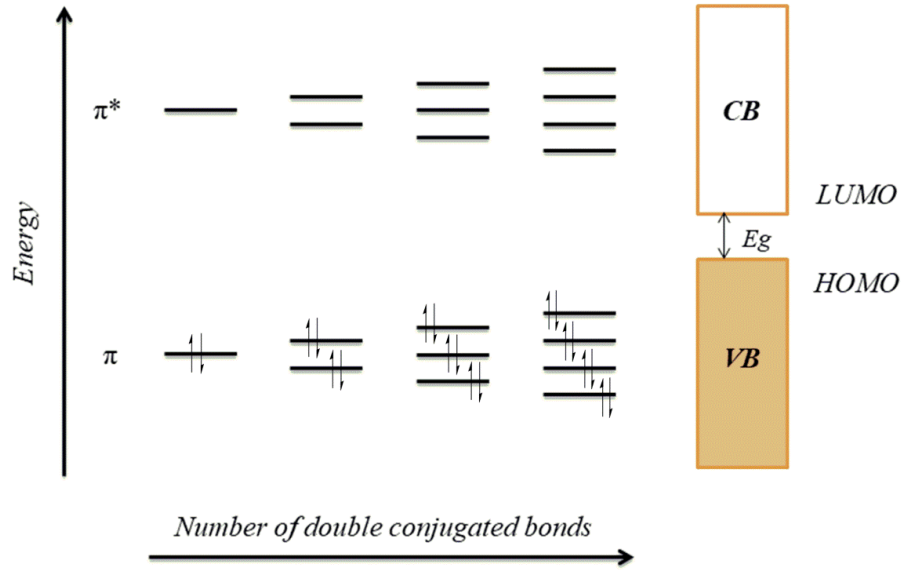

Figure 2. Generic scheme of a "band model" for conjugated polymers.

As shown in Figure 2, the increase of the extent of conjugation thus results in a decrease of Eg that promotes the jump of excited electron from the higher energy molecular occupied orbital (HOMO) of the valence band to the lower energy molecular not occupied orbital (LUMO) of the conduction band.

The improvement of conductivity is closely related to conjugation length of polymer which is not usually high due to the presence of impurities and/or structural defects as terminal groups of macromolecular backbone.

1.3. Doping

The high enhancement of electrical conductivity is usually obtained by doping[6] of polymeric material by several methods such as electrochemical, charge injection, photochemical and chemical doping. In general, the process consists of a reaction between target polymer (with high electron affinity and low ionization potential values) and an electron-acceptor or electron-donor specie with consequent generation of polycations or polyanions, respectively. The oxidation or reduction reaction allows the charge transfer and increases the charge mobility.

When oxidation occurs, the doping is considered positive (p type) and electron-acceptor species are usually used, such as Br_2, I_2, AsF_5, H_2SO_4, $HClO_4$, $FeCl_3$, $AlCl_3$. The addition of an oxidant leads to the formation of radical-cationic and positively charged species along the macromolecular chain with consequent creation of polarons and/or bi-polarons (Figure 3). These promote a further charge delocalization and the decrease of Eg combined with the increase of conductivity of material.

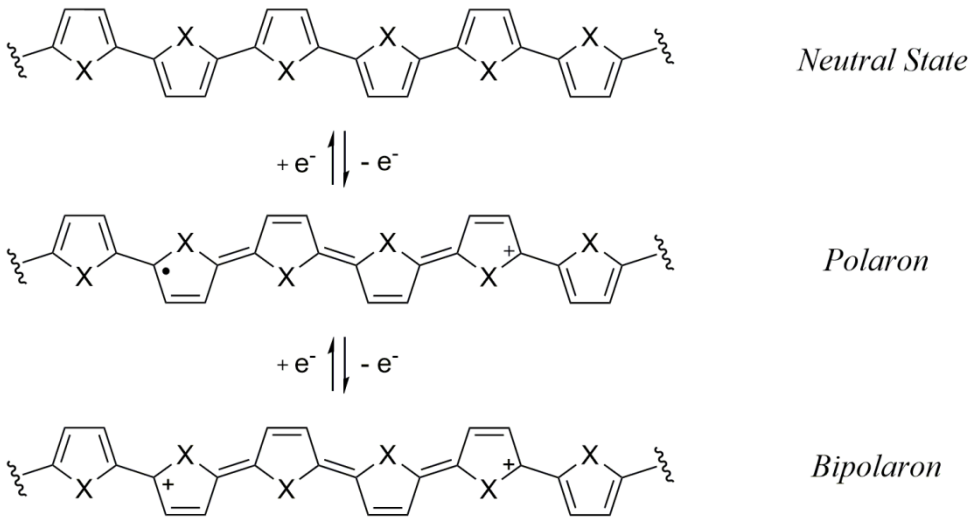

Figure 3. Example of generation of cationic polaron and bipolaron.

Both polarons and bipolarons can move along the macromolecular backbone leading to generation of delocalized structural deformations named quinoid, which result in the enhancement of π level and the reduction of the band gap.

When reduction occurs the doping is considered negative (n type) and electro-donor species usually used, such as Li, Na, K, involve the generation of anionic polarons that act equally to cationic ones.

According to the choice of oxidizing or reducing agents, the conductive properties of polymer can be changed obtaining results that influence the final application.

2. Polythiophenes and poly-alkylthiophenes

In last years, the attention has been focused on conductive polymers with particular interest about polythiophene (PT) and poly-alkylthiophenes (PATs).[7,8] These aromatic poly-heterocycles present rings linked to each other through α positions (2 and 5, Figure 4).

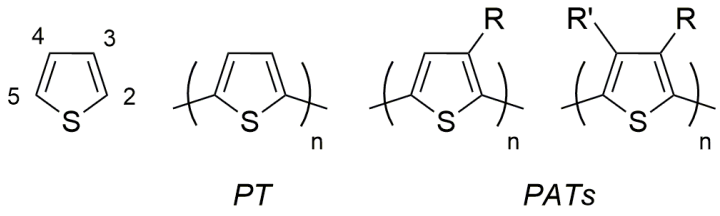

Figure 4. Example of polythiophenes.

Polythiophenes are polymeric materials with interesting properties as high conductivity (10-100 S/cm), resistance to heat and low toxicity. Besides, the high value of redox potential (E° = 0,70 V) provides a great stability to material (up to 350°C in air and up to 900°C in inert atmosphere).

The degradation temperature, lower than the melting point, leads to have a non-fusible and insoluble polythiophenic material in common organic solvents combined with hard processing.

In the case of poly-alkylthiophenes, the presence of a flexible side chain in position 3 - and eventually 3,4 - of thiophene ring solves the issue. The substituent decreases the packing and the interaction between macromolecular main chains: the decrease of crystallinity results in an improvement of solubility and workability. The right length of flexible alkylic side chain (4-6 carbon atoms) is the key point to achieve a processable material combined with a low decrease of final conductivity properties.

The decline of planarity of aromatic rings and the resultant low charge delocalization along the macromolecular backbone reduce the extension of the conjugation system and the conductivity and increase the Eg value.

Besides, the loss of symmetry due to the alkylic side chain results in three different possible α couplings of repeating units: head-to-tail (HT o 2-5'), tail-to-tail (TT o 5-5') head-to-head (HH o 2-2'). A poly-alkylthiophene which contains only HT couplings can be defined regioregular; otherwise, the polymer is considered regioirregular (Figure 5).

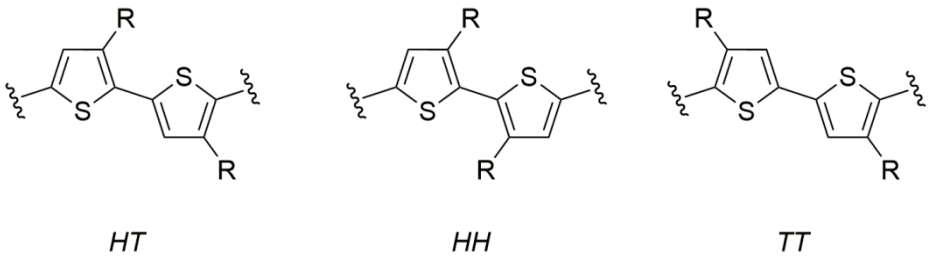

Figure 5. The regioisomeric dyads in generic poly-alkylthiophenes.

The structural isomerism given by different thiophenic units couplings also affects the conjugation of the system with consequences on the electrical behaviour of material: the steric hindrance in HH and/or TT couplings hinders the free rotation of C-C bonds determining the loss of planarity. The presence of regioregularity leads to the increase of planarity, balancing the presence of internal plasticizer.

2.1. Synthetic routes for polythiophenes

2.2. Oxidative polymerization with ferric chloride

The oxidative polymerization is a synthetic route which involves the use of ferric chloride ($FeCl_3$) as oxidizing and polymerising agent thanks to its Lewis acid character. The resulting polymers are not regioregular but the easiness, sustainability and low toxicity of the process make this polymerization widely used on large scale.

This polymerization is also called mixture polymerization due to the use of two different solvents: $FeCl_3$ is solubilized into a small amount of nitromethane (CH_3NO_2) in order to be added to the system containing anhydrous chloroform ($CHCl_3$) as solvent reaction in which the oxidant is insoluble. This condition is necessary to ensure the coordination with thiophene monomer and to maintain active coordination deficits (d orbitals of Fe^{3+}) allowing the polymerization. If the doping agent ($FeCl_3$) is used in solution or in presence of water it would be inactive: ferric trichloride is mainly in the form of dimer (Fe_2Cl_6) and is lacking in coordination gaps.

Another important feature is the use of stronger excess of oxidant agent than the thiophene monomer (1:4 molar ratio), as shown in Figure 6.

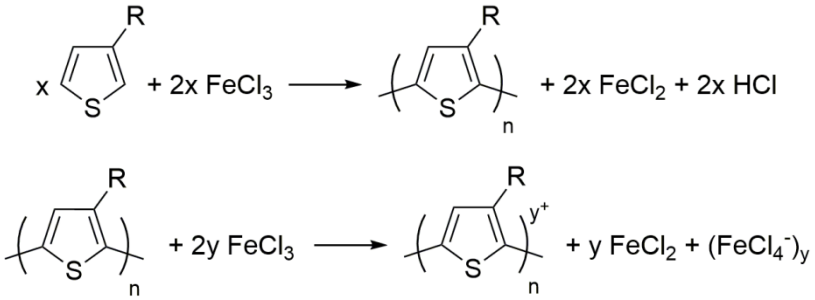

Figure 6. Oxidative polymerization of a poly-alkylthiophene.

The polymerization mainly consists of two oxidation-reduction reactions with the oxidation of monomer at first combined with the oxidation of the obtained polymer to give a doped polythiophene. The hydrochloric acid developed involves the risk of final product degradation and for this purpose it's removed by a high flow rate of an inert gas during the reaction and by the use of an excess of oxidant to give $HFeCl_4$.

In detail, the reaction mechanism consists of several steps: the coordination of thiophene ring to the empty orbital of iron leads to the generation of radical-cation. By the loss of a proton, a radical is formed and it couples with the next monomer molecule thus losing protons which combine with the oxidant (Figure 7).[9]

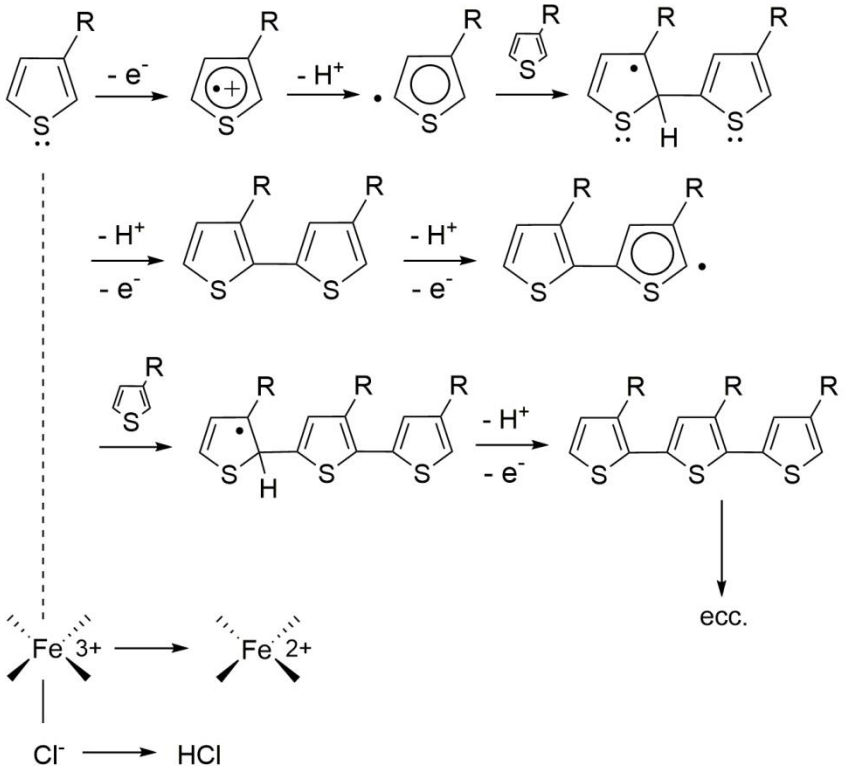

Figure 7. Mechanism of polymerization with $FeCl_3$.

This results in polythiophene with high average molecular weight, good yield of reaction but low regioregularity (70-80% HT). Starting from symmetrically substituted monomers (3,4-alkylthiophenes), it's possible to overcome this disadvantage obtaining regioregular polythiophenes.

2.3. Grignard Metathesis Polymerization (GRIM Method)

The most known regiospecific synthesis of poly-3alkylthiophenes is the polymerization conceptualized by McCullough in the 1990s.

The first strategic route proposed involved the synthesis of 2-bromo-5-(bromomagnesium)-3-alkylthiophene as the starting monomer and its subsequent polymerization in presence of [1,3-bis(diphenylphosphino)propane] nickel (II) chloride ($Ni(dppp)Cl_2$), as shown in Figure 8.[10]

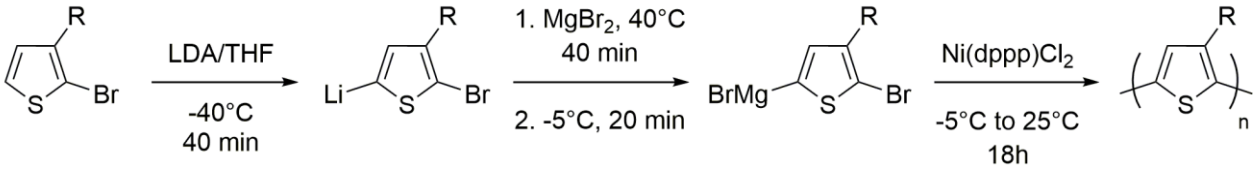

Figure 8. Polymerization proposed by McCullough.

The synthesis is based on the use of 3-alkylthiophenes substituted in position 2 and 5 of the ring with good leaving groups capable of participating in elimination reactions to promote the desired polymerization.

The severe conditions of the synthesis (i.e. low temperature, high sensibility of reagents, purity degree of intermediates) have prompted McCullough himself to design an alternative strategy to obtain a polymer with the same characteristics.

The synthesis proposed is called GRIM (Grignard Metathesis Polymerization),[11,12] and involves the use of 2,5-dibromo-3-alkylthiophene as starting monomer (Figure 9). The subsequent reaction with methylmagnesiumbromide (CH_3MgBr) leads to the main formation of a Grignard intermediate in position 5 of thiophene ring (distribution of isomers a:b is around 80:20) and, finally, the polymerization through cross-coupling with the same catalyst.[13]

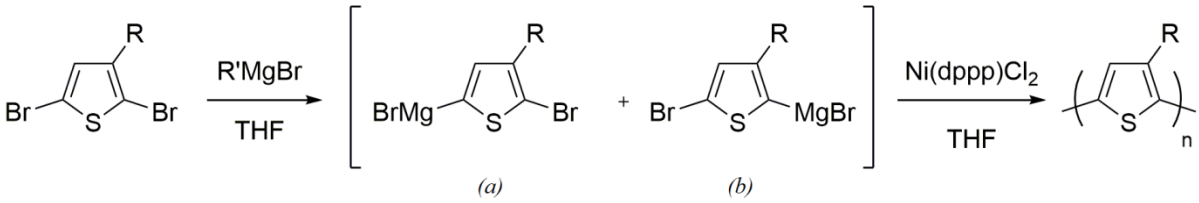

Figure 9. GRIM method.

In addition to be an easy and fast process, the main advantage of the proposed synthesis is the possibility to obtain products with high purity and yield reaction. Moreover, the enhancement of electrical and optical properties of the final material justifies the costs of synthesis.

The GRIM method is also referred to Kumada catalyst transfer condensative polymerization (KCTCP)[14] and involves several steps which are reported in Figure 10. Two equivalents of monomer in presence of the catalyst lead to the formation of a bis(organo)nickel compound followed by a reductive elimination to give an associated pair of thiophenic dimer (5,5'-dibromo-bithienyl with TT coupling) and Ni^0 (III). After this transmetalation step, the initiating specie takes part to the catalytic cycle where oxidative additions and reductive eliminations lead to the chain growth.

The obtained polymer shows HT couplings with the exception of the end chains due to polymerization mechanism.

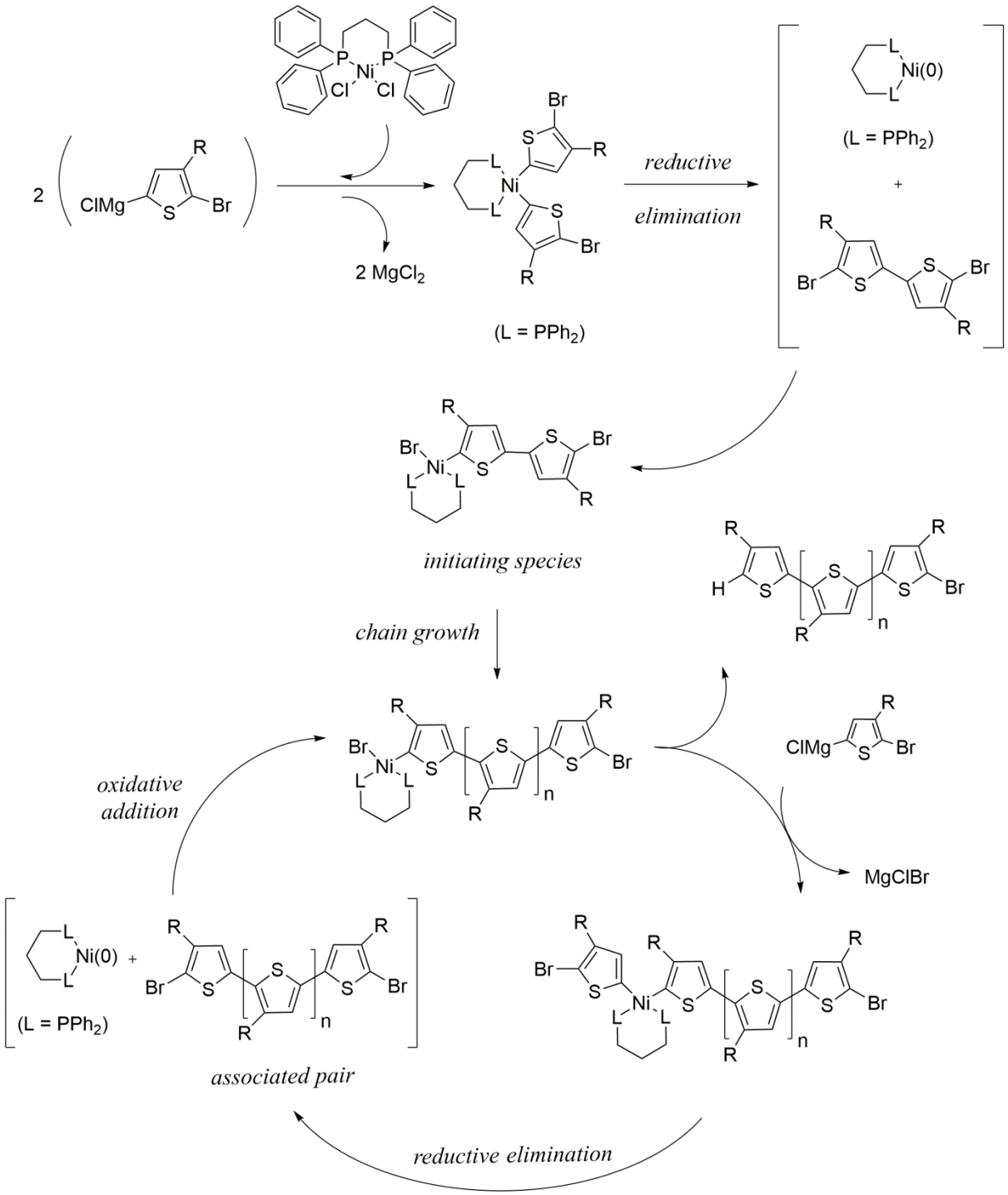

Figure 10. Catalytic mechanism for the growth of chains with GRIM method.

The main disadvantage of this polymerization resides in the obtainment of low average molecular weights due to its mechanism, during which the system becomes heterogeneous thus limiting the chain growth.

3. Final applications

Due to their interesting optical and electrical properties, π-conjugated polymers and in particular poly-alkylthiophenes are widely used in several electronic field and they are employed in rechargeable batteries, electrochromic displays (ECDs), polymer light emitting diodes (pLEDs), chemical sensors, organic field effect transistors (OFETs) and polymeric solar cells (PSCs).[15]

3.1. Organic photovoltaic solar cells (OSCs)

Due to fast decrease of fossil resources and the growing trend towards renewable/clean energies, several studies have been conducted in order to exploit solar energy as an alternative source. To make this possible with sustainable costs and eco-friendly techniques, latest researches have been directed towards the development of organic solar cells based on polymeric photoactive layers (PSCs).[16]

Photovoltaic devices usually show a sandwich structure where the photo-active layer is enclosed between two electrodes (cathode and anode). Depending on the type of active layer used, solar cells can have several architectures such as single layer, bilayer, multilayer or bulk-heterojunction (BHJ) (Figure 11). The high charge recombination in single layer cells and the issues related to low interface area in bilayer or multilayer devices makes BHJ structure the most attractive architecture for several studies.

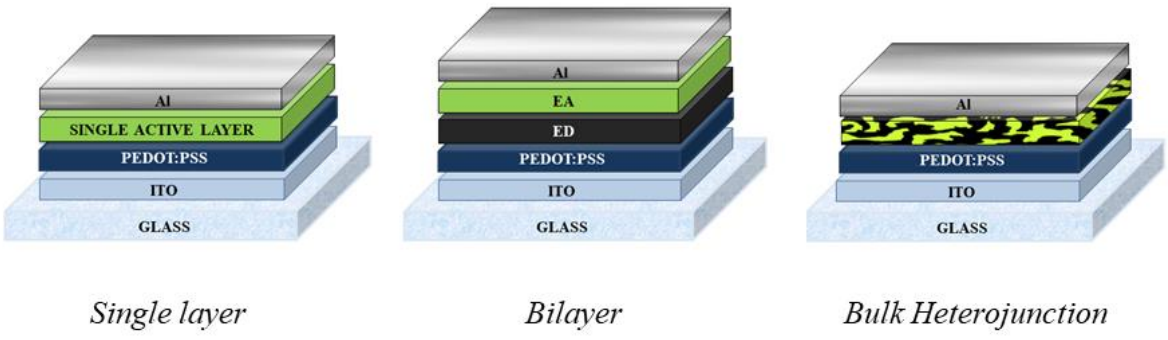

Figure 11. Three different architectures of photo-active layer in a generic PSC.

Generally, photovoltaic devices are based on the so called "photovoltaic effect" which consists in the interaction between electro-magnetic solar radiation and electrons in the valence band of semiconducting material.

The mechanism of PSCs (Figure 12) is composed by four fundamental steps:

- *photoabsorption*: the sunlight promotes the electron hopping from valence band (HOMO level) to conduction band (LUMO level) resulting in the generation of excitons (i.e. hole-electron pairs strongly bounded by Coulombic attraction);

- *exciton diffusion* toward the donor-acceptor interface (p-n junction) by a chemical potential gradient;
- *hopping* of electron from LUMO of donor to LUMO of acceptor material with consequently charge transfer;
- *collecting* of generated free charges to the respective electrodes giving a potential gradient inside the photovoltaic device.

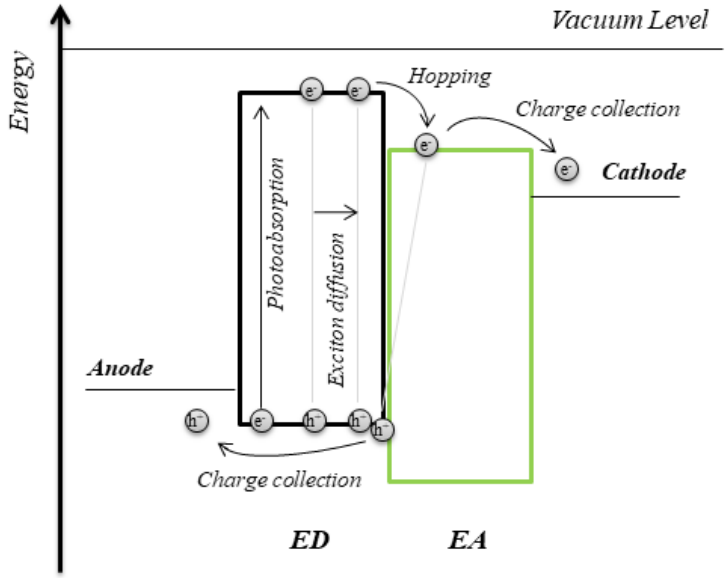

Figure 12. Scheme of the photo-mechanism in a photovoltaic device.

The presence of an electron-acceptor specie is the main requirement to avoid the fall of electrons to the fundamental state and the subsequent loss of absorbed energy as light or heat. Usually, the ED and EA materials need to have high ionization potential (IP) and great electronic affinity (EA) values, respectively.

Another key point of the process is that the LUMO of donor and the LUMO of the acceptor material must be in succession between each other in order to guarantee the high speed of the hopping step. Besides, the energy gap between LUMO levels is higher than binding energy of excitons to avoid the charge recombination and the decrease of final power conversion efficiency.

3.2. Solar cell parameters

The working principle behind a photovoltaic device can be graphically described by a curve of charge density (J) vs. voltage (V) as shown in Figure 13.

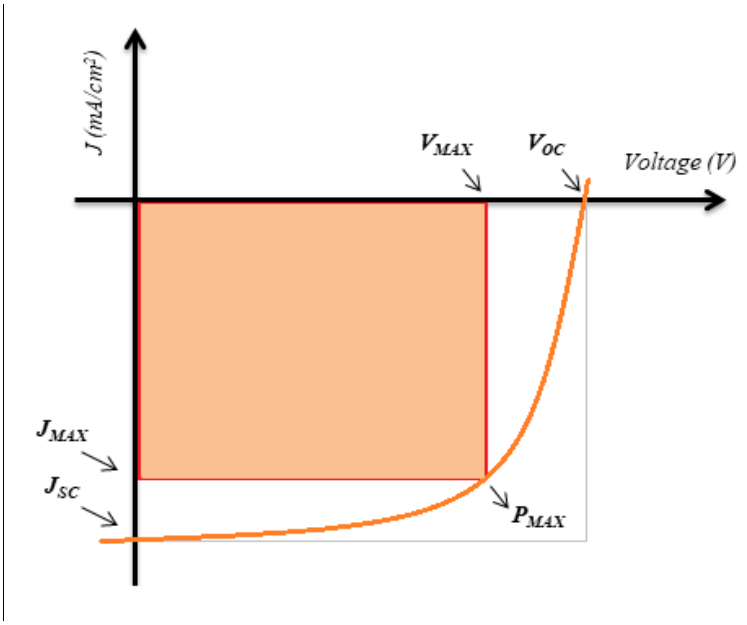

Figure 13. J/V curve obtained testing a solar cell.

The performance of a photovoltaic device depends on several parameters and it is measured in terms of conversion efficiency (η). This is the ratio between the maximum achievable power (P_{MAX}) and the power of incident light (P_{IN}) and it can be described as following:

$$\eta = \frac{P_{MAX}}{P_{IN}} = \frac{V_{OC} \cdot J_{SC} \cdot FF}{P_S}$$

The P_{max} can be also described through other parameters:

- *open circuit voltage* (V_{OC}): the maximum voltage obtainable in absence of current (J = 0 mA/cm^2) and is related to the energy gap between the LUMO of the acceptor and the HOMO of the donor material;
- *short current density* (J_{SC}): the maximum current amount on the surface cell generated by the device in short circuit conditions (V = 0 Volt);
- *fill factor* (FF): a parameter that considers the non-ideality of the device and matches with the area of the orange rectangle in Figure 13.

In an ideal device, the fill factor is 1 (V_{MAX} = V_{OC} and J_{SC} = J_{MAX}) and for this reason its measured value is an important parameter to give truthful information about the device.

Finally, the power conversion efficiency is also defined PCE as it indicates the ratio between the amounts of photons converted and the power delivered by the cell when it is connected to an electrical circuit.

3.3. Device optimization

In order to avoid oxidation phenomena and improve hole extraction and collection, the photoactive layer is typically not placed in direct contact with the anode but a hole transport layer (HTL) is commonly deposited between the ITO and the active layer. The most used HTL is made of poly(3,4-ethyl-enedioxythiophene):poly(styrenesulfonate) (PEDOT:PSS) due to its eco-friendly solution processability, high conductivity, stability and high light trasmittance.[17]

Otherwise, in common BHJ solar cells the photoactive layer is directly in contact with the cathode surface, with possible migration of metal atoms into the active layer during deposition and subsequent decrease of the open-circuit voltage (V_{oc}).[18] Therefore, with a view to avoid these interactions and both increase the power conversion efficiency (PCE) and V_{OC} of BHJ devices, several polythiophenic electrolytes with different pendant cationic moieties have been used as interlayer between the photoactive and cathode films with the aim to modify the interface.[19-21] The presence of a ionic moiety on the conjugated polyelectrolyte – acting as electron transporting layer (ETL) – seems to improve the final performance of the device by changing interactions at the cathode interface due to the increase of polarity. In fact, the consequently modified dipole moment generates a capacitive double layer and allows an easier charge transport and collection.[22-24] The reduction of the work-function of the cathode results in a lower resistance at the interface, thus leading to a higher fill factor (FF), short-circuit current density (J_{sc}), open-circuit voltage (V_{oc}) and, consequently, power conversion efficiency (PCE). Moreover, the recombination is reduced due to a better charge carriers mobility.[25]

Another interesting feature is the solubility of polymer electrolytes in environmental-friendly polar solvents such as alcohols (i.e. methanol, ethanol, isopropanol) and water. The possibility to process the interlayer from more green solvents means an enhancement of sustainability of the final device.

4. Fullerene and its applications

4.1. Main characteristics of fullerene

Since its discovery in 1985, the family of fullerenes has been widely studied and the attention has been focused with extremely interest on the most representative fullerene C_{60} (*buckminsterfullerene*).[26,27] This molecule can be produced by the arc discharge of graphite electrodes and it is composed by 60 carbon atoms chemically equivalent. These are ordered in a hollow sphere (truncated-icosahedral structure, I_h) in which 12 pentagons and 20 hexagons are fused together and carbon atoms are linked to each other through sp^2 ibridization.[28]

Due to its driving force, fullerene is considered unstable from a thermodynamic perspective: alternating single (C_5-C_5) and double (C_5-C_6) bonds in the polyenic structure allow it to behave as an electron poor olefin and to participate as electrophilic reagent into typical alkene reactions.[29]

4.2. Fullerene derivatives

Due to the low solubility of fullerene in common organic solvents, several studies have been conducted in order to avoid this inconvenient through functionalization of C_{60}.[30] In this contest, a wide variety of reactions have been exploited to obtain fullerene derivatives: cycloaddition ([1+2], [2+2], [3+2] Prato Reaction, [4+2] Diels-Alder), cyclopropanation (the nucleophilic addition so called Bingel or Bingel-Hirsch Reaction), radical functionalization and electrophilic reactions.[31,32]

Recently, novel properties of fullerene have been investigated (radical scavenger, biological activity, ecc) and these studies have allowed to expand the application fields of this material also in medical and biological applications.[33] However, in these cases the main requirement is the solubility in low toxic solvents, i.e. ethanol and water.

In order to make C_{60} water/alcohol soluble, several different approaches[34] have been developed such as:

- solvent exchange method (i.e. fullerene aggregates in solvent suspension);
- long-term stirring in water;
- incorporation into water-soluble supramolecular structures;
- chemical reaction on fullerene surface.

Its high tendency to form aggregates involves that the main approach used is to synthesize fullerene derivatives by attaching polar moieties to its surface. The most employed functional groups are dialkyl malonate, pyrrolidine derivatives, sultone and hydroxyl groups,[35-39] as shown in Figure 14.

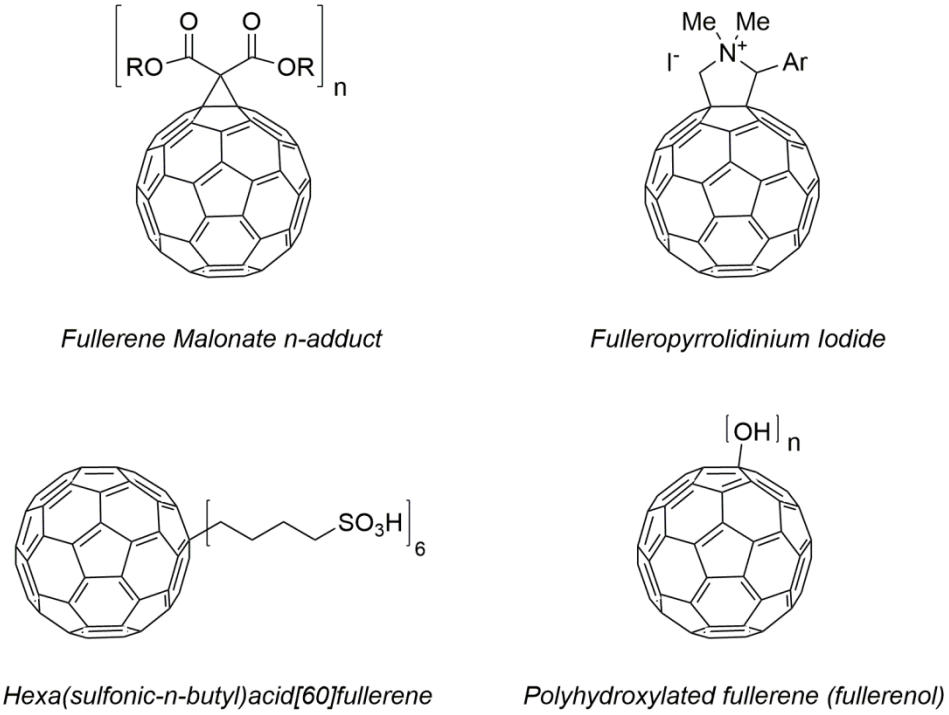

Fullerene Malonate n-adduct

Fulleropyrrolidinium Iodide

Hexa(sulfonic-n-butyl)acid[60]fullerene

Polyhydroxylated fullerene (fullerenol)

Figure 14. Examples of water-soluble fullerene derivatives.

4.3. C_{60} in photovoltaic solar cells

Fullerene derivatives are widely used in several areas such as biomedical application (e.g. inhibitor of HIV protease) and optoelectronic devices (PSCs, OFETs). Moreover, C_{60} shows interesting features: biocompatibility, antioxidant properties, high electron affinity, small reorganization energy, absorption of visible light and excellent electron-accepting properties. In 1992, Heeger and Wudl's research group observed the fast electron transfer from a polyphenylenevinylene derivative (MEH-PPV) to C_{60}.[40] This observation led to the use of conjugated polymers and fullerene derivatives as electron-donors (ED) and electron-acceptors (EA) materials in PSCs, respectively.[41]

However, the conventional fullerene derivative used in photovoltaic field (i.e. BHJ PSCs) is [6,6]-Phenyl-C_{61}-butyric acid methyl ester ($PC_{61}BM$). This material was firstly synthetized by Wudl's group in 1995 and its wide use is due to its good solubility in several common organic solvents and its excellent electronic properties.[42] Besides, other fullerene materials could also be used in photovoltaic field: fulleropyrrolidine, [6,6]-Phenyl-C_{71}-butyric acid methyl ester ($PC_{71}BM$) and Indene-C_{60} bis-adduct (Figure 15).

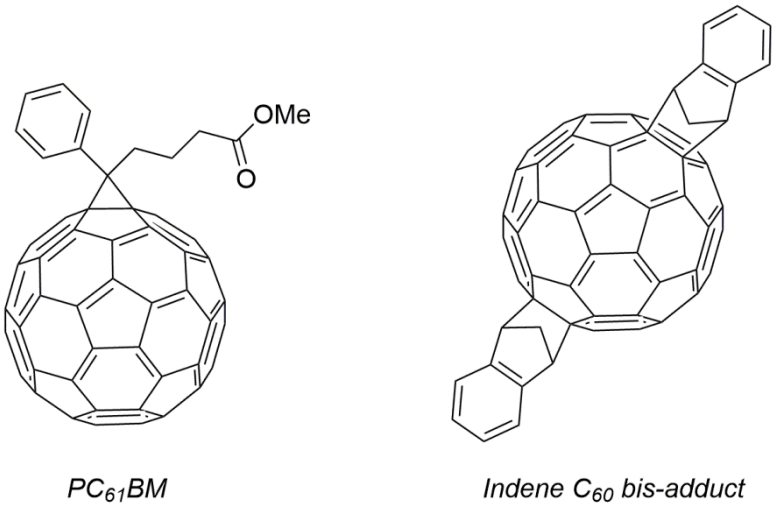

Figure 15. Fullerene derivatives used in photovoltaic devices.

References

1. D. W. Hatchett, M. Josowicz, *Chem. Rev.*, **2008**, *108*, 746-769.
2. J. Ouyang, *Acta Phys. – Chim. Sin*, **2018**, *34*, 1211–1220.
3. S. C. Rasmussen, *ACS Symposium Series*, **2011**, *1080*, 147–163.
4. C. K. Chiang, C. B. Fincher, Jr., Y. W. Park, A. J. Heeger, H. Shirakawa, E.J. Louis, S. C. Gau, A. G. MacDiarmid, *Physical Review Letters*, **1977**, *39*, 1098-1101.
5. J. L. Bredas, G. B. Street, *Acc. Chem. Res*, **1985**, *18*, 309-315.
6. A. Di Terje, A. Skotheim, J. R. Reynold, *Handbook of Conducting Polymers*, CRC Press, **2007**.
7. T. P. Kaloni, P. K. Giesbrecht, G. Schreckenbach, M. S. Freund, *Chem. Mater*., **2017**, *29*, 10248−10283.
8. G. Schopf, G. Koßmehl, *Polythiophenes – Electrically Conductive Polymers*, Springer-Verlag Berlin Heidelberg New York, **1997**.
9. V. M. Niemi, P. Knuuttila, J. E. Österholm, J. Korvola, *Polymer*, **1992**, *33*, 1559-1562.
10. R. D. McCullough, R. D. Lowe, M. Jayaraman, D. L. Anderson, *J. Org. Chem.*, **1993**, *58*, 904–912.
11. R. D. McCullough, *Adv. Mater.*, **1998**, *10*, 93-116.
12. R. S. Loewe, P. C. Ewbank, J. Liu, L. Zhai, R. D. McCullough, *Macromolecules*, **2001**, *34*, 4324-4333.
13. M. Iovu, E. Sheina, R. Gil, R. McCullough, *Macromolecules*, **2005**, *38*, 8649-8656.
14. A. Kiriy, V. Senkovskyy, M. Sommer, *Macromol. Rapid Commun*., **2011**, *32*, 1503- 1517.
15. T. M. S. K. Pathiranage, D. S. Dissanayake, C. N. Niermann, Y. Ren, M. C. Biewer, M. C. Stefan, *Journal of Polymer Science, Part A: Polymer Chemistry*, **2017**, *55*, 3327–3346.
16. A. R. Murad, A. Iraqi, S. B. Aziz, S. N. Abdullah, M. A. Brza, *Polymers*, **2020**, *12*, 2627.
17. F. Zhang, M. Johansson, M. R. Andersson, J. C. Hummelen, O. Inganäs, *Adv. Mater.*, **2002**, *14*, 662-665.
18. K. Suemori, T. Miyata, M. Yokoyama, M. Hiramoto, *Appl. Phys. Lett.*, **2004**, *85*, 6269-6271.
19. J. H. Seo, A. Gutacker, Y. Sun, H. Wu, F. Huang, Y. Cao, U. Scherf, A. J. Heeger, and G. C. Bazan, *J. Am. Chem. Soc*., **2011**, *133*, 8416-8419.
20. J. Luo, H. B. Wu, C. He, A. Y. Li, W. Yang, Y. Cao, *Appl. Phys. Lett*., **2009**, *95*, 043301.
21. H. Zeng, X. Zhu, Y. Liang, X. Guo, *Polymers*, **2015**, *7*, 333-372.
22. H. Wu, F. Huang, Y. Mo, W. Yang, D. Wang, J. Peng, Y. Cao, *Adv. Mater*., **2004**, *16*, 1826-1830.
23. J. Kesters, S. Govaerts, G. Pirotte, J. Drijkoningen, M. Chevrier, N. Van den Brande, et al., *ACS Appl. Mater. Interfaces*, **2016**, *8*, 6309–6314.

24. B.H. Lee, I.H. Jung, H.Y. Woo, H.-K. Shim, G. Kim, K. Lee, *Adv. Funct. Mater*., **2014**, *24*, 1100–1108.

25. Z. He, C. Zhong, X. Huang, W. Wong, H. Wu, L. Chen, S. Su, and Y. Cao, *Adv. Mater*, **2011**, *23*, 4636-4643.

26. H. W. Kroto, J. R. Heath, S. C. O'Brien, R. F. Curl, R. E. Smalley *Nature*, **1985**, *318*, 162-163.

27. H. W. Kroto, A. W. Allaf, S. P. Balm, *Chem. Rev*., **1991**, *91*, 1213-1235.

28. W. Krätschmer, L. D. Lamb, K. Fostiropoulos, D. R. Huffman, *Nature*, **1990**, *347*, 354-358.

29. F. Wudl, A. Hirsch, K. C. Khemani, T. Suzuki, P. M. Allemand, A. Kosch, H. Heckert, G. Srdanov, H. M. Webb, *American Chemical Society*, **1992**, *161*.

30. R. S. Ruoff, D. S. Tse, R. Malhotra, D. C. Lorents, *J. Phys. Chem*, **1993**, *97*, 3379-3383.

31. A. M. Lòpez, A. Mateo-Alonso, M. Prato, *J. Mater. Chem.*, **2011**, *21*, 1305-1318.

32. X. K. Chua, M. Pumera, *Chem. Soc. Rev.*, **2013**, *42*, 3222.

33. E. Nakamura, H. Isobe, *Accounts of Chemical Research*, **2003**, *36*, 807-815.

34. Z. Markovic, V. Trajkovic, *Biomaterials*, **2008**, *29*, 3561-3573.

35. H. Li, S. A. Haque, A. Kitaygorodskiy, M. J. Meziani, M. Torres-Castillo, Y. Sun, *Org. Lett.*, **2006**, *8*, 5641-5643.

36. C. Li, C. Chueh, H. Yip, F. Ding, X. Li, A. K.-Y. Jen, *Adv. Mater*., **2013**, *25*, 2457-2461.

37. Y. Chi, J. B. Bhonsle, T. Canteenwala, J.-P. Huang, J. Shiea, B.-J. Chen, L. Y. Chiang, *Chemistry Letters*, **1998**, 465-466.

38. K. Kokubo, K. Matsubayashi, H. Tategaki, H. Takada, T. Oshima, *ACS Nano*, **2008**, *2*, 327-333.

39. L. O. Husebo, B. Sitharaman, K. Furukawa, T. Kato, L. J. Wilson, *J. Am. Chem. Soc*., **2004**, *126*, 12055-12064.

40. N. S. Sariciftci, L. Smilowitz, A. J. Heeger, F. Wudl, *Science*, **1992**, *258*, 1474- 1476.

41. B. Kraabel, C. H. Lee, D. McBranch, D. Moses, N. S. Sariciftci, A. J. Heeger, *Chem. Phys. Lett*., **1993**, *213*, 389-394.

42. G. Yu, J. Gao, J. C. Hummelen, F. Wudl, A. J. Heeger, *Science*, **1995**, *270*, 1789-1791.

CHAPTER II: STUDY OF GRIGNARD METATHESIS POLYMERIZATION (GRIM)

1. Introduction

1.1 Overview

Since a high value of regioregularity (HT linkages) is the first key point to improve the final optical and conductive properties of the polymeric photoactive materials,[1] the GRIM (Grignard Metathesis) polymerization is the most employed regiospecific method for the synthesis of poly(3-alkylthiophene)s.[2-5]

The latest version proposed by McCullough involves the generation of the Grignard intermediate starting from the monomer 2,5-dibromo-3-alkylthiophene and the subsequent cross-coupling reaction of polymerization in presence of a Nickel-based catalyst.

The GRIM method results to be an easy and fast process to obtain products with high purity by straightforward reactions and it has been widely used. Indeed, several studies have been conducted in order to optimize operative conditions such as the choice of the Grignard reagent (e.g. t-BuMgCl, MeMgBr, MeMgCl), the temperature (reflux, room temperature or less) and the reaction time (minutes or hours).[6,7]

1.2. Aim of the chapter

In order to study the optimal GRIM time reaction at room temperature to synthetize a regioregular poly[3-(6-bromohexyl)thiophene] (PT6Br) – useful for further post-functionalization reactions – the 2,5-dibromo-3-(6-bromohexyl)thiophene (2,5BT6Br) was prepared and subsequently used as the starting monomer to be polymerized.

The structural properties of products and the time reaction were investigated by ^{1}H-NMR spectrometry.

This chapter is an extracted part of "Influence of the active layer structure on the photovoltaic performance of water-soluble polythiophene-based solar cells" M. Lanzi, D. Quadretti, M. Marinelli, Y. Ziai, E. Salatelli, F. Pierini, *Polymers*, 2021, 13, 1640.

The study of regiospecific polymerization and the synthetic results reported in this chapter were performed by Antonia Grieco under the supervision of the author, or by the author herself.

2. Results and discussion

2.1. Synthesis

The synthesis of the starting monomer 2,5-dibromo-3-(6-bromohexyl)thiophene (2,5BT6Br) for the GRIM polymerization involved several steps: protection of target alkylic chain with subsequent cross-coupling reaction with 3-bromothiophene,[8] deprotection and, finally, dibromination of thiophene ring (Scheme 1).[9]

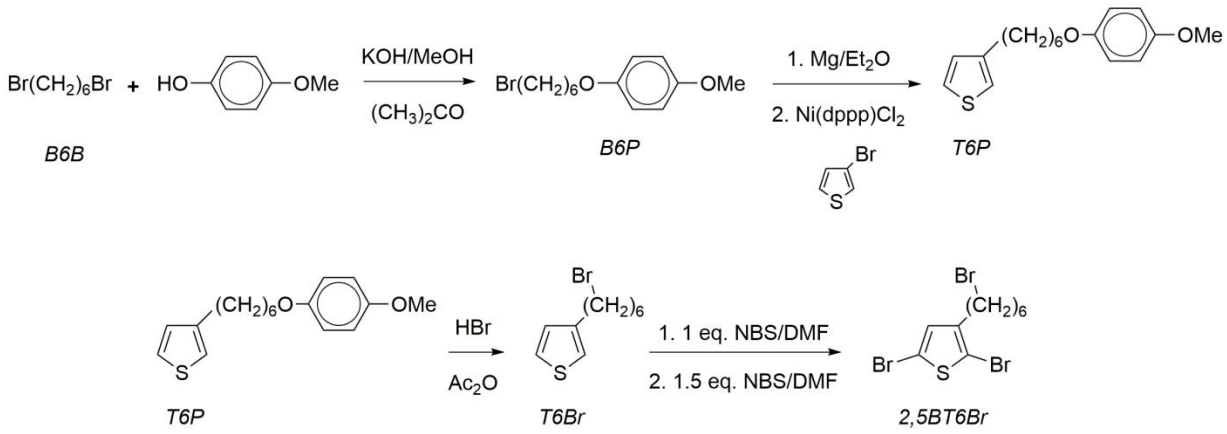

Scheme 1. Synthetic route to synthetize the starting monomer.

At first, the commercially available 1,6-dibromohexane (B6B) was protected on one side with the ethereal p-methoxyphenol group to obtain the subsequent formation of the Grignard reagent on a single bromide function avoiding side reactions. Moreover, the protection allows to maintain the possibility to restore the bromide group later.

In detail, the reaction was conducted under reflux conditions in presence of KOH to promote the formation of KBr (not soluble in reaction solvent) and the contemporary etherification reaction between the generated 1,6-bromohexanol and p-methoxyphenol.

Then, the second step involved the cross-coupling reaction between the obtained 1-bromo-6-(p-methoxyphenoxy)hexane (B6P) and 3-bromothiophene to give 3-[6-(p-methoxyphenoxy)hexyl]thiophene (T6P). Also in this case, the intermediate is a Grignard reagent resulting from the reaction of B6P with magnesium in reflux conditions for 20 hours and with anhydrous diethyl ether as solvent. Afterwards, the intermediate was quickly transferred to a second system where cross-coupling with 3-bromothiophene took place in presence of [1,3-bis(diphenylphosphino)propane] nickel (II) chloride ($Ni(dppp)Cl_2$).

The cross-coupling reaction between a Grignard reagent and an alkyl halide occurs through the catalytic mechanism proposed by Tamao-Sumitani-Kumada and is schematically reported in Scheme 2.[10-11]

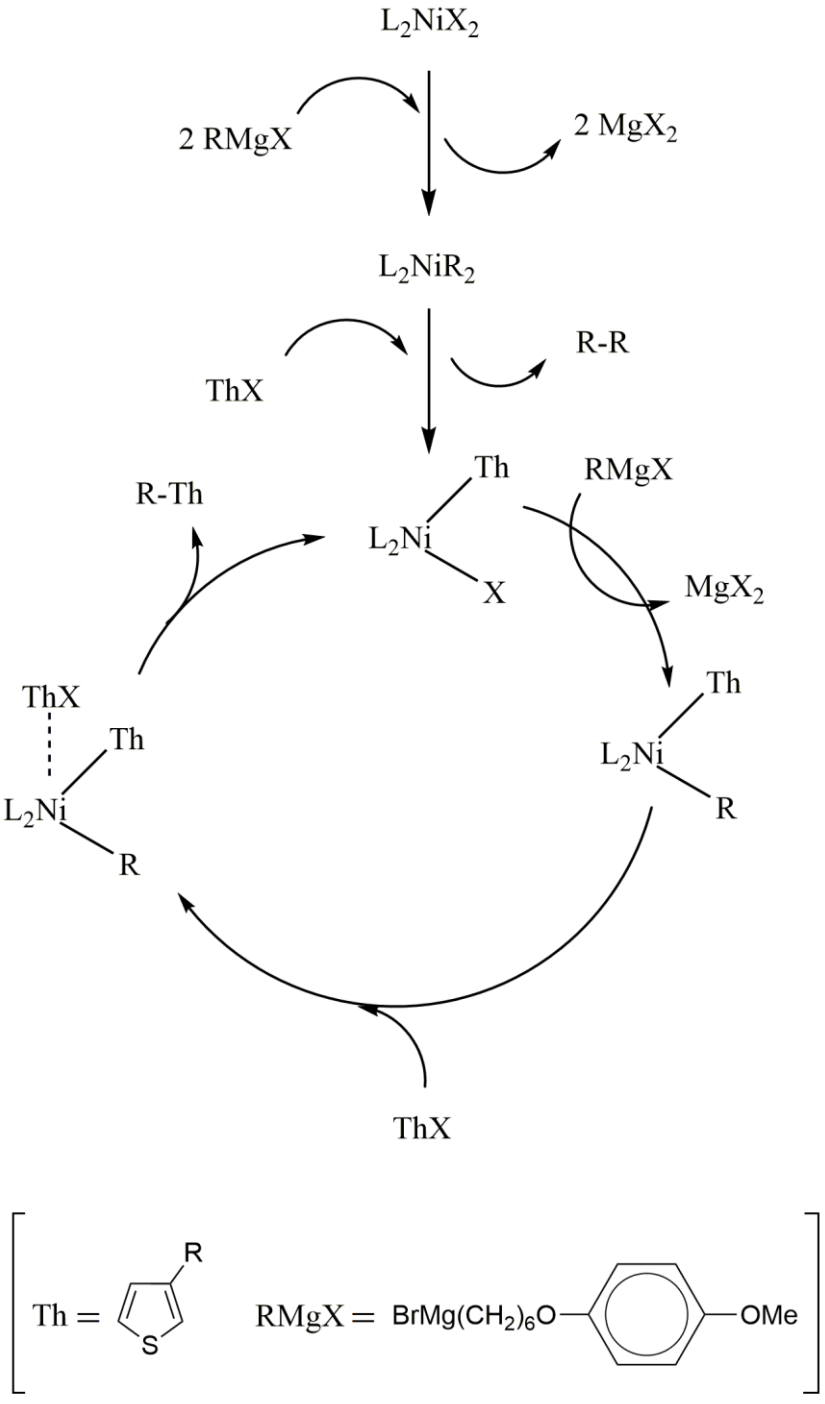

Scheme 2. Generic scheme of Tamao-Sumitani-Kumada cross-coupling.

The Nickel based catalyst chosen is the most efficient catalyst for this type of reactions.[12] Despite the effectiveness of the catalyst, the resulting product required intensive purification (recrystallization, clean-up with silica and steam distillation) because by-products are inevitably formed (Figure 1) resulting in a low reaction yield.

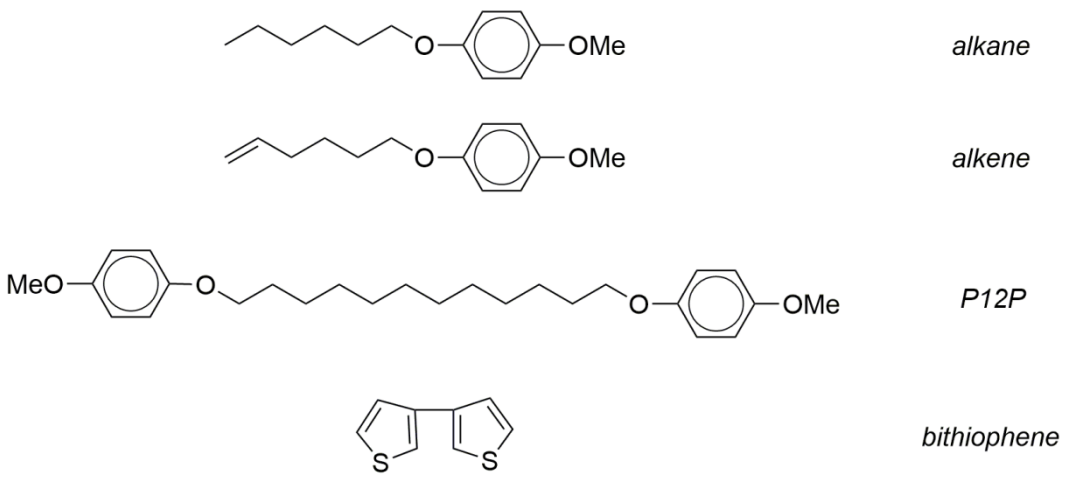

Figure 1. By-products of coupling reaction of B6P with 3-bromothiophene.

The formation of by-products can be ascribed to the presence of water and the dehydrohalogenation of intermediate giving the "alkane" and "alkene", respectively. Besides, Grignard reagent and 3-bromothiophene can react with themselves causing the generation of a dimer (P12P) and "bithiophene", respectively.

The third step was the deprotection of T6P to restore the bromide group at the end of side chain giving 3-(6-bromohexyl)thiophene (T6Br). The reaction involved the use of hydrobromic acid in hard conditions (90°C) and the presence of acetic anhydride to eliminate water residue. Despite the unavoidable loss of product due to reaction with silica (substitution of bromide with hydroxyl group), the crude product was purified by chromatography column.

Finally, the monomeric precursor T6Br was dibrominated with N-bromosuccinimide (NBS) in two steps and with different equivalents in order to promote the bromination both in position 2 and 5 of thiophene ring giving the corresponding 2,5-dibromo-3-(6-bromohexyl)thiophene (2,5BT6Br).

Once synthetized the dibrominated monomer it's possible to proceed with GRIM polymerization as reported in Scheme 3.

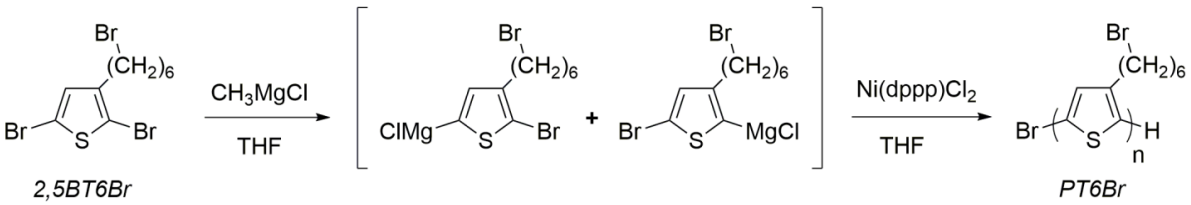

Scheme 3. Synthetic route of synthesis of PT6Br through GRIM method.

The synthesis involved the processing of 2,5BT6Br with CH_3MgCl under reflux conditions and the consequent generation of a mixture of regiochemical isomers, i.e. Grignard organomagnesium intermediates. Their typical distribution is around 80:20 of 2-bromo-5-chloromagnesium-3-(6-

bromohexyl)thiophene and 5-bromo-2-chloromagnesium-3-(6-bromohexyl)thiophene, respectively. The latter isomer does not participate in the catalytic cycle due to the steric hindrance of alkylic side chain in position 3 of thiophene ring and this contributes to the low reaction yield.

The second step of reaction provided a cross-coupling of the Grignard intermediate (2-bromo-5-chloromagnesium-3-(6-bromohexyl)thiophene) with Ni(dppp)Cl_2. As previously discussed, this catalyst was chosen due to its high selectivity in cross-coupling reaction with Grignard intermediates which, in this case, allows to obtain a regioregular polymer.

The reaction – defined as a quasi-living polymerization - was conducted at room temperature in order to avoid the shift of regioisomers toward to the formation of the undesired isomer in position 2.[13,14]

To determine the optimal reaction time (90 minutes), the degree of polymerization after the addition of the catalyst was followed by quenching two portions of the reaction mixture after 30 and 60 minutes which were subsequently analyzed by ^{1}H-NMR.

2.2. NMR characterization

The chemical structure of all the synthetized products (B6P, T6P, T6Br and 2,5BT6Br) and the polymer PT6Br were verified by ^{1}H-NMR and ^{13}C-NMR spectroscopy.

In detail, ^{1}H-NMR spectrum reported in Figure 2a confirms the protection of 1,6-dibromohexane to 1-bromo-6-(p-methoxyphenoxy)hexane (B6P) by the presence of signal at 3.91 ppm ascribable to methylenic protons linked to oxygen atom of p-methoxyphenol group.

The success of subsequently cross-coupling reaction with 3-bromothiophene to obtain 3-[6-(p-methoxyphenoxy)hexyl]thiophene (T6P) is given by the spectrum reported in Figure 2b, which shows the absence of the triplet at 3.42 ppm (ascribable to -CH_2Br) combined with the presence of signal at 2.65 ppm attributable to the two methylenic protons in position 3 of thiophene ring.

Then, the synthesis of 3-(6-bromohexyl)thiophene (T6Br) through deprotection of T6P in order to restore bromide moiety is confirmed by the presence of triplet signal at 3.41 ppm, as show in Figure 2c.

Finally, the evidence of dibromination of T6Br to give 2,5-dibromo-3-(6-bromohexyl)thiophene (2,5BT6Br), the monomer of GRIM reaction, is given by the disappearance of the signal ascribable to the aromatic protons - position 2 and 4 of thiophene ring – in the spectrum reported in Figure 2d.

As for ^{1}H-NMR, also ^{13}C-NMR gave confirmations about the success of previously discussed reaction (Figure 3).

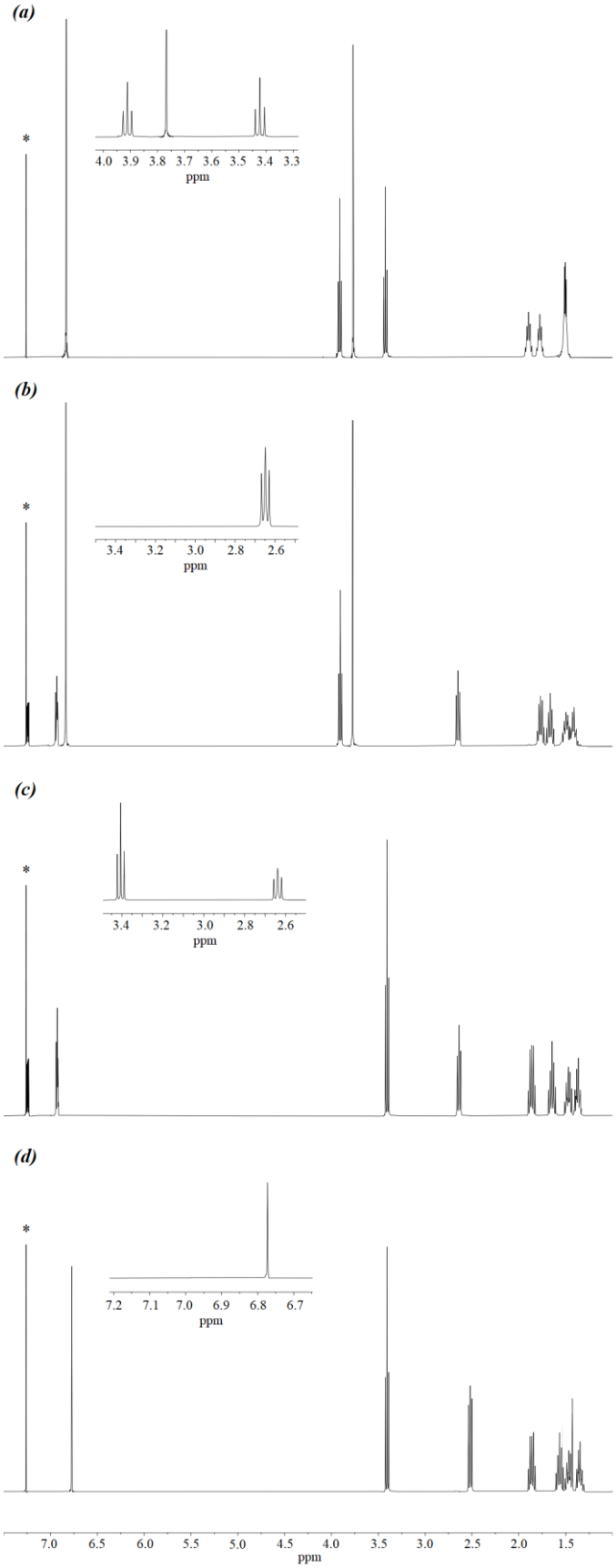

Figure 2. ^{1}H-NMR spectra of B6P (*a*), T6P (*b*), T6Br (*c*) and 2,5BT6Br (*d*). Asterisk: solvent resonance ($CDCl_3$). Inset: expanded region.

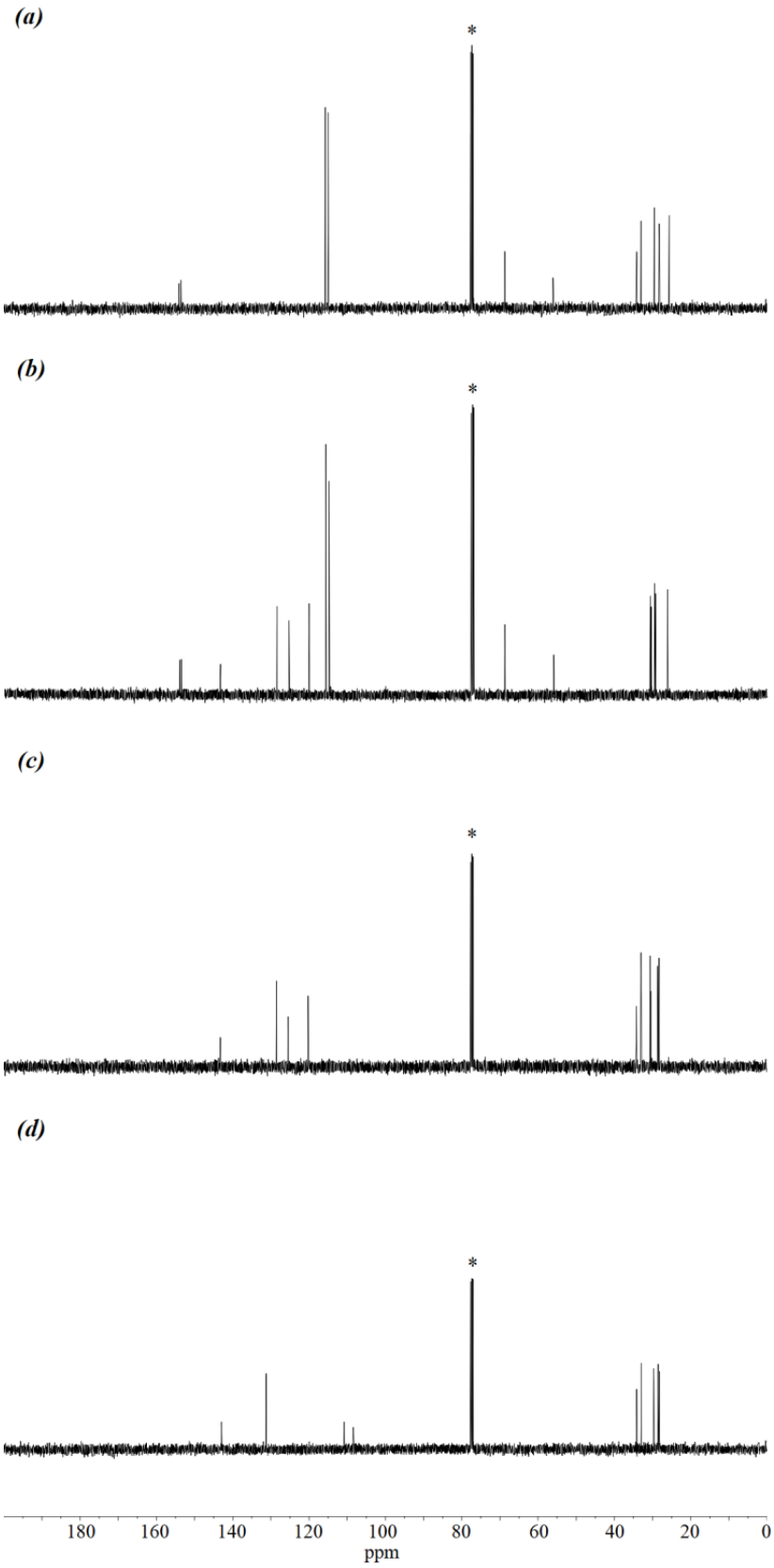

Figure 3. ^{13}C-NMR spectra of B6P (*a*), T6P (*b*), T6Br (*c*) and 2,5BT6Br (*d*). Asterisk: solvent resonance ($CDCl_3$).

The synthesis of PT6Br by GRIM reaction was followed by ^{1}H-NMR spectroscopy by collecting three reaction mixture samples at different reaction times (30, 60 and 90 minutes) after the addition of the Ni(dppp)Cl_2 catalyst. The obtained spectra are shown in Figure 4, while chemical shifts and assignments are shown in Table 1.

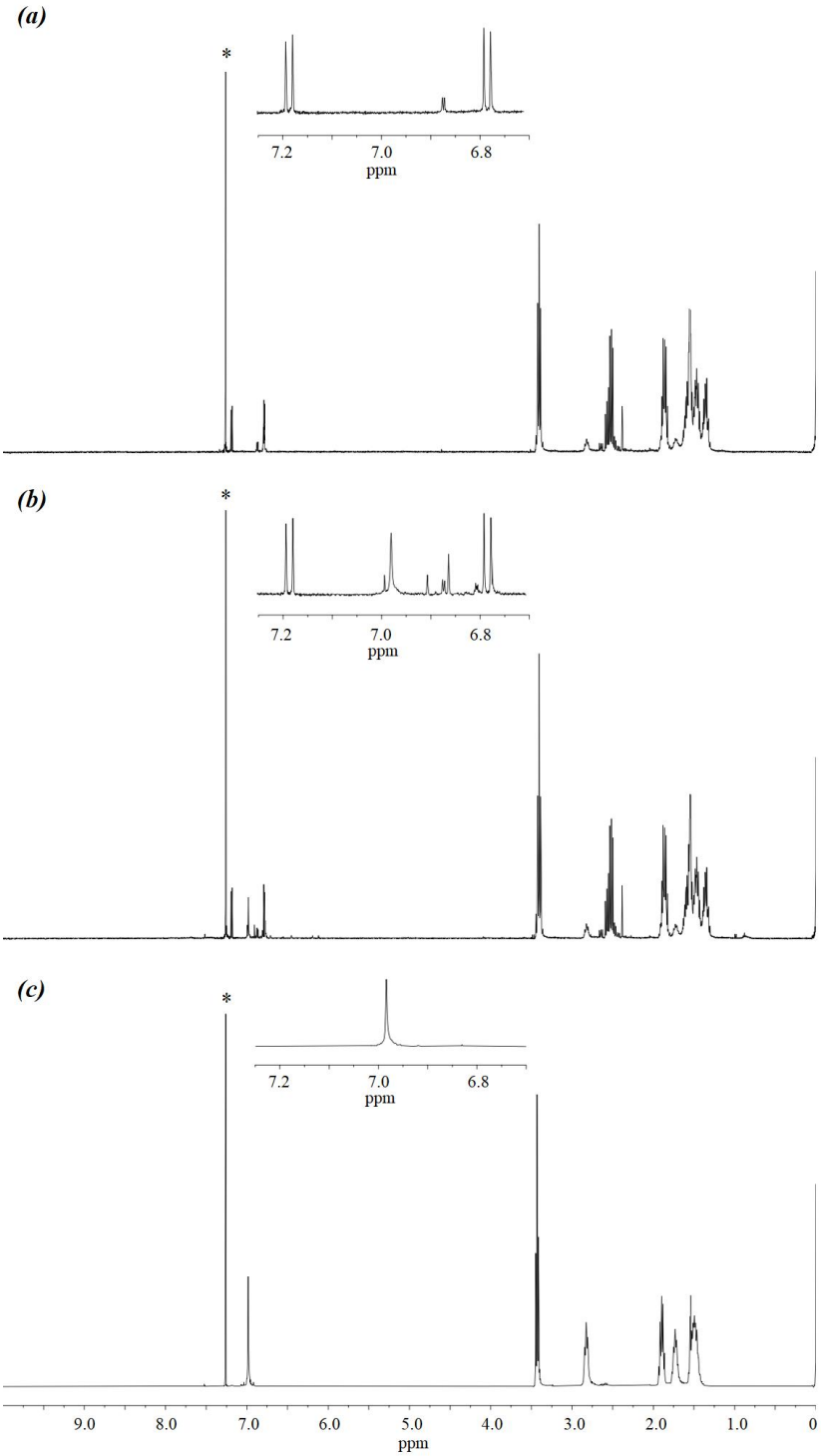

Figure 4. ^{1}H-NMR spectra of PT6Br after 30 minutes (*a*), 60 minutes (*b*) and 90 minutes (*c*). Asterisk: solvent resonance ($CDCl_3$). Inset: expansion of the aromatic region.

Table 1. Chemical shift (ppm) and assignments of the three samples collected after 30 minutes (*a*), 60 minutes (*b*) and 90 minutes (*c*).

***a* (ppm)**	***b* (ppm)**	***c* (ppm)**	***Assignments***	***Ref.***
7.19 6.88 6.79 3.41	7.19 6.88 6.79 3.41	-	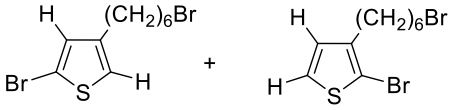	[7]
-	7.00 6.81 2.39	2.59	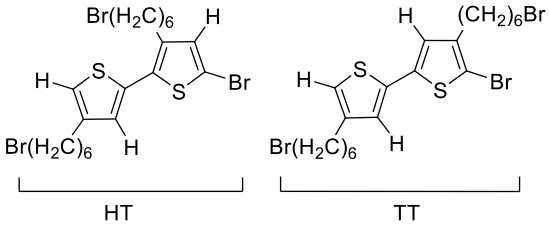	[15,17,18]
-	6.98 6.91 6.87 2.83 2.65	6.98 3.43 2.83	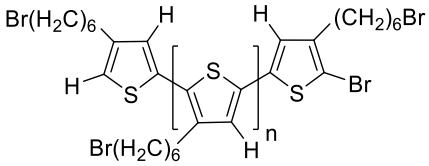	[14,15,16]
1.86 1.56 1.47 1.36	1.86 1.73 1.56 1.47 1.36	1.90 1.73 1.49	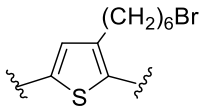	

The ^{1}H-NMR spectrum collected 30 minutes after the onset of the reaction (Figure 4a) essentially shows only the signals ascribable to reagents, i.e. the quenched isomers deriving from the Grignard intermediate.

After 60 minutes (Figure 4b), the spectrum obtained reveals some differences: the peaks related to two or more thiophenic units linked to each other are also shown while Grignard intermediates are still clearly present. The signals at 6.81 ppm and 7.00 ppm are ascribable to the first TT linkage between the two starting thiophenic units and to the polymeric backbone growing with TT-HT linkages, respectively and suggest that the polymerization is still taking place in the reaction system.

Indeed, after 90 minutes (Figure 4c), the exclusive presence of peaks related to the main polymeric chain – with HT linkages and bromide groups in the side chain – indicates that polymerization has occurred determining the success of polymerization.

^{1}H-NMR spectroscopy was also used to estimate the percentage of head-to-tail linkages (95% HT) in the macromolecular backbone of the final PT6Br. In fact, the regioregularity degree can be evaluated by the integral ratio of the signals centered at 2.83 ppm (HT dyads) and 2.59 ppm (HH and TT dyads).

Finally, ^{13}C-NMR spectrum of PT6Br (Figure 5) also confirmed the structure and the success of polymerization after 90 minutes.

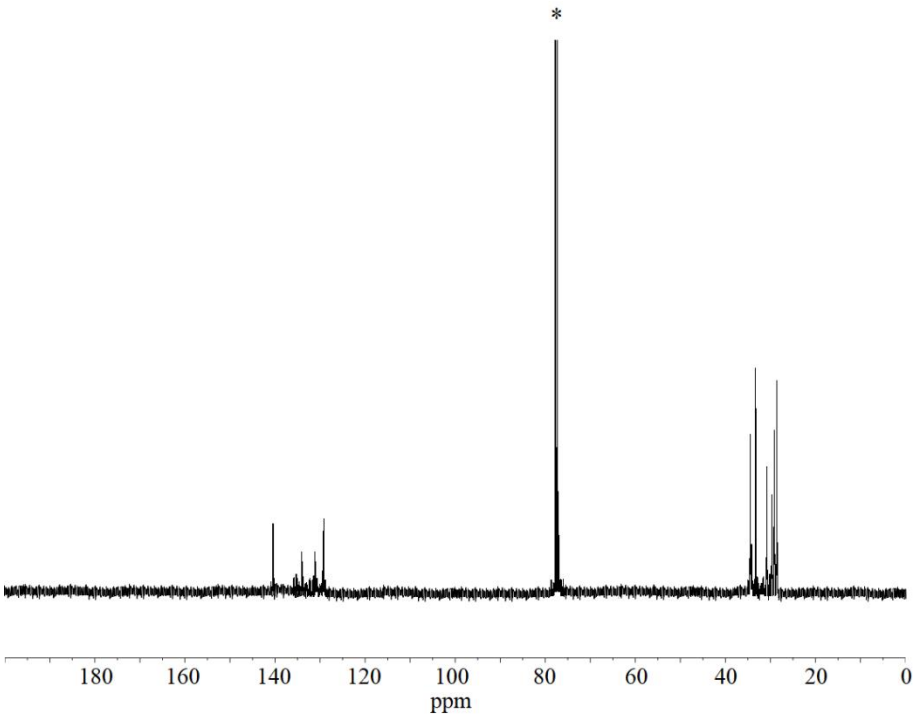

Figure 5. ^{13}C-NMR spectrum of PT6Br. Asterisk: solvent resonance ($CDCl_3$).

2.3. Conclusions

In conclusion, the synthesis of a model monomer has allowed to find a suitable reaction time (90 minutes) for the second catalyzed step of GRIM reaction (performed at room temperature) for ω-bromoalkylthiophene derivatives like the 2,5BT6Br used in this study.

All products were widely characterized through spectroscopy techniques (NMR and FT-IR) and through ^{1}H-NMR it was possible to follow the reaction at different times.

3. Experimental section

3.1. Materials

[1,3-bis(diphenylphosphino)propane] nickel (II) chloride ($Ni(dppp)Cl_2$), methylmagnesium chloride (CH_3MgCl, 3.0 M solution in THF), p-methoxyphenol, 3-bromothiophene (97%), N,N-dimethylformamide (DMF, 99.8%), hydrochloric acid (HCl, >37%), sodium hydroxide (NaOH, ≥98%), N-bromosuccinimide (NBS, 99%), tetrahydrofuran (THF, >99.9%), diethyl ether (Et_2O, >99.5%), petroleum ether (Etp, >90%), acetone (>99%) and chloroform ($CHCl_3$, 99.0-99.4%) were purchased from Sigma Aldrich Chemical Co. Acetic anhydride (Ac_2O, >97%) was purchased from Acros Organics (USA). Hydrobromic acid (HBr, 48%) and potassium hydroxide (KOH) were purchased from Fluka (Switzerland). n-Heptane (99.4%) and cyclohexane were purchased from VWR Chemicals (France). Methanol (MeOH, >99.8%) was purchased from Honeywell (Germany). 1,6-Dibromohexane (B6B, >97%) was purchased from TCI (Tokyo). Sodium sulfate (Na_2SO_4, anhydrous) and sodium bicarbonate ($NaHCO_3$, puriss.) were purchased from Riedel-deHaën (Poland). Magnesium (Mg) for Grignard were purchased from Merck (Germany). The solvent used for the Grignard Metathesis Polymerization (GRIM) was dried with a sodium-potassium alloy under reflux and stored over molecular sieves before the use. Diethyl ether and THF were freshly distilled before use to remove the stabilizer. All other materials were used as received. All manipulations involving moisture-sensitive reagents were performed under argon atmosphere in flame-dried glassware.

3.2. Synthesis

3.2.1. Synthesis of 1-bromo-6-(p-methoxyphenoxy)hexane (B6P)

32.3 g (0.571 mol) of KOH and 49.6 g (0.359 mol) of p-methoxyphenol were dissolved in 80.0 mL of methanol. In a two neck-flask containing 126 mL (0.820 mol) of 1,6-dibromohexane (B6B) in 160 mL of acetone, the solution was added drop-wise in 90 minutes under stirring and then the system was refluxed for 1h.

The system was cooled down to room temperature, the mixture was filtered on a Buckner filter – in order to remove KBr - and the solid was washed several times with acetone (3 × 100 mL). After filtration, the solvent was removed under reduce pressure and the crude product was recovered in 1000 mL of hot diethyl ether. Then, the solution was filtered again, washed with a solution of NaOH 2% (4 × 150 mL) and distilled water up to neutrality (3 × 100 mL). The organic phase was dried with Na_2SO_4, filtered and the solvent was removed under reduce pressure. The crude product was purified by three crystallizations in hot petroleum ether followed by clean-up with SiO_2 obtaining 92.4 g (0.322) of B6P as white solid (yield 80%).

^{1}H-NMR ($CDCl_3$, ppm): δ 6.83 (s, 4H, aromatic C*H*), 3.91 (t, 2H, CH_2O), 3.77 (s, 3H, OCH_3), 3.42 (t, 2H, CH_2Br), 1.90 (m, 2H, CH_2CH$_2$O), 1.78 (m, 2H, CH_2CH$_2$Br), 1.50 (m, 4H, (CH_2)$_2$).

^{13}C-NMR ($CDCl_3$, ppm): δ 154.07, 153.54 (aromatic *C*-O), 115.78, 114.98 (aromatic *C*H), 68.73 (*C*H$_2$O), 56.09 (O*C*H$_3$), 34.16 (*C*H$_2$Br), 33.05, 29.55, 28.29, 25.66 (aliphatic *C*H$_2$).

FT-IR (KBr, cm^{-1}): 3104, 2937, 2862, 2835, 1513, 1466, 1384, 1291, 1242, 1113, 1036, 826, 742, 646, 532.

3.2.2. Synthesis of 3-[6-(p-methoxyphenoxy)hexyl]thiophene (T6P)

150 mL of dry diethyl ether were added dropwise to a reaction system containing 20.0 g (69.6 mol) of B6P and 1.75 g (72.0 mmol) of Mg. The mixture was refluxed for 20h, under stirring and inert atmosphere.

The Grignard intermediate was then transferred via cannula and added dropwise to the second reaction system containing 5.70 mL (60.1 mmol) of 3-bromothiophene and 71.0 mg (0.131 mmol) of catalyst [1,3-bis(diphenylphosphino)propane] nickel (II) chloride (Ni(dppp)Cl_2) and the system was refluxed for 16h, under stirring and in an inert atmosphere.

The mixture was cooled down to room temperature, poured in 200 mL of HCl 2% and extracted with 100 mL of diethyl ether. The organic phase was washed with distilled water up to neutrality, dried with Na_2SO_4, filtered and the solvent was removed under reduced pressure.

The crude product was purified by recrystallization from 1.50 L of petroleum ether (Etp) followed by clean-up with silica and steam distillation obtaining 6.12 g (21.1 mmol) of T6P (yield 36%).

^{1}H-NMR ($CDCl_3$, ppm): δ 7.24 (m, 1H, Th *H*5), 6.94 (m, 2H, Th *H*4 + *H*2), 6.83 (d, 4H, aromatic C*H*), 3.91 (t, 2H, CH_2O), 3.77 (s, 3H, OCH_3), 2.65 (t, 2H, ThCH_2), 1.77 (m, 2H, CH_2CH$_2$O), 1.66 (m, 2H, ThCH$_2$CH_2), 1.50 (m, 2H, aliphatic CH_2), 1.41 (m, 2H, aliphatic CH_2).

^{13}C-NMR ($CDCl_3$, ppm): δ 154.03, 153.61 (aromatic *C*-O), 143.38 (Th *C*3), 128.59 (Th *C*4), 125.45 (Th *C*5), 120.19 (Th *C*2), 115.78, 114.96 (aromatic *C*H), 68.91 (*C*H$_2$O), 56.09 (O*C*H$_3$), 30.81, 30.52, 29.65, 29.38, 26.22 (aliphatic *C*H$_2$).

FT-IR (KBr, cm^{-1}): 3103, 3002, 2928, 2916, 2856, 2845, 1510, 1467, 1453, 1292, 1238, 1220, 1112, 1069, 1037, 829, 809, 774, 748, 715, 593, 526.

3.2.3. Synthesis of 3-(6-bromohexyl)thiophene (T6Br)

14.7 mL (0.130 mol) of HBr 48% were slowly added to 19.7 mL (0.204 mol) of acetic anhydride ((CH$_3$CO)$_2$CO, 98%). The obtained solution was added dropwise to a flask containing 6.16 g (21.2 mmol) of T6P and the mixture was heated at 90°C for 24h, protected from light.

The system was cooled down to room temperature and the crude product was added to 200 mL of ice/distilled water and extracted with petroleum ether (8 × 100 mL). The organic phase was washed with 250 mL of a saturated solution of $NaHCO_3$ and then with distilled water up to neutrality, dried with Na_2SO_4, filtered and the solvent was removed under reduced pressure.

The crude product was purified by chromatography column on silica gel with heptane:diethyl ether (95:5) giving 2.37 g (9.59 mmol) of a colorless oil (yield 45%).

^{1}H-NMR ($CDCl_3$, ppm): δ 7.24 (m, 1H, Th *H*5), 6.93 (m, 2H, Th *H*4 + *H*2), 3.41 (t, 2H, C*H*$_2$Br), 2.64 (t, 2H, ThC*H*$_2$), 1.86 (m, 2H, C*H*$_2$CH$_2$Br), 1.64 (m, 2H, ThCH$_2$C*H*$_2$), 1.47 (m, 2H, aliphatic C*H*$_2$), 1.36 (m, 2H, aliphatic C*H*$_2$).

^{13}C-NMR ($CDCl_3$, ppm): δ 143.22 (Th *C*3), 128.55 (Th *C*4), 125.52 (Th *C*5), 120.25 (Th *C*2), 34.28 (*C*H$_2$Br), 33.06, 30.66, 30.46, 28.72, 28.31 (aliphatic *C*H$_2$).

FT-IR (KBr, cm^{-1}): 3104, 3049, 2924, 2856, 1537, 1465, 1435, 1246, 1215, 1080, 831, 753, 685, 634, 561.

3.2.4. Synthesis of 2,5-dibromo-3-(6-bromohexyl)thiophene (2,5BT6Br)

1.01 g (4.10 mmol) of T6Br were dissolved in 4.00 mL of DMF in a three neck-flask equipped with a drip funnel containing 0.730 g (4.10 mmol) of N-bromosuccinimide (NBS) dissolved in 4.10 mL of DMF. The solution of NBS was added dropwise to the system in an inert atmosphere and allowed to react under stirring at room temperature for 6h, protected from light.

Subsequently, a second solution of 1.09 g (6.15 mmol) of NBS in 6.20 mL of DMF was slowly added to the system and the mixture was reacted at room temperature for 24h, under stirring and inert atmosphere.

The crude product was added to 130 mL of a half saturated solution of NaCl and extracted with petroleum ether (5 × 100 mL). The organic phase was then washed with distilled water up to neutrality, dried with Na_2SO_4, filtered and concentrated under reduced pressure.

The crude product was purified by chromatography column on silica gel with cyclohexane obtaining 1.24 g (3.06 mmol) of a colorless oil (yield 75%).

^{1}H-NMR ($CDCl_3$, ppm): δ 6.77 (s, 1H, Th *H*4), 3.41 (t, 2H, C*H*$_2$Br), 2.52 (t, 2H, ThC*H*$_2$), 1.86 (m, 2H, C*H*$_2$CH$_2$Br), 1.56 (m, 2H, ThCH$_2$C*H*$_2$), 1.47 (m, 2H, aliphatic C*H*$_2$), 1.34 (m, 2H, aliphatic C*H*$_2$).

^{13}C-NMR ($CDCl_3$, ppm): δ 142.97 (Th *C*3), 131.24 (Th *C*4), 110.81 (Th *C*5), 108.44 (Th *C*2), 34.19 (*C*H$_2$Br), 33.00, 29.70, 29.64, 28.50, 28.23 (aliphatic *C*H$_2$).

FT-IR (KBr, cm^{-1}): 3090, 2932, 2855, 1541, 1461, 1436, 1418, 1254, 1233, 1186, 1001, 826, 727, 645.

3.2.5. Synthesis of poly[3-(6-bromohexyl)thiophene] (PT6Br)

0.66 mL of a 3.0 M CH_3MgCl solution (1.98 mmol) in THF was added to 800 mg (1.98 mmol) of 2,5BT6Br in 16.0 mL of anhydrous THF. The mixture was refluxed for 2h under stirring and in an inert atmosphere. The system was then cooled down to room temperature and 5.37 mg (0.0099 mmol) of catalyst ($Ni(dppp)Cl_2$) were added. At 30 and 60 minutes two portions of the reaction mixture were taken out while the remaining part was stirred for 90 minutes. At the end of polymerization, the three portions of the crude product were treated with 15.0 mL of HCl 2.5 M and extracted with 90.0 mL of $CHCl_3$. The organic phase was subsequently treated with 100 mL of HCl 1.0 M, washed with 100 mL of aqueous $NaHCO_3$ and with distilled water until neutrality, dried over Na_2SO_4, filtered and concentrated to a small volume under reduced pressure.

The crude product obtained after 90 minutes of reaction was precipitated into 300 mL of cold MeOH/HCl (1% HCl v/v) under stirring. The resulting dark brown powder was filtered on a cellulose extraction thimble (33 × 94 mm), washed with MeOH, and recovered with $CHCl_3$ using a Soxhlet apparatus. The mixture was concentrated, reprecipitated in cold MeOH/HCl (0.2% HCl v/v), and then filtered on a PTFE membrane (0.45 μm pore size) giving 103 mg (0.420 mmol) of reddish PT6Br (yield 21%).

^{1}H-NMR ($CDCl_3$, ppm): δ 6.98 (s, 1H, Th *H*4), 3.43 (t, 2H, C*H*$_2$Br), 2.83, 2.59 (t, 2H, ThC*H*$_2$), 1.95-1.84 (m, 2H, C*H*$_2$CH$_2$Br), 1.78-1.67 (m, 1H, ThCH$_2$C*H*$_2$), 1.58-1.40 (m, 4H, (C*H*$_2$)$_2$).

^{13}C-NMR ($CDCl_3$, ppm): δ 140.31 (Th *C*3), 134.91 (Th *C*5), 131.23 (Th *C*2), 129.01 (Th *C*4), 34.59 (*C*H$_2$Br), 33.97, 30.61, 29.83, 29.17, 28.55 (aliphatic *C*H$_2$).

FT-IR (KBr, cm^{-1}): 3052, 2928, 2855, 1511, 1459, 1257, 1089, 832, 728, 645, 562.

3.3. Methods

^{1}H-NMR and ^{13}C-NMR spectra were recorded on a Varian Mercury Plus 400 (400 MHz) spectrometer at room temperature using TMS as internal standard in deuterated solvents. Chemical shifts are given in ppm.

FT-IR spectra were taken on KBr disk using a Perkin Elmer Spectrum One spectrophotometer.

References

1. C. H. Woo, B. C. Thompson, B. J. Kim, M. F. Toney, J. M. Frechet, *J. Am. Chem. Soc*., **2008**, *130*, 16324-16329.
2. R. D. McCullough, *Adv. Mater.*, **1998**, *10*, 93-116.
3. R. S. Loewe, S. M. Khersonsky, R. D. McCullough, *Adv. Mater*, **1999**, *11*, 250-253.
4. R. S. Loewe, P. C. Ewbank, J. Liu, L. Zhai, R. D. McCullough, *Macromolecules*, **2001**, *34*, 4324-4333.
5. L. Zhai, R. L. Pilston, K. L. Zaiger, K. K. Stokes, R. D. McCullough, *Macromolecules*, **2003,** *36*, 61-64.
6. S. Hladysh, D. Bondarev, J. Vohlídal, D. Vrbata, J. Zedník, *Eur. Polym. J.*, **2016**, *83*, 367-376.
7. R. H. Lohwasser, M. Thelakkat, *Macromolecules*, **2011**, *44*, 3388-3397.
8. P. Bäuerle, F. Würthner, S. Heid, *Angew. Chem. Int. Ed. Engl.*, **1990**, *29*, 419-420.
9. S. Miyanishi, K. Tajima, K. Hashimoto, *Macromolecules*, **2009**, *42*, 1610-1618.
10. K. Tamao, K. Sumitani, Y. Kiso, M. Zembayashi, A. Fujioka, S. Kodama, I. Nakajima, A. Minato, M. Kumada, *Bull, Chem. Soc. Jpn.*, **1976**, *49*, 1958-1969.
11. K. Tamao, K. Sumitani, M. Kumada, *J. Am. Chem. Soc.*, **1972**, *94*, 4374.
12. M. P. Bhatt, H. D. Magurudeniya, P. Sista, E. E. Sheina, M. Jeffries-EL, B. G. Janesko, R. D. McCullough, M. C. Stefan, *J. Mater. Chem. A*, **2013**, 1, 12841.
13. R. Miyakoshi, A. Yokoyama, T. Yokozawa, *J. Am. Chem. Soc*., **2005**, *127*, 17542.
14. M. Iovu, E. Sheina, R. Gil, R. McCullough, *Macromolecules*, **2005** , *38*, 8649-8656.
15. T. Chen, X. Wu, R. D. Rieke, *J. Am. Chem. Soc.*, **1995**, *117*, 233-244.
16. F. P. V. Koch, P. Smith, M. Heeney, *J. Am. Chem. Soc.*, **2013**, *135*, 13695-13698.
17. M. Zagòrska, B. Krische, *Polymer*, **1990**, *31*, 1379-1383.
18. M. Jeffries-el, R. D. McCullough, *Macromolecules*, **2005**, *38*, 10346-10352.

CHAPTER III: STUDY OF PHOTOACTIVE LAYERS IN BHJ SOLAR CELLS

1. Introduction

1.1 Overview

In recent years, bulk-heterojunction (BHJ) solar cells have been widely studied for their peculiarities and advantages.[1-3] In detail, the resulting enhanced interface area between the two components – electron-donor (ED) and electron-acceptor (EA) materials – can promote an efficient generation and subsequent transport of free-charge carriers.[4]

The use of proper photoactive materials in a physical blend is the main requirement for the correct operation of the device. Several studies have demonstrated that interesting features can be obtained by using polythiophenes as ED material, in particular poly-alkoxythiophene with several oxygen atoms in side chains.[5] The presence of an ether-functionalized side chain directly linked to the thiophene ring provides an improved final solubility in common organic solvents,[6] reduced band gap, low oxidation potential, increase in optical behavior and conductivity and an enhancement of interaction with the EA material.[7] Moreover, the introduction of an oxygen atom directly linked to the thiophenic ring can increase the electronic density of the π-conjugated backbone and, when the polymer also shows a high regioregularity degree and an appropriate average molecular weight, the final material can exhibit very promising optical properties and electrical conductivity.[8,9]

1.2. Aim of the chapter

In order to evaluate the influence of oxygen atoms, three poly-alkoxythiophene derivatives were synthetized with different ethereal side chains of different length and in different position of thiophene rings. Besides, they were investigated as electron-donor materials for bulk heterojunction (BHJ) polymeric solar cells with the aim to obtain the best photovoltaic performances.

The structural properties were investigated by spectroscopy techniques (^{1}H-NMR, ^{13}C-NMR, FT-IR, UV-Vis), thermogravimetric analysis (TGA), differential scanning calorimetry (DSC) and external quantum efficiency (EQE). Finally, the final materials were tested as photoactive materials in organic solar devices.

The external quantum efficiency (EQE) measurements were carried out in collaboration with Prof. Filippo Pierini of Department of Biosystem and Soft Matter – Institute of Fundamental Technological Research, Polish Academy of Science (Warsaw, Poland).

The electrochemical measurements (CV) were carried out in collaboration with Prof. Domenica Tonelli's research group at the Department of Industrial Chemistry "Toso Montanari" - Bologna (BO), Italy.

The synthesis of poly[3,4-bis(6-methoxyhexyl-1-oxy)thiophene] [P(3,4TO6OMe)] and poly[3,4-bis(10-methoxydecyl-1-oxy)thiophene] [P(3,4TO10OMe)] with the related synthetic results reported in this chapter were performed by Nicola Iannacci and Simone Rofani, respectively, under the supervision of the author or by the author herself.

2. Results and discussion

2.1. Synthesis

The synthetic approach followed to prepare photoactive materials was based on the functionalization of different monomeric precursors with the same substituent (methoxide group) and their subsequent polymerization – through GRIM method to synthetize poly[3-(6-methoxyhexyl)thiophene] (PT6OMe) and by the oxidative polymerization with $FeCl_3$ for symmetric monomers - in order to obtain poly-alkoxythiophenes with high degrees of regioregularity.

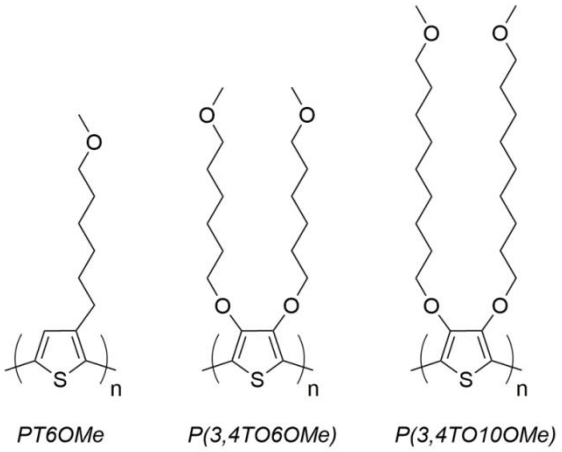

Figure 1. Scheme of synthetized polymers.

With the aim to compare highly regioregular polymers between them, the monomer 2,5-dibromo-3-(6-methoxyhexyl)thiophene was polymerized through the Grignard Metathesis Polymerization in presence of a nickel based catalyst, as reported in literature by my research group.[10]

The resulting polymer presents a high degree of regioregularity but it bears only one side chain in position 3 of thiophene ring. In order to study the effect of two side chains, it has been tried to synthetize a disubstituted polythiophene with the same side chains (Figure 2).

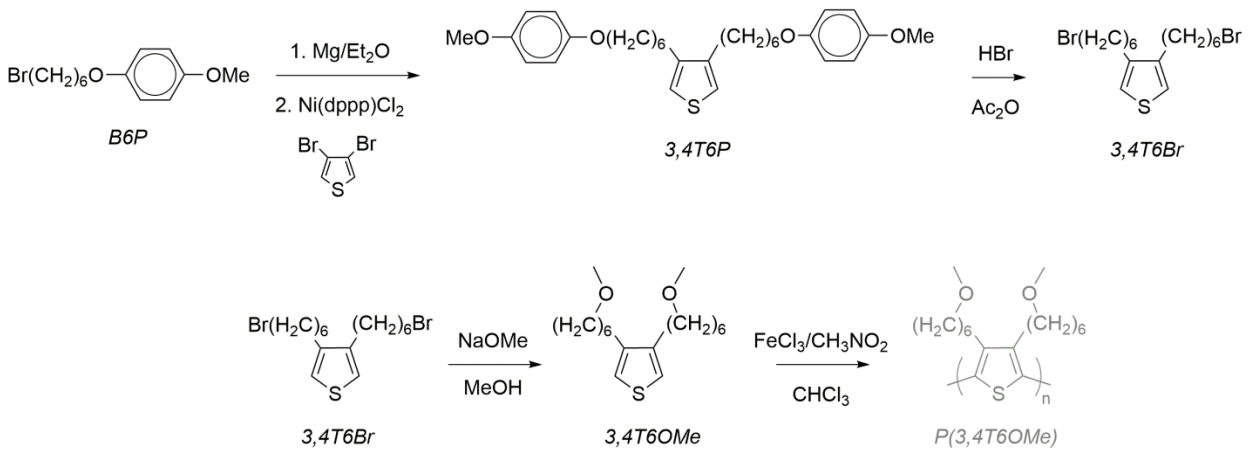

Figure 2. Synthetic route followed to obtain P(3,4T6OMe).

In detail, the synthetic process provided the cross-coupling reaction with the protected alkylic chain (B6P) with 3,4-dibromothiophene and the consequent deprotection to obtain 3,4-bis(6-bromohexyl)thiophene (3,4T6Br), similarly to the synthesis of 3-(6-bromohexyl)thiophene (T6Br) previously illustrated in Chapter II.

Then, the monomeric precursor 3,4T6Br was subjected to a SN_2 reaction with sodium methoxide (NaOMe 30% in MeOH), which involved the bromide group at the end of side chain. The reaction was conducted under reflux conditions for 4 hours. The subsequent polymerization was conducted through an oxidative reaction with $FeCl_3$ for 5 hours. Despite the high reaction time, only short oligomers were obtained (Mn = 1.5 kDa, Xn = 5, PDI = 1.2) and this is probably due to the high stability of the monomer and its reduced tendency to be oxidized.

Disubstituted alkoxy monomeric precursors were obtained by transetherification reaction between 3,4-dimethoxythiophene and the corresponding synthetized alkylic chain (6-bromo-1-hexanol or 10-bromo-1-decanol). Then, they were also subjected to a substitution reaction with sodium methoxide, under reflux conditions for 2 hours or more. Due to the presence of a good leaving group, the functionalization could easily produce the desired monomers 3,4-bis(6-dimethoxyhexyl-1-oxy)thiophene (3,4TO6OMe) and 3,4-bis(10-dimethoxydecyl-1-oxy)thiophene (3,4TO10OMe). Then, monomers were reacted with $FeCl_3$ in dry chloroform for ~ 20/25 minutes under inert conditions to obtain the corresponding polymers poly[3,4-bis(6-methoxyhexyl-1-oxy)thiophene] [P(3,4TO6OMe)] and poly[3,4-bis(10-methoxydecyl-1-oxy)thiophene] [P(3,4TO10OMe)].

The average molecular weights were determined through GPC analysis of the soluble fractions of the synthetized polymers (Table 1) and revealed comparable polymerization degrees.

Table 1. Polymers' characteristics.

	Yield reaction (%)	*HT (%)* [a]	*Mn (kDa)* [b]	X_n [b]	*PDI* [b]
PT6OMe	64	94	39.7	202	1.77
P(3,4TO6OMe)	56	100	64.6	189	1.22
P(3,4TO10OMe)	64	100	53.7	126	1.27

[a] Determined by ^{1}H-NMR; [b] Determined by GPC chromatography.

2.2. NMR characterization

All the synthesized polymers were characterized by NMR spectrometry (^{1}H-NMR and ^{13}C-NMR) to confirm their chemical structure.

The analysis of ^{1}H-NMR spectra of monomers 3,4TO6OMe and 3,4TO10OMe shows the total absence of methylenic protons in α position to -Br group (~ 3.40 ppm) evidencing the successful functionalization of precursors 3,4TO6Br and 3,4TO10Br with methoxide group. In particular, the triplet and the singlet signals around 3.36 and 3.33 ppm, respectively - ascribable to the methylenic protons near to the oxygen atom of methoxide moiety - confirm the complete substitution of bromide group (Figure 3 and Figure 4).

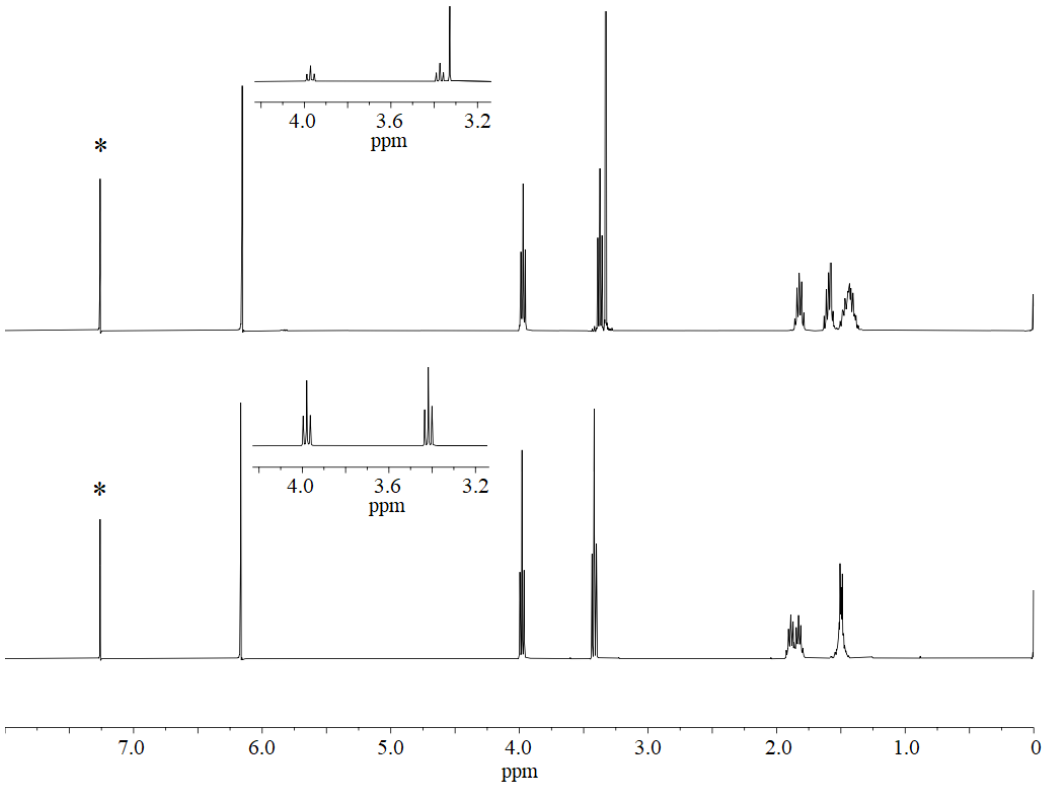

Figure 2. ^{1}H-NMR spectra of 3,4TO6Br (bottom) and 3,4TO6OMe (top). Asterisk: solvent resonance ($CDCl_3$). Inset: expanded region showing protons near to heteroatoms.

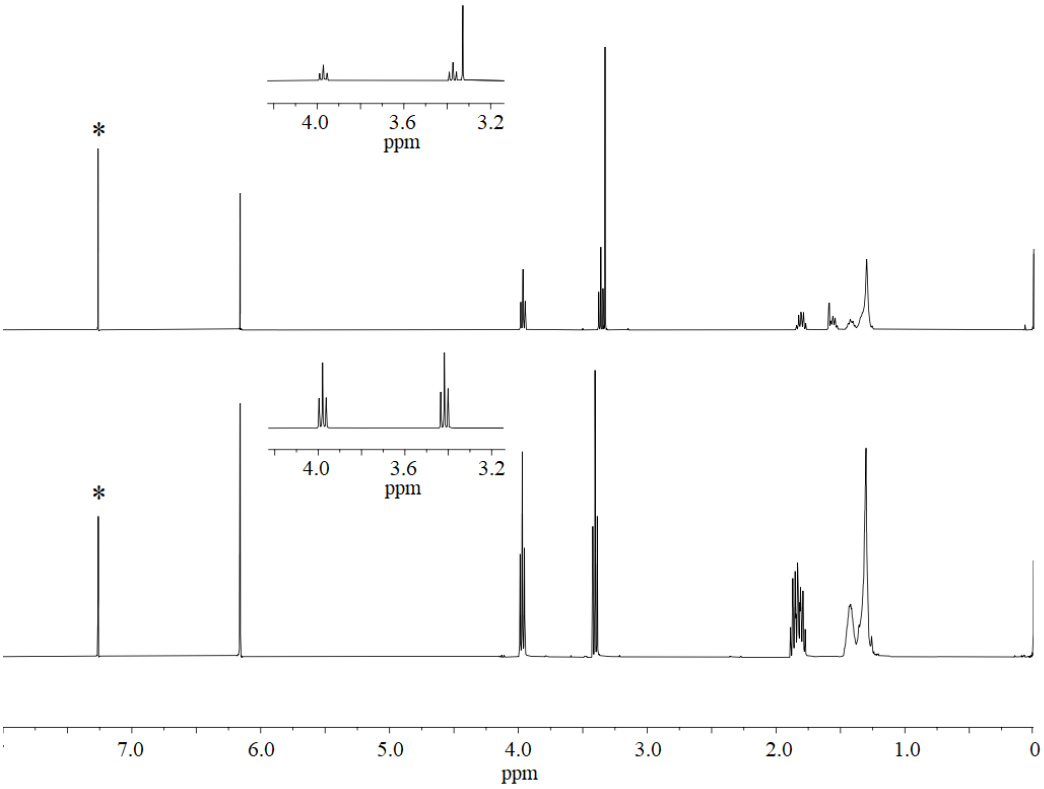

Figure 3. ^{1}H-NMR spectra of 3,4TO10Br (bottom) and 3,4TO10OMe (top). Asterisk: solvent resonance ($CDCl_3$). Inset: expanded region showing protons near to heteroatoms.

The subsequent polymerizations through GRIM method and oxidative polymerization with $FeCl_3$ to give PT6OMe and two poly(3,4-dialkoxythiophenes) P(3,4TO6OMe) and P(3,4TO10OMe), respectively, were confirmed by ^{1}H-NMR analyses which spectra are reported in Figure 5.

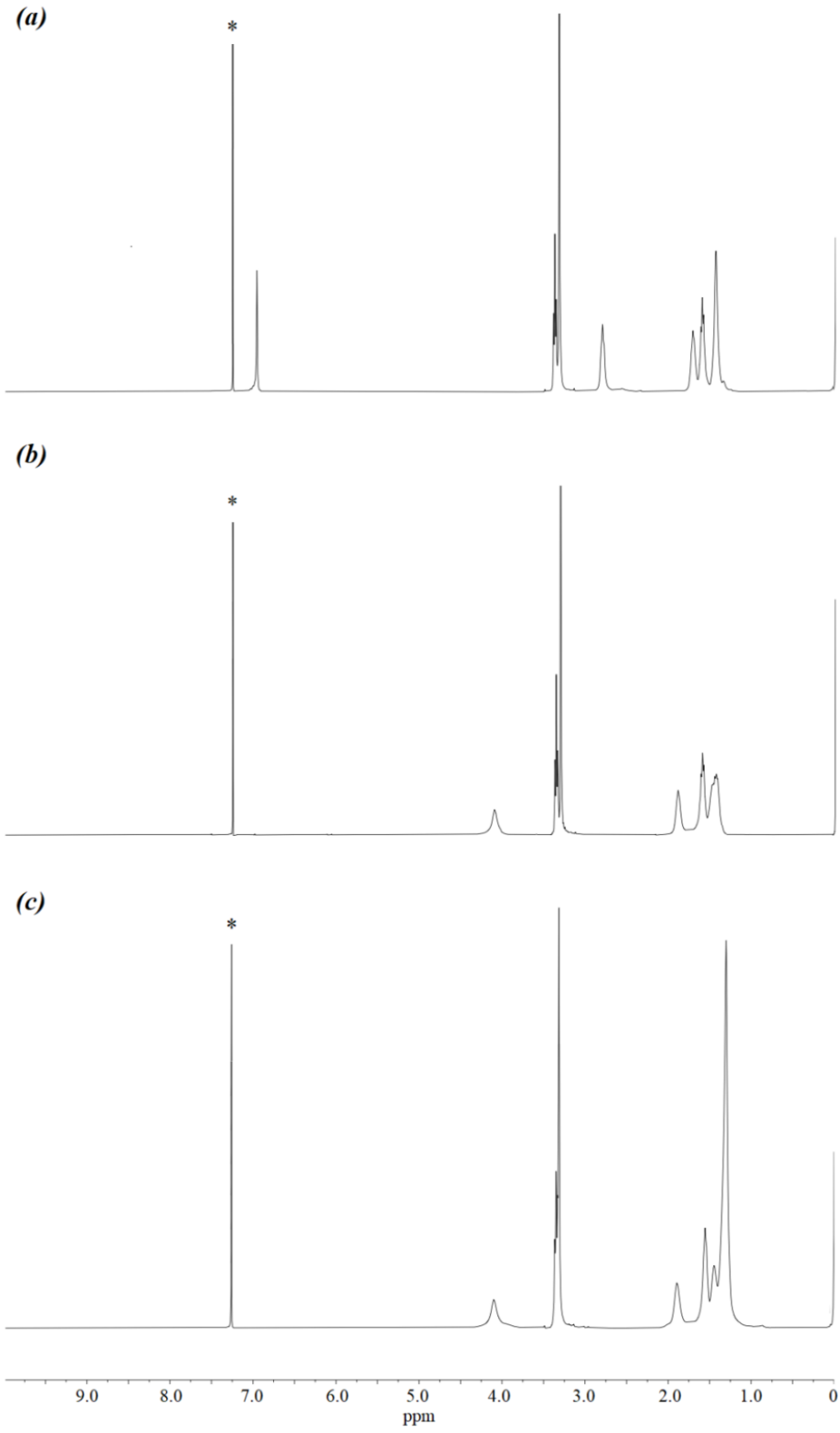

Figure 5. ^{1}H-NMR spectra of PT6OMe (*a*), P(3,4TO6OMe) (*b*) and P(3,4TO10OMe) (*c*). Asterisk: solvent resonance ($CDCl_3$).

2.3. FT-IR characterization

FT-IR spectroscopy further confirms the chemical structure of all synthetized products and resulting polymers PT6OMe, P(3,4TO6OMe), P(3,4TO10OMe) whose spectra are reported in Figure 6.

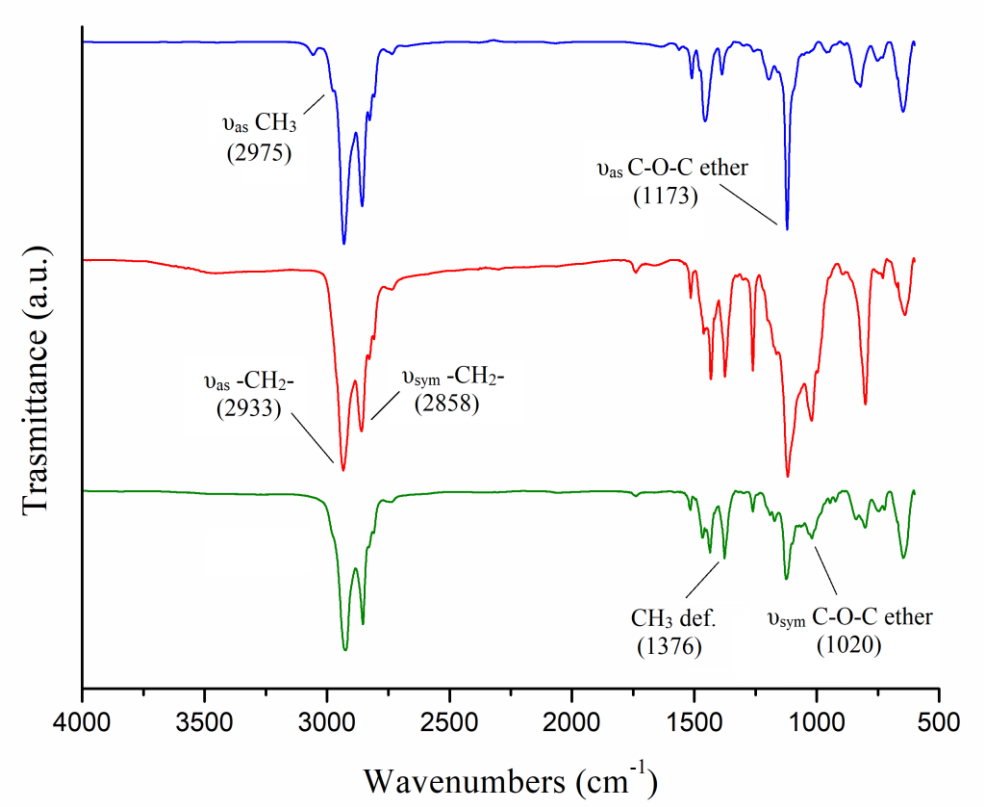

Figure 6. FT-IR spectra of PT6OMe (blue line), P(3,4TO6OMe) (red line) and P(3,4TO10OMe) (green line).

The presence of two bands ascribable to methoxide group at the end of side chain (~ 2975 and 1376 cm^{-1}) in IR spectra confirms the functionalization and substitution of bromide group which is also evidenced by the absence of peaks ascribable to -Br terminal group at ~ 640 and 560 cm^{-1}. Moreover, in the FT-IR spectra of disubstituted poly-alkoxythiophenes can also be found the presence of C-O-C asymmetric stretching bonds at ~ 1120 cm^{-1} (ascribable to methoxide terminal groups) and at ~ 1170 cm^{-1} (ascribable to ethereal bond next to thiophene).

2.4. Thermal properties

The thermal stability of synthetized polymers PT6OMe, P(3,4TO6OMe) and P(3,4TO10OMe) has been evaluated by TGA analysis under oxidizing atmosphere (air), at a heating scan rate of 10°C min^{-1} and up to 600°C (Figure 7 and Table 2).

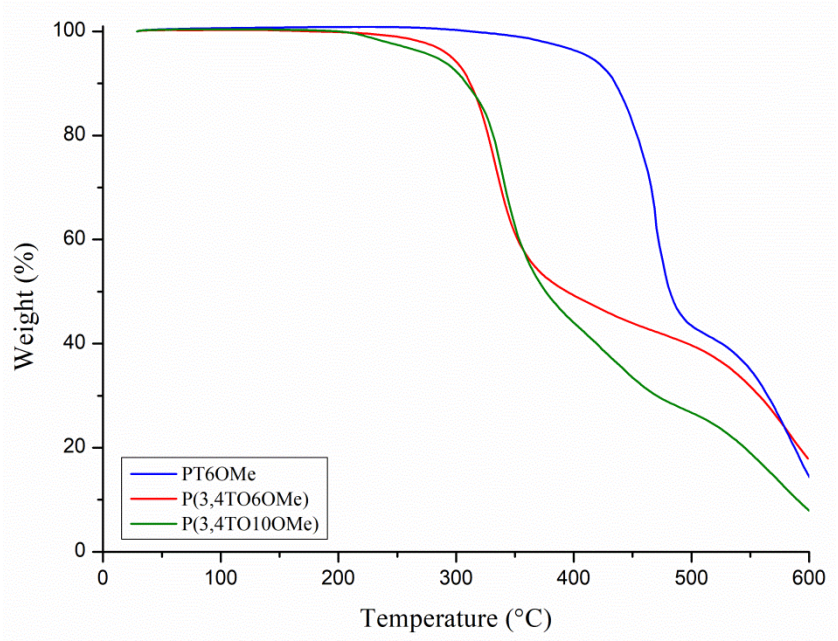

Figure 7. TGA curves of photoactive materials.

In detail, the TGA curves of all the examined samples show two main weight losses that can be ascribed to the aliphatic side chain scission (up to 300°C) and to the macromolecular backbone combustion (up to 500°C), respectively. Higher values can be observed for PT6OMe owing to the lower steric hindrance of monosubstituted repeating units, as reported in Table 2. Moreover, the two disubstituted poly-alkoxythiophenes show comparable first decomposition temperatures but at ~ 400°C the curves profiles change due to the different length of side chains.

The synthesized samples, however, may be considered stable enough to be used as photoactive materials in organic photovoltaic devices.

Table 2. Decomposition (T_d) and glass-transition (T_g) temperatures of polymers.

	T_d (°C) [a]	$T_{d,max}$ (°C) [b]	T_g (°C) [c]	T_m (°C) [c]	T_c (°C) [c]
PT6OMe	417	437	54	178	131
P(3,4TO6OMe)	307	333	64	153	126
P(3,4TO10OMe)	327	341	37	128	106

[a] Determined by the onset point of the first inflection; [b] calculated from the first derivative of the weight/temperature curve; [c] evaluated by DSC analysis.

Thermal properties of polymers have been evaluated by DSC analyses which were carried out under nitrogen atmosphere with a heating ramp of 10°C min^{-1} from -30°C up to 220°C and the relative curves are reported in Figure 8.

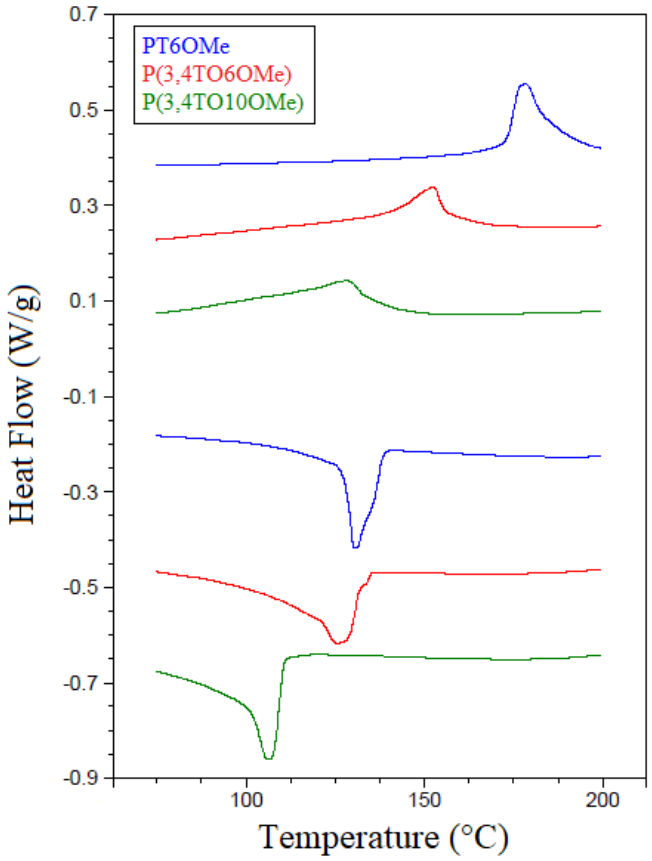

Figure 8. DSC curves profiles of melting and crystallization transitions of synthetized photoactive materials.

All polymeric samples show a slight endothermic flexure ascribable to the glass transition temperature (T_g) (Table 2). Contrary to expectations, the highest T_g value was obtained analyzing P(3,4TO6OMe), thus confirming its singular behavior: it is therefore possible to state that the consequences of the steric hindrance given by the presence of two side chains can be strongly reduced by combining the proper length of side chain with the ethereal bonds linked to thiophene ring. Moreover, the increase of plastifying effect of the side chains – from one to two and with increased length - induces the decrease of melting and crystallization temperatures in DSC curves (Figure 8). Nevertheless, the high degree of symmetry – and the consequent conformational order - of all examined samples allowed the obtainment of semi-crystalline materials, an important requirement to use them as photoactive layers.

2.5. Optical properties (UV-Vis characterization)

In order to evaluate the optical properties, synthetized materials were analyzed by UV-Vis spectroscopy in solution and in films obtained by drop-casting on quartz slides solution of polymers in chloroform and chlorobenzene. The normalized absorption spectra are reported in Figure 9 while their associated data are reported in Table 3.

Table 3. Maximum absorption wavelengths (nm) of polymers in solution and in thin films drop-cast from chlorinated solvents.

	Solvent	***λ_{max} solution 10^{-5} M (nm)***	***λ_{max} film (nm)***	***Solubility (mg/mL)***
PT6OMe	Chloroform	442	523	28
	Chlorobenzene	455	514	14
P(3,4TO6OMe)	Chloroform	533, 565	554, 601	9
	Chlorobenzene	537, 574	557, 601	11
P(3,4TO10OMe)	Chloroform	533, 564	549, 596	17
	Chlorobenzene	539, 576	548, 595	9

The analysis of the obtained values and optical profiles suggests that the use of one of these solvents doesn't involve appreciable shift of the maximum absorption wavelengths (λ_{max}) both in solution and in solid state. Moreover, the values of the poly(3,4-dialkoxythiophenes) are comparable between them.

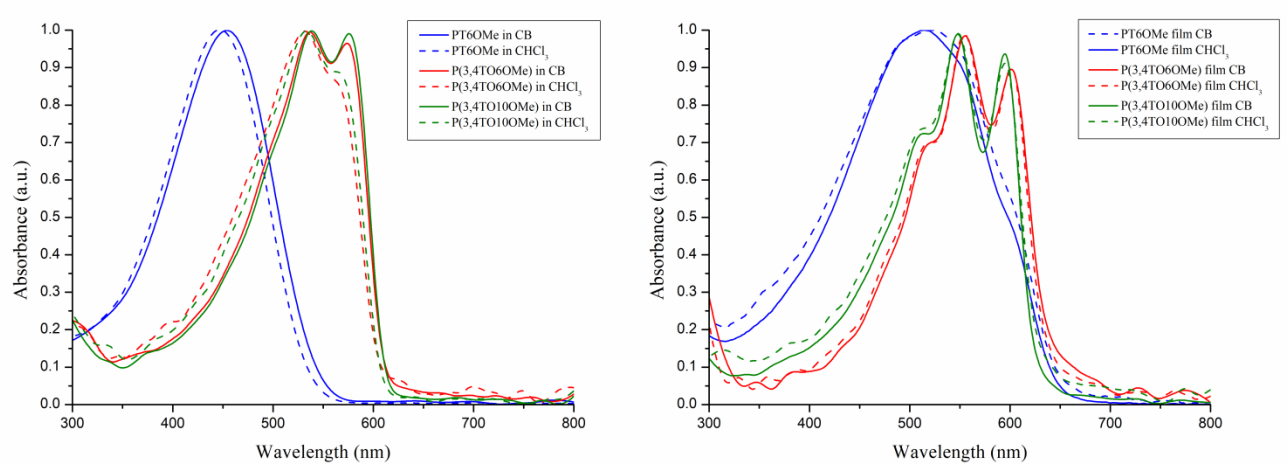

Figure 9. Normalized UV-Vis spectra of polymers in solution (left) and in solid state (right).

The main observation can be made on the absorption profile of PT6OMe which presents only a side chain without an oxygen atom directly linked to the thiophene ring. The high solubility of this polymer leads to have an ordered macromolecular organization which is expressed by a notable bathochromic shift of λ_{max} in solid state (~ 60-80 nm).[11] Nevertheless, highest values of absorption can be observed when oxygen atoms are present in side chains, i.e. when disubstituted poly-alkoxythiophenes were analysed. Moreover, the high degree of symmetry leads to have both a red shift of the λ_{max} and the evidence of two electronic transitions ($\pi \rightarrow \pi^*$ and $n \rightarrow \pi^*$) in UV-Vis spectra both in solution and in film.

2.6. Electrochemical properties (CV)

The potentials of photoactive materials PT6OMe, P(3,4TO6OMe) and P(3,4TO10OMe) were evaluated by cyclic voltammetry (CV). In Table 4 are reported the electrochemical parameters of synthesized polymers in thin films obtained by drop-casting their solution in chloroform on Pt electrode.

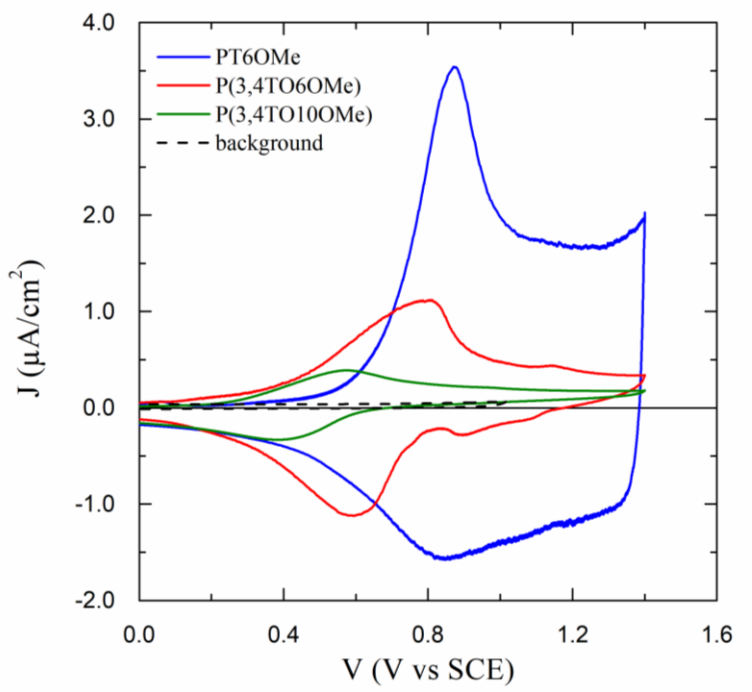

Figure 10. Cyclic voltammetries of photoactive materials at 0.1 V s^{-1}.

As shown in Figure 10, oxidation of the synthetized materials can be considered reversible due to the presence of both anodic and cathodic potential picks. Moreover, during this reversible process it was observed an electrochromic effect, an interesting characteristic in optoelectronic field.

Table 4. Electrochemical and optical properties of synthesized polymer in thin film.

	E_{ox} (V) [a]	HOMO (eV)	LUMO (eV)	$E_{g,\,opt}$ (eV) [b]
PT6OMe	+0.66	-4.90	-2.99	1.91
P(3,4TO6OMe)	+0.37	-4.61	-2.56	2.05
P(3,4TO10OMe)	+0.25	-4.49	-2.52	1.97

[a] Onset potential of anodic scan; [b] Optical bandgap in film.

The different electrochemical properties of the three polymers are ascribable to the degree of electronic delocalization over the polyconjugated backbones. The presence of oxygen atoms – with a consequent enhancement of the electron density - directly linked to the thiophene ring promotes the decrease of oxidation potential (Table 4).[12,13]

While the energy levels of the highest occupied molecular orbitals (HOMO) were evaluated by CV according to the following equation:

$$HOMO\ (eV) = -\ e\ (E_{ox} + 4.24)$$

where 4.24 V is the SCE absolute potential, the energy levels of the lowest unoccupied molecular orbital (LUMO) were evaluated indirectly since the reduction potentials resulted to be outside the electrochemical stability window of the electrolyte. LUMO levels were then calculated from HOMO levels and the optical bandgaps ($E_{g,opt}$) obtained from the UV–Vis spectra of the films by the equation:

$$LUMO\ (eV) = HOMO + E_{g,opt}$$

To explain the obtained values, in Figure 11 are reported the energy levels values of synthetized materials employed in a photovoltaic device with BHJ architecture. The LUMO levels distance between electron-donor and electron-acceptor is an important requirement to guarantee the correct process of hopping in a solar cell.

By comparing the synthetized materials with poly-(3-hexylthiophene) (P3HT)[14] as electron-donor reference, the energy gap between LUMO energy levels of ED and EA materials are able to guarantee the hopping and exciton dissociation at the donor/acceptor interface in a BHJ solar cell.

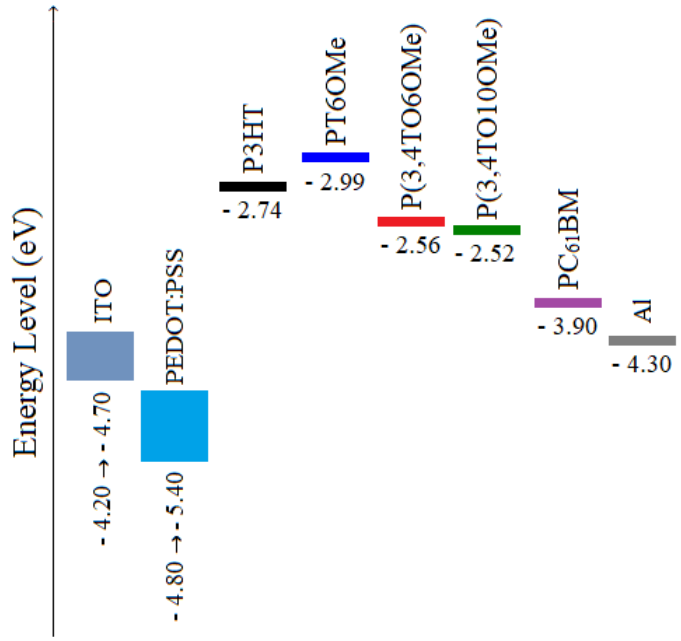

Figure 11. Energy-level alignment of OPVs layers (ITO, PEDOT:PSS and Al)[15] and comparison between P3HT and synthetized materials.

2.7. Photovoltaic properties

The photocurrent density-voltage (J/V) characteristics of the cells prepared using the photoactive layer with each of three synthesized electron-donor (ED) materials - PT6OMe, P(3,4TO6OMe) and P(3,4TO10OMe) – respectively, measured under illumination of AM 1.5 G (100 mW/cm^2), are shown in Figure 12. The final structure of the prepared cells was: ITO/PEDOT:PSS/ED:$PC_{61}BM$ (1:1 w/w)/Al. Detailed information on open circuit voltage (V_{OC}), short-circuit current density (J_{SC}), fill factor (FF) and photoconversion efficiency (PCE) are collected in Table 5.

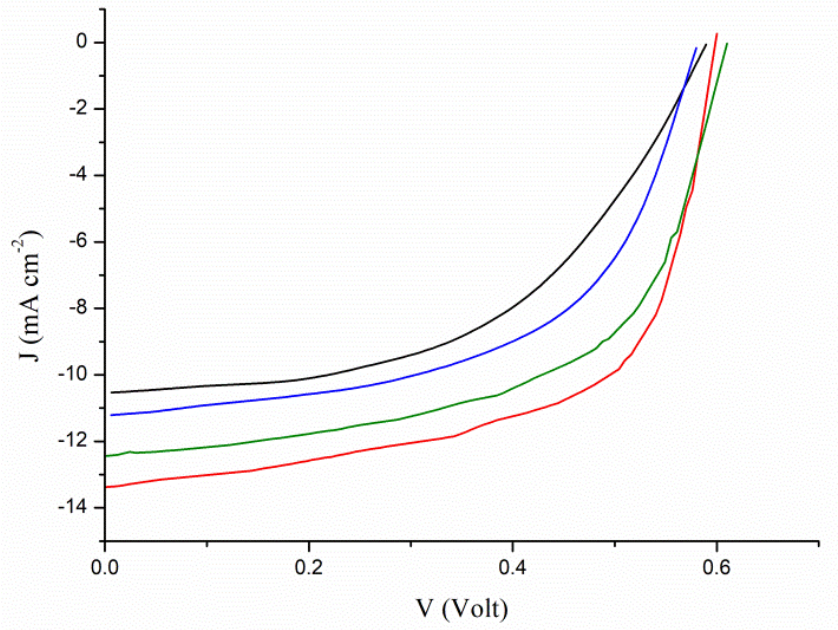

Figure 12. J/V curves obtained from tested cells based on P3HT (black line), PT6OMe (blue line), P(3,4TO6OMe) (red line) and P(3,4TO10OMe) (green line) as ED materials.

Taking as a reference the device composed by the photoactive blend poly-(3-hexylthiophene) (P3HT) and $PC_{61}BM$ and comparing the photovoltaic parameters obtained, it appears that devices prepared with an increasing number of oxygen atoms in side chain provides an enhancement in power conversion efficiency (PCE) and current density (J_{SC}). The electron-donating effect of the oxygen atom(s) directly linked to the thiophenic ring in addition to the presence of methoxide end group allow to achieve good photovoltaic properties.

Besides, the lower length of side chains allows to have a better extension of conjugation in terms of enhanced orbital overlapping between aromatic thiophenes of macromolecular backbone and this is also confirmed by the highest photovoltaic parameters obtained (Table 5).

Table 5. Short-circuit current density (J_{SC}) open-circuit voltage (V_{OC}), fill factor (FF) and power conversion efficiency (PCE) of tested photovoltaic devices.

	J_{sc} (mA cm^{-2}) [a]	V_{oc} (V)	FF	PCE (%)
P3HT:PC$_{61}$BM	10.55	0.59	0.59	3.68
PT6OMe:PC$_{61}$BM	11.21	0.58	0.61	3.96
P(3,4TO6OMe):PC$_{61}$BM	13.41	0.60	0.61	4.91
P(3,4TO10OMe):PC$_{61}$BM	12.47	0.61	0.60	4.56

[a] from J/V curves.

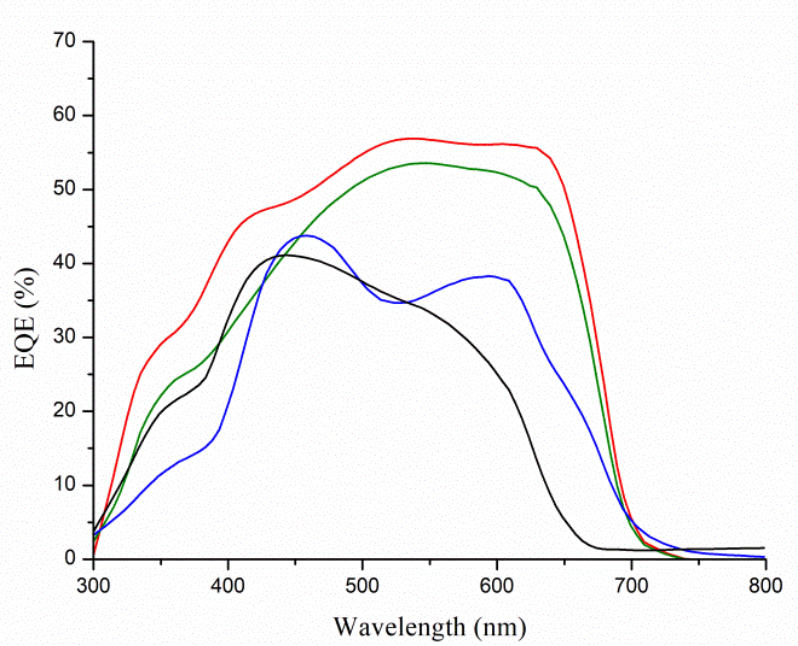

Figure 13. EQE spectra of P3HT (black line), PT6OMe (blue line), P(3,4TO6OMe) (red line) and P(3,4TO10OMe) (green line).

Analyzing the photo-current response wavelength for the cell based on the synthetized electron-donor materials range from 300 to 800 nm and compared with P3HT as reference, the curves show different behaviors. In case of PT6OMe the obtained curve presents two feature peaks (~ 460 and 590 nm) while in curves of P(3,4TO6OMe) and P(3,4TO10OMe) they are not detectable (Figure 13).

The disubstituted poly-alkoxythiophenes present EQE profiles that follow the trend observed in the UV-Vis spectra of polymers in solid state, indicating that the whole absorption effectively contributes to the photocurrent. Moreover, by introducing oxygen atoms in side chains of poly(3,4-dialkoxythiophenes) is possible to obtain EQE_{max} values at ~ 60%, as for P(3,4TO6OMe).

2.8. Conclusions

The three polythiophene derivatives with different ethereal side chains PT6OMe, P(3,4TO6OMe) and P(3,4(TO10OMe) were successfully synthetized starting from the corresponding functionalized monomers. The obtained polymers were highly soluble in a wide range of organic solvents and easily workable in thick free-standing films, owing to their semicrystalline structure. Their morphology also positively influences their thermal stability characteristics. Finally, the optical, electrochemical and photovoltaic properties also highlight the beneficial effects of the presence of oxygen atoms in the side chain.

3. Experimental section

3.1. Materials

[1,3-bis(diphenylphosphino)propane] nickel (II) chloride ($Ni(dppp)Cl_2$), methylmagnesium bromide (CH_3MgBr, 1M in butylether), tetrahydrofuran (THF, >99.9%), toluene (C_7H_8, >99.9%), diethyl ether (Et_2O, >99.5%), ethyl acetate (EtOAc, >99.5%), petroleum ether (Etp, >90%), 3-methoxythiophene (98%) and chloroform ($CHCl_3$, 99.0-99.4%) were purchased from Sigma Aldrich Chemical Co. (USA). Hexane (≥99%) and dichloromethane (CH_2Cl_2, ≥99.9%) were purchased from Sigma Aldrich (France). Nitromethane (CH_3NO_2, ≥98.5%), hydrochloridric acid (HCl, ≥37%), hydrobromic acid (HBr, 48%) and ferric trichloride ($FeCl_3$, ≥98%) were purchased from Fluka (Switzerland). 3,4-dimethoxythiophene (>98%) and 3,4-dibromothiophene (98%) were purchased from Tokyo Chemical Industry (Japan). n-Heptane (99.4%) was purchased from VWR Chemicals (France). Magnesium (Mg) for Grignard were purchased from Merck (Germany). P-Toluensulfonic acid monohydrate (pTSA) and acetic anhydride (Ac_2O, 99%) were purchased from Carlo Erba (Italy). Sodium sulfate (Na_2SO_4, anhydrous) and sodium bicarbonate ($NaHCO_3$) were purchased from Riedel-deHaën (Poland). Sodium methoxide solution (NaOMe 30% wt in methanol) was purchased from Acros Organics. Methanol (MeOH, >99.8%) was purchased from Honeywell (Germany). In order to remove the stabilizer, diethyl ether and THF were freshly distilled before the use. All other materials were used as received. All manipulations involving moisture-sensitive reagents were performed under argon atmosphere.

3.2. Synthesis

3.2.1. Synthesis of 3,4-bis[6-(4-methoxyphenoxy)hexyl]thiophene (3,4T6P)

113 mL of dry diethyl ether were added dropwise to a reaction system containing 10.0 g (35.0 mmol) of 1-bromo-6-(p-methoxyphenoxy)hexane (B6P) - previously synthetized - and 88.0 mg (36.0 mmol) of Mg. The mixture was refluxed for 5h, under stirring and inert atmosphere.

The Grignard intermediate was then transferred via cannula and added dropwise to the second reaction system containing 3.50 g (14.6 mmol) of 3,4-dibromothiophene and 37.9 mg (0.70 mmol) of catalyst [1,3-bis(diphenylphosphino)propane] nickel (II) chloride ($Ni(dppp)Cl_2$) and the system was refluxed for 16h, under stirring and in an inert atmosphere.

The mixture was cooled down to room temperature, poured in 150 mL of HCl 2% and extracted with 100 mL of diethyl ether. The organic phase was washed with distilled water up to neutrality, dried with Na_2SO_4, filtered and the solvent was removed under reduced pressure.

The crude product was purified by clean-up with silica in 500 mL of hot petroleum ether (Etp) followed steam distillation and crystallization obtaining 1.50 g (3.02 mmol) of 3,4T6P (yield 20%).

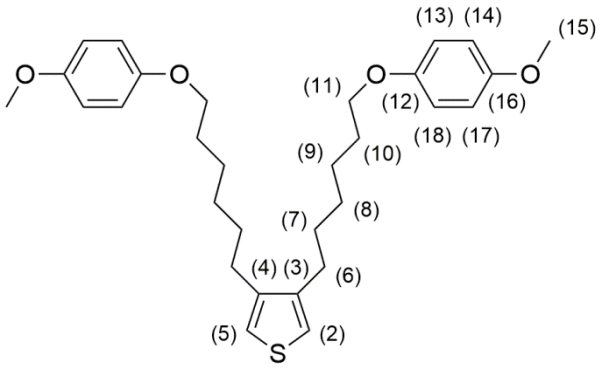

^{1}H-NMR ($CDCl_3$, ppm): δ 6.89 (s, 2H, Th *H*2+*H*5), 6.83 (s, 4H, *H*13+*H*14+*H*17+*H*18), 3.91 (t, 2H, *H*11), 3.76 (s, 3H, *H*15), 2.52 (t, 2H, *H*6), 1.77 (m, 2H, *H*10), 1.66 (m, 2H, *H*7), 1.47 (m, 4H, *H*8+*H*9).

^{13}C-NMR ($CDCl_3$, ppm): δ 154.35 (*C*16), 153.93 (*C*12), 142.52 (*C*3+*C*4), 120.70 (*C*2+*C*5), 116.09 (*C*13+*C*18), 115.29 (*C*14+*C*17), 69.23 (*C*11), 56.40 (*C*15), 30.24, 30.02, 30.00, 29.39, 26.63 (aliphatic *C*H_2).

FT-IR (KBr, cm^{-1}): 3104, 3083, 2994, 2940, 2921, 2855, 2832, 1590, 1508, 1475, 1463, 1390, 1290, 1234, 1178, 1106, 1038, 866, 826, 811, 741.

3.2.2. Generic procedure for the synthesis of n-bromohexyl-1-oxy (B(CH_2)$_n$OH)

In a three neck flask, diol was dissolved in toluene and the solution was heated at 120°C. Under inert flux, a solution of HBr 48% was dropwise added at the system and the reaction mixture was allowed to react under reflux for 72h. The crude product was treated with distilled water up to neutrality, the organic phase was dried over Na_2SO_4, filtered and concentrated under reduced pressure. The obtained residue was purified by silica gel column chromatography (EtOAc:Etp, 1:1) to give a colorless oil.

3.2.2.1. Synthesis of 6-bromo-1-hexanol (B6OH)

9.90 g (83.7 mmol) of 1,6-hexandiol; 126 mL of toluene; 11.4 mL (101 mmol) of HBr 48%; 10.8 g (60.1 mmol) of a colorless oil were obtained (yield 72%). ^{1}H-NMR ($CDCl_3$, ppm): δ 3.65 (t, 2H, C*H*$_2$OH), 3.41 (t, 2H, C*H*$_2$Br), 1.87 (m, 2H, C*H*$_2$CH$_2$OH), 1.58 (m, 2H, C*H*$_2$CH$_2$Br), 1.47 (m, 2H, C*H*$_2$), 1.39 (m, 2H, C*H*$_2$). ^{13}C-NMR ($CDCl_3$, ppm): δ 63.14 (*C*H$_2$OH), 34.16 (*C*H$_2$Br), 33.05, 32.86, 28.28, 25.28 (aliphatic *C*H_2). FT-IR (KBr, cm^{-1}): 3339, 2932, 2859, 1053, 728, 644, 561.

3.2.2.2. Synthesis of 10-bromo-1-decanol (B10OH)

10.0 g (56.3 mmol) of 1,10-decandiol; 86.0 mL of toluene; 7.60 mL (67.5 mmol) of HBr 48%; 8.61 g (36.3 mmol) of a colorless oil were obtained (yield 65%). ^{1}H-NMR ($CDCl_3$, ppm): δ δ 3.63 (t, 2H, C*H*$_2$OH), 3.40 (t, 2H, C*H*$_2$Br), 1.85 (m, 2H, C*H*$_2$CH$_2$OH), 1.56 (m, 2H, C*H*$_2$CH$_2$Br), 1.42

(m, 2H, CH_2), 1.29 (m, 10H, (CH_2)$_5$). ^{13}C-NMR ($CDCl_3$, ppm): δ 63.40 (*C*H_2OH), 34.38 (*C*H_2Br), 33.16, 33.11, 29.80, 29.70, 29.68, 29.07, 28.49, 26.05 (aliphatic *C*H_2). FT-IR (KBr, cm^{-1}): 3338, 2925, 2854, 1056, 722, 645, 562.

3.2.3. Synthesis of monomeric precursors

3.2.3.1. Synthesis of 3,4-bis(6-bromohexyl)thiophene (3,4T6Br)

177 mg (0.356 mmol) of 3,4-bis(6-(4-methoxyphenoxy)hexyl)thiophene (3,4T6P) previously synthetized were added to a solution of 0.54 mL (5.70 mmol) of acetic anhydride and 0.40 mL of hydrobromic acid (HBr 48%). The mixture was allowed to react at 90°C for 24h.

The system was then cooled down to room temperature and the crude product was added to 10 mL of distilled water and ice and subsequently extracted with petroleum ether (2 × 20 mL). The organic phase was washed with 50 mL of a saturated solution of $NaHCO_3$ and with distilled water up to neutrality (2 × 50 mL), dried on Na_2SO_4, filtered and concentrated under reduced pressure.

Finally, the purification by silica gel column chromatography (heptane/diethyl ether 9:1) allowed to obtain 81 mg (0.197 mmol) of 3,4T6Br as colorless oil (yield 55%).

^{1}H-NMR ($CDCl_3$, ppm): δ 6.89 (s, 2H, Th *H*2+*H*5), 3.42 (t, 4H, C*H*$_2$Br), 2.51 (t, 4H, ThC*H*$_2$), 1.88 (t, 4H, C*H*$_2$CH$_2$Br), 1.64 (m, 4H, ThCH$_2$C*H*$_2$), 1.54-1.38 (m, 8H, 2 × (C*H*$_2$)$_2$).

^{13}C-NMR ($CDCl_3$, ppm): δ 142.01 (Th *C*3+*C*4), 120.48 (Th *C*2+*C*5), 34.28 (*C*H_2Br), 33.08, 29.79, 29.01, 28.39 (aliphatic *C*H_2).

FT-IR (KBr, cm^{-1}): 3099, 2928, 2855, 1507, 1462, 1436, 1257, 1234, 867, 786, 643, 560.

3.2.3.2. Generic procedure for synthesis of 3,4-dialkoxythiophenes

Alkoxy-bromide chain (B6OH or B10OH) and p-toluensulfonic acid monohydrate (pTSA) were dissolved in anhydrous toluene in a neck flask equipped with a cooling system. Subsequently, 3-methoxythiophene or 3,4-dimethoxythiophene was added to the system under inert atmosphere. The mixture was allowed to react under reflux for 22h.

The system was then cooled down to room temperature, the solvent was removed under reduced pressure and the crude product was recovered in CH_2Cl_2. The organic phase was extracted with saturated solution of $NaHCO_3$, washed with water until neutrality and dried under vacuum. Finally, the purification by silica gel column chromatography (hexane/EtOAc 85:15) allowed to obtain the monomeric precursor.

3.2.3.2.1. Synthesis of 3,4-bis(6-bromohexyl-1-oxy)thiophene (3,4TO6Br)

1.88 g (10.4 mmol) of 6-bromo-1-hexanol (B6OH); 0.066 g (0.347 mmol) of p-toluensulfonic acid monohydrate (pTSA); 15.0 mL of anhydrous toluene; 0.42 mL (3.47 mmol) of 3,4-

dimethoxythiophene; the mixture was allowed to react under reflux for 22h; 100 mL of CH_2Cl_2; 50.0 mL of saturated solution of $NaHCO_3$; 712 mg (1.61 mmol) of 3,4TO6Br were obtained (yield 46%).

^{1}H-NMR ($CDCl_3$, ppm): δ 6.17 (d, 2H, Th *H*2+*H*5), 3.98 (t, 4H, ThOC*H*$_2$), 3.42 (t, 4H, C*H*$_2$Br), 1.89 (m, 2H, C*H*$_2$CH$_2$O), 1.83 (m, 2H, C*H*$_2$CH$_2$Br), 1.50 (m, 4H, (C*H*$_2$)$_2$).

^{13}C-NMR ($CDCl_3$, ppm): δ 147.75 (Th *C*3+*C*4), 97.36 (Th *C*2+*C*5), 70.60 (*C*H$_2$O), 34.11 (*C*H$_2$Br), 33.01, 29.19, 28.24, 25.58 (aliphatic *C*H$_2$).

FT-IR (KBr, cm^{-1}): 3109, 3002, 2937, 2859, 1563, 1499, 1467, 1242, 1144, 1048, 866, 747, 644, 560.

3.2.3.2.2. Synthesis of 3,4-bis(10-dibromodecyl-1-oxy)thiophene (3,4TO10Br)

0.422 mL (3.54 mmol) 3,4-dimethoxythiophene; 2.52 g (0.0106 mol) B10OH; 67.3 mg (0.354 mmol) pTSA; 50.0 mL toluene; the mixture was allowed to react under reflux for 24h; 100 mL of CH_2Cl_2; 50.0 mL of saturated solution of $NaHCO_3$; 1.20 g (2.16 mmol) of 3,4TO10Br were obtained (yield 61%).

^{1}H-NMR ($CDCl_3$, ppm): δ 6.16 (s, 2H, Th *H*2+*H*5), 3.97 (t, 2H, ThOC*H*$_2$), 3.41 (t, 2H, C*H*$_2$Br), 1.85 (m, 2H, C*H*$_2$CH$_2$Br), 1.81 (m, 2H, C*H*$_2$CH$_2$O), 1.42 (bm, 2H, C*H*$_2$), 1.30 (bm, 10H, (C*H*$_2$)$_5$).

^{13}C-NMR ($CDCl_3$, ppm): δ 147.86 (Th *C*3+*C*4), 97.21 (Th *C*2+*C*5), 70.88 (ThO*C*H$_2$), 34.37 (*C*H$_2$Br), 33.17, 29.77, 29.70, 29.66, 29.35, 29.10, 28.51, 26.28 (aliphatic *C*H$_2$).

FT-IR (KBr, cm^{-1}): 3109, 2927, 2853, 1563, 1499, 1466, 1259, 1203, 1152, 1018, 870, 723, 644, 561.

3.2.4. Synthesis of monomer by functionalization with sodium methoxide

The monomeric precursor dissolved in methanol was fast added to a flask containing a solution of NaOMe 30% in MeOH. The mixture was allowed to react under reflux for 2h (or more). The system was cooled down to room temperature and distilled water was added to the mixture. Then, the crude product was extracted with diethyl ether. The organic phase was washed with water to neutrality, dried with Na_2SO_4, filtered and concentrated under reduced pressure.

3.2.4.1. Synthesis of 3,4-bis(6-methoxyhexyl)thiophene (3,4T6OMe)

81 mg (0.197 mmol) of 3,4T6Br; 3.0 mL of methanol; 0.19 mL (0.987 mmol) of NaOMe 30% in MeOH; the system was heated until reflux and was allowed to react for 4h; 25.0 mL of distilled water; 53.0 mg (0.169 mmol) of 3,4T6OMe as colorless oil were obtained (yield 86%).

^{1}H-NMR ($CDCl_3$, ppm): 6.88 (s, 2H, Th *H*2+*H*5), 3.37 (t, 4H, C*H*$_2$O), 3.33 (s, 6H, C*H*$_3$), 2.50 (t, 4H, ThC*H*$_2$), 1.61 (m, 8H, (C*H*$_2$)$_4$), 1.40 (m, 8H, (C*H*$_2$)$_4$).

^{13}C-NMR ($CDCl_3$, ppm): δ 142.28 (Th *C*3+*C*4), 120.29 (Th *C*2+*C*5), 73.32 (*C*H_2O), 58.90 (O*C*H_3), 29.97, 29.92, 29.79, 29.08, 26.39 (aliphatic *C*H_2).

FT-IR (KBr, cm^{-1}): 3094, 2976, 2928, 2857, 1508, 1479, 1462, 1387, 1229, 1206, 1194, 1120, 958, 868, 783.

3.2.4.2. Synthesis of 3,4-bis(6-methoxyhexyl-1-oxy)thiophene (3,4TO6OMe)

200 mg (0.452 mmol) of 3,4TO6Br; 2.0 mL of methanol; 0.127 mL (0.678 mmol) of NaOMe 30% in MeOH; the system was heated until reflux and was allowed to react for 3h; 19.0 mL of distilled water; 132 mg (0.383 mmol) of 3,4TO6OMe as white solid were obtained (yield 85%).

^{1}H-NMR ($CDCl_3$, ppm): 6.15 (s, 2H, Th *H*2+*H*5), 3.97 (t, 2H, ThOCH_2), 3.37 (t, 2H, CH_2OCH_3), 3.33 (s, 3H, OCH_3), 1.82 (m, 2H, ThOCH_2CH_2), 1.58 (m, 2H, CH_2CH_2OCH_3), 1.43 (m, 4H, (CH_2)$_2$).

^{13}C-NMR ($CDCl_3$, ppm): δ 147.83 (Th *C*3+*C*4), 97.25 (Th *C*2+*C*5), 73.12 (*C*H_2OCH_3), 70.77 (ThO*C*H_2), 58.90 (O*C*H_3), 29.93, 29.34, 26.28, 26.21 (aliphatic *C*H_2).

FT-IR (KBr, cm^{-1}): 3103, 2976, 2940, 2859, 1564, 1499, 1472, 1378, 1229, 1206, 1157, 1120, 1031, 873, 735.

3.2.4.3. Synthesis of 3,4-bis(10-methoxydecyl-1-oxy)thiophene (3,4TO10OMe)

300 mg (0.541 mmol) of 3,4(TO10Br); 0.152 mL (0.818 mmol) di NaOMe 30% in MeOH; 1.81 mL of MeOH; the system was heated until reflux and was allowed to react for 5h; 23.0 mL of distilled water; 210 mg (0.460 mmol) of 3,4TO10OMe as were obtained (yield 85%).

^{1}H-NMR ($CDCl_3$, ppm): δ 6.16 (s, 2H, Th *H*2+*H*5), 3.97 (t, 2H, ThOCH_2), 3.36 (t, 2H, CH_2OCH_3), 3.33 (s, 3H, OCH_3), 1.81 (m, 2H, ThOCH_2CH_2), 1.56 (m, 2H, CH_2CH_2OCH_3), 1.43 (m, 2H, aliphatic CH_2), 1.30 (bm, 10H, (CH_2)$_5$).

^{13}C-NMR ($CDCl_3$, ppm): δ 147.88 (Th *C*3+*C*4), 97.20 (Th *C*2+*C*5), 73.31 (*C*H_2OCH_3), 70.91 (ThO*C*H_2), 58.87 (O*C*H_3), 30.00, 29.87, 29.83, 29.71, 29.35, 26.48, 26.29 (aliphatic *C*H_2).

FT-IR (KBr, cm^{-1}): 3103, 2974, 2921, 2848, 1563, 1499, 1471, 1378, 1210, 1202, 1157, 1123, 1043, 875, 724.

3.2.5. Oxidative polymerization of monomers with $FeCl_3$

$FeCl_3$ dissolved in CH_3NO_2 was added by drop-wise in a flask containing monomer and anhydrous chloroform. The mixture was allowed to react under vigorous flux of argon at room temperature. Then, THF were added to the system and allowed to stir for 50 minutes.

The crude product was recovered with $CHCl_3$ and threated with HCl 2%, up to exhaustive extraction of the iron (III) ion, and washed with distilled water up to neutrality. The organic phase

was dried over Na_2SO_4, filtered and concentrated to reduced volume. The solution of polymer in $CHCl_3$ was added by drop-wise in 300 mL of methanol, the precipitate formed was filtered on PTFE membrane (0.45 μm pore size) and washed several times with methanol.

3.2.5.1. Synthesis of poly[3,4-bis(6-methoxyhexyl)thiophene] [P(3,4T6OMe)]

106 mg (0.653 mol) of $FeCl_3$; 0.64 mL of CH_3NO_2; 50.0 mg (0.16 mmol) of 3,4T6OMe; 3.50 mL of anhydrous chloroform; the mixture was allowed to react under vigorous flux of argon for 5h at room temperature; 8.0 mL of THF; 20.0 mL of $CHCl_3$; 44 mg of an orange dense oil.

3.2.5.2. Synthesis of poly[3,4-bis(6-methoxyhexyl-1-oxy)thiophene] [P(3,4TO6OMe)]

192 mg (1.16 mmol) of $FeCl_3$; 1.16 mL of CH_3NO_2; 100 mg (0.290 mmol) of 3,4TO6OMe; 6.30 mL of anhydrous chloroform; the mixture was allowed to react under vigorous flux of argon for 25 minutes at room temperature; 10.0 mL of THF; 30.0 mL of $CHCl_3$; 56.0 mg (0.163 mmol) of P(3,4TO6OMe) as dark purplish solid were obtained (yield 56%).

^{1}H-NMR ($CDCl_3$, ppm): δ 4.28-3.94 (bs, 2H, ThOCH_2), 3.36 (t, 2H, CH_2OCH_3), 3.31 (s, 3H, OCH_3), 2.02-1.80 (m, 2H, ThOCH_2CH_2), 1.73-1.55 (bm, 2H, CH_2CH_2OCH_3), 1.54-1.31 (bm, 4H, (CH_2)$_2$).

^{13}C-NMR ($CDCl_3$, ppm): δ 145.20 (Th *C*3+*C*4), 116.92 (Th *C*2+*C*5), 73.56 (*C*H_2OCH_3), 73.10 (ThO*C*H_2), 58.86 (O*C*H_3), 30.56, 30.07, 26.53, 26.33 (aliphatic *C*H_2).

FT-IR (Ge, cm^{-1}): 2975, 2858, 1515, 1462, 1432, 1375, 1261, 1163, 1117, 1021, 730.

3.2.5.3. Synthesis of poly[3,4-bis(10-dimethoxydecyl-1-oxy)thiophene] [P(3,4TO10OMe)]

145 mg (0.876 mmol) of $FeCl_3$; 0.88 mL of CH_3NO_2; 100 mg (0.219 mmol) of 3,4TO10OMe; 4.75 mL of anhydrous chloroform; the mixture was allowed to react under vigorous flux of argon for 23 minutes at room temperature; 10.0 mL of THF; 30.0 mL of $CHCl_3$; 64 mg (0.141 mmol) of P(3,4TO10OMe) as dark purplish solid were obtained (64 yield %).

^{1}H-NMR ($CDCl_3$, ppm): δ 4.37-3.80 (bs, 2H, ThOCH_2), 3.35 (bt, 2H, CH_2OCH_3), 3.31 (bs, 3H, OCH_3), 2.03-1.80 (m, 2H, ThOCH_2CH_2), 1.66-1.51 (bm, 2H, CH_2CH_2OCH_3), 1.50-1.40 (bs, 2H, (CH_2), 1.39-1.12 (bs, 10H, (CH_2)$_5$).

^{13}C-NMR ($CDCl_3$, ppm): δ 145.12 (Th *C*3+*C*4), 116.89 (Th *C*2+*C*5), 73.56 (*C*H_2OCH_3), 73.18 (ThO*C*H_2), 58.75 (O*C*H_3), 30.54, 30.05, 29.96, 29.87, 26.46, 26.40 (aliphatic *C*H_2).

FT-IR (Ge, cm^{-1}): 2973, 2922, 2853, 1516, 1465, 1435, 1376, 1261, 1173, 1125, 1020, 723.

3.2.6. Synthesis of poly[3-(6-methoxyhexyl)thiophene] (PT6OMe)

2.86 mL (2.86 mmol) of a 1M solution of methylmagnesium bromide in n-butylether were added to a three-neck flask containing 100 mg (2.81 mmol) of 2,5-dibromo-3-(6-methoxyhexyl)thiophene – previously synthetized by my research group - dissolved in 15.7 mL of anhydrous THF. The system was heated until reflux conditions and then 1.0 mg (0.0018 mmol) of Ni(dppp)Cl_2 were added. The mixture was allowed to react under inert atmosphere and refluxed for 2h. The crude product was poured in 200 mL of methanol, filtered on PTFE septum (0.45 μm) and washed several times with fresh methanol obtaining 493 mg (2.51 mmol) of polymer (64% yield).

^{1}H-NMR ($CDCl_3$, ppm): δ 6.97 (s, 1H, Th *H*4), 3.38 (t, 2H, C*H*$_2$OCH$_3$), 3.33 (s, 3H, OC*H*$_3$), 2.81, 2.57 (bs, 2H, ThC*H*$_2$), 1.72 (bs, 2H, C*H*$_2$CH$_2$OCH$_3$), 1.60 (bt, 2H, ThCH$_2$C*H*$_2$), 1.44 (bs, 4H, aliphatic C*H*$_2$).

^{13}C-NMR ($CDCl_3$, ppm): δ 140.14 (Th *C*3), 134.04 (Th *C*5), 130.89 (Th *C*2), 128.99 (Th *C*4), 73.20 (*C*H$_2$OCH$_3$), 58.88 (O*C*H$_3$), 30.86 (Th*C*H$_2$), 29.98, 29.77, 29.73, 26.39 (aliphatic (*C*H$_2$)$_n$).

FT-IR (Ge, cm^{-1}): 3057, 2930, 2856, 1510, 1456, 1387, 1256, 1121, 1090, 822, 751.

3.3. NMR spectra

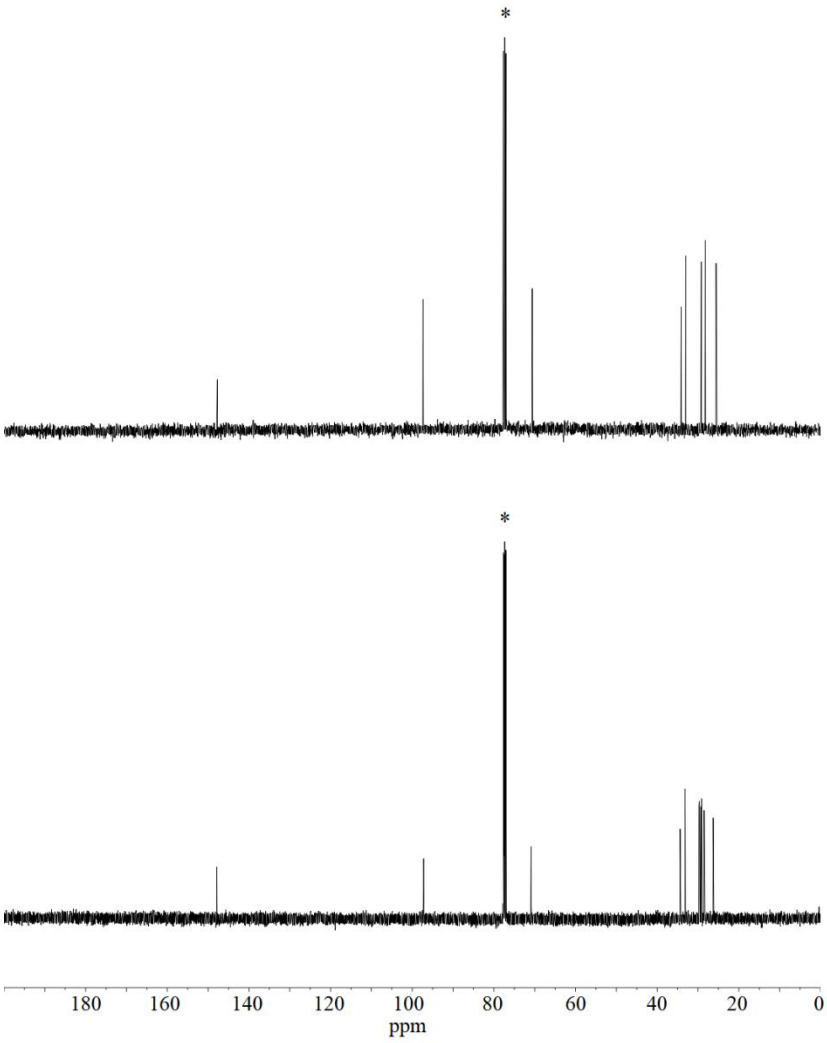

Figure 14. ^{13}C-NMR spectra of 3,4TO6Br (top) and 3,4TO10Br (bottom). Asterisk: solvent resonance ($CDCl_3$).

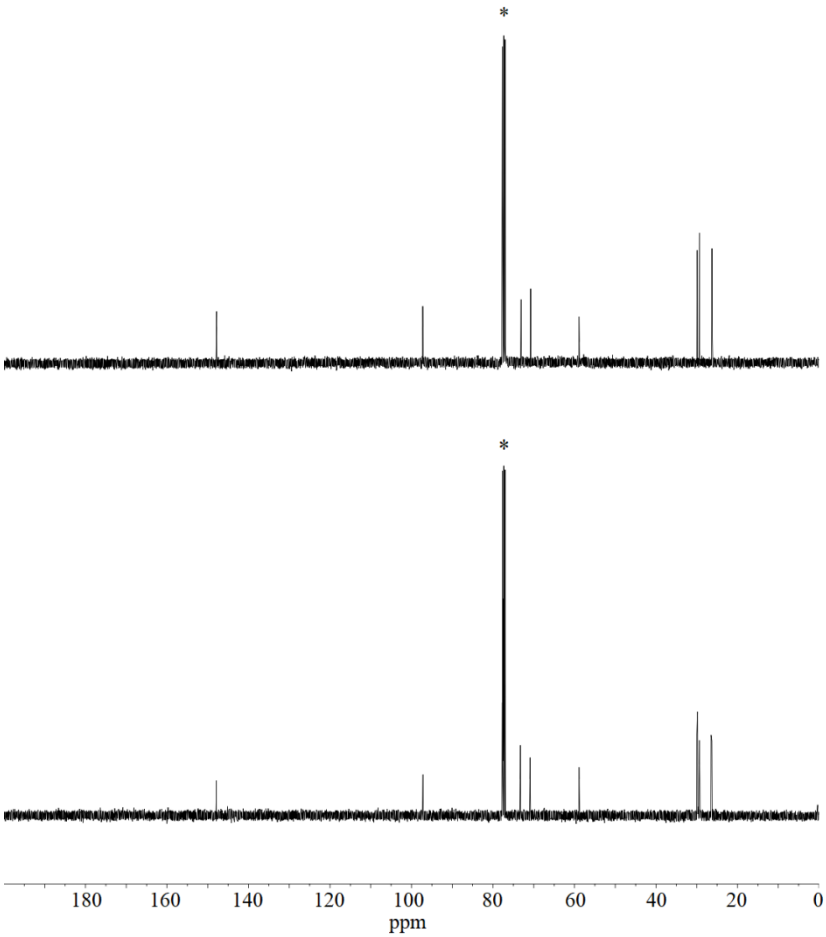

Figure 15. ^{13}C-NMR spectra of 3,4TO6OMe (top) and 3,4TO10OMe (bottom). Asterisk: solvent resonance ($CDCl_3$).

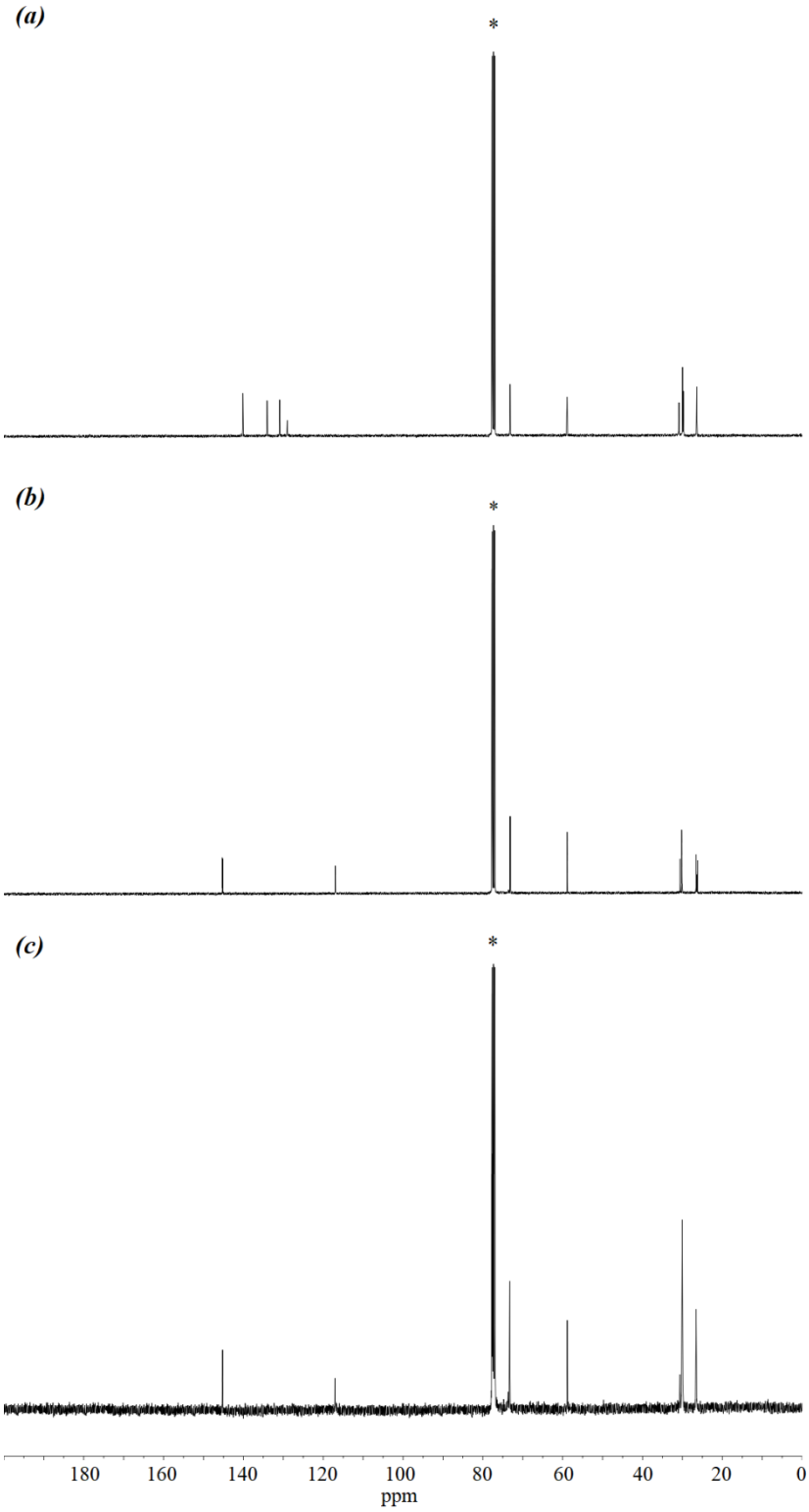

Figure 16. ^{13}C-NMR spectra of PT6OMe (*a*), P(3,4TO6OMe (*b*) and P(3,4TO10OMe) (*c*). Asterisk: solvent resonance ($CDCl_3$).

3.4. FT-IR assignments

Table 6. Main IR absorption bands (cm^{-1}) of PT6OMe.

PT6OMe	***Assignments***
3057	υ C-H β thiophene
2930	υ_{as} -CH_2- side chain
2856	υ_{sym} -CH_2-
1510	υ_{as} -C=C- thiophene
1456	υ_{sym} C=C thiophene
1387	CH_3 deformation
1256	υ C-C thiophene-thiophene
1121	υ_{as} C-O-C ether
1090	δ –CH thiophene
822	γ C-H thiophene 2, 3, 5-trisubstituted
751	rocking -CH_2-
-	*υ* C-Br aliphatic

Table 7. Main IR absorption bands (cm^{-1}) of P(3,4T6OMe) and precursors.

3,4T6P	***3,4T6Br***	***3,4T6OMe***	***Assignments***
3104	-	-	υ C–H phenyl ring
3083	3099	3094	υ C–H (aromatic α H)
2994	-	2976	υ_{as} CH_3
2940	-	-	υ_{sym} CH_3
2921	2928	2928	υ_{as} -CH_2- side chain
2855	2855	2857	υ_{sym} -CH_2- side chain
1508	1507	1508	υ_{as} -C=C- thiophene
1475, 1463	1462, 1436	1479, 1462	υ_{sym} -C=C- thiophene
1390	-	1387	CH_3 deformation
1290, 1234	1257, 1234	1229, 1206	υ C-C thiophene ring
1178, 1106	-	1194, 1120	υ_{as} C-O-C ether
1038	-	958	υ_{sym} C-O-C ether
866	867	868	γ C-H thiophene 3,4-disubstituted
826, 811	-	-	γ C-H phenyl ring
741	786	783	Rocking -CH_2-
-	643, 560	-	*υ* C-Br aliphatic

Table 8. Main IR absorption bands (cm^{-1}) of P(3,4TO6OMe) and precursors.

B6OH	*3,4TO6Br*	*3,4TO6OMe*	*P(3,4TO6OMe)*	*Assignments*
3339	-	-	-	υ –OH
-	3109	3103	-	υ C–H (aromatic α H)
-	-	2976	2975	υ_{as} CH_3
2932	2937	2940	2933	υ_{as} $-CH_2-$ side chain
2859	2859	2859	2858	υ_{sym} $-CH_2-$ side chain
-	1563	1564	1515	υ_{as} -C=C- thiophene
-	1499, 1467	1499, 1472	1462, 1432	υ_{sym} -C=C- thiophene
-	-	1378	1375	CH_3 deformation
-	1242, 1202	1229, 1206	1261	υ C-C thiophene ring
	1144	1157, 1120	1163, 1117	υ_{as} C-O-C ether
-	1048	1031	1021	υ_{sym} C-O-C ether
1053	-	-	-	υ C-OH
-	866	873	-	γ C-H thiophene 3,4-disubstituted
728	747	735	730	Rocking $-CH_2-$
644, 561	644, 560	-	-	*υ* C-Br aliphatic

Table 9. Main IR absorption bands (cm^{-1}) of P(3,4TO10OMe) and precursors.

B10OH	*3,4TO10Br*	*3,4TO10OMe*	*P(3,4TO10OMe)*	*Assignments*
3338	-	-	-	υ –OH
-	3109	3103	-	υ C–H (aromatic α H)
-	-	2974	Emb.	υ_{as} CH_3
2925	2927	2921	2922	υ_{as} $-CH_2-$ side chain
2854	2853	2848	2853	υ_{sym} $-CH_2-$ side chain
-	1563	1563	1516	υ_{as} -C=C- thiophene
-	1499, 1466	1499, 1471	1465, 1435	υ_{sym} -C=C- thiophene
-	-	1378	1376	CH_3 deformation
-	1259, 1203	1210, 1202	1261	υ C-C thiophene ring
	1152	1157, 1123	1173, 1125	υ_{as} C-O-C ether
1056	-	-	-	υ C-OH
-	1018	1043	1020	υ_{sym} C-O-C ether
-	870	875	-	γ C-H thiophene 3,4-disubstituted
722	723	724	723	Rocking $-CH_2-$
645, 562	644, 561	-	-	*υ* C-Br aliphatic

υ = stretching; γ = out of plane bending; δ = in-plane bending.

3.5. Methods

^{1}H-NMR and ^{13}C-NMR spectra were recorded on a Varian Mercury Plus 400 (400 MHz) spectrometer at room temperature using TMS as internal standard in deuterated solvents. Chemical shifts are given in ppm.

FT-IR spectra were taken on Ge or KBr disks using a Perkin Elmer Spectrum One spectrophotometer.

The molecular weight was determined by gel permeation chromatography (GPC) using $CHCl_3$ solutions on a HPLC Lab Flow 2000 apparatus equipped with a Rheodyne 7725i injector, a Phenomenex MXM 5 μm mixed bed column and an RI K-2301 KNAUER detector. The calibration curve was recorded using monodisperse polystyrene standards.

UV-Vis spectra were collected by using Perkin Elmer Lambda 19 spectrophotometer using either around 10^{-5} M polymer solutions in spectroquality solvents in Suprasil quartz cuvettes (1 × 1 cm) or films on quartz slides drop-cast through the use of Doctor Blade.

Sample decomposition temperatures were recorder on NETZSCH TG 209 F1 Libra operating in air flux and it was used to determine sample decomposition temperatures by heating from 30°C to 600°C with a ramp of 10°C min^{1}. A TA Instruments Q2000 differential scanning calorimeter (DSC) was used for the thermal analysis by varying the temperature from -30 to 220°C with a heating and cooling ramp of 10°C min^{-1} in a nitrogen atmosphere.

Cyclic voltammetry (CV) analyses were performed in a three compartments glass cell under inert pressure and at room temperature by using CHI Instrument 660C. Polymers were deposited by drop casting (5 deposition of 1μL) from chloroform solutions (1 mg/mL) on Pt electrode (2 mm diameter). Auxiliary electrode was a disk of Pt and the reference electrode was aqueous saturated calomel electrode (SCE). Supporting electrolyte used was a solution of $C_{16}H_{36}F_6NP$ (0.1 mol/L) while the solvent was chosen in order to avoid the dissolution of film (acetonitrile). Cyclic analyses were performed at 0.1 V/s and SCE absolute potential is 4.24 eV.

3.5.1. Solar cells

The ITO glass substrate (2 × 2 cm, surface resistance 21 Ω/sq) was etched on one side by using a 10% wt aqueous solution of HCl and heated at 60°C for 10 min, in order to obtain an area of 1.5 × 1 cm covered by indium tin oxide. The glass was then cleaned using distilled water, 2-propanol and dried with a nitrogen flow (final resistance12 Ω/sq). Poly(3,4-ethylenedioxythiophene):polystyrene sulfonic acid (PEDOT:PSS, 2.8 wt% dispersion in water, viscosity 20 cps) was diluted 1:1 v/v with 2-propanol, sonicated for 15 min using an ultrasonic bath (Elmasonic S 30H), filtered on a Gooch G2 and the resulting solution (viscosity 12 cps) deposited over the previously treated ITO glass with

the doctor blading technique using a Sheen Instrument Model S265674, leaving only a small (0.5 × 1 cm) area uncovered at the opposite side of the previously etched area. The PEDOT:PSS film was heated in a Buchi GKR-50 glass oven at 120°C for 90 min under vacuum (10^{-3} mmHg).

A solution made by mixing 2.5 mg of electron-donor material and 2.5 mg of $PC_{61}BM$ in 0.5 mL of chlorobenzene was sonicated for 15 min and deposited by using Doctor Blade on the slide in order to cover the PEDOT:PSS layer. The sample was then annealed in the glass oven under vacuum (10^{-3} mmHg) at 120°C for 45 min.

Finally, a thin film of Al (electrode, 50 nm of thickness) was deposited over the polymeric layer through a shadow mask using an Edwards 6306A coating system operating at 10^{-6} mmHg. The active area of the cell was 1 × 1 cm^2. The current-voltage characteristics were measured in air using a Keithley 2401 source meter under the illumination of an Abet Technologies LS150 Xenon Arc Lamp Source AM 1.5 Solar Simulator (100 mW/cm^2) calibrated with an ILT 1400-BL photometer.

The structure of the final devices was made of: ITO (80 nm)/PEDOT:PSS (100 nm)/active layer (150 nm)/Al (50 nm). The solar cell spectral response was measured using a 7-SC Spec III Modularized Solar Cell Spectral Test System (SevenStar Optics, Beijing, PRC). Layer thickness was measured using a FTPAdvances FTPadv-2 Film Thickness Probe (Sentech GmbH, Germany) equipped with the FTPExpert software.

References

1. L. Lu, T. Zheng, Q. Wu, A. M. Schneider, D. Zhao, L. Yu, C*hem. Rev.*, **2015**, *115*, 12666–12731.
2. G. Wang, F. S. Melkonyan, A. Facchetti, T. J. Marks, *Angew. Chem. Int. Ed*., **2019**, *58*, 4129 – 4142.
3. Q. Liang, Z. Hu, J. Yao, Y. Yin, P. Wei, Z. Chen, W. Li, J. Liu, *J. Polym. Sci*., **2022**, *60*, 917–944.
4. G. Yu, J. Gao, J. C. Hummelen, F. Wudl, A. J. Heeger, *Science*, **1995**, *270*, 1789.
5. C. Cui, W.-Y. Wong, *Macromol. Rapid Commun*., **2016**, *37*, 287-302.
6. E. Villa, E. Agosti, C. Castiglioni, M. C. Gallazzi, G. Zerbi, *J. Chem. Phys*., **1996**, *105*, 9461.
7. E. E. Sheina, S. M. Khersonsky, E. G. Jones, R. D. McCullough, *Polym. Prepr*., **2003**, *44*, 843-844.
8. G. Koeckelberghs, M. Vangheluwe, C. Samyn, A. Persoons, T. Verbiest, *Macromolecules*, **2005**, *38*, 5554-5559.
9. G. Daoust, M. Leclerc, *Macromolecules*, **1991**, *24*, 455-459.
10. M. Lanzi, L. Paganin, *European Polymer Journal*, **2008**, *44*, 3987-3996.
11. C. Shi, Y. Yao, Y. Yang, Q. B. Pei, *J. Am. Chem. Soc*., **2006**, *128*, 8980.
12. X. Hu, L. G. Xu, *Polymer*, **2000**, *41*, 9147.
13. Y.-L. Yang, Y.-H. Lee, Y.-P. Lee, C.-J. Chiang, C. Shen, C.-C. Wu, Y. Ohta, T. Yokozawa, C.-A. Dai, *Polym. Int*., **2014**, *63*, 2068-2075.
14. J. Hou, Z. Tan, Y. Yan, Y. He, C. Yang, Y. Li, *J. Am. Chem. Soc*, **2006**, *128*, 4911-4916.
15. S. A. Rutledge, A. S. Helmy, *J. Appl. Phys*., **2013**, *114*, 133708.

CHAPTER IV: SYNTHESIS OF A WATER-SOLUBLE FULLERENE DERIVATIVE

1. Introduction

1.1 Overview

The main disadvantages of C_{60} are its reduced solubility in several common organic solvents (except toluene and chlorinated aromatics), the high hydrophobicity and its high aptitude to form aggregates in solutions. Chemical modification of fullerene could be the key to make it able to exploit its properties. Indeed, the main electron-acceptor (EA) material used in BHJ solar cells is [6,6]-Phenyl-C_{61}-butyric acid methyl ester ($PC_{61}BM$), a fullerene ester-derivative. Its good solubility and miscibility with π-conjugated polymers as P3ATs allow the device to perform quite well when they are mixed together in a photoactive blend.[1,2]

In addition to the chemical structure of material, the solvent used for the deposition of the blend and the annealing conditions play an important role in the film formation and consequently on the final device efficiency.[3]

1.2. Aim of the chapter

In order to prepare completely green active layers of BHJ cells, a water/alcohol soluble fullerene derivative was synthetized and tested as electron-acceptor material in photovoltaic devices.[4] The solubility in the same solvents of the two photoactive materials improves the compatibility between them promoting a higher contact area with the consequent enhancement of the photocurrent generation and the improvement of the final efficiency of device.

The structural properties of EA material were investigated by spectroscopic techniques (^{1}H-NMR, ^{13}C-NMR, FT-IR), its absorption profile was evaluated through UV-Vis in solid state and the energy of its LUMO level was determined by cyclic voltammetry (CV).

This chapter is an extracted part of "Influence of the active layer structure on the photovoltaic performance of water-soluble polythiophene-based solar cells" M. Lanzi, D. Quadretti, M. Marinelli, Y. Ziai, E. Salatelli, F. Pierini, *Polymers*, 2021, 13, 1640.

The electrochemical measurements (CV) were carried out in collaboration with National Research Council (CNR) - Institute for Organic Synthesis and Photoreactivity (ISOF), Bologna (BO), Italy.

2. Results and discussion

2.1. Synthesis

The adopted synthetic route provides a nucleophilic addition of a malonate to C_{60} by the modified Bingel-Hirsch (BH) reaction.[5] In detail, the procedure involves a nucleophilic [2+1] cycloaddition between the fullerene and a halogenated malonate (i.e. bromo- or iodomalonate) in the presence of DBU or NaH as a strong base.[6]

Starting from a commercially available reagent 2-amino-1,3-propanediol (serinol), the first step of this synthetic strategy[7] involves a condensation reaction between serinol and diethylmalonate to give serinolamide which was subsequently protected with acetic groups to give the corresponding ester N,N'-Bis{2-(acetyloxy)-1-[(acetyloxy)methyl]ethyl}-malonamide (P-Ser) (Scheme 1).

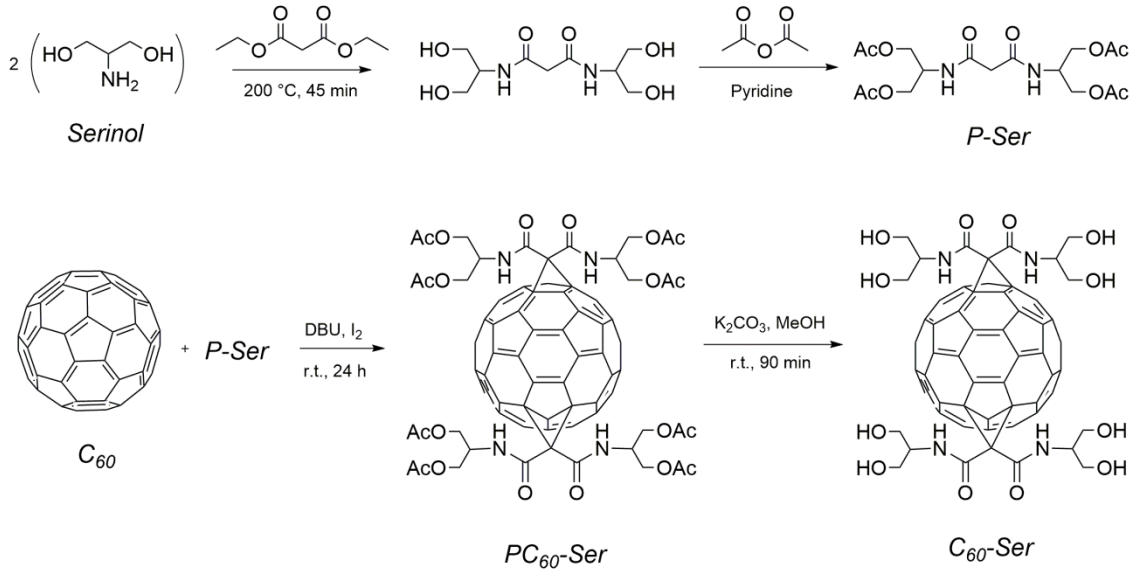

Scheme 1. Synthetic route to obtain fullerene derivative C_{60}-Ser.

The replacement of one [6-6] fullerene double bond takes place through a cyclopropanation reaction in situ with I_2 and in presence of DBU as a base[8] to give the halogenated malonate intermediate and, subsequently, the protected malonodiserinolamide fullerene (PC_{60}-Ser). The stoichiometry of reagents was established with the aim of obtaining a bis-adduct product as it was previously reported that the deprotected mono-adduct is poorly soluble in water.[9] The final basic methanolysis at room temperature allows to obtain the water-soluble fullerene derivative C_{60}-Ser.

2.2. NMR characterization

The chemical structure of the fullerene derivative C_{60}-Ser and its precursors (P-Ser and PC_{60}-Ser) were verified by ^{1}H-NMR and ^{13}C-NMR spectroscopy.

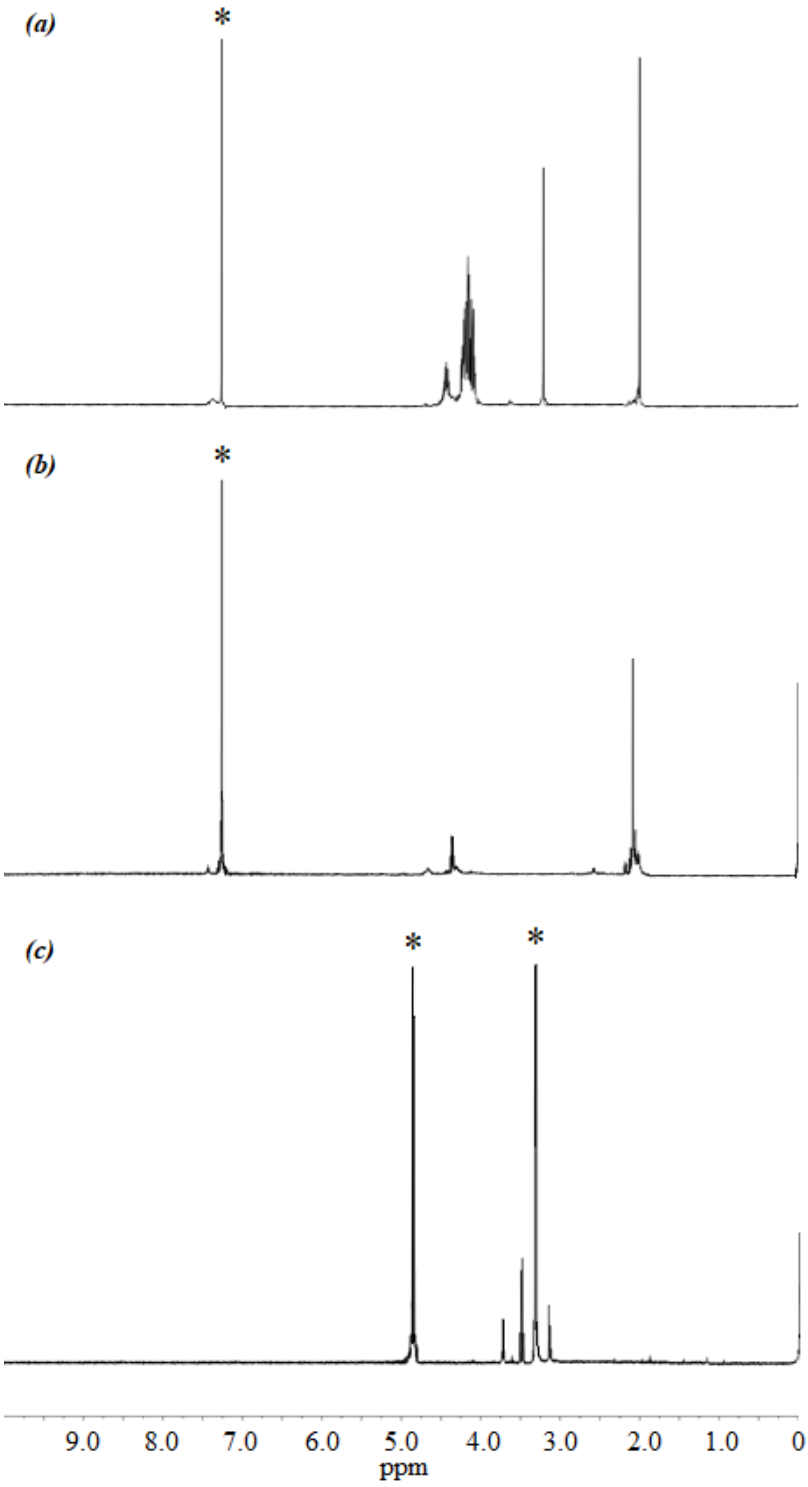

Figure 1. ^{1}H-NMR spectra of P-Ser *(a)*, PC_{60}-Ser *(b)* and C_{60}-Ser *(c)*. Asterisk: solvent resonances **(**$CDCl_3$ and CD_3OD**)**.

By comparing the spectra of the protected serinol P-Ser with PC_{60}-Ser (Figure 1a and 1b, respectively), it's possible to confirm that the reaction on the fullerene surface has occurred. In detail, the signal at 3.21 ppm ascribable to the COC*H*$_2$CO protons of P-Ser is absent in PC_{60}-Ser spectrum as expected. A further confirmation is given by ^{13}C-NMR spectra of PC_{60}-Ser (Figure 2b)

in which the signal at 73.19 ppm is attributable to substituted C_{60}, in addition to the signal at 143.30 ppm ascribable to fullerene.

The subsequent deprotection of malonic groups of PC_{60}-Ser to give the water-soluble fullerene derivative (C_{60}-Ser) is confirmed by ^{1}H-NMR spectrum of the latter (Figure 1c) in which the absence of the signals at 4.35 and 2.09 ppm ascribable to the acetoxy group protons in the side chains (OCH_2 and CH_3), can be observed. Similarly to PC_{60}-Ser, the ^{13}C-NMR spectrum of C_{60}-Ser further confirms that the fullerene is directly linked to malonamide derivative by the presence of the signals at 141.00 and 73.04 ppm (Figure 2c).

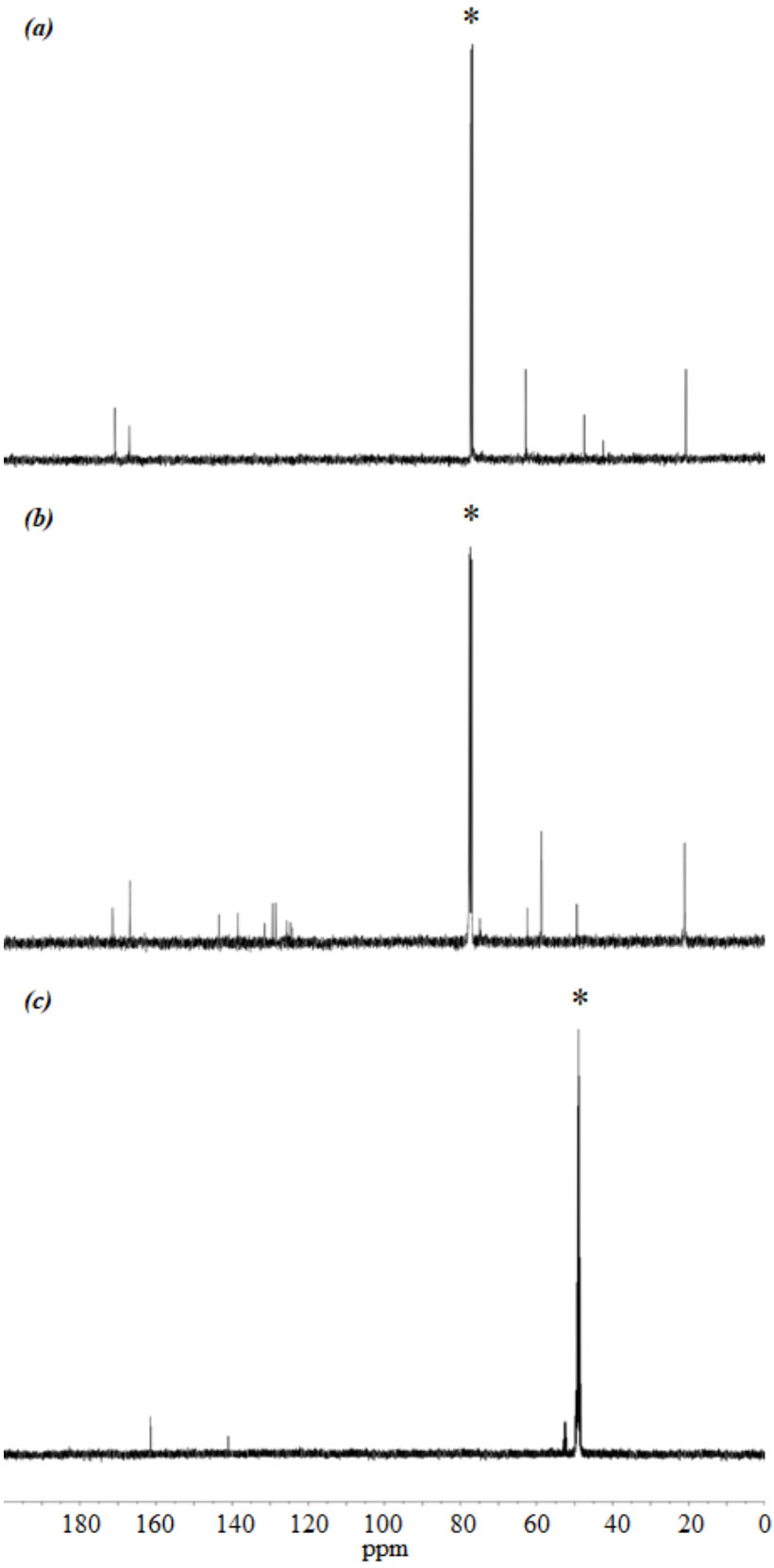

Figure 2. ^{13}C-NMR spectra of P-Ser *(a)*, PC_{60}-Ser *(b)* and C_{60}-Ser *(c)*. Asterisk: solvent resonances ($CDCl_3$ and CD_3OD).

2.3. FT-IR characterization

According to NMR characterization, FT-IR spectroscopy can also give another confirm of the successful of reactions and allows the identification of the signals belonging to the fullerene derivatives and P-Ser. The IR absorption bands of all materials are shown in Figure 3 and their assignments are reported in Table 1.

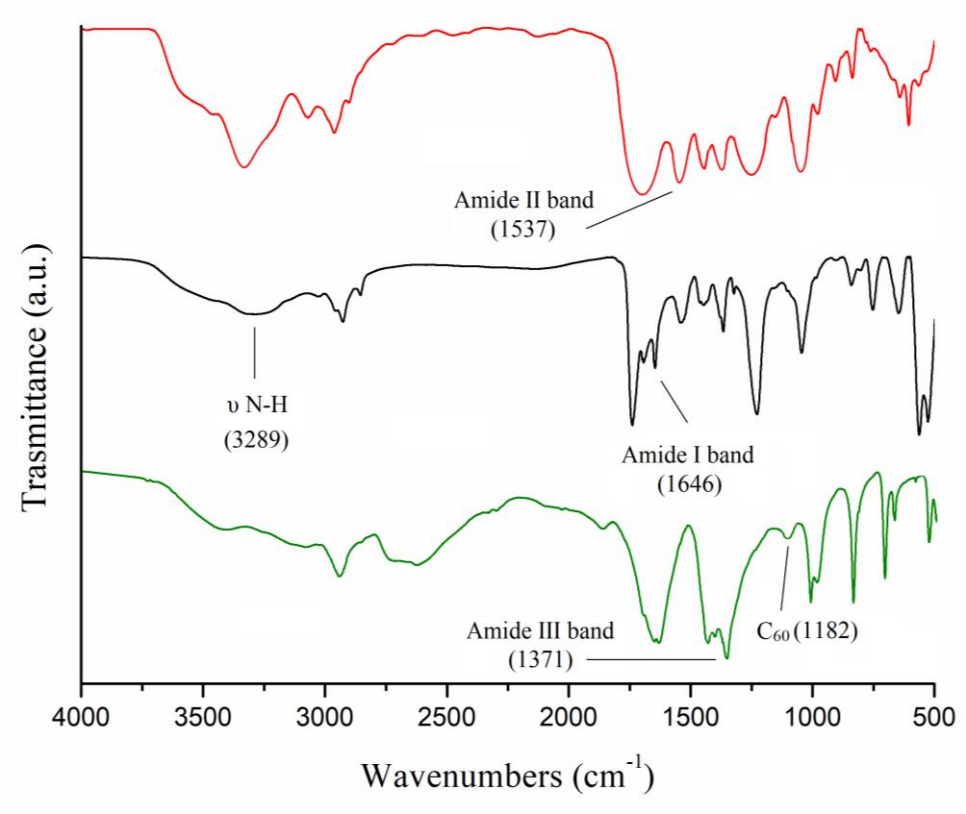

Figure 3. FT-IR spectra of P-Ser (*red line*), PC_{60}-Ser (*black line*) and C_{60}-Ser (*green line*).

At first, the structure of protected malonamide is confirmed by the absence of absorptions at 1401 cm^{-1} - ascribable to the bending out of plane of –OH bond - and by the presence of typical amide absorption bands (I, II, III). Moreover, the absorption bands at 1428, 1180, 561 and 526 cm^{-1} confirm the presence of fullerene in PC_{60}-Ser. The absence of the bands ascribable to the stretching of C=O ester and -$OCOCH_3$ is a further confirm of the successful reaction of deprotection of PC_{60}-Ser to C_{60}-Ser.

Table 1. Main IR absorption bands (cm^{-1}) of P-Ser, PC_{60}-Ser and C_{60}-Ser.

P-Ser	*PC_{60}-Ser*	*C_{60}-Ser*	*Assignments*
3301	3289	3405	υ N-H
2961	2926	2948	υ_{as} -CH_2-
2902	2853	2623	υ_{sym} -CH_2-
1737	1739	-	υ C=O ester
1661	1646	1649	Amide I band, υ C-O
1537	1543	1548	Amide II band, δ N-H
-	1428	1429	fullerene
-	-	1401	γ OH
1370	1366	1371	Amide III band, υ C-N
1242	1228	-	υ_{as} -$OCOCH_3$
-	1180	1182	fullerene
-	561, 526	576, 526	fullerene

υ = stretching; γ = out of plane bending; δ = in-plane bending.

2.4. Optical properties (UV-Vis characterization)

The optical properties of C_{60}-Ser were evaluated in the solid state using film on quartz slide deposited by Doctor Blade from its solution in methanol (MeOH). The resulting normalized absorption spectrum is reported in Figure 4 in comparison with that of a film of $PC_{61}BM$ - drop-cast from chlorobenzene (CB) – a fullerene derivative commercially available.

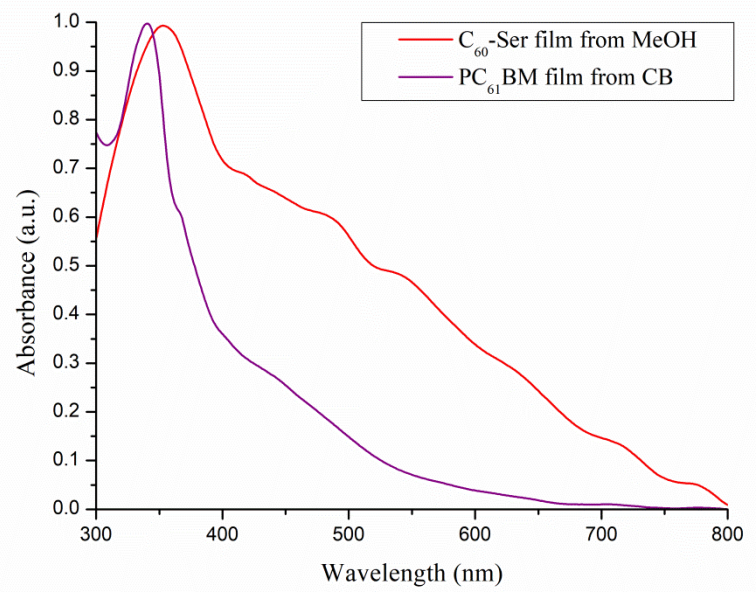

Figure 4. Normalized UV-Vis spectrum of C_{60}-Ser and $PC_{61}BM$ in thin film.

First of all, it's possible to notice the red-shift (or bathocromic shift) of the maximum absorption wavelength (λ_{max}) from 342 nm ($PC_{61}BM$) to 356 nm (C_{60}-Ser) ascribable to different structure of the compounds and of the solvents used for their deposition. Moreover, the range of absorption of

C_{60}-Ser is wider and its spectrum is more structured than that of $PC_{61}BM$, suggesting a more effective light absorption, an important feature for the final application in BHJ solar cell.

2.5. Electrochemical properties (CV)

The properties of C_{60}-Ser were evaluated also through cyclic voltammetry with the aim to define its LUMO level. The analysis was conducted on a thin film drop cast from methanol on a Pt electrode and using a mixture of solvents (0.1 mol/L $(C_4H_9)_4NClO_4$ in CH_3CN:C_7H_8 (25:75)). previously chosen in order to avoid the dissolution of the cast film.[10]

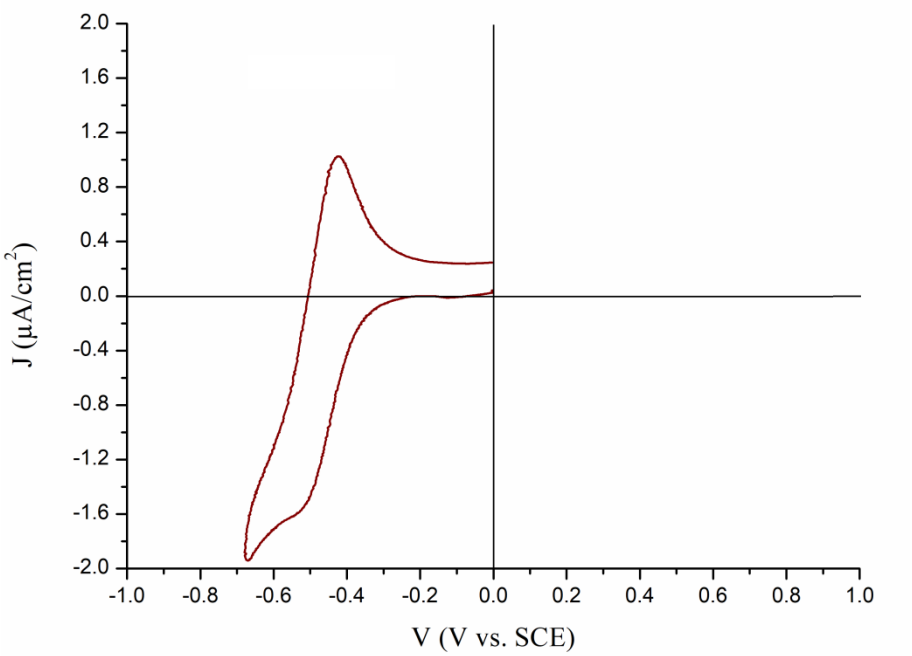

Figure 5. Cyclic voltammetry of C_{60}-Ser in film.

As show in Figure 5, C_{60}-Ser shows a reversible reduction wave at -0.37 V suggesting that the presence of substituents on fullerene surface does not affect the electron-accepting properties of the carbon cage in solid state.

Table 2. Redox potentials and energy levels of C_{60}-Ser in thin film.

	E_{ox} (V)	E_{red} (V) [a]	HOMO (eV)	LUMO (eV)
C_{60}-Ser	-	-0.37	-	-3.87

[a] Calculated by onset; SCE absolute potential 4.24 eV.

The lowest unoccupied molecular orbital (LUMO) energy was estimated according to the following relation:

$$LUMO = -q\ (E_{red} + 4.24)$$

where q is electronic charge and E_{red} is the onset reduction potential (V).

In view of the final application, in Figure 6 are reported the energy level values of all materials employed in a solar cell with BHJ architecture (P3HT as reference for ED material). The LUMO energy is the key for an estimation of the electron affinity (EA), which is the main feature for the electron-accepting materials.

Comparing $PC_{61}BM$ (-3.90 eV) and C_{60}-Ser (-3.87 eV) LUMO levels, it's possible to verify that fullerene derivatives show higher values than fullerene C_{60} (-4.50 eV).[11] The energy levels of the two electron-acceptor materials are very close to each other but the water/alcohol solubility of synthesized fullerene derivative makes it a more valuable EA material for sustainable photovoltaic applications. Moreover, the energy gap between ED LUMO (P3HT, -2.74 eV)[12] and EA LUMO (C_{60}-Ser, -3.87 eV) levels should be enough to drive the exciton dissociation at the donor/acceptor interface in a BHJ solar cell.

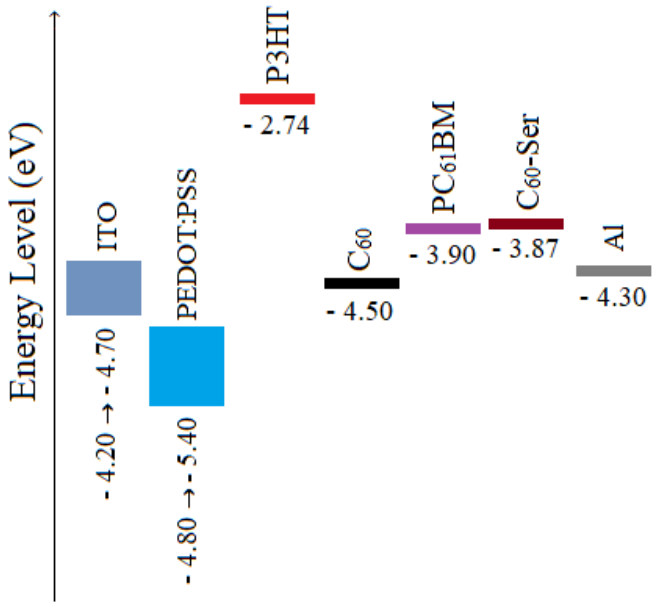

Figure 6. Energy-level alignment of OPVs layers (ITO, PEDOT:PSS and Al)[13] and comparison between C_{60} and its derivatives levels.

2.6. Conclusions

A maloserinolamide fullerene bis-adduct has been successfully prepared with the aim to obtain a water-soluble EA material for BHJ PSCs. Its optical and electrochemical properties has allowed to test C_{60}-Ser in a photovoltaic device in which the photoactive layer was drop-cast from methanol. The good final solubility (>5 mg/ml) in polar solvents allows to enhance the sustainability of device assembling owing to the decreased toxicity of the employed solvents.

3. Experimental section

3.1. Materials

Fullerene (C_{60}, 98%), toluene (C_7H_8, >99.9%), ethyl acetate (EtOAc, >99.5%) and pyridine (>99.0%) were purchased from Sigma Aldrich Chemical Co. (USA). Methanol (MeOH, >99.8%) was purchased from Honeywell (Germany). 1,8-Diazabicyclo[5.4.0]undec-7-ene(1,5-5) (DBU, >99%) was purchased from Fluka Chemika. 2-Amino-1,3-propanediol (Serinol, >98.0%) was purchased from TCI (Tokyo). Diethyl malonate (99%) and acetic anhydride (Ac_2O, 99%) were purchased from Carlo Erba (Italy). Iodine resublimed (I_2) was purchased from Merck (Germany). All materials were used as received. All manipulations involving moisture-sensitive reagents were performed under argon atmosphere in flame-dried glassware.

3.2. Synthesis

3.2.1. Synthesis of N,N'-Bis{2-(acetyloxy)-1-[(acetyloxy)methyl]ethyl}-malonamide (P-Ser)

In a loosely capped Pyrex tube, 0.98 g of serinol (2-amino-1,3-propanediol, 10.9 mmol) and 0.72 mL (4.57 mmol) of diethyl malonate were mixed and heated at 200°C for 45 min under stirring. After evaporation of EtOH, the system was cooled down to room temperature and then the deep orange solid residue was treated with 4.0 mL of Ac_2O and 4.0 mL of pyridine. The mixture was allowed to react under stirring for 20 h at room temperature. Subsequently 3.0 mL of methanol were carefully added after cooling the system to 0 °C.

The solvents were removed under vacuum and the residue was recovered in 30 mL of EtOAc. The solid was then extracted with a diluted solution of $CuSO_4$ (10^{-3} M, 3 × 20 mL), washed with distilled water (3 × 30 mL) and finally extracted with a saturated solution of NaCl. The organic phase was dried with Na_2SO_4 and filtered to give 0.631 g (1.51 mmol, 33% yield) of deep orange oil.

^{1}H-NMR ($CDCl_3$, ppm): δ 7.34 (b, 2H, N*H*), 4.43 (m, 2H, C*H*NH), 4.16 (m, 8H, OCH_2), 3.21 (s, 2H, COCH_2CO), 2.07 (s, 12H, CH_3).

^{13}C-NMR ($CDCl_3$, ppm): δ 170.91 (CH_3*C*OO), 167.15 (*C*ONH), 62.65 (O*C*H_2), 47.61 (*C*HNH), 42.64 (CO*C*H_2CO), 20.89 (*C*H_3).

FT-IR (Ge, cm^{-1}): 3301, 2961, 2902, 1737, 1661, 1537, 1370, 1242.

3.2.2. Synthesis of protected malonodiserinolamide fullerene (PC_{60}-Ser)

In a round-bottom flask, 0.0644 g (0.0894 mmol) of fullerene (C_{60}) were dissolved in 110 mL of anhydrous toluene. 0.187 g (0.447 mmol) of P-Ser, 0.13 mL (0.894 mmol) of DBU and 0.113 g

(0.447 mmol) of I_2 were added to the system. The mixture was left to react for 24 h under stirring and inert atmosphere at room temperature.

The organic phase was washed with distilled water (2 × 100 mL) and a saturated solution of NaCl (1 × 100 mL). After drying with Na_2SO_4 and concentrating at reduced pressure, 0.174 g (0.112 mmol, 25% yield) of PC_{60}-Ser were obtained.

^{1}H-NMR ($CDCl_3$, ppm): δ 7.39 (br d, J=7.78 Hz, 2H, N*H*), 4.69 (m, 2H, C*H*NH), 4.35 (dd, 8H, OCH_2), 2.09 (s, 12H, CH_3).

^{13}C-NMR ($CDCl_3$, ppm): δ 171.01 (CH_3*C*OO), 166.80 (*C*ONH), 143.30, 138.25, 131.57, 129.36, 128.55, 125.62, 125.45, 125.42, 73.19 (C_{60}), 62.78 (O*C*H_2), 58.79 (OC*C*CO), 49.45 (*C*HNH), 21.11 (*C*H_3).

FT-IR (Ge, cm^{-1}): 3289, 2926, 2853, 1739, 1646, 1543, 1428, 1366, 1228, 1880, 561, 526.

3.2.3. Synthesis of the malonodiserinolamide fullerene (C_{60}-Ser)

In a system containing 40.0 mL of methanol and 40.0 mL of a saturated solution of K_2CO_3, 0.100 g (0.0644 mmol) of PC_{60}-Ser were carefully added. The mixture was left to react under stirring at room temperature for 90 min. The organic phase was removed and the dark brown solid was dried under vacuum. The solid was washed several times with MeOH, filtered on a PTFE membrane (0.45 μm pore size) and dried, giving 0.0678 g (0.0557 mmol, 87% yield) of C_{60}-Ser.

^{1}H-NMR (CD_3OD, ppm): δ 3.73 (m, 4H, CH_2OH), 3.48 (m, 4H, CH_2OH), 3.13 (m, 2H, C*H*NH).

^{13}C-NMR (CD_3OD, ppm): δ 161.42 (*C*ONH), 141.00 (C_{60}), 52.72 (HO*C*H_2), 52.50 (CO*C*CO), 52.28 (*C*HNH).

FT-IR (KBr, cm^{-1}): 3405, 2948, 1649, 1429, 1401, 1371, 1182, 576, 526.

3.3. Methods

^{1}H-NMR and ^{13}C-NMR spectra were recorded on a Varian Mercury Plus 400 (400 MHz) spectrometer at room temperature using TMS as internal standard in deuterated solvents. Chemical shifts are given in ppm.

FT-IR spectra were taken on Ge or KBr disks using a Perkin Elmer Spectrum One spectrophotometer.

UV-Vis spectra were run by using a Perkin Elmer Lambda 19 spectrophotometer with films drop-cast on quartz slides through the use of Doctor Blade.

Cyclic voltammetry (CV) analyses were performed in a three compartments glass cell under Ar pressure and at room temperature by using an AMEL 5000 Electrochemical System. Polymers were deposited by drop casting from methanol solutions on Pt electrode (1 mm diameter). Auxiliary electrode was Pt wire spiral and reference electrode was aqueous saturated calomel electrode (SCE). Supporting electrolyte used was a solution of $(C_4H_9)_4NClO_4$ (0.1 mol/L) while the solvent was chosen in order to avoid the dissolution of film (acetonitrile/toluene, 25:75). SCE absolute potential is 4.24 eV.

References

1. N. S. Sariciftci, L. Smilowitz, A. J. Heeger, F. Wudl, *Science*, **1992**, *258*, 1474- 1476.
2. B. Kraabel, C. H. Lee, D. McBranch, D. Moses, N. S. Sariciftci, A. J. Heeger, *Chem. Phys. Lett*., **1993**, *213*, 389-394.
3. H. Hoppe, N. S. Sariciftci, *J. Mater. Chem.*, **2006**, *16*, 45-61.
4. M. Lanzi, D. Quadretti, M. Marinelli, Y. Ziai, E. Salatelli, F. Pierini, *Polymers*, **2021**, *13*, 1640.
5. A. Hirsch, O. Vostrowsky, *Eur. J. Org. Chem.*, **2001**, *5*, 829-848.
6. C. Bingel, *Chem. Ber*., **1993**, *126*, 1957-1959.
7. T. Wharton, V. U. Kini, R. A. Mortis, L. J. Wilson, *Tetrahedron Letters*, **2001**, *42*, 5159-5162.
8. T. Shirosaki, R. Harisaki, M. Horikawa, H. Sakurai, S. Nagaoka, H. Ihara, *Synthetic Communications*, **2014**, *44*, 275-279.
9. T. Wharton, L. J. Wilson, *Bioorganic & Medicinal Chemistry*, **2002**, *10*, 3545–3554.
10. M. Marinelli, M. Lanzi , F. Pierini, Y. Ziai, A. Zanelli, D. Quadretti, F. Di Maria, E. Salatelli, *Polymers*, **2022**, *14*, 3965.
11. K. Akaike, K. Koyasu, K. Sakai, T. Nishi, Y. Kamizuru, T. Nishi, Y. Ouchi, K. Seki, *Appl. Phys. A*, **2009**, *95*, 309-313.
12. J. Hou, Z. Tan, Y. Yan, Y. He, C. Yang, Y. Li, *J. Am. Chem. Soc.*, **2006**, *128*, 4911-4916.
13. S. A. Rutledge, A. S. Helmy, *J. Appl. Phys*., **2013**, *114*, 133708.

CHAPTER V: SYNTHESIS OF ALCOHOL-SOLUBLE POLYTHIOPHENES AS ELECTRO-DONOR MATERIALS FOR BHJ SOLAR CELLS

1. Introduction

1.1 Overview

The production of organic solar cells (OPVs) very often requires the consumption of large amounts of chlorinated and/or aromatic organic toxic solvents. The future technologies are clearly needed to make progress toward the study of large-scale environmentally friendly techniques.

For this reason, water/alcohol soluble conjugated polymers (WSCPs) have attracted growing attention in recent years.[2-5] The solubility of π-conjugated polymers in polar solvents, in particular poly(3-alkyl)thiophenes, can be achieved and tailored by incorporating hydrophilic ionic moieties – such as imidazolium,[6,7] amino,[8] or phosphine groups[9] – to monomer and/or polymer side chains to obtain conjugated polyelectrolytes (CPEs). The main characteristic of these materials is the possibility to combine the good optical properties of polythiophenes with the final solubility in solvents which are safer than common organic solvents.

1.2. Aim of the chapter

In order to study water/alcohol soluble materials, several CPEs with different functional groups at the end of side chain (imidazole, phosphine and phosphate groups) were synthetized. The investigation of materials was carried out in order to check in which case better results can be achieved.

The structural properties were investigated by spectroscopy techniques (^{1}H-NMR, ^{13}C-NMR, ^{31}P-NMR, FT-IR, UV-Vis), thermogravimetric analysis (TGA) and differential scanning calorimetry (DSC). The final materials were tested as photoactive layers in organic solar devices obtaining promising results of photoconversion efficiency (PCE) using tributylphosphine as side chain polar moiety.

The electrochemical measurements (CV) were carried out in collaboration with National Research Council (CNR) - Institute for Organic Synthesis and Photoreactivity (ISOF), Bologna (BO), Italy.

The synthesis of poly{3-[6-(tributylphosphonium)-hexyl]-thiophene}bromide (PT6buP^{+}Br^{-}) and poly{3-[6-(1-methyl-1H-imidazol-3-ium)-hexyl]-thiophene}bromide (PT6I) and the synthetic results reported in this chapter were performed by Antonia Grieco and Simone Rofani respectively, under the supervision of the author, or by the author herself.

2. Results and discussion

2.1. Synthesis

In order to synthetize different water/alcohol soluble polymers through post-functionalization reactions (Scheme 1), three regioregular poly[3-(6-bromohexyl)thiophene]s (PT6Br) of different molecular weights were firstly prepared by GRIM method[10] (as reported in Chapter II) and their main characteristics are reported in Table 1.

Table 2. Main characteristics of starting polymers.

	Yield (%)	*HT (%)* [a]	*Mn (kDa)* [b]	*PDI* [b]
PT6Br_1	44	92%	34.6	1.13
PT6Br_2	24	95%	14.9	1.15
PT6Br_3	21	94%	11.0	1.18

[a] Determined by ^{1}H-NMR; [b] Determined by GPC chromatography.

The choice to post-functionalize polymeric precursor instead of synthetizing a functionalized monomer is mainly due to the lack of solubility which could be a limiting factor for its further polymerization reactions. Moreover, through post-functionalization the configurational regularity of the resulting polymer cannot be affected by the substitution reaction. For these reasons, the regioregularity degree of the ionic functionalized polythiophenes is pre-determined in the polymeric precursors (up to 90% HT dyads), as well as the mean degree of polymerization, thus faciliting the characterization of the final material being polyelectrolytes hardly soluble in common organic solvents.

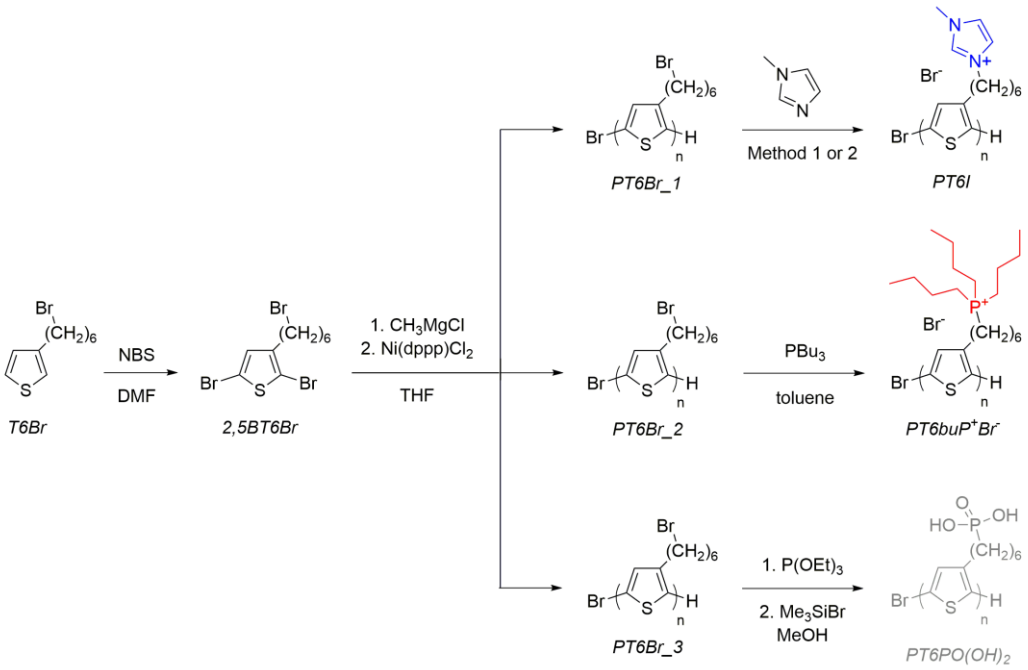

Scheme 1. Scheme of synthetic procedures to obtain alcohol soluble polythiophenes.

The first synthetic route involved the post-functionalization of PT6Br_1 by reaction with 1-methylimidazolium. Two methods were chosen in order to synthetize poly{3-[6-(1-methyl-1H-imidazol-3-ium)-hexyl]-thiophene}bromide (PT6I). The first method was proposed by Bondarev et al.[11,12] and involved the use of several solvents to give good reaction yield, unlike the second method (yield 13%). Although the latter procedure involves the use of anhydrous solvent and is simpler than the first one,[13] Bondarev's method resulted to be the best procedure to synthetize PT6I (Table 2).

As the previous way, the second synthetic route also involved a post-functionalization by a SN_2 reaction on the bromoalkylic side chain of PT6Br_2 and in presence of an excess of tributylphosphine (PBu_3, 1:10). In detail, the polymeric precursor was allowed to react under reflux conditions with phosphine in toluene. In this way, the formed polyelectrolyte poly{3-[6-(tributylphosphonium)-hexyl]-thiophene}bromide ($PT6buP^+Br^-$) resulted to be insoluble in common organic solvents like toluene, giving a precipitate which was easily recovered from the reaction system. The main advantage of the reaction with phosphines is the possibility to obtain the complete post-functionalization of side chain substituents.[8,9] As for PT6I, the resulting average molecular weight was calculated from its precursor (Table 2).

The third synthetic route also involved a post-functionalization reaction on bromide group of PT6Br_3 but with the aim to obtain an alcohol-soluble neutral (non-ionic) polythiophene. The polymeric precursors were allowed to react with triethyl phosphite followed by hydrolysis of phosphonic ester moiety with bromotrimethylsilane in methanol.[14] At first, the polymer was functionalized with triethylphosphite through the Arbuzov reaction, also known as the Michaelis-Arbuzov rearrangement.[15]

In detail, the reaction involved the bromide group at the end of side chain and a trialkyl phosphite to give the corresponding dialkyl phosphonate. The subsequent step consisted of McKenna Reaction, a transeterification reaction in presence of bromotrimethylsilane, followed by a methanolysis providing the phosphonic acid derivative.[16,17]

Although the first reaction gave a good yield of functionalization with triethylphosphite (80%), the subsequent step produced a burgundy solid which was difficult to characterize due to the low solubility both in organic and polar solvents.

Table 2. Main features of post-functionalized polymers calculated from precursors.

	Yield reaction (%)	*Ionic content (%)* [a]	*HT (%)* [b]	*Mn (kDa)* [b]	*PDI* [b]
PT6I	88	90	92%	34.0	1.13
PT6buP$^+$Br$^-$	98	100	95%	27.2	1.15

[a] Determined by ^{1}H-NMR; [b] Determined by GPC chromatography.

With the aim to improve solubility and optical properties maintaining the same cationic moiety (tributylphosphium group), it has been then decided to synthetize a polythiophene with a polyetheral side chain. By introducing oxygen atoms on the alkyl chain it's possible to increase the polymer polarity and to improve the interaction between macromolecules and solvent. Moreover, the electron-donor effect of the oxygen atoms yields the π system more electron-rich than a common poly(3-alkylthiophene), thus favoring the coplanar conformation and the consequently decreasing of energy band gap.

At first, the synthetic route involved the protection of a hydroxyl group of tetraethylene glycol in presence of triethylamine which was necessary to remove the generated hydrocloridric acid. The following etherification reaction with the glycol tosylate and 3-methoxythiophene in presence of p-toluenesulfonic acid gave the corresponding thiophenic ether (Scheme 2).[18] The resulting product was unstable and for this reason not characterizable or usable for the following reactions.

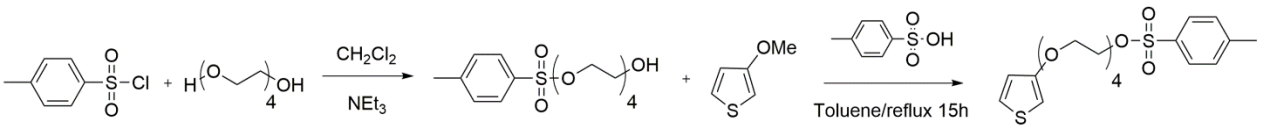

Scheme 2. Synthesis of polyetheralthiophene.

Due to the difficulty to obtain a polythiophene with several oxygen atoms in side chain, the project was then focused on another synthetic strategy starting from 3,4-dimethoxythiophene (Scheme 3).

The presence of two oxygen atoms directly linked to thiophene ring further enhances the electron-donating effect due to the higher charge delocalization.

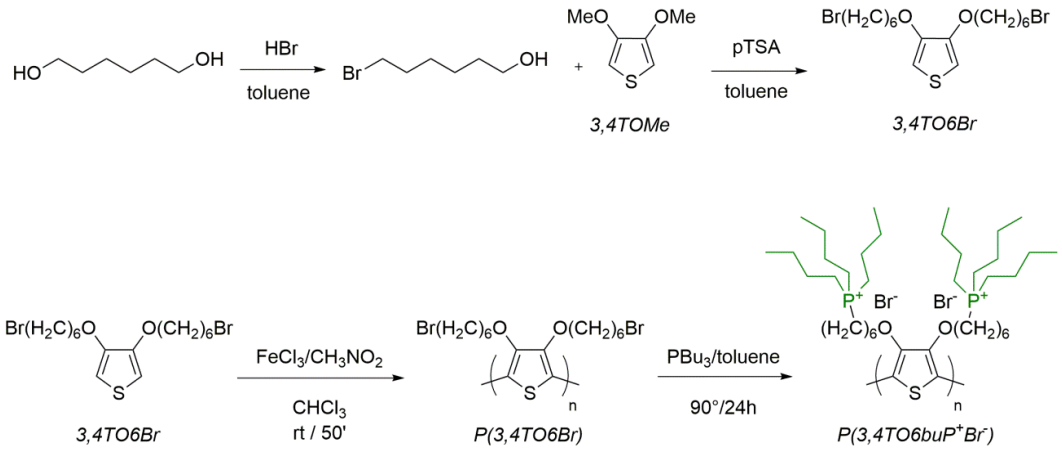

Scheme 3. Synthesis of poly[3,4-bis(6-bromohexyl-1-tributylphosphonium)thiophene]dibromide.

In detail, the hydroxyl side chain with a bromide group was synthetized[19] starting from 1,6-hexanediol with the aim to maintain the bromide group at the end of side chain after the transetherification reaction with 3,4-dimethoxythiophene (3,4TOMe).[20] The mechanism involved acid conditions (p-toluenesulfonic acid, pTSA) providing the formation of the corresponding ether 3,4-(6-bromohexyl-1-oxy)thiophene (3,4TO6Br).

The symmetry of the monomeric precursor, as the equivalency of α positions of thiophene ring, allowed to proceed with oxidative polymerization with ferric trichloride ($FeCl_3$) - usually used as not regiospecific polymerization – obtaining the corresponding polymer poly[3,4-bis(6-bromohexyl-1-oxy)thiophene] [P(3,4TO6Br), Mn = 42.4 kDa, Xn = 96, PDI = 1.48].

Moreover, the bromide groups at the end of side chains allowed the post-functionalization of the resulting polymer with tributylphosphine - considered the most performing cationic group from a synthetic point of view, as previously discussed – to obtain poly[3,4-bis(6-bromohexyl-1-tributylphosphonium)thiophene]dibromide [P(3,4TO6buP$^+$Br$^-$), Mn = 81.1 kDa, PDI = 1.48].

2.2. NMR Characterization

All the synthesized products were characterized by ^{1}H-NMR and ^{13}C-NMR spectrometry to evaluate their chemical structure and purity degree.

At first, ^{1}H-NMR spectroscopy was used to evaluate the percentage of head-to-tail linkages (up to 90%) in the macromolecular backbone of the PT6Br - the polymeric precursor of both ionic poly(3-alkylthiophenes) PT6I and PT6buP$^+$Br$^-$ - since the regioregularity degree can be determined by the integral ratio of the signals centered at 2.83 ppm (HT dyads) and 2.59 ppm (HH and TT dyads) (Figure 1).

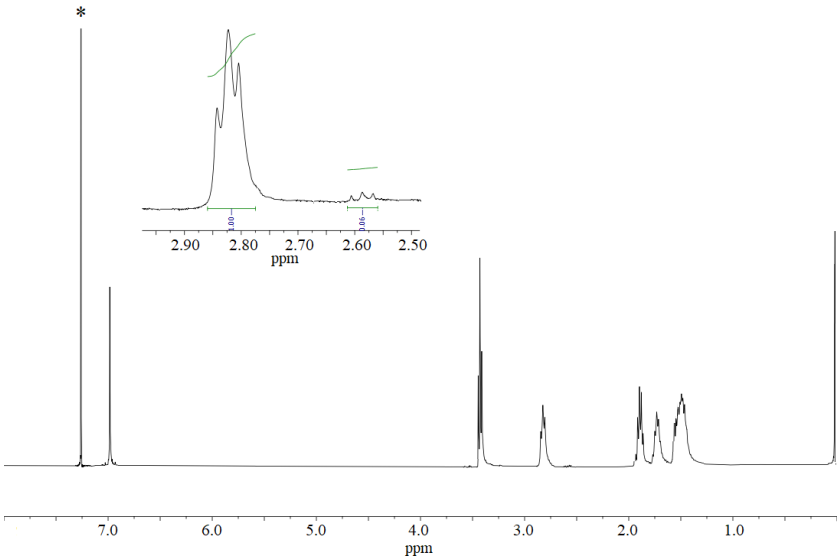

Figure 1. ^{1}H-NMR spectrum of a regioregular PT6Br. Asterisk: solvent resonance ($CDCl_3$).

The occurrence of post-functionalization reactions with 1-methylimidazolium and tributylphosphine to give PT6I and PT6buP^{+}Br^{-}, respectively, was verified by both ^{1}H-NMR and ^{13}C-NMR.

In particular, when analyzing ^{1}H-NMR spectra (Figure 2), the presence of two broad triplets at 4.19 ppm and 2.24 ppm can be attributed to the methylenic protons in α- positions to the cationic imidazole and phosphine group, respectively.

In PT6I spectrum, the presence of a triplet at 3.43 ppm - ascribable to methylenic protons in α-position to bromide group – indicates the non-complete substitution of -Br with 1-methylimidazolium (yield of post-functionalization 90%). Differently, the total absence of signals ascribable to protons of halogenated moieties in PT6buP^{+}Br^{-} evidences the total substitution reaction with phosphonium group, which typically occurs when phosphines are used as nucleophile reagents.

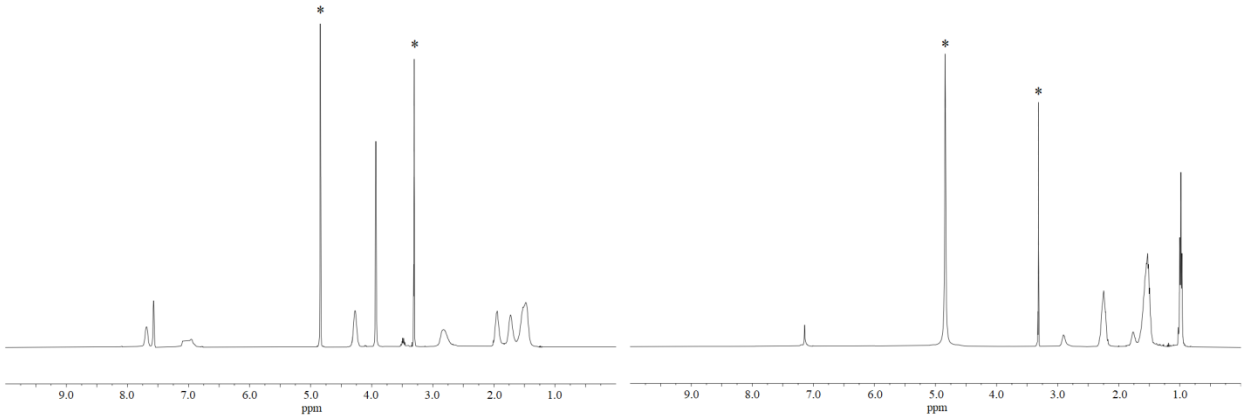

Figure 2. ^{1}H-NMR spectra of PT6I (left) and PT6buP^{+}Br^{-} (right). Asterisk: solvent resonance (CD_3OD).

For the disubstituted cationic polythiophene P(3,4TO6buP^{+}Br^{-}), the comparison of ^{1}H-NMR spectra of monomer 3,4TO6Br and polymeric precursor P(3,4TO6Br) evidences the disappearance of the doublet at 6.17 ppm ascribable to thiophenic protons due to the polymerization in α-positions. In this case, the degree of HT linkage wasn't determined due to the symmetry of monomer, determining the absence of signals ascribable to HH and TT dyads in the spectrum. Moreover, the broadening of signals can further confirm the successful reaction (Figure 3a and 3b).

As for PT6buP^{+}Br^{-}, the ^{1}H-NMR spectrum of post-functionalized polymer P(3,4TO6buP^{+}Br^{-}) shows the presence of a broad signal at 2.23 ppm that can be ascribed to the eight methylenic protons in α- position to the ionic group (Figure 3c).

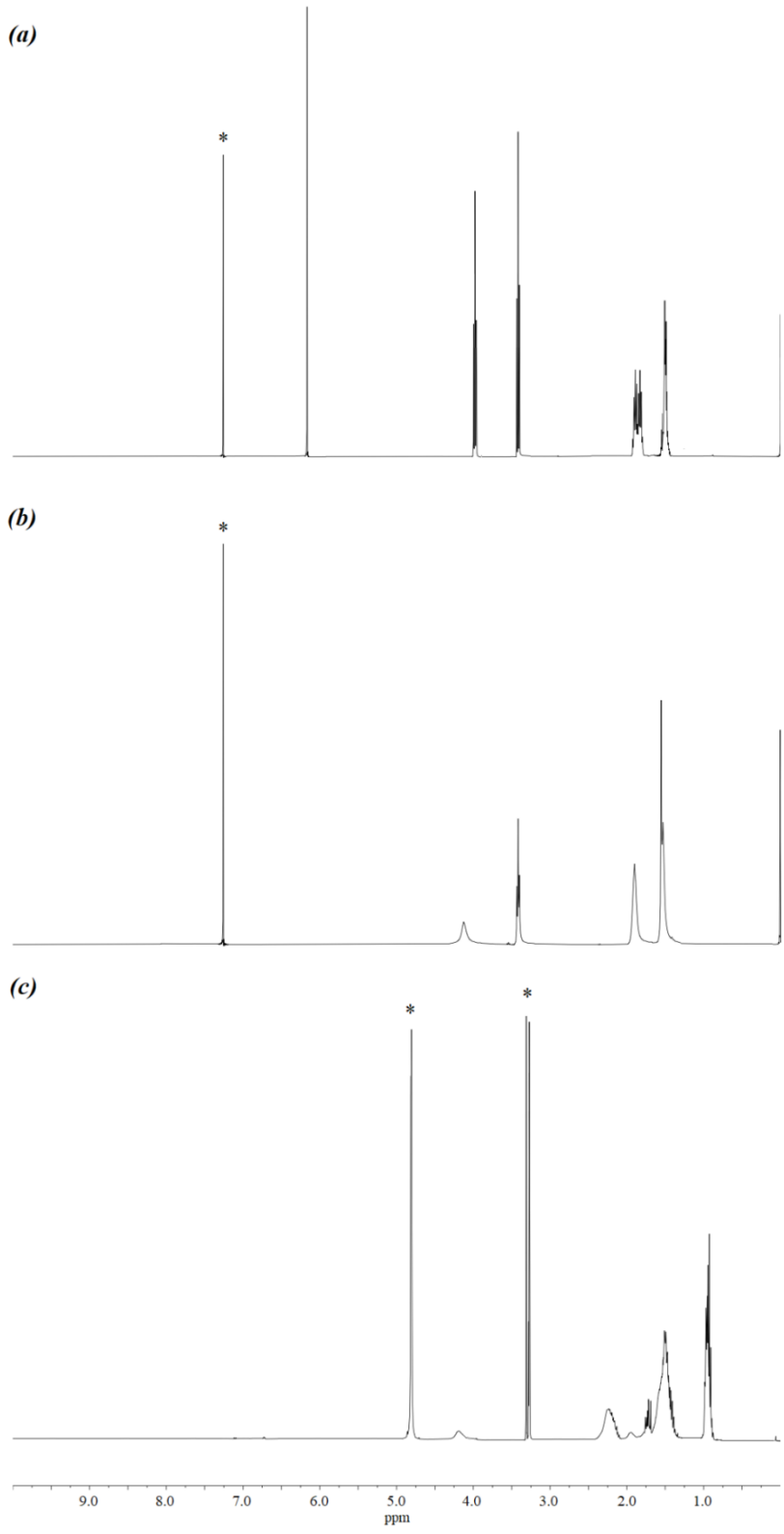

Figure 3. ^{1}H-NMR spectra of 3,4TO6Br (*a*), P(3,4TO6Br) (*b*) and P(3,4TO6buP^{+}Br^{-}) (*c*). Asterisk: solvent resonances ($CDCl_3$ and CD_3OD).

Finally, the ^{31}P-NMR spectra of PT6buP^{+}Br^{-} and P(3,4TO6buP^{+}Br^{-}) reported in Figure 4 also confirm the complete absence of unreacted tributylphosphine and the complete post-functionalization of precursors, as previously verified.

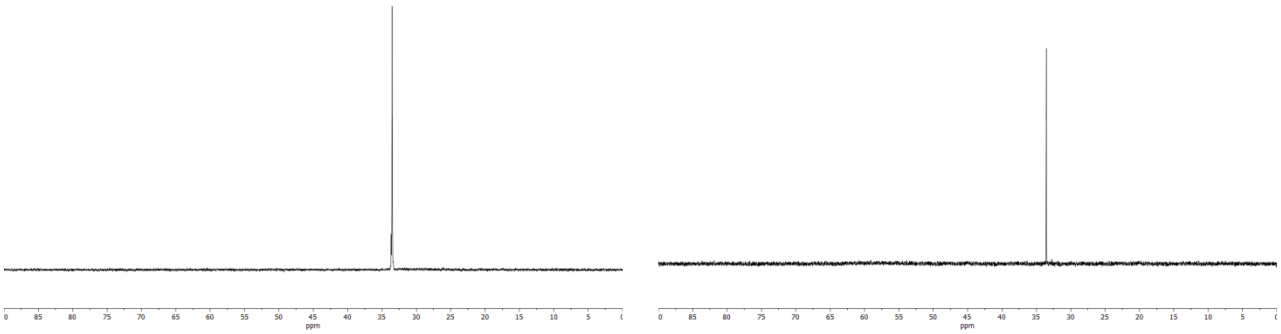

Figure 4. ^{31}P-NMR spectra of PT6buP^{+}Br^{-} (left) and P(3,4T6ObuP^{+}Br^{-}) (right).

2.3. FT-IR characterization

FT-IR spectroscopy gave another confirm of the occurrence of polymerization and subsequent post-functionalization reactions (Table 3 and Figure 5).

Table 3. Main IR absorption bands (cm^{-1}).

PT6Br	***PT6I***	***PT6buP^{+}Br^{-}***	***Assignments***
-	3145	-	υ_{as} C-H imidazolium
3052	Emb.	3053	υ C-H β thiophene
-	3078	-	υ_{sym} C-H imidazolium
-	-	2957	υ_{as} –CH_3 phosphonium group
2928	2930	2929	υ_{as} -CH_2- side chain and phosphonium group
2855	2856	2870	υ_{sym} -CH_2- and –CH_3
-	1627, 1572	-	υ_{as} imidazolium ring
1511	1511	1513	υ_{as} -C=C- thiophene
1459	1461	1463	υ_{sym} C=C thiophene and -CH_2- deformation phosphonium group
-	1451	-	υ_{sym} imidazolium ring
-	-	1410	γ_{as} P-CH_2-R
-	-	1378	-CH_3 deformation phosphonium group
1257	1259	1232	υ C-C thiophene-thiophene
-	1178	-	υ_{as} N-CH_3
-	1169	-	υ_{sym} N-CH_3
1089	1098	1099	δ –CH thiophene
-	1044	-	δ –CH imidazolium
832	832	833	γ C-H thiophene 2, 3, 5-trisubstituted
-	752	-	γ C-H imidazolium
728	725	723	rocking -CH_2-
645, 562	644, 560	-	υ C-Br aliphatic

υ = stretching; γ = out of plane bending; δ = in-plane bending.

The IR spectrum (Figure 5) of brominated polythiophene PT6Br (black line) shows peaks at 645 and 562 cm^{-1} which are characteristic of the aliphatic C–Br stretching. The desired post-functionalization with methylimidazole and tributylphosphonium groups are confirmed by the presence of the bands at 2957, 2929, 2870, 1463, 1378 cm^{-1} and at 3145, 3078, 1627, 1572, 1451, 1044, 752 cm^{-1}, respectively (Table 3).

Moreover, the complete disappearance of the bands related to C-Br stretching in FT-IR spectrum of PT6buP^{+}Br^{-} evidences the complete post-functionalization of the polymeric precursor, as already stated.[8]

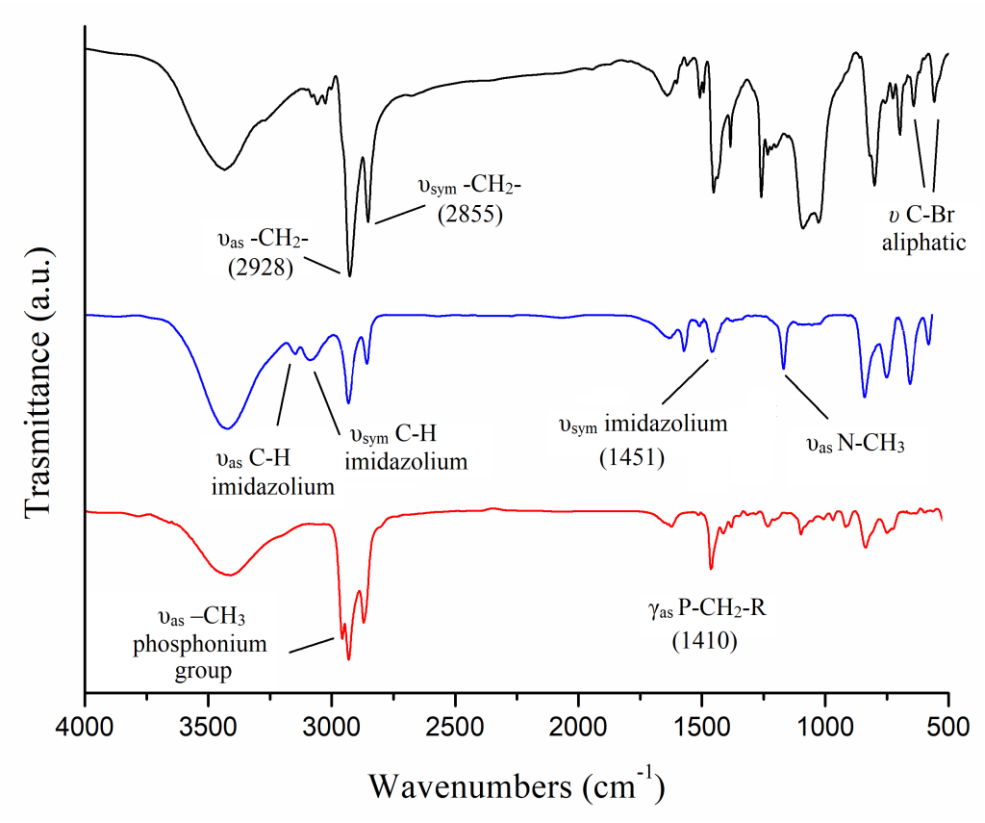

Figure 5. FT-IR spectra of PT6Br (black line), PT6I (blue line) and PT6buP^{+}Br^{-} (red line).

Also in the case of disubstituted polythiophene, occurrence of the desired reactions was confirmed by IR spectroscopy and the main absorption bands with relative assignments are reported in Table 4 and Figure 6.

Table 4. Main IR absorption bands (cm^{-1}) of polymers and precursors.

3,4TO6Br	*P(3,4TO6Br)*	*P(3,4TO6buP$^+$Br$^-$)*	*Assignments*
3109	-	-	υ C–H (aromatic α H)
-	-	2958	υ_{as} –CH_3 (phosphonium group)
2937	2937	2933	υ_{as} -CH_2- (side chain and phosphonium group)
2859	2859	2872	υ_{sym} -CH_2- and –CH_3
1563	1509	1511	υ_{as} -C=C- thiophene
1499, 1467	1456, 1433	1464,1431	υ_{sym} -C=C- thiophene
-	-	1379	–CH_3 deformation (phosphonium group)
1242	1240	1230	Vibration thiophene ring
1144	1170	1147	υ_{as} C-O-C ether
1048	1049	1097	υ_{sym} C-O-C ether
866	-	-	γ C-H thiophene 3,4-bisubstituted
747	728	726	Rocking -CH_2-
644, 560	643,560	-	*υ* C-Br aliphatic

υ = stretching; γ = out of plane bending; δ = in-plane bending.

Going from the obtained spectra of starting monomer 3,4TO6Br and related polymer P(3,4TO6Br), the disappearance of bands at 3109 and 866 cm^{-1} - ascribable to C–H stretching of aromatic α protons and of thiophene 3,4-disubstituted, respectively – confirms that polymerization has occurred. As for PT6buP$^+$Br$^-$, the subsequent complete post-functionalization with tributylphosphine is confirmed by the presence of the bands at 2958, 2933, 2872 and 1379 cm^{-1} and by the disappearance of the bands of C-Br stretching (Figure 6).

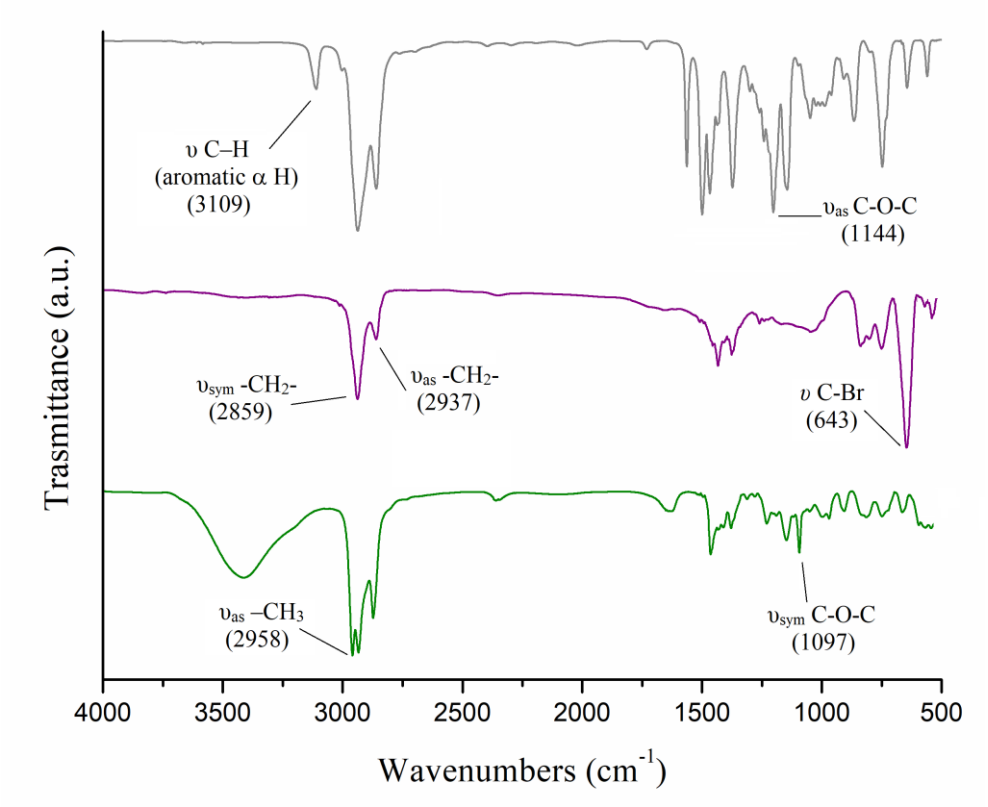

Figure 6. FT-IR spectra of 3,4TO6Br (grey line), P(3,4TO6Br) (purple line) and P(3,4TO6buP$^+$Br$^-$) (green line).

2.4. Thermal properties

The thermal stability of PT6I, PT6buP$^+$Br$^-$ and P(3,4TO6buP$^+$Br$^-$) were evaluated by TGA analysis under oxidizing atmosphere (air), at a heating scan rate of 10°C min^{-1} and up to 600°C (Figure 7 and Table 4).

The TGA curves of all the examined samples show three main weight losses that can be ascribed to the elimination of ionic moiety (up to 200°C), to the aliphatic side chain scission (up to 250°C) and to the macromolecular backbone combustion (up to 400°C), respectively. For PT6buP$^+$Br$^-$, the negligible first loss of weight at ~ 100°C is ascribable to the presence of traces of moisture due to the strong hydrophilicity of the single phosphonium group. This phenomenon is not particularly evident for the other polyelectrolytes probably due to the steric hindrance of methylimidazolium and of the two phosphonium groups of PT6I and P(3,4TO6buP$^+$Br$^-$), respectively.

The synthesized samples, however, may be considered stable enough to be used as photoactive materials in organic photovoltaic devices.

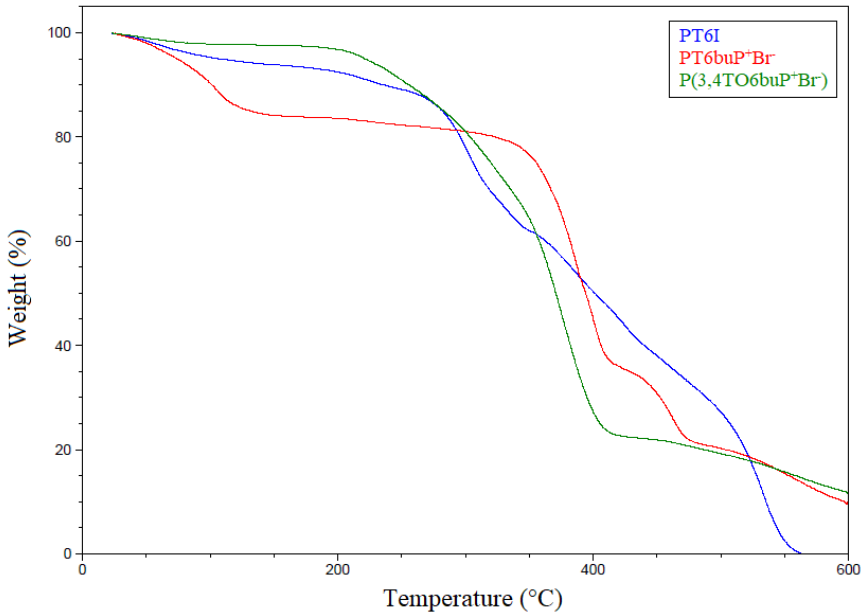

Figure 7. TGA thermograms of cationic polymers.

Table 4. Decomposition (T_d) and glass-transition (T_g) temperatures of polymers.

	T_d (°C) [a]	$T_{d,max}$ (°C) [b]	T_g (°C) [c]
PT6I	280	303	69
PT6buP$^+$Br$^-$	355	402	43
P(3,4TO6buP$^+$Br$^-$)	212	221	48

[a] Determined by the onset point of the first inflection; [b] calculated from the first derivative of the weight/temperature curve; [c] evaluated by DSC analysis.

The DSC analysis was carried out under nitrogen atmosphere with a heating ramp of 10°C min^{-1} from -20°C up to 200°C and the relative curves are reported in Figure 8.

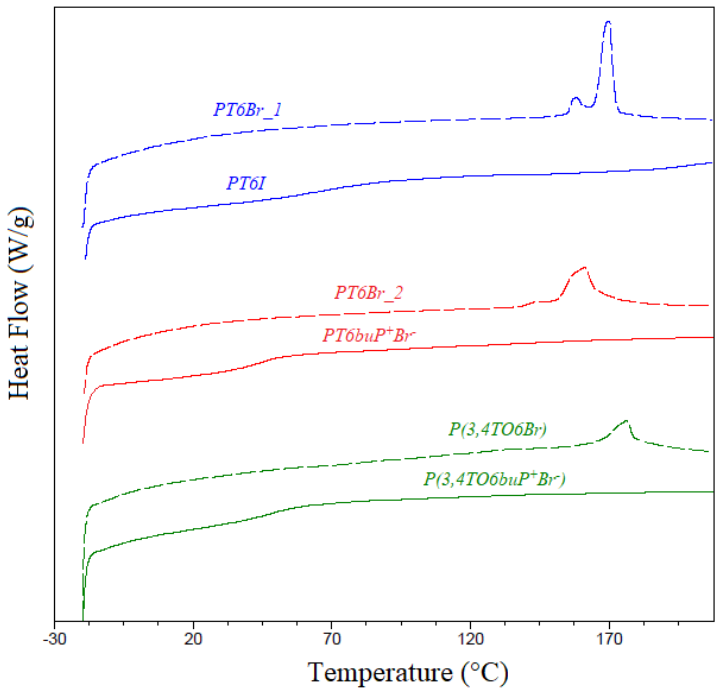

Figure 8. DSC curves of cationic polymers.

All polymeric samples show the endothermic flexure ascribable to the glass transition temperature (T_g), a value that decreases when the tributylphosphonium group is linked to the side chain (Table 4). Moreover, the presence of ionic side chain moiety causes the absence of melting and crystallization peaks in DSC curves of all samples, evidencing the amorphous nature of these materials. On the contrary, brominated polymeric precursors show evident melting peaks ascribable to their semicrystalline state.

2.5. Optical properties (UV-Vis characterization)

The optical properties of ionic conjugated polymers were analyzed by UV-Vis spectroscopy both in solution and in solid state, by drop-casting their solution onto quartz slides. Their normalized absorption spectra and assignments are shown in Figure 9 and Table 5.

Table 5. Wavelengths of maximum absorption of synthetized polymers in several polar solvents and their solubility.

	Solvent	***λ_{max} solution 10^{-5}M (nm)***	***λ_{max} film (nm)***	***Solubility (mg/mL)***
PT6I	Methanol	446	534	<5
	Ethanol	449	515	
	Water	508	511	
PT6buP$^+$Br$^-$	Methanol	425	445	>50
	Ethanol	426	444	
	Water	447	444	35
P(3,4TO6buP$^+$Br$^-$)	Methanol	520	528	48
	Ethanol	525	533	43
	Water	511	527	12

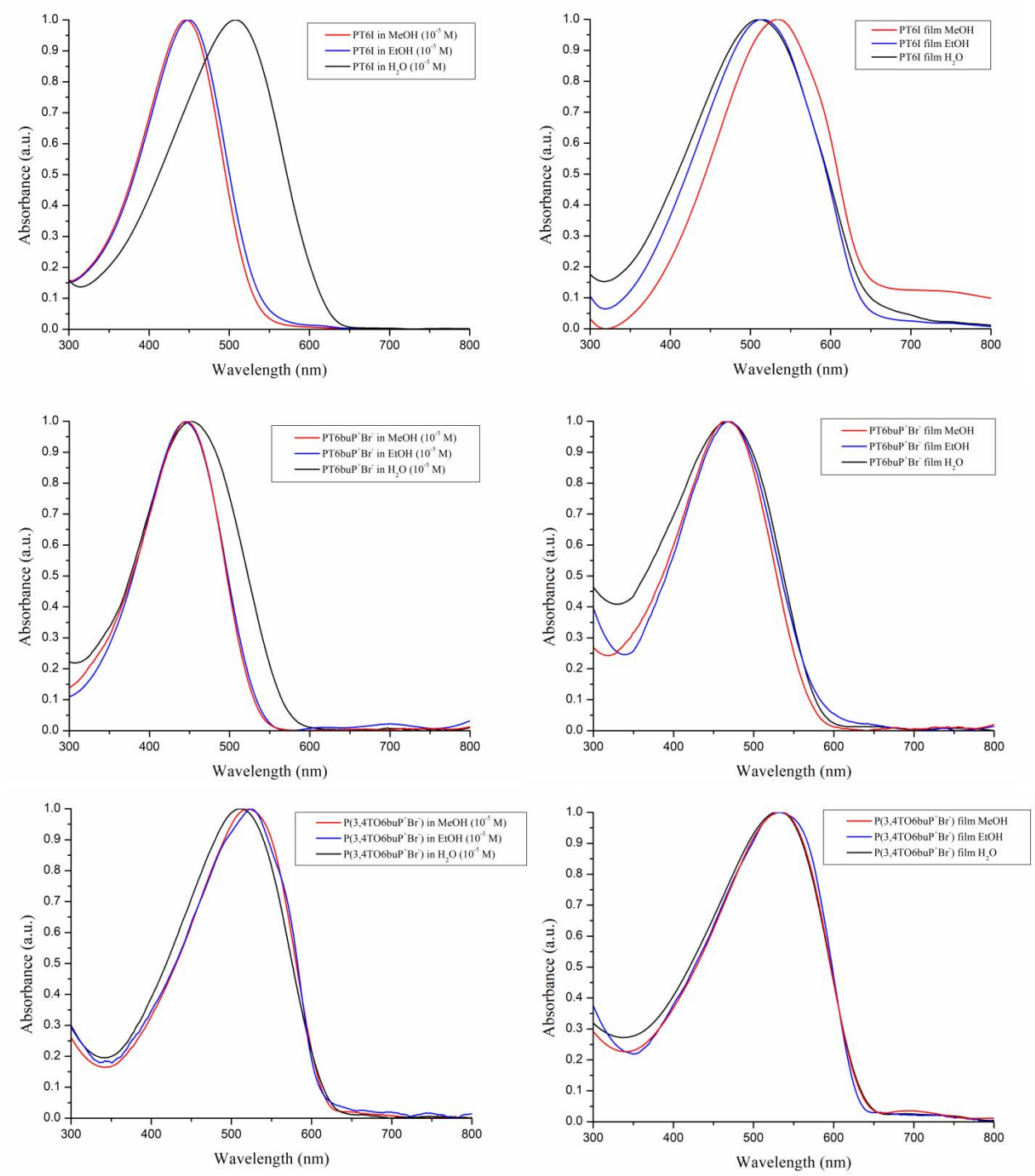

Figure 9. Normalized UV-Vis spectra of CPEs in solution (left column) and in thin film by drop-casting from different solvents (right column).

The UV-Vis spectral profiles of the three cationic polymers result to be essentially independent from the solvents employed for their dissolution and subsequent deposition (water, methanol and ethanol). Moreover, all samples both in solution and in solid state don't show any aggregation of macromolecular chains. As expected, the best values were obtained in solid state due to the

enhancement of organization of the macromolecular backbones, with the exception of disubstituted polyelectrolyte owing to the high steric hindrance of their side chains.

In view of this and considering the solubility and filming properties (Table 5), ethanol was used as filming solvent for the preparation of cell with the aim to obtain more sustainable and eco-friendly devices.

2.6. Electrochemical properties (CV)

In order to study the behavior of synthesized materials, potentials of ionic photoactive layers were evaluated by cyclic voltammetry (CV). In Figure 10 are reported the CV curves of synthetized polymers in thin films obtained by drop-casting their solution in ethanol on Pt electrodes in acetonitrile/toluene (25:75).

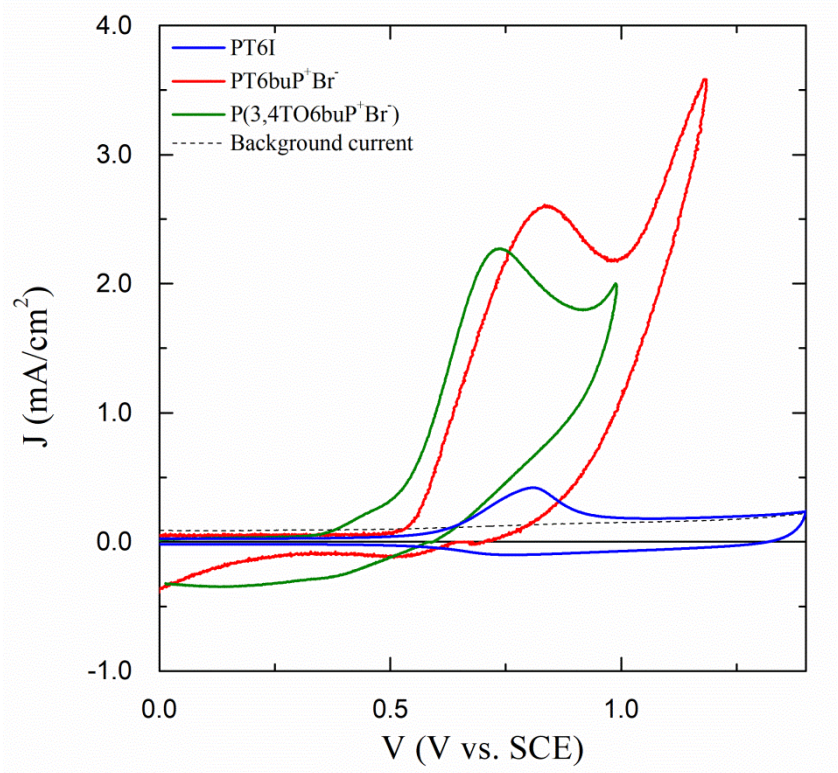

Figure 10. CV curves of PT6I (blue line), PT6buP$^+$Br$^-$ (red line) and P(3,4TO6buP$^+$Br$^-$) (green line).

Table 6. Electrochemical and optical properties of synthesized materials in thin film.

	E_{ox} (V) [a]	HOMO (eV)	LUMO (eV)	E_g (eV) [b]
PT6I	+0.61	-4.85	-2.93	1.92
PT6buP$^+$Br$^-$	+0.54	-4.78	-2.59	2.19
P(3,4TO6buP$^+$Br$^-$)	+0.53	-4.77	-2.79	1.98

[a] Calculated by onset; [b] E_g optical.

As shown in Figure 10, the CV curves of analyzed materials can be considered not reversible and only the anodic peak can be observed due to the presence of only oxidation phenomena.

While the energy levels of the highest occupied molecular orbitals (HOMO) were evaluated by CV according to the following equation:

$$HOMO\ (eV) = -\ e\ (E_{ox} + 4.24)$$

where 4.24 V is the SCE absolute potential, the energy levels of the lowest unoccupied molecular orbital (LUMO) were evaluated indirectly since the reduction potentials resulted to be outside the electrochemical stability window of the electrolyte. LUMO levels were then calculated from HOMO levels and the optical bandgaps ($E_{g,opt}$) obtained from the UV–Vis spectra of the films with the equation:

$$LUMO\ (eV) = HOMO + E_{g,opt}$$

The obtained LUMO energy levels values are schematically reported in Figure 11.

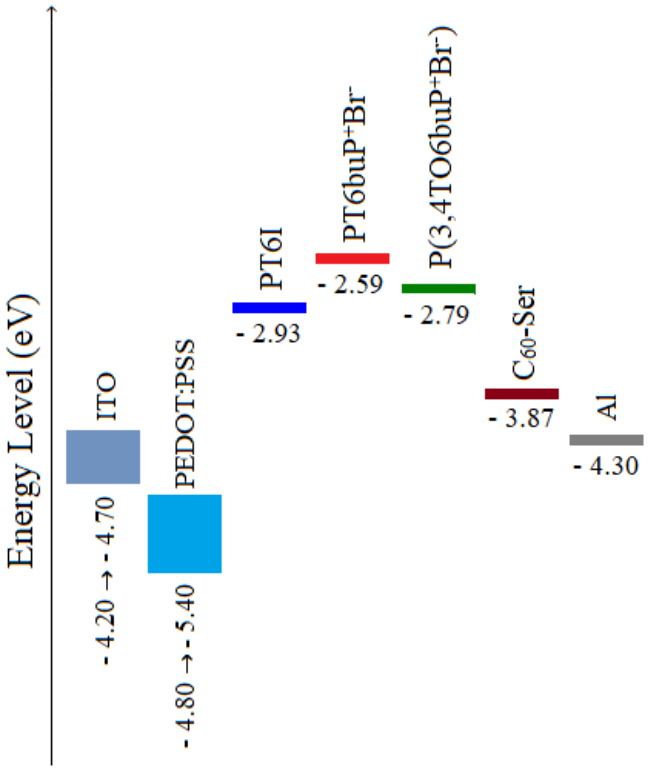

Figure 11. Energy-level alignment of OPVs layers (ITO, PEDOT:PSS and Al)[21] and comparison between synthetized electron-donor photoactive materials.

Observing the energy level values obtained (Table 6) and by comparing them with the reference material poly(3-hexylthiophene) (P3HT) – which presents a comparable E_g optical value of 2.02 eV[22] – it's possible to confirm that the synthetized cationic polymers can be employed as electron-donor materials in a photovoltaic device.

2.7. Photovoltaic properties

Water/alcohol soluble polymers PT6I, PT6buP$^+$Br$^-$ and P(3,4TO6buP$^+$Br$^-$) were tested as photoactive layer for the building up of solar devices. Photovoltaic properties were investigated by adopting the device configuration ITO/PEDOT:PSS/photoactive layer/Al in which polymers were tested in blend with C_{60}-Ser, the previously synthetized electron-acceptor fullerene derivative. Photovoltaic performance parameters are shown in Table 7.

Table 7. Short-circuit current density (J_{SC}), open-circuit voltage (V_{OC}), fill factor (FF) and power conversion efficiency (PCE) of tested solar cell.

	J_{sc} (mA cm^{-2}) [a]	***V_{oc} (V)***	***FF***	***PCE (%)***
PT6I:C_{60}-Ser	9.85	0.59	0.59	3.43
PT6buP$^+$Br$^-$:C_{60}-Ser	10.68	0.59	0.57	3.59
P(3,4TO6buP$^+$Br$^-$):C_{60}-Ser	13.32	0.60	0.60	4.79

[a] From J/V curves.

Current density-voltage curves shown in Figure 12 evidence that both phosphonic polymers are characterized by a profile which is different from that of imidazole polyelectrolyte. This is probably due to the different solubility and ability to film of the employed materials and the steric hindrance of side chains.

Besides, the presence of two oxygen atoms directly linked to the thiophene ring effectively offsets the presence of two tributylphosphonium side moieties and results in the best value of power conversion efficiency (PCE).

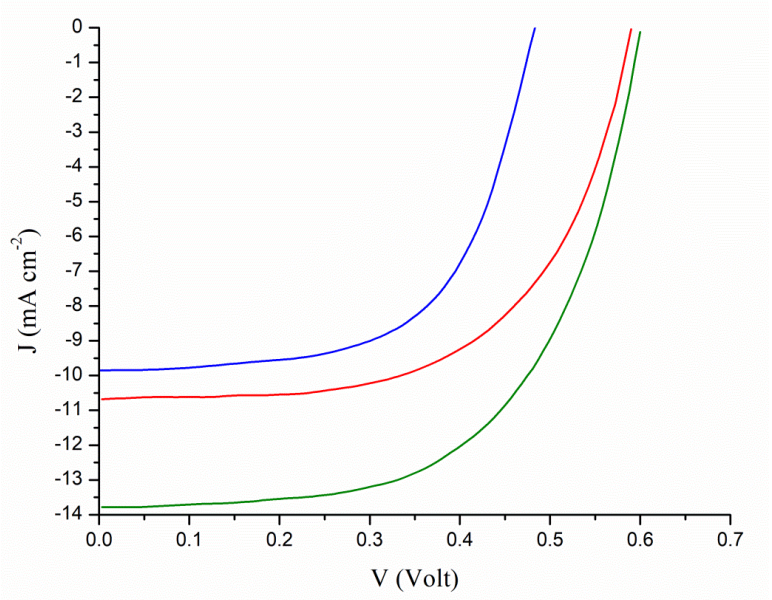

Figure 12. Current density-voltage (J/V) for the cell tested with ED material PT6I (blue line), PT6buP$^+$Br$^-$ (red line) and P(3,4TO6buP$^+$Br$^-$) (green line) under AM 1.5 one-sun illumination.

2.8. Conclusions

Three different ionic electron-donor polythiophenes were successfully synthesized using an easy and effective post-polymerization approach on three polythiophene derivatives. The effective post-functionalization was confirmed by spectroscopy analyses, which also made it possible to determine the substitution degree (complete in case of tributylphosphium group).

Final materials showed good solubility in water, as well as in methanol and ethanol, in particular in case of the two phosphonium polyelectrolytes PT6buP^{+}Br^{-} and P(3,4TO6buP^{+}Br^{-}). Thermal analyses confirmed the stability of synthetized materials and the tested devices showed good photovoltaic properties.

In detail, P(3,4TO6buP^{+}Br^{-}) showed the best optical and electrochemical properties, confirming that thiophenes functionalized with oxygen atoms and phosphonium groups can give an alcohol-soluble material with promising photovoltaic properties.

3. Experimental section

3.1. Materials

Tributylphosphine (97%), 1-methylimidazole (>99%), 1,6-hexandiol (99%), tetrahydrofuran (THF, >99.9%), toluene (C_7H_8, >99.9%), diethyl ether (Et_2O, >99.5%), trimethylamine (NEt_3, >98%), ethyl acetate (EtOAc, >99.5%) and chloroform ($CHCl_3$, 99.0-99.4%) were purchased from Sigma Aldrich Chemical Co. (USA). Triethylphosphite (for synthesis) were purchased from Sigma Aldrich (China). Petroleum ether (Etp, >90%) was purchased from Sigma Aldrich (Israel). Hexane (≥99%) and dichloromethane (≥99.9%) were purchased from Sigma Aldrich (France). Methanol (MeOH, >99.8%) was purchased from Honeywell (Germany). Dimethylsulfoxide (DMSO) and p-Toluensulfonic acid monohydrate (p-TSA) were purchased from Carlo Erba. Sodium sulfate (Na_2SO_4, anhydrous) and sodium bicarbonate ($NaHCO_3$, puriss.) were purchased from Riedel-deHaën (Poland). Nitromethane (CH_3NO_2, ≥98.5%), hydrobromic acid (HBr, 48%), hydrochloric acid (HCl, ≥37%), toluene-4-sulforide chloride and ferric chloride ($FeCl_3$, ≥98%) were purchased from Fluka (Switzerland). Cyclohexane and acetonitrile were purchased from VWR Chemicals (France). 3-Methoxythiophene (99%) was purchased from Alfa Aesar. 3,4-Dimethoxythiophene (>98%) was purchased from TCI (Japan). Poly[3-(6-bromohexyl)-thiophene] (PT6Br) and fullerene derivative (C_{60}-Ser) were synthetized as reported in previous Chapters. Diethyl ether and THF were freshly distilled before use to remove the stabilizer. All other materials were used as received. All manipulations involving moisture-sensitive reagents were performed under argon atmosphere in flame-dried glassware.

3.2. Synthesis of ionic electron-donor materials

3.2.1. Synthesis of poly{3-[6-(1-methyl-1H-imidazol-3-ium)-hexyl]-thiophene}bromide (PT6I)

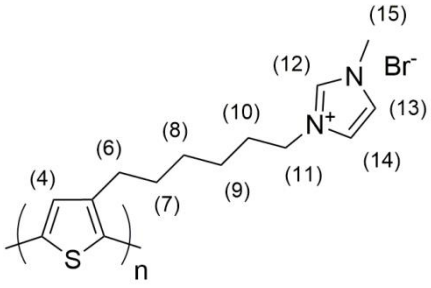

Method 1

300 mg (1.22 mmol) of PT6Br were dissolved in 40.0 mL of THF and added in a three-neck flask containing 15.0 mL of DMSO, 15.0 mL of methanol and 10.0 mL of water. 1.95 mL (24.4

mmol) of 1-methylimidazolium were added and the system was heated until reflux conditions for 48h.

The system was cooled down to room temperature and the crude product was added to 400 mL of THF. The precipitate was then filtered on PFTE membrane (pore size 0.45 μm), recovered in methanol and the solvent was finally removed under reduced pressure obtaining 350 mg (1.07 mmol) of dark purplish solid (yield 88%).

Method 2

50.0 mg (0.204 mmol) of PT6Br dissolved in 6.0 mL of anhydrous $CHCl_3$ were added in a three-neck flask containing 0.162 mL (2.04 mmol) of 1-methylimidazolium and the system was heated until reflux conditions for 48h.

The system was cooled down to room temperature and the crude product was washed several times with THF and recovered with methanol obtaining 9.0 mg (0.026 mmol) of PT6I as dark purplish solid (yield 13%).

^{1}H-NMR (CD_3OD, ppm): δ 7.61 (bs, 1H, *H*12), 7.50 (bs, 1H, *H*13), 7.14-6.86 (bm, 1H, *H*14+*H*4), 4.19 (bt, 2H, *H*11), 3.87 (s, 3H, *H*15), 3.43 (t, 2H, C*H*$_2$Br), 2.83-2.47 (bm, 2H, *H*6), 1.88 (bm, 2H, *H*10), 1.78-1.59 (bm, 2H, *H*7), 1.58-1.25 (bm, 4H, *H*8+*H*9).

^{13}C-NMR (CD_3OD, ppm): δ 141.64 (Th *C*3), 137.75 (*C*12), 135.04 (Th *C*2), 131.8 (Th *C*5), 130.48 (Th *C*4), 125.06 (*C*13), 123.84 (*C*14), 51.03 (*C*11), 36.78 (*C*15), 31.63, 31.32, 30.38, 30.12, 27.33 (aliphatic *C*H_2).

FT-IR (Ge, cm^{-1}): 3145, 3078, 2930, 2856, 1627, 1572, 1511, 1461, 1451, 1259, 1178, 1169, 1098, 1044, 832, 752, 725, 644, 560.

3.2.2. Synthesis of poly{3-[6-(tributylphosphonium)-hexyl]-thiophene}bromide (PT6buP$^+$Br$^-$)

200 mg (0.816 mmol) of PT6Br were dissolved in 12.0 mL of toluene in a three-neck round-bottom flask. Subsequently 2.0 mL (8.0 mmol) of tributylphosphine was added and the system was left to react at 90 °C for 24h, under stirring and in an inert atmosphere. The supernatant was removed and the polyelectrolyte formed on the flask surface was recovered with methanol, washed with Et_2O and dried under vacuum, obtaining 359 mg (0.802 mmol) of PT6buP$^+$Br$^-$ as a dark red solid (yield 98%).

^{1}H-NMR (CD_3OD, ppm): δ 7.13 (s, 1H, Th *H*4), 2.90 (bs, 2H, ThC*H*$_2$), 2.24 (bt, 8H, (C*H*$_2$)$_4$P$^+$), 1.83-1.69 (bm, 2H, ThCH$_2$C*H*$_2$), 1.68-1.44 (bm, 18H, (C*H*$_2$)$_n$), 0.98 (m, 9H, C*H*$_3$).

^{13}C-NMR (CD_3OD, ppm): δ 141.64 (Th *C*3), 134.87 (Th *C*5), 131.63 (Th *C*2), 130.38 (Th *C*4), 31.42, 30.23, 29.67, 25.06, 24.91, 24.47, 22.46 (aliphatic *C*H_2), 19.52 (*C*H$_2$P$^+$), 19.04 (P$^+$*C*H$_2$), 13.87 (*C*H_3).

^{31}P-NMR (CD_3OD, ppm): δ 33.31.

FT-IR (Ge, cm^{-1}): 3053, 2957, 2929, 2870, 1513, 1463, 1410, 1378, 1232, 1099, 833, 723.

3.2.3. Synthesis of 6-bromo-1-hexanol (B6OH)

In a three-neck flask, 9.90 g (83.7 mmol) of 1,6-hexandiol were dissolved in 126.0 mL of toluene. The solution was heated at 120°C and 11.4 mL (101 mmol) of HBr 48% was dropwise added at the system under inert flux. The reaction mixture was allowed to react under reflux for 72h. The crude product was treated with distilled water (2 × 150 mL), the organic phase was dried over Na_2SO_4, filtered and concentrated under reduced pressure. The obtained residue was purified by silica gel column chromatography (EtOAc:Etp, 1:1) to give 10.8 g (60.1 mmol) of a colorless oil (yield 72%).

^{1}H-NMR ($CDCl_3$, ppm): δ 3.65 (t, 2H, C*H*$_2$OH), 3.41 (t, 2H, C*H*$_2$Br), 1.87 (m, 2H, C*H*$_2$CH$_2$OH), 1.58 (m, 2H, C*H*$_2$CH$_2$Br), 1.47 (m, 2H, C*H*$_2$), 1.39 (m, 2H, C*H*$_2$).

^{13}C-NMR (100 MHz, $CDCl_3$, ppm): δ 63.14 (*C*H$_2$OH), 34.16 (*C*H$_2$Br), 33.05 (*C*H$_2$CH$_2$OH), 32.86 (*C*H$_2$CH$_2$Br), 28.28 (*C*H$_2$CH$_2$CH$_2$OH), 25.28 (*C*H$_2$CH$_2$CH$_2$Br).

FT-IR (KBr, cm^{-1}): 3339, 2932, 2859, 1053, 728, 644, 561.

3.2.4. Synthesis of 3,4-bis(6-bromohexyl-1-oxy)thiophene (3,4TO6Br)

In a two-neck flask, equipped with a cooling system, 500 mg (3.47 mmol) of 3,4-dimethoxythiophene were dissolved in 80.0 mL of dry toluene. Subsequently, 1.88 g (10.4 mmol) of 6-bromo-1-hexanol and a catalytic amount (66.0 mg, 0.347 mmol) of p-toluenesulfonic monohydrate acid were added under stirring. The mixture was refluxed for 24h under inert atmosphere. After removing solvent, the crude product was recovered with 100.0 mL of dichloromethane and then it was extracted with 50.0 mL of a saturated solution of $NaHCO_3$. The organic phase was washed with distilled water (3 × 100 mL), dried over Na_2SO_4, filtered and concentrated under reduced pressure. The residue was subjected to column chromatography (hexane:EtOAc, 85:15) to give 0.301 g (0.681 mmol, 20% yield) of a dark yellow-greenish oil.

^{1}H-NMR ($CDCl_3$, ppm): δ 6.17 (d, 2H, Th *H*2+*H*5), 3.98 (t, 4H, C*H*$_2$O), 3.42 (t, 4H, C*H*$_2$Br), 1.89 (m, 2H, C*H*$_2$CH$_2$O), 1.83 (m, 2H, C*H*$_2$CH$_2$Br), 1.50 (m, 4H, (C*H*$_2$)$_2$).

^{13}C-NMR ($CDCl_3$, ppm): δ 147.75 (Th *C*3+*C*4), 97.36 (Th *C*2+*C*5), 70.60 (*C*H$_2$O), 34.11 (*C*H$_2$Br), 33.01 (*C*H$_2$CH$_2$O), 29.19 (*C*H$_2$CH$_2$Br), 28.24, 25.58 (aliphatic *C*H$_2$).

FT-IR (KBr, cm^{-1}): 3109, 3002, 2937, 2859, 1563, 1499, 1467, 1242, 1144, 1048, 866, 747, 644, 560.

3.2.5. Synthesis of poly[3,4-bis(6-bromohexyl-1-oxy)thiophene] [P(3,4TO6Br)]

In a three-neck flask, 0.21 g (0.475 mmol) of previously synthetized 3,4TO6Br were dissolved in 12.0 mL of dry chloroform. Then, 0.314 mg (1.94 mmol) of ferric thrichloride ($FeCl_3$, 98%) dissolved in 1.89 mL of nitromethane in a dripper were added at the solution in 5 minutes. The mixture was allowed to react for 45 minutes, under vigorous inert flow and under stirring. After the reaction time, 10.0 mL of tetrahydrofuran were added and the system was allowed under stirring for 50 minutes.

Then the mixture was added drop by drop to 340 mL of a solution of MeOH/HCl (5%) under stirring. The precipitate was filtered on PTFE membrane (0.45 μm pore size) and washed several times with methanol. The solid was recovered with 100 mL of chloroform and the organic phase was washed with HCl 2% up to exhaustive extraction of the iron (III) ion (negative NH_4SCN test). Subsequently the crude product was washed with distilled water until neutrality. The mixture was dried over Na_2SO_4, filtered and concentrated under reduced pressure to give 0.115 g (0.261 mmol, 55% yield) of reddish polymer.

^{1}H-NMR ($CDCl_3$, ppm): δ 4.13 (b, 4H, C*H*$_2$O), 3.42 (t, 4H, C*H*$_2$Br), 1.90 (b, 8H, C*H*$_2$CH$_2$O + C*H*$_2$CH$_2$Br), 1.55 (b, 8H, (C*H*$_2$)$_2$).

^{13}C-NMR ($CDCl_3$, ppm): δ 145.23 (Th *C*3+*C*4), 116.92 (Th *C*2+*C*5), 73.47 (*C*H$_2$O), 34.23 (*C*H$_2$Br), 33.11, 30.45, 28.52, 25.70 (aliphatic *C*H$_2$).

FT-IR (KBr, cm^{-1}): 3109, 3002, 2937, 2859, 1563, 1499, 1467, 1242, 1144, 1048, 866, 747, 644, 560.

3.2.6. Synthesis of poly[3,4-bis(6-bromohexyl-1-tributylphosphonium)thiophene]dibromide [P(3,4TO6buP$^+$Br$^-$)]

In a three-neck round-bottom flask, 50.0 mg (0.114 mmol) of P(3,4TO6Br) were dissolved in 4.0 mL of toluene. Then 0.284 mL (1.14 mmol) of tributylphosphine were added under stirring and in an inert atmosphere. The system was left to react at 90 °C for 24 h. The supernatant was removed and the polyelectrolyte formed, filmed on the flask surface, was recovered with methanol, washed with diethyl ether and dried under vacuum, to obtain 0.094 g (0.111 mmol, 98% yield) of P(3,4TO6buP$^+$Br$^-$) as a black cherry solid.

^{1}H-NMR (CD_3OD, ppm): δ 4.17 (b, 4H, C*H*$_2$O), 2.41-2.09 (b, 16H, C*H*$_2$P$^+$), 1.95 (b, 4H, C*H*$_2$CH$_2$O), 2.03-1.88 (b, 4H, C*H*$_2$CH$_2$O), 1.67-1.34 (b, 32H, (C*H*$_2$)$_2$), 1.02-0.87 (m, 18H, C*H*$_3$).

^{13}C-NMR (CD_3OD, ppm): δ 154.72 (Th *C*3+*C*4), 129.08 (Th *C*2+*C*5), 66.90 (*C*H$_2$O), 28.15, 27.50, 25.25, 24.81, 24.65, 24.61 (aliphatic *C*H$_2$), 19.22 (*C*H$_2$P$^+$), 13.90 (*C*H$_3$).

^{31}P-NMR (CD_3OD, ppm): δ 33.37.

FT-IR (Ge, cm^{-1}): 2958, 2933, 2872, 1511, 1464, 1431, 1379, 1230, 1147, 1097, 726.

3.3. Synthesis of non-ionic electron-donor materials

3.3.1. Synthesis of poly[3-(6-diethylphosphonate)hexylthiophene] [PT6PO(OEt)$_2$]

100 mg (0.408 mmol) of PT6Br were added to a three-neck flask containing 8.0 mL (0.046 mol) of triethylphosphite. The system was heated at 120°C for 24h, under inert atmosphere. The system was cooled down to room temperature and the crude product was filtered on PTFE filter, washed with methanol obtaining 67.4 mg (0.223 mmol) of a partially substituted product (reaction yield 55%; functionalization yield 80%).

3.3.2. Synthesis of poly[3-(6-phosphonic acid)hexylthiophene] [PT6PO(OH)$_2$]

37.0 mg (0.123 mmol) of PT6PO(OEt)$_2$ were dissolved in 5.0 mL of dichloromethane and then were added 0.16 mL (1.23 mmol) of triethylammine and 0.17 mL (1.23 mmol) of bromotrimethyl silane. The system was allowed under inert atmosphere and under stirring for 4 h. Subsequently, 25.0 mL of methanol was added and the suspension allow to decant. Finally, the surnatant was removed obtaining a purplish solid which was not characterizable.

3.4. Synthesis of non-ionic electron-donor materials polyethereal

3.4.1. Synthesis of 2-(2-(2-(2-hydroxyehoxy)ethox)ethoxy)ethyl-4-methylbenzenesulfonate

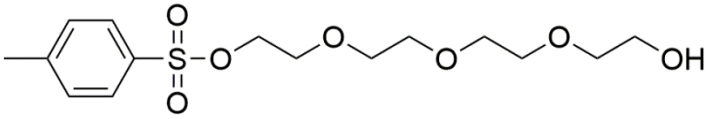

25.48 g (131.2 mmol) of tetraethylene glycol and 2.02 mL (19.7 mmol) of triethylamine were solubilized in 20.0 mL of CH_2Cl_2. The flask was placed in a bath of ice and water and 2.52 g (13.2 mmol) toluene sulfonyl chloride in 20.0 mL of CH_2Cl_2 were added dropwise under stirring.

The solution was stirred overnight at room temperature and then the mixture was poured in 100 mL of distilled water. The crude product was extracted with CH_2Cl_2 (2 × 100 mL), dried with Na_2SO_4, filtered and concentrated under reduced pressure.

The crude product was purified by chromatography column on silica gel with CH_2Cl_2:acetonitrile (3:1 and then 1:1) obtaining 1.63 g (5.21 mmol) of a yellowish oil (yield 40%).

^{1}H-NMR ($CDCl_3$, ppm): δ 7.80 (dt, 2H, aromatic C*H*), 7.35 (d, 2H, aromatic C*H*), 4.16 (t, 2H, Ts-OCH_2), 3.70 (m, 4H, Ts-OCH$_2$CH_2+CH_2OH), 3.64-3.59 (m, 10H, (CH_2)$_5$), 2.53 (bs, 1H, O*H*), 2.44 (s, 3H, CH_3).

^{13}C-NMR ($CDCl_3$, ppm): δ 144.8, 133.1, 129.8, 124.6 (aromatic *C*H), 70.7, 70.6, 70.5, 69.7, 69.6, 69.3 ((*C*H$_2$O)$_n$), 68.7 (*C*H$_2$OH), 61.7 (Ts-O*C*H$_2$), 21.6 (*C*H$_3$).

FT-IR (KBr, cm^{-1}): 3451, 2873, 1931, 1598, 1494, 1452, 1356, 1249, 1175, 1018, 923, 818, 664, 555.

3.4.2. Synthesis of 2-(2-(2-(2-thiophene-3-yloxy)ethox)ethoxy)ethyl-4-methylbenzenesulfonate

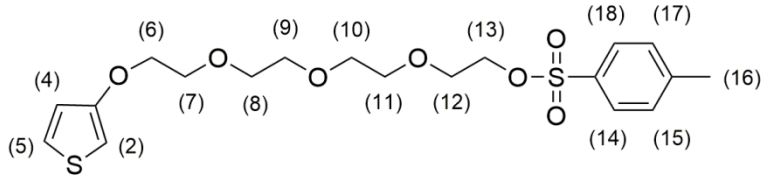

1.00 g (3.20 mmol) of sulfonate was added to a three-neck flask containing 0.213 mL (2.13 mmol) of 3-methoxythiophene, 6.40 mL of toluene and 81.2 mg (0.427 mmol) of p-toluenesulfonic acid monohydrate as a catalyst. The system was heated to reflux for 14 h under stirring and under inert atmosphere. The system was then cooled down to room temperature and the reaction solvent was removed under reduced pressure.

The crude product was purified by chromatography column on silica gel with cyclohexane:EtOAc (1:1) obtaining 324 mg (0.753 mmol) of a product that was not stable over time (yield 35%).

^{1}H-NMR ($CDCl_3$, ppm): δ 7.79 (d, 2H, aromatic C*H*), 7.65 (dd, 1H, *H*5), 7.33 (d, 2H, aromatic C*H*), 6.77 (dd, 1H, *H*4), 6.25 (dd, 1H, *H*2), 4.15-4.11 (m, 2H, *H*6), 3.83 (m, 4H, *H*7+*H*13), 3.68 (m, 2H, *H*12), 3.64 (m, 8H, *H*9+*H*10+*H*11+*H*12), 2.44 (s, 3H, *H*16).

3.5. NMR spectra

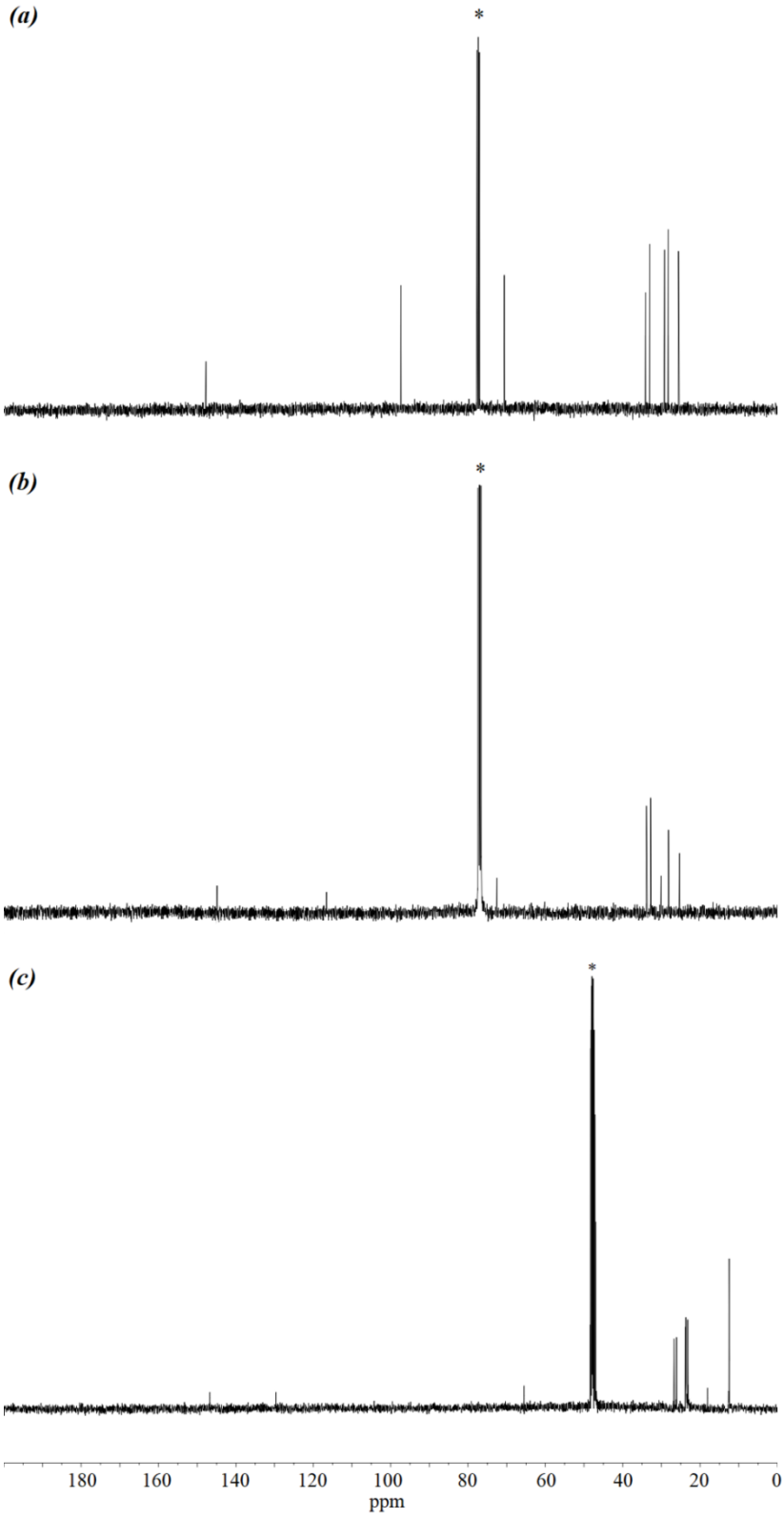

Figure 12. ^{13}C-NMR spectra of 3,4TO6Br (*a*), P(3,4TO6Br) (*b*) and P(3,4TO6buP^{+}Br^{-}) (*c*). Asterisk: solvent resonances ($CDCl_3$ and CD_3OD).

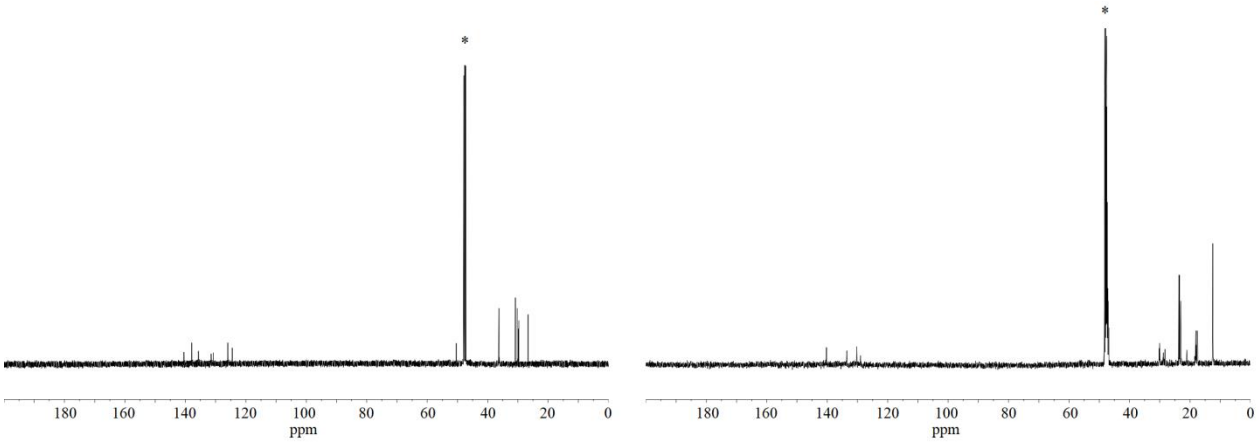

Figure 13. ^{13}C-NMR spectra of PT6I (left) and PT6buP^{+}Br^{-} (right). Asterisk: solvent resonance (CD_3OD).

3.6. Methods

^{1}H-NMR, ^{13}C-NMR and ^{31}P-NMR spectra were recorded on a Varian Mercury Plus 400 (400 MHz) spectrometer at room temperature using TMS as internal standard in deuterated solvents. Chemical shifts are given in ppm.

FT-IR spectra were taken on Ge or KBr disks using a Perkin Elmer Spectrum One spectrophotometer.

The molecular weight of polymeric precursors was determined by gel permeation chromatography (GPC) using THF solutions on a HPLC Lab Flow 2000 apparatus equipped with a Rheodyne 7725i injector, a Phenomenex MXL 5 μm mixed bed column and an RI K-2301 KNAUER detector. The calibration curve was recorded using monodisperse polystyrene standards.

UV-Vis spectra were collected by using Perkin Elmer Lambda 19 spectrophotometer using either around 10^{-5} M polymer solutions in spectroquality solvents in Suprasil quartz cuvettes (1 × 1 cm) or films on quartz slides drop-cast through the use of Doctor Blade.

Sample decomposition temperatures were determined by using a TA Instruments Q600 thermogravimetric analyzer (TGA) by heating from 30°C to 600°C with a ramp of 10°C min^{1} in oxidant atmosphere (air). DSC analyses were conducted by using a TA Instruments Q2000 differential scanning calorimeter (DSC) by varying the temperature from -20 to 200°C with a heating and cooling ramp of 10°C min^{-1} in a nitrogen atmosphere.

Cyclic voltammetry (CV) analyses were performed in a three compartments glass cell under Ar pressure and at room temperature by using an AMEL 5000 Electrochemical System. Polymers were deposited by drop casting from methanol solutions on Pt electrode (1 mm diameter). Auxiliary electrode was Pt wire spiral and reference electrode was aqueous saturated calomel electrode (SCE). Supporting electrolyte used was a solution of $(C_4H_9)_4NClO_4$ (0.1 mol/L) while the solvent was chosen in order to avoid the dissolution of film (acetonitrile/toluene, 25:75). SCE absolute potential is 4.24 eV.

3.6.1. Solar cells

The ITO glass substrate (2 × 2 cm, surface resistance 21 Ω/sq) was etched on one side by using a 10% wt aqueous solution of HCl and heated at 60°C for 10 min, in order to obtain an area of 1.5 × 1 cm covered by indium tin oxide. The glass was then cleaned using distilled water, 2-propanol and dried with a nitrogen flow (final resistance12 Ω/sq). Poly(3,4-ethylenedioxythiophene):polystyrene sulfonic acid (PEDOT:PSS, 2.8 wt% dispersion in water, viscosity 20 cps) was diluted 1:1 v/v with 2-propanol, sonicated for 15 min using an ultrasonic bath (Elmasonic S 30H), filtered on a Gooch G2 and the resulting solution (viscosity 12 cps) deposited over the previously treated ITO glass with

the doctor blading technique using a Sheen Instrument Model S265674, leaving only a small (0.5 × 1 cm) area uncovered at the opposite side of the previously etched area. The PEDOT:PSS film was heated in a Buchi GKR-50 glass oven at 120°C for 90 min under vacuum (10^{-3} mmHg).

A solution made by mixing 2.5 mg of polyelectrolyte and 2.5 mg of C_{60}-Ser in 0.5 mL of methanol was sonicated for 15 min and deposited by using Doctor Blade on the slide in order to cover the PEDOT:PSS layer. The sample was then annealed in the glass oven under vacuum (10^{-3} mmHg) at 120°C for 45 min.

Finally, a thin film of Al (electrode, 50 nm of thickness) was deposited over the polymeric layer through a shadow mask using an Edwards 6306A coating system operating at 10^{-6} mmHg. The active area of the cell was 1 × 1 cm^2. The current-voltage characteristics were measured in air using a Keithley 2401 source meter under the illumination of an Abet Technologies LS150 Xenon Arc Lamp Source AM 1.5 Solar Simulator (100 mW/cm^2) calibrated with an ILT 1400-BL photometer.

The structure of the final devices was made of: ITO (80 nm)/PEDOT:PSS (100 nm)/active layer (150 nm)/Al (50 nm). The solar cell spectral response was measured using a 7-SC Spec III Modularized Solar Cell Spectral Test System (SevenStar Optics, Beijing, PRC). Layer thickness was measured using a FTPAdvances FTPadv-2 Film Thickness Probe (Sentech GmbH, Germany) equipped with the FTPExpert software.

References

1. S. Das, D. P. Chatterjee, R. Ghosh, A. K. Nandi, *RSC Adv.*, **2015**, *5*, 20160-20177.
2. C. Duan, K. Zhang, C. Zhong, F. Huang, Y. Cao, *Chem. Soc. Rev.*, **2013**, *42*, 9071-9104.
3. M. Lanzi, E. Salatelli, L. Giorgini, A. Mucci, F. Pierini, F. P. Di-Nicola, *Eur. Polym. J.*, **2017**, *97*, 378-388.
4. F. Huang, H. Wu, Y. Cao, *Chem. Soc. Rev.*, **2010**, *39*, 2500-2521.
5. M. Lanzi, E. Salatelli, L. Giorgini, M. Marinelli, F. Pierini, *Polymer*, **2018**, *149*, 273-285.
6. T. Ghoos, J. Brassinne, C. Fustin, J. Gohy, M. Defour, N. Van Den Brande, B. Van Mele, L. Lutsen, D. J. Vanderzande, W. Maes, *Polymer*, **2013**, *54*, 6293-6304.
7. P. Urbánek, A. Di Martino, S. Gladyš, I. Kuřitka, A. Minařík, E. Pavlova, D. Bondarev, *Synth. Met.*, **2015**, *202*, 16-24.
8. S. Hladysh, A. Murmiliuk, J. Vohlídal, D. Havlíček, V. Sedlařík, M. Štěpánek, J. Zedník, *Eur. Polym. J.*, **2018**, *100*, 200-208.
9. S. Hladysh, D. Bondarev, J. Vohlídal, D. Vrbata, J. Zedník, *Eur. Polym. J.*, **2016**, *83*, 367-376.
10. R. D. McCullough, *Adv. Mater.*, **1998**, *10*, 93-116.
11. P. Urbánek, A. Di Martino, S. Gladyš, I. Kuřitka, A. Minařík, E. Pavlova, D. Bondarev, *Synth. Met.*, **2015**, *202*, 16-24.
12. D. Bondarev, J. Zedník, I. Šloufová, A. Sharf, M. Prochazka, J. Pfleger, J. Vohlídal, *J. Polym. Sci. Polym. Chem.*, **2010**, *48*, 3073.
13. C. Zhang, K. Du, X. Zhang, X. Zheng, G. Cao, F. Zhang, F. Feng, *Dyes and Pigments*, **2019**, *170*, 107581.
14. K. K. Stokes, K. Heuzé, R. D. McCullough, *Macromolecules*, **2003**, *36*, 7114-7118.
15. A. K. Bhattacharya, G. Thyagarajan, *Chem. Rev*., **1981**, *81*, 415-430.
16. K. M. Błazewska, *J. Org. Chem*., **2014**, *79*, 408-412.
17. C. M. Sevrain, M. Berchel, H. Couthon, P.-A. Jaffrès, *Beilstein J. Org. Chem*., **2017**, *13*, 2186-2213.
18. Y. Li, M. Zhou, Y. Wang, Q. Pan, Q. Gong, Z. Xia, Y. Li, *Carbon*, **2019**, *147*, 519-531.
19. J. Chang, S. Zhang, Y. Jiang, L. Xu, J. Yu, W. Zhou, X. Sun, *ChemMedChem*, **2013**, *8*, 976-984.
20. X. Chen, Q. Qu, *Sol. Energy Mater. Sol. Cells*, **2018**, *179*, 270-275.
21. S. A. Rutledge, A. S. Helmy, *J. Appl. Phys*. **2013**, *114*, 133708.
22. J. Hou, Z. Tan, Y. Yan, Y. He, C. Yang, Y. Li, *J. Am. Chem. Soc*, **2006**, *128*, 4911-4916.

CHAPTER VI: SYNTHESIS OF A DOUBLE-CABLE WATER-SOLUBLE COPOLYMER

1. Introduction

1.1 Overview

Among the different types of organic photovoltaic (OPVs) devices, the bulk-heterojunction (BHJ) cells are the most attractive due to the possibility to combine easy processability with high final efficiency. In detail, in the BHJ architecture the active layer is usually composed by a physical blend between an electron-donor (ED, a π-conjugated polymer) and an electron-acceptor (EA, usually a fullerene derivative) material. The main issue of this architecture is the generation of a phase separation that does not allow an ideal transport of charges and affects consequently the blend morphology and its thermal stability, with final efficiency-limiting factor. Moreover, the miscibility of the two components is also an essential factor to be considered.

In order to obtain optimized and enhanced structures, it's possible to prepare a double-cable material in which the electron-acceptor group (EA) is directly linked to the end of the side chains of the polyconjugated backbone by chemical modification of the polymeric structure.[1] However, earlier studies have proved that the content of the EA group, e.g. fullerene, should be appropriate to obtain a good solubility in common organic solvents combined with an efficient collection of electrons during charge separation.[2]

Moreover, the electron-donor unit (ED) should be selected with suitable characteristics with the aim to obtain an alcohol-soluble polymer.[3-6] Final solubility of π-conjugated polymers in polar solvents can be achieved and tailored by linking phosphine groups,[7] i.e. a hydrophilic ionic moiety, to polymer side chain. Therefore, a double-cable polymer could combine both solubility in more green solvents with a reduced distance between the units bearing side chains functionalized with ionic moiety (tributylphosphine) and an acceptor group (fullerene).

1.2. Aim of the chapter

In order to synthetize the new alcohol-soluble double-cable poly{[3-(6-tributylphosphonium)thiophene]bromide-*co*-3-(6-fullerenylhexyl)thiophene} (P[(T6buP^{+}Br^{-})-*co*-(T6F)]), the regioregular poly[3-(6-hexyl)thiophene] (PT6Br) - obtained through GRIM Method – was post-functionalized in two steps obtaining a copolymer with both a C_{60}-fullerene moiety (electron-acceptor unit) and an ionic phosphonium group (electron-donor unit) at the end of a hexamethylenic side chain. The reduced distance between the EA and ED materials could lead to an

improved morphology and photoconversion efficiency of photovoltaic devices, exploiting the excellent solubility in polar solvents of phosphine-substituted polythiophene-based materials.

The structural properties were investigated by spectroscopy techniques (^{1}H-NMR, ^{13}C-NMR, ^{31}P-NMR, FT-IR, UV-Vis), thermogravimetric analysis (TGA), differential scanning calorimetry (DSC), X-ray diffraction (XRD), atomic force microscopy (AFM) and external quantum efficiency (EQE). The final materials were tested as active media in organic solar devices prepared with halogen-free solvents resulting in eco-friendly photovoltaic cells.

This chapter is an adapted part of "Influence of the active layer structure on the photovoltaic performance of water-soluble polythiophene-based solar cells" M. Lanzi, D. Quadretti, M. Marinelli, Y. Ziai, E. Salatelli, F. Pierini, *Polymers*, 2021, 13, 1640.

The atomic force microscopy (AFM) and external quantum efficiency (EQE) measurements were carried out in collaboration with Prof. Filippo Pierini of Department of Biosystem and Soft Matter – Institute of Fundamental Technological Research, Polish Academy of Science (Warsaw, Poland).

2. Results and discussion

2.1. Synthesis

The adopted synthetic route involves several steps, such as the synthesis of a regioregular polymeric precursor, poly[3-(6-bromohexyl)thiophene] (PT6Br) from 2,5-dibromo-3-(6-bromohexyl)thiophene (2,5BT6Br),[8,9] as previously discussed in Chapter II.

In order to improve performance of final device, a high value of regioregularity of polymer is the first key point to improve the final optical and conductive properties of the photoactive material. For this purpose, the regiospecific GRIM (Grignard Metathesis)[10-12] polymerization method was adopted to obtain the regioregular precursor PT6Br with a high percentage of HT linkages (95%).

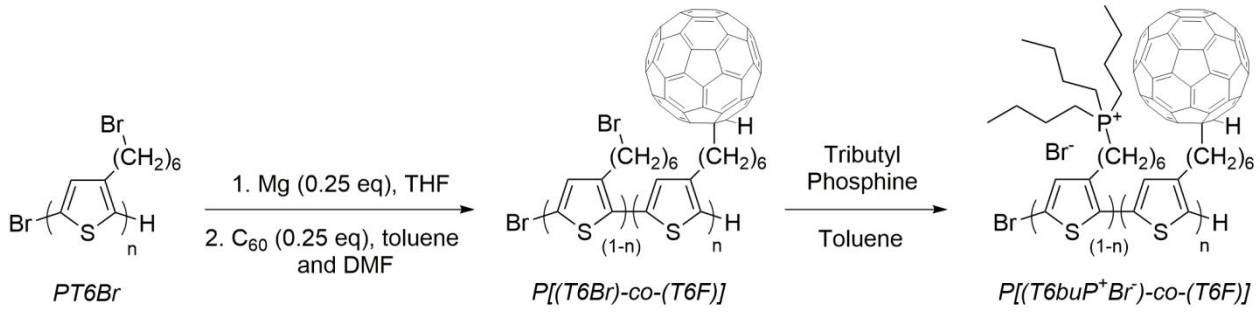

Scheme 1. Synthesis of the water-soluble double-cable copolymer P[T6buP^{+}Br^{-})-*co*-(T6F)].

Starting from PT6Br, the synthetic route involved two post-functionalization reactions (Scheme 1). The first one relates to a Grignard reaction on a specific amount of units (0.25 eq) of side chains

and the reaction of the intermediate with fullerene (C_{60}), according to the procedure previously developed by my research group.[2] The resulting double-cable copolymeric precursor P[(T6Br)-*co*-(T6F)] presents 7% fullerene content, a percentage that did not compromise the final solubility of material.

The obtained product was then post-functionalized with tributylphosphine under reflux conditions in toluene for 5 hours, a reduced time if compared to that reported in literature, in order to prevent any loss of C_{60} from the side chains.[7] Finally, the obtained copolymer P[(T6buP$^+$Br$^-$)-*co*-(T6F)] presented both ionic and fullerene moieties and its main characteristics were determined from values obtained from GPC analysis of precursor (Table 1).

Table 3. Polymers characteristics.

	Reaction Yield (%)	***Ionic group content (%mol)*** [a]	***C_{60} content (%mol)*** [a]	***Mn (kDa)***	***PDI***
PT6Br	21	-	-	14.9 [b]	1.15 [b]
P[(T6Br)-co-(T6F)]	85	-	7	17.6 [c]	1.15 [c]
P[(T6buP$^+$Br$^-$)-co-(T6F)]	78	93	7	29.1 [c]	1.15 [c]

[a] Determined by ^{1}H-NMR; [b] Determined by GPC chromatography; [c] Calculated from the molecular mass of the corresponding polymeric precursor.

The low average molecular weight obtained for PT6Br - polymeric precursor, $X_n = 61$ - is due to polymerization mechanism, during which the system becomes heterogeneous, thus limiting the chain growth.

2.2. NMR Characterization

All the synthesized products were characterized by ^{1}H-NMR and ^{13}C-NMR spectrometry to evaluate their chemical structure and purity degree.

In detail, ^{1}H-NMR spectrum of the double-cable precursor copolymer P[(T6Br)-*co*-(T6F)] (Figure 1, blue line) clearly shows the characteristic peaks - singlet peak at 7.41 ppm and broad multiplet at 3.56 ppm, ascribable to the fullerene proton and methylenic protons in the α-position to C_{60}, respectively – that are only present when the fullerene is directly linked to the side chain. By the ratio of the signals at 3.56 and at 3.45 ppm - related to CH_2C$_{60}$ and CH_2Br, respectively - a 7% fullerene content can be estimated for the precursor copolymer.

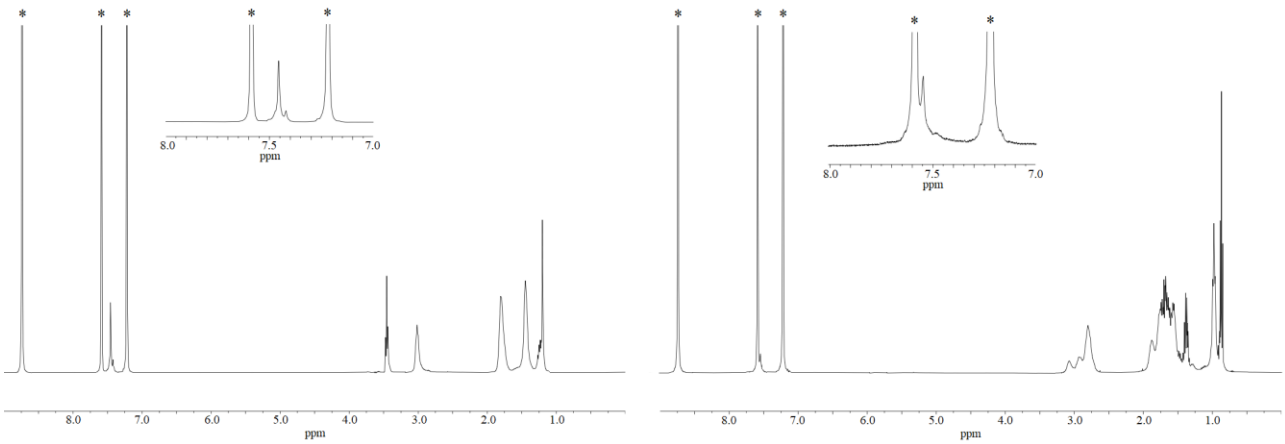

Figure 1. ^{1}H-NMR spectra of P[(T6Br)-*co*-(T6F)] (left) and P[(T6buP^{+}Br^{-})-*co*-(T6F)] (right). Asterisk: solvent resonances (pyridine-d_5). Inset: expansion of the aromatic region.

The occurrence of the subsequent post-functionalization with tributylphosphine to give P[(T6buP^{+}Br^{-})-*co*-(T6F)] was also verified by ^{1}H-NMR, as well as ^{31}P-NMR spectroscopy. In ^{1}H-NMR spectrum (Figure 1, green line), the broad multiplet at 2.75 ppm is ascribable to the eight methylenic protons in α- and α'-position to the cationic phosphine group. Moreover, the total absence of signal ascribable to -Br moiety evidences the total substitution reaction with phosphonium group, which typically occurs when phosphines are used as nucleophile reagents as previously verified.

Indeed, when ^{13}C-NMR spectra of PT6Br, P[(T6Br)-*co*-(T6F)] and P[(T6buP^{+}Br-)-*co*-(T6F)] (Figure 2) are compared to each other, a further confirmation that the post-functionalizations took place is obtained.

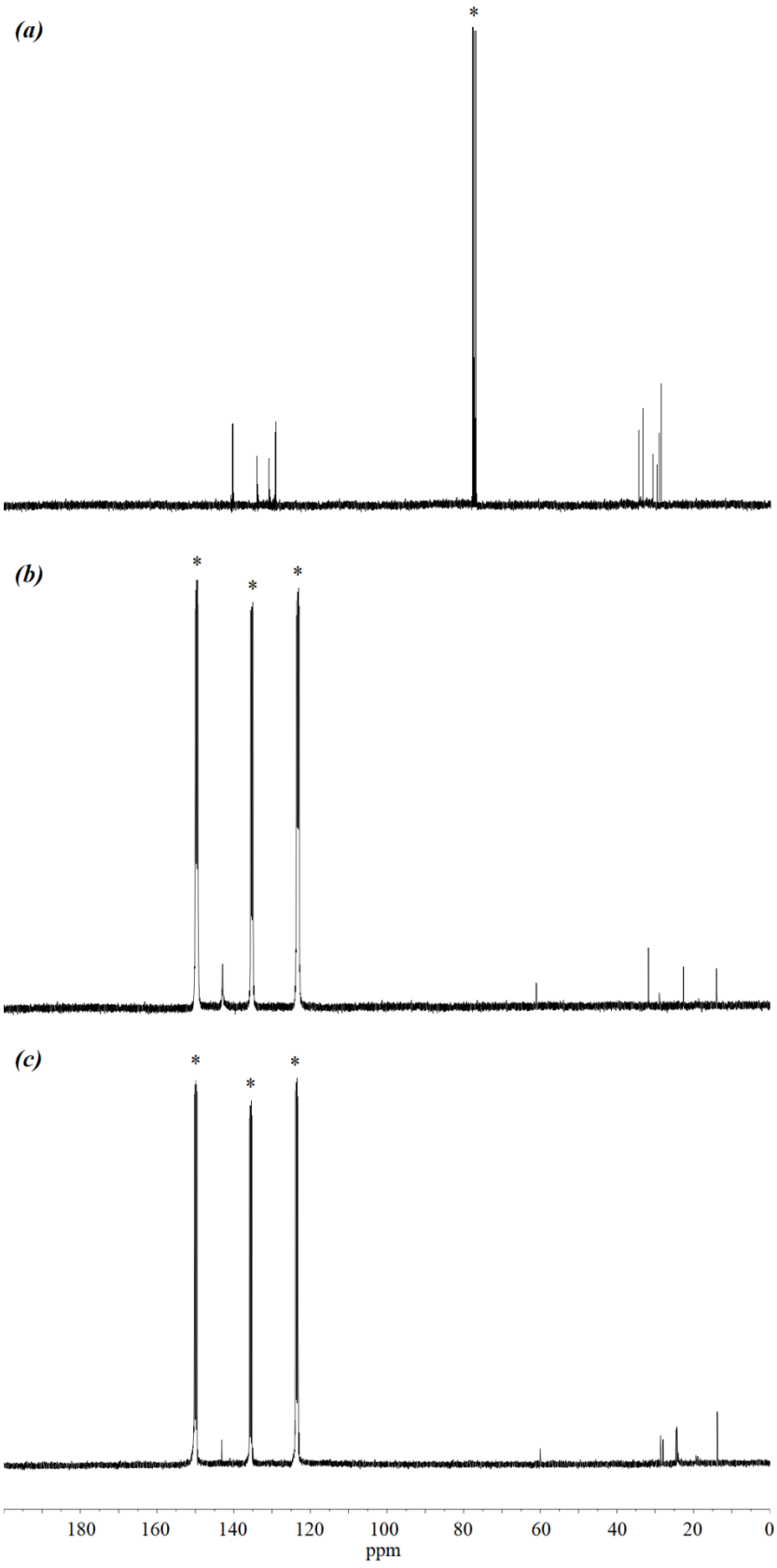

Figure 2. ^{13}C-NMR spectra of PT6Br (*a*), P[(T6Br)-*co*-(T6F)] (*b*) and P[(T6buP^{+}Br^{-})-*co*-(T6F)] (*c*). Asterisk: solvent resonances ($CDCl_3$ and pyridine- d_5).

Moreover, the ^{31}P-NMR spectrum of ionic copolymer P[(T6buP^{+}Br^{-})-*co*-(T6F)] (Figure 3) shows only a signal at 37.84 ppm that also confirms the complete absence of unreacted tributylphosphine, as previously verified by ^{1}H-NMR.

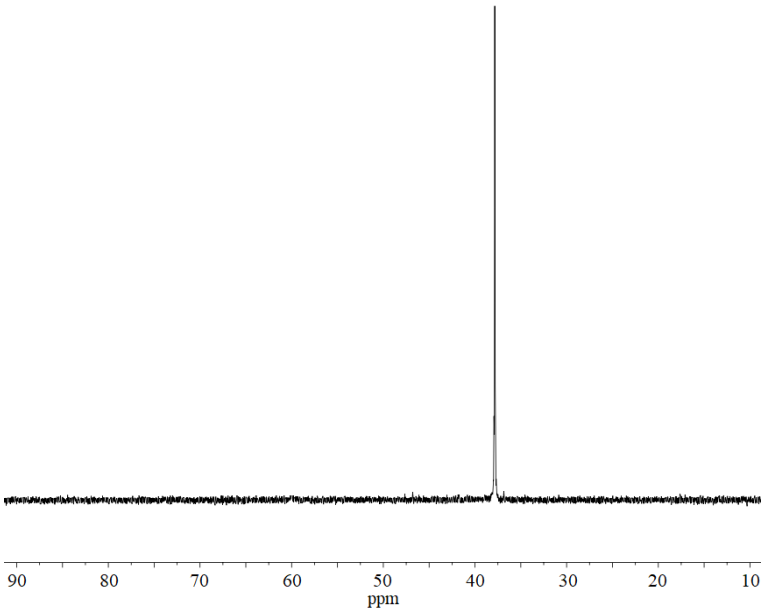

Figure 3. ^{31}P-NMR spectrum of P[(T6buP^{+}Br^{-})-*co*-(T6F)].

2.3. FT-IR characterization

FT-IR spectroscopy gave another confirm of the occurrence of polymerization and subsequent post-functionalization reactions. The main IR absorption bands of precursor polymer (PT6Br), double-cable copolymers (P[(T6Br)-*co*-(T6F)] and P[(T6buP^{+}Br^{-})-*co*-(T6F)]) and their assignments are reported in Figure 4 and Table 2.

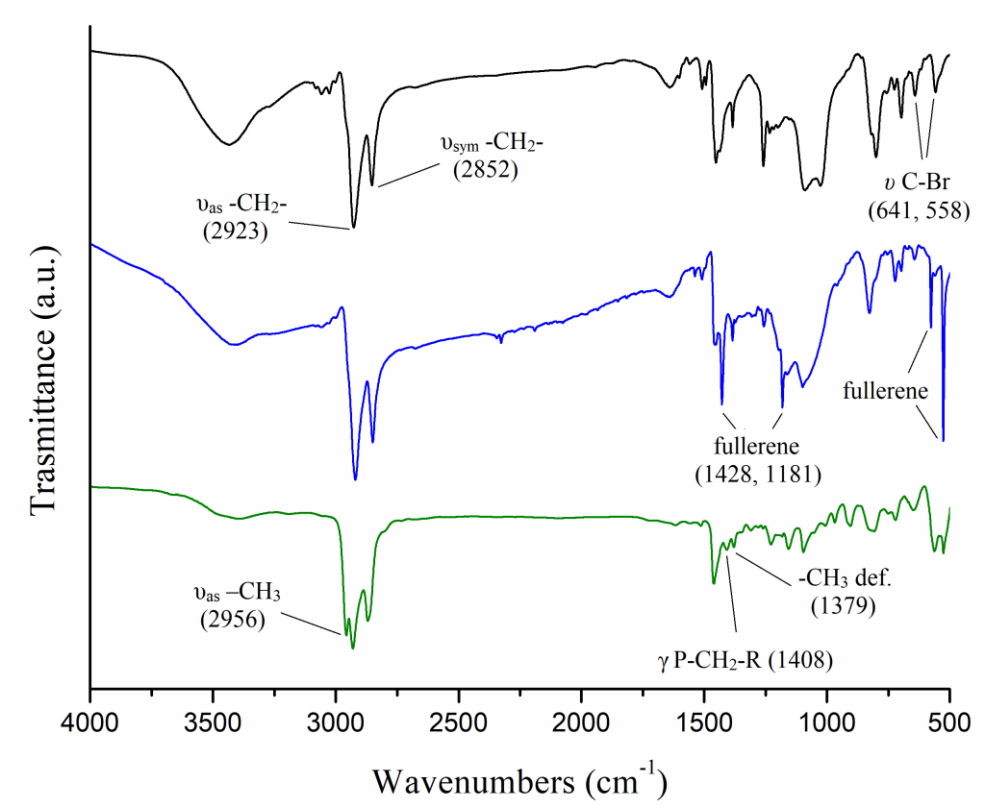

Figure 4. FT-IR spectra of PT6Br (black line), P[(T6Br)-*co*-(T6F)] (blue line) and P[(T6buP$^+$Br$^-$)-*co*-(T6F)] (green line).

The FT-IR spectra of brominated derivatives show peaks at 641, 558 cm^{-1} for PT6Br (black line) and 644, 557 cm^{-1} for P[(T6Br)-*co*-(T6F)] (blue line), which are characteristic of the terminal -Br atom in the side chain. The desired post-functionalization with C_{60}-fullerene in the side chains is then confirmed by the presence of the absorptions at 1428, 1181, 562, and 526 cm^{-1} in P[(T6Br)-*co*-(T6F)] and at 1427, 1180, 576 and 526 cm^{-1} in P[(T6buP$^+$Br$^-$)-*co*-(T6F)] (green line).

Besides, the appearance of the bands at 2956, 2927, 2869, 1461, and 1379 cm^{-1} in P[(T6buP$^+$Br$^-$)-*co*-(T6F)] spectrum - ascribable to the tributylphosphonium group - as well as the disappearance of the bands related to C-Br stretching, evidence the complete post-functionalization of the polymeric precursor. Moreover, the presence of bands at 1427, 1180, 576 and 526 cm^{-1} ascribable to fullerene linked to the side chains also in cationic double-cable copolymer spectrum is a further confirm that the second substitution reaction on copolymer doesn't affect the other units.

Table 2. Main IR absorption bands (cm^{-1}) of polymers.

PT6Br	*P[(T6Br)-co-(T6F)]*	*P[(T6buP$^+$Br$^-$)-co-(T6F)]*	*Assignments*
3058	3053	3052	υ C-H β thiophene
-	-	2956	υ_{as} –CH_3 (phosphonium group)
2923	2918	2927	υ_{as} -CH_2- (side chain and phosphonium group)
2852	2849	2869	υ_{sym} -CH_2- and –CH_3
1508	1509	1514	υ_{as} -C=C- thiophene
1434	1452	1461	-CH_2- deformation (phosphonium group) and υ_{sym} C=C thiophene
-	1428	1427	fullerene
-	-	1408	γ P-CH_2-R
-	-	1379	-CH_3 deformation (phosphonium group)
1259	1257	1228	υ C-C thiophene-thiophene
-	1181	1180	fullerene
1089	1099	1096	δ –CH thiophene
800	826	808	γ C-H thiophene 2, 3, 5-trisubstituted
725	722	721	rocking -CH_2-
641, 558	644, 557	-	*υ* C-Br aliphatic
-	562, 526	576, 526	fullerene

υ = stretching; γ = out of plane bending; δ = in-plane bending.

2.4. Thermal properties

The thermal stability of polymeric precursor and double-cable copolymers was determined by TGA under oxidizing atmosphere (air), at a heating scan of 10°C min^{-1} and up to 600°C (Figure 5).

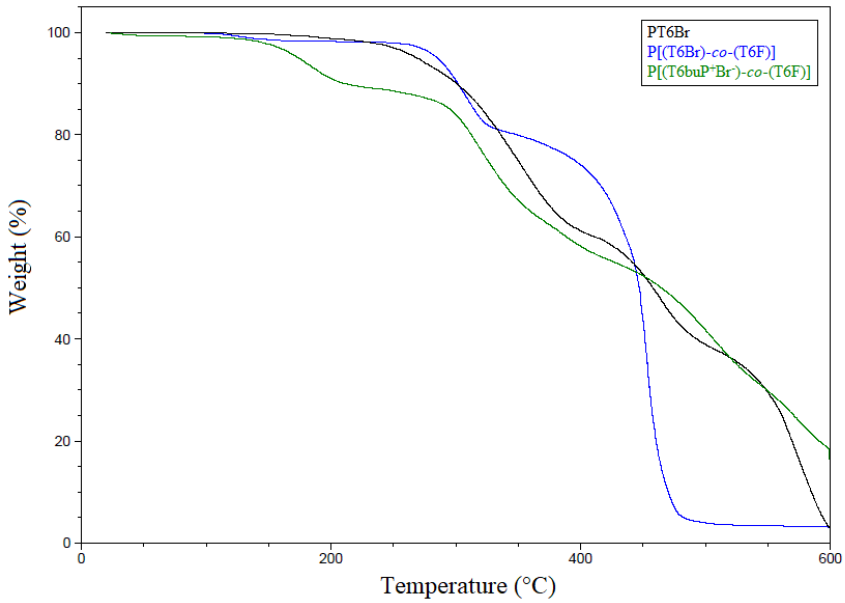

Figure 5. TGA thermograms of homo- and co-polymers.

While in the TGA curve of PT6Br the first main weight losses can be ascribed to the elimination of –Br group, side chains and degradation of macromolecular backbone, for the two copolymers the weight changes can be related to different losses (i.e. fullerene and phosphonium pendant groups).

In detail, the copolymer P[(T6Br)-*co*-(T6F)] shows a thermal behavior quite different from its respective precursor PT6Br, and this might be ascribed to the steric hindrance of fullerene linked to the side chain. Indeed, even though a small weight loss at around 155°C is shown in the P[(T6buP$^+$Br$^-$)-*co*-(T6F)] sample, it is possible to observe two main weight losses instead of the three observed in the copolymeric precursor. The synthesized samples, however, may be considered stable enough to be used as photoactive materials in organic photovoltaic devices due to their high degradation temperatures (~ 260-290°C).

Table 3. Glass-transition (T_g), melting (T_m), crystallization (T_c) and initial decomposition (T_d) temperatures of polymers.

	T_d (°C) [a]	T_g (°C) [b]	T_m (°C) [b]	T_c (°C) [b]
PT6Br	282	55	164	95
P[(T6Br)-co-(T6F)]	260	77	148	86
P[(T6buP$^+$Br$^-$)-co-(T6F)]	296	27	-	-

[a] Calculated by onset point on first inflection in TGA curves; [b] Determined by DSC analyses.

The DSC analysis was carried out under nitrogen atmosphere with a heating ramp of 10°C min^{-1} from -20°C up to 200°C and the relative curves are reported in Figure 6.

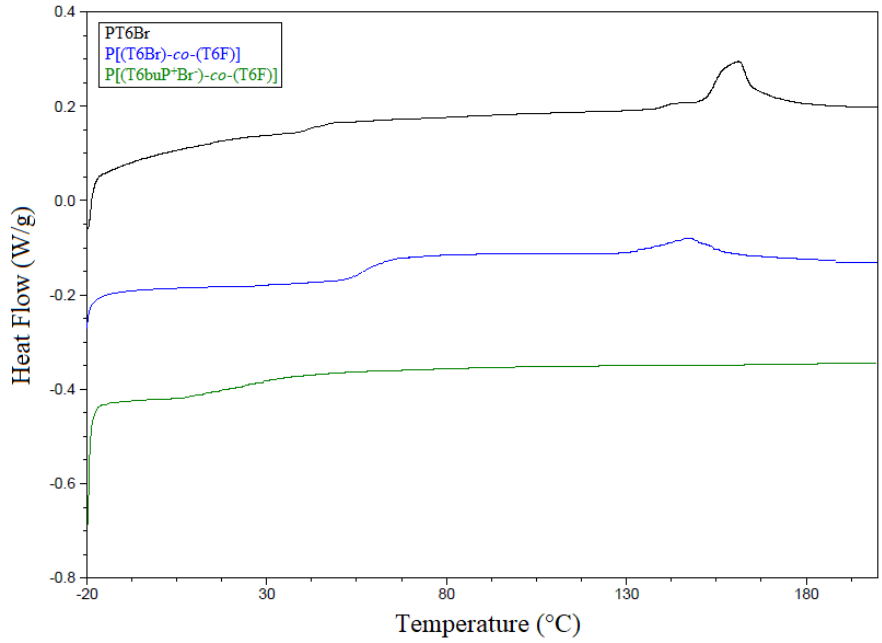

Figure 6. DSC curves of homo- and co-polymers.

All polymeric samples show an endothermic flexure at low values, ascribable to the glass transition temperature (T_g), a value that decreases when the tributylphosphonium group is linked to the side chain.

The presence of two different side chains determines the decrease of melting and crystallization temperatures in comparison with PT6Br values (Table 3). In detail, an amount of 7% of fullerene has a small effect on first-order transitions while the presence of ionic side chain moiety (93%) determines the absence of melting and crystallization peaks in DSC curve of P[(T6buP$^+$Br$^-$)-*co*-(T6F)].

2.5. Optical properties (UV-Vis characterization)

The optical properties of PT6Br and co-polymers P[(T6Br)-*co*-(T6F)] and P[(T6buP$^+$Br$^-$)-*co*-(T6F)] were analyzed by UV-Vis spectroscopy both in solution and in solid state, by drop-casting their solution onto quartz slides. Their normalized absorption spectra and assignments are shown in Figure 7 and Table 4.

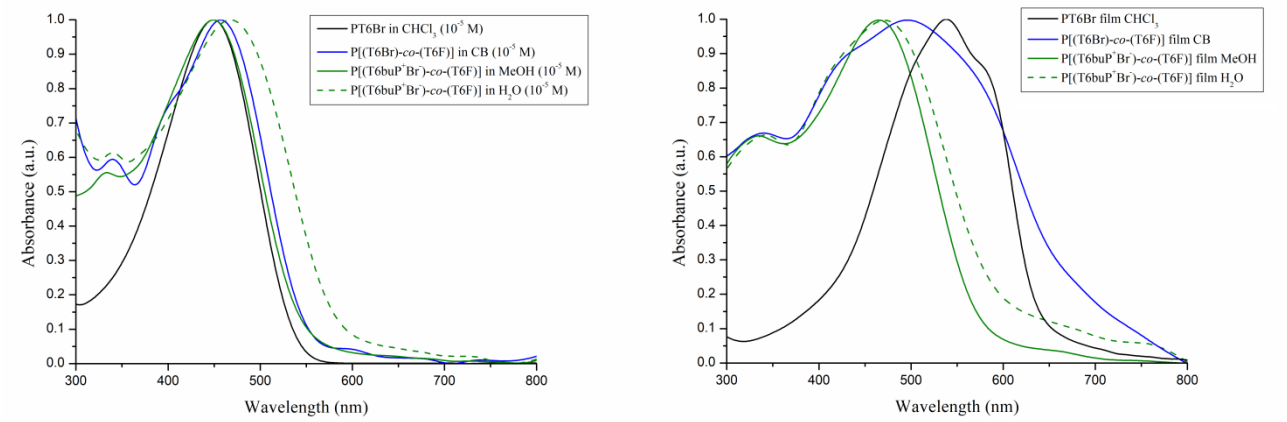

Figure 7. UV-Vis spectra of homopolymer and double-cable copolymers in solution and in thin film by drop-casting from different solvents.

About spectra of polymers in solution, the maximum absorption wavelength (λ_{max}) at ~ 450-460 nm is ascribable to the $\pi \rightarrow \pi^*$ electronic transition that typically occurs in the conjugated polymer main chain. In copolymer precursor spectrum, it's possible to notice the fullerene contribute to absorption profile at ~330 nm, that also influences the optical behavior of ionic copolymer in different solvents (water and methanol).

The spectra of both double-cable copolymers in the solid state show a different behavior, evidencing a broader profile than homopolymer PT6Br. Besides, the bulky and hindering nature of the fullerene units inserted in the side chain - whose absorption contribution is clearly evident also in this case – involves a rather strong blue-shift of the λ_{max} of the thiophene system for P[(T6Br)-*co*-(T6F)] if compared to its precursor.

The subsequent post-functionalization with tributylphosphine to give P[(T6buP$^+$Br$^-$)-*co*-(T6F)] results in a more blue-shifted absorption maximum. This behavior may be ascribed to the enhancement of steric hindrance of lateral side chains (93% of tributylphosphonium groups) combined with different solvents used for depositions. Nevertheless, the broader profiles of two copolymers and the wide range of absorption makes them attractive materials in opto-electronic applications.

Table 4. Maximum absorption wavelengths of polymers in solution and thin films.

	Solvents	***λ_{max} solution 10^{-5} M (nm)***	***λ_{max} film (nm)***
PT6Br	Chloroform	457	538
P[(T6Br)-co-(T6F)]	Chlorobenzene	339, 456	340, 496
P[(T6buP$^+$Br$^-$)-co-(T6F)]	Water	342, 468	343, 471
	Methanol	333, 450	334, 465

2.6. X-ray diffraction

The X-ray diffraction (XRD) profiles of the PT6Br and of the two copolymers P[(T6Br)-*co*-(T6F)] and P[(T6buP$^+$Br$^-$)-*co*-(T6F)] in film are shown in Figure 8.

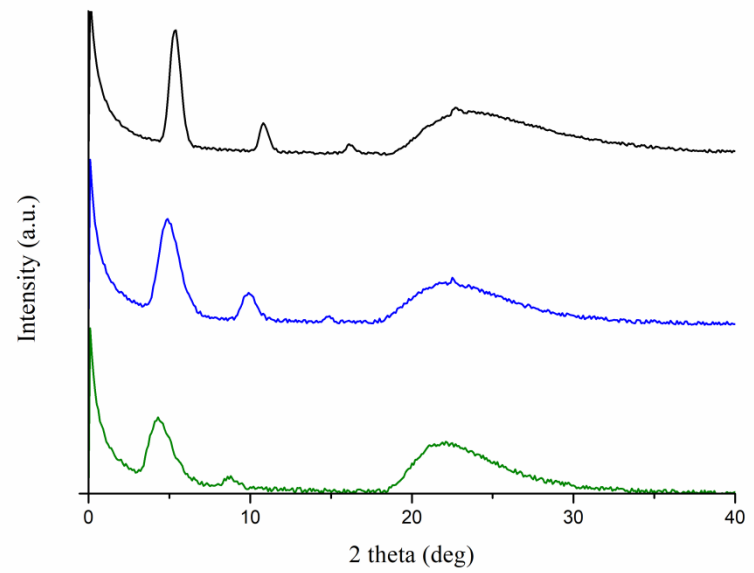

Figure 8. X-ray diffractograms of PT6Br (black line), P[(T6Br)-*co*-(T6F)] (blue line) and P[(T6buP$^+$Br$^-$)-*co*-(T6F)] (green line).

Samples exhibit the (100) reflection ascribable to the side chain lamellar distance and the corresponding high order reflection (200), while the third order reflection (300) is only present in PT6Br and P[(T6Br)-*co*-(T6F)] diffractograms (Table 5).

Table 5. Structural parameters of samples.

Sample	*Low-angle diffractions (degrees)*	*High-angle diffractions (degrees)*	*On plane Th chains distances (Å)*	*Planes stacking distances (Å)*	*Crystallites mean size (L) (nm)*
PT6Br	5.34; 10.82; 16.19	22.68	16.5	3.92	15.6
P[(T6Br)-co-(T6F)]	4.91; 9.89; 14.84	22.51	17.9	3.95	6.74
P[(T6buP$^+$Br$^-$)-co-(T6F)]	4.34; 8.71	21.61	20.3	4.09	5.33

The weak peaks at wide angles superimposed to the broad amorphous halo correspond to the on-plain chain distances. The lamellar spacings and the planes stacking distances range from 3.92 to 4.09 Å and 16.5 to 20.3 Å, respectively. The crystallites main size (L) - calculated using Scherrer's relation[13] - indicates the presence of some microcrystalline domains in the essentially amorphous phase of the examined polymeric films.

2.7. Photovoltaic properties

Water/alcohol soluble double-cable polymer P[(T6buP$^+$Br$^-$)-*co*-(T6F)] was tested as photoactive layer for the building up of solar device and compared with its copolymeric precursor P[(T6Br)-*co*-(T6F)].[2] Photovoltaic properties were investigated by adopting the device configuration ITO/PEDOT:PSS/photoactive layer/Al in which copolymers were tested as a single material. Photovoltaic performance parameters are shown in Table 6.

Table 6. Short-circuit current density (J_{SC}), open-circuit voltage (V_{OC}), fill factor (FF) and power conversion efficiency (PCE) of tested solar cell.

Sample	J_{SC} *(mA cm^{-2})* [a]	V_{OC} *(V)*	*FF*	*PCE (%)*
P[(T6Br)-co-(T6F)]	10.4	0.67	0.55	3.55
P[(T6buP$^+$Br$^-$)-co-(T6F)]	8.51	0.61	0.60	3.11

[a] From J/V curves.

Current density-voltage curves shown in Figure 9 evidence that both double-cable copolymers are characterized by a high photo-current ascribable to the presence of the fullerene group chemically linked to the polyconjugated backbone, thus avoiding phase-separation and aggregation phenomena usually observed when the electron acceptor molecule is only physically blended with the electron donor polymer. This result is particularly promising since, with the proposed approach, electron-donor and electron-acceptor moieties can be collected within a single material which, at the

same time, can be applied to different surfaces avoiding the use of toxic or non-environment friendly solvents.

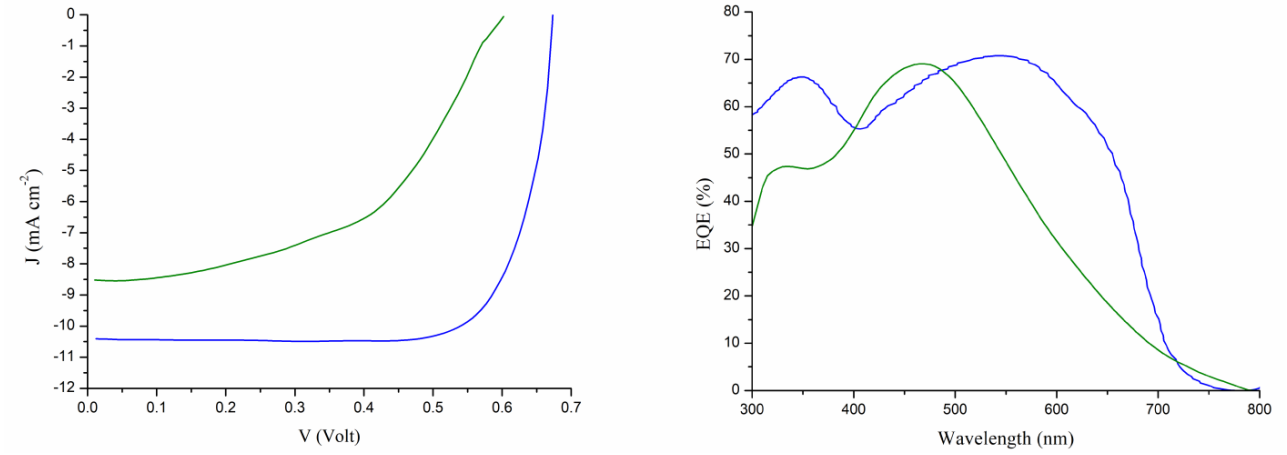

Figure 9. Current density-voltage (J/V) for the cell tested under AM 1.5 one-sun illumination (left) and EQE spectrum (right) of P[(T6Br)-*co*-(T6F)] (blue line) and P[(T6buP$^+$Br$^-$)-*co*-(T6F)] (green line).

EQE spectra of P[(T6buP$^+$Br$^-$)-*co*-(T6F)] and its copolymeric precursor P[(T6Br)-*co*-(T6F)] are reported in Figure 9. Both the obtained curves show two feature peaks and the quantum efficiency (EQE) profiles follow the trend observed in the absorption spectra of copolymers in thin film, suggesting that the harvested photons over the whole absorption spectrum can contribute to the final photo-current. The observed EQE values (EQE_{max} ~70%) indicate an efficient charge collection when the electron-acceptor material (fullerene) is directly linked to the electron-donor main chain.[2] Moreover, the introduction of ionic moieties in side chains allow to obtain a promising material with a good solubility in green solvents.

2.8. Morphological analysis

The morphological features of the active layers made by P[(T6buP$^+$Br$^-$)-*co*-(T6F)] were analyzed by FE-SEM and AFM techniques (Figure 10).

By observing the obtained images, the active layer of the single-material based cell obtained using the synthesized double-cable polymer is extremely flat and does not show any micro- or nanoscale defect or tendency to form aggregates. The results collected using these high-resolution imaging techniques confirm the absence of phase separation and the outstanding uniformity of the P[(T6buP$^+$Br$^-$)-*co*-(T6F)] structure and justify the photovoltaic performances obtained with this sample. The uniformity, stability, and absence of imperfections reveal an enhanced hierarchical nano- and microstructuration of the single-material double-cable layer driven by the proposed chemical structure optimization, which is the key for the development of highly efficient single-material organic photovoltaic solar cells.

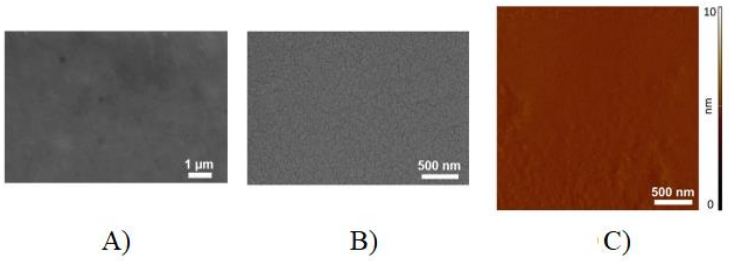

Figure 10. Morphological structure of the active layer surface of the organic photovoltaic cell. FE-SEM (A-B) and AFM topographical images (C) of P[(T6buP^{+}Br^{-})-*co*-(T6F)].

2.9. Conclusions

A new double-cable donor-acceptor polythiophene derivative was successfully synthesized using an easy and effective post-polymerization approach on a regioregular poly[3-(6-bromohexylthiophene)] (PT6Br) by means of a Grignard coupling reaction with C_{60}-fullerene and the subsequently substitution with tributylphosphine group. The successful anchorage of C_{60} to the PT6Br backbone and the complete functionalization of the remaining bromide moieties were confirmed by spectroscopy analysis, which also allowed to determine the substitution degree.

The final material showed good solubility in water, as well as methanol, and was successfully used as a single-material photoactive layer in organic photovoltaic solar cells. The copolymer sample showed good photovoltaic properties, confirming the pivotal effect of the chemical structure on the electronic characteristics of the photoactive blend. Indeed, the EA group directly linked to the polythiophenic ED backbone can reduce the distance between the two electroactive systems, making possible an effective exciton dissociation and a fast charge-transport to the electrodes. The suggested synthetic approach – leading to a single copolymeric electron-donor material which contains both water-solubilizing groups and electron-acceptor moieties at the same time – provides a simple and versatile architecture for the construction of efficient donor-acceptor intramolecular polymers.

3. Experimental section

3.1. Materials

Tributylphosphine (97%), fullerene (C_{60}, 98%), N,N-dimethylformamide (DMF, 99.8%), toluene (C_7H_8, >99.9%), diethyl ether (Et_2O, >99.5%), and chloroform ($CHCl_3$, 99.0-99.4%) were purchased from Sigma Aldrich Chemical Co. n-Heptane (99.4%) was purchased from VWR Chemicals (France). Methanol (MeOH, >99.8%) was purchased from Honeywell (Germany). Magnesium (Mg) was purchased from Merck (Germany). Diethyl ether and THF were freshly distilled before use to remove the stabilizer while all other materials were used as received. All manipulations involving moisture-sensitive reagents were performed under argon atmosphere in flame-dried glassware.

3.2. Synthesis of water-soluble double-cable copolymer

3.2.1. Synthesis of poly [3-(6-bromohexyl)thiophene-co-3-(6-fullerenylhexyl)thiophene] (P[(T6Br)-co-(T6F)]) by post-functionalization of PT6Br

103 mg (0.420 mmol) of PT6Br and 2.6 mg (0.105 mmol) of Mg were added into 5.0 mL of anhydrous THF in a first reaction system. The mixture was allowed to react under reflux for 2h, under stirring and in an inert atmosphere. Subsequently the system was cooled down to room temperature and the reaction mixture was transferred to the second reaction system containing 1.0 mL of DMF, 100 mL of anhydrous toluene and 114 mg (0.158 mmol) of fullerene C_{60}. The mixture was left to react at room temperature for 22h under vigorous stirring. After the reaction time, 1.0 mL of a solution of NH_4Cl 2.0 M was added to quench the reaction mixture. The crude product was extracted with a half-saturated solution of NaCl (2 × 100 mL) and washed with distilled water until neutrality. The organic phase was dried under vacuum and the obtained solid was recovered with 50 mL of $CHCl_3$ and slowly added to 350 mL of n-heptane. The dark brown precipitate was filtered on a PTFE membrane (0.45 μm pore size) and dried, giving 104 mg (0.357 mmol, 85% yield) of copolymer.

^{1}H-NMR (pyridine-d_5, ppm): δ 7.45 (s, 1H, Th *H*4), 7.41 (s, 1H, C_{60}-*H*), 3.57 (bm, 2H, CH_2C_{60}), 3.45 (bt, 2H, CH_2Br), 3.01 (bt, 2H, ThCH_2), 1.88-1.66 (bm, 4H, CH_2CH_2Br + $CH_2CH_2C_{60}$), 1.54-1.32 (bm, 2H, ThCH_2CH_2), 1.32-1.12 (bm, 8H, $(CH_2)_2CH_2CH_2$Br + $(CH_2)_2CH_2CH_2C_{60}$).

^{13}C-NMR (pyridine-d_5, ppm): δ 143.13 (C_{60}), 134.99, 122.96 (Thiophene *C*), 60.05 (CH_2C_{60}), 32.03 (CH_2Br), 29.20, 22.89 (aliphatic CH_2).

FT-IR (KBr, cm^{-1}): 3053, 2918, 2849, 1509, 1452, 1428, 1384, 1257, 1181, 1099, 826, 722, 644, 557, 562, 526.

3.2.2. Synthesis of poly{[3-(6-tributylphosphonium)thiophene]bromide-co-3-(6-fullerenylhexyl)thiophene} (P[(T6buP$^+$Br$^-$)-co-(T6F)]) by post-functionalization of P[(T6Br)-co-(T6F)])

100 mg (0.323 mmol) of P[(T6Br)-*co*-(T6F)] was added to 0.57 mL (2.27 mmol) of tributylphosphine dissolved in 5.0 mL of toluene in a three-neck flask, under inert atmosphere. The mixture was left to react at 90°C for 5h under stirring.

The system was cooled down to room temperature and the supernatant was removed. The dark brown-reddish solid was recovered in 30.0 mL of MeOH, washed with diethyl ether and dried under vacuum, giving 121 mg (0.252 mmol, 78% yield) of ionic copolymer.

^{1}H-NMR (pyridine-d_5, ppm): δ 7.54 (s, 1H, Th *H*4), 7.47 (s, 1H, C_{60}-*H*), 3.56 (bm, 2H, C*H*$_2$C$_{60}$), 3.07 (bm, 2H, ThC*H*$_2$(CH$_2$)$_5$C$_{60}$), 2.92 (bm, 2H, ThC*H*$_2$(CH$_2$)$_5$P$^+$), 2.79 (bm, 2H, C*H*$_2$P$^+$), 1.94-1.82 (bm, 8H, P$^+$(CH$_2$)$_3$ + C*H*$_2$CH$_2$C$_{60}$), 1.82-1.12 (m, 12H, (C*H*$_2$)$_3$CH$_2$P$^+$ + (C*H*$_2$)$_3$CH$_2$CH$_2$C$_{60}$), 1.04-0.81 (bm, 9H, C*H*$_3$).

^{13}C-NMR (pyridine-d_5, ppm): δ 143.11 (*C*$_{60}$), 134.97, 122.95 (Thiophene *C*), 60.12 (*C*H$_2$C$_{60}$), 28.59, 27.95, 24.42, 24.34, 24.30, 24.25, 24.19, 23.96 (aliphatic *C*H$_2$), 19.37 (*C*H$_2$P$^+$), 18.90 (P$^+$*C*H$_2$), 13.80 (*C*H$_3$).

^{31}P-NMR (CD$_3$OD, ppm): δ 37.84.

FT-IR (Ge, cm^{-1}): 3052, 2956, 2927, 2869, 1514, 1461, 1427, 1408, 1379, 1228, 1180, 1096, 808, 721, 576, 526.

3.3. Methods

^{1}H-NMR, ^{13}C-NMR and ^{31}P-NMR spectra were recorded on a Varian Mercury Plus 400 (400 MHz) spectrometer at room temperature using TMS as internal standard in deuterated solvents. Chemical shifts are given in ppm.

FT-IR spectra were taken on Ge or KBr disks using a Perkin Elmer Spectrum One spectrophotometer.

The molecular weight was determined by gel permeation chromatography (GPC) using THF solutions on a HPLC Lab Flow 2000 apparatus equipped with a Rheodyne 7725i injector, a Phenomenex MXL 5 μm mixed bed column and an RI K-2301 KNAUER detector. The calibration curve was recorded using monodisperse polystyrene standards.

UV-Vis spectra were collected by using Perkin Elmer Lambda 19 spectrophotometer using either around 10^{-5} M polymer solutions in spectroquality solvents in Suprasil quartz cuvettes (1 × 1 cm) or films on quartz slides drop-cast through the use of Doctor Blade.

Sample decomposition temperatures were determined by using a TA Instruments Q600 thermogravimetric analyzer (TGA) by heating from 30°C to 600°C with a ramp of 10°C min^{1} in oxidant atmosphere (air). DSC analyses were conducted by using a TA Instruments Q2000 differential scanning calorimeter (DSC) by varying the temperature from -20 to 200°C with a heating and cooling ramp of 10°C min^{-1} in a nitrogen atmosphere.

X-ray diffraction data were recorded at room temperature by using a CuKα (λ = 1.5406 Å) radiation source (Philips PW 1050) and a Bragg-Brentano diffractometer (Philips PW 1710) equipped with a graphite monochromator in the diffracted beam. The 2θ range between 2.0 and 90.0° was scanned by 881 steps of 0.1° with a counting time of 15 s for each step. The XRD characterization was carried out on polymer films on glass slides deposited by using Doctor Blade (~ 100 nm of thickness) and after an annealing treatment by heating sample films at 120°C for 45 min under vacuum.

Field emission scanning electron microscopy (FE-SEM) was performed by using a FEI Nova NanoSEM 450 microscope at an accelerating voltage of 10 kV and a working distance of about 4 mm. Samples were covered with a gold layer (8 nm of thickness), using a SC7620 Polaron mini sputter coater (Quorum Technologies Ltd., Ashford, UK) before performing the electron microscopy imaging. The sample surface topography was evaluated with an atomic force microscope (AFM, Ntegra, NT-MDT) equipped with a silicon cantilever (HA_NC, NT-MDT, tip radius of 10 nm and spring constant of 12 N/m). Measurements were performed in a semi-contact mode with a resonance frequency of around 150 kHz and a scanning rate of 0.5 Hz, while the size of the scanned sample was 2.75 μm × 2.75 μm per image.

3.3.1. Solar cells

The ITO glass substrate (2 × 2 cm, surface resistance 21 Ω/sq) was etched on one side by using a 10% wt aqueous solution of HCl and heated at 60°C for 10 min, in order to obtain an area of 1.5 × 1 cm covered by indium tin oxide. The glass was then cleaned using distilled water, 2-propanol and dried with a nitrogen flow (final resistance12 Ω/sq). Poly(3,4-ethylenedioxythiophene):polystyrene sulfonic acid (PEDOT:PSS, 2.8 wt% dispersion in water, viscosity 20 cps) was diluted 1:1 v/v with 2-propanol, sonicated for 15 min using an ultrasonic bath (Elmasonic S 30H), filtered on a Gooch G2 and the resulting solution (viscosity 12 cps) deposited over the previously treated ITO glass with the doctor blading technique using a Sheen Instrument Model S265674, leaving only a small (0.5 × 1 cm) area uncovered at the opposite side of the previously etched area. The PEDOT:PSS film was heated in a Buchi GKR-50 glass oven at 120°C for 90 min under vacuum (10^{-3} mmHg).

A solution made by mixing 5.0 mg of P[(T6buP^{+}Br^{-})-*co*-(T6F)] in 0.5 mL of methanol was sonicated for 15 min and deposited by using Doctor Blade on the slide in order to cover the PEDOT:PSS layer. The sample was then annealed in the glass oven under vacuum (10^{-3} mmHg) at 120°C for 45 min.

Finally, a thin film of Al (electrode, 50 nm of thickness) was deposited over the polymeric layer through a shadow mask using an Edwards 6306A coating system operating at 10^{-6} mmHg. The active area of the cell was 1 × 1 cm^2. The current-voltage characteristics were measured in air using a Keithley 2401 source meter under the illumination of an Abet Technologies LS150 Xenon Arc Lamp Source AM 1.5 Solar Simulator (100 mW/cm^2) calibrated with an ILT 1400-BL photometer.

The structure of the final devices was made of: ITO (80 nm)/PEDOT:PSS (100 nm)/active layer (150 nm)/Al (50 nm). The solar cell spectral response was measured using a 7-SC Spec III Modularized Solar Cell Spectral Test System (SevenStar Optics, Beijing, PRC). Layer thickness was measured using a FTPAdvances FTPadv-2 Film Thickness Probe (Sentech GmbH, Germany) equipped with the FTPExpert software.

References

1. M. Lanzi, E. Salatelli, T. Benelli, D. Caretti, L. Giorgini, F. P. Di-Nicola, *J. Appl. Polym. Sci.*, **2015**, *132*, 42121.
2. M. Lanzi, E. Salatelli, M. Marinelli, F. Pierini, *Macromol. Chem. Phys*., **2020**, *221*, 1900433.
3. C. Duan, K. Zhang, C. Zhong, F. Huang, Y. Cao, *Chem. Soc. Rev.*, **2013**, *42*, 9071-9104.
4. M. Lanzi, E. Salatelli, L. Giorgini, A. Mucci, F. Pierini, F. P. Di-Nicola, *Eur. Polym. J.*, **2017**, *97*, 378-388.
5. F. Huang, H. Wu, Y. Cao, *Chem. Soc. Rev.*, **2010**, *39*, 2500-2521.
6. M. Lanzi, E. Salatelli, L. Giorgini, M. Marinelli, F. Pierini, *Polymer*, **2018**, *149*, 273-285.
7. S. Hladysh, D. Bondarev, J. Vohlídal, D. Vrbata, J. Zedník, *Eur. Polym. J.*, **2016**, *83*, 367-376.
8. S. Miyanishi, K. Tajima, K. Hashimoto, *Macromolecules*, **2009**, *42*, 1610-1618.
9. R. H. Mitchell, Y. Lai, *J. Org. Chem.*, **1979**, *44*, 4733-4735.
10. R. D. McCullough, *Adv. Mater.*, **1998**, *10*, 93-116.
11. M. C. Stefan, M. P. Bhatt, P. Sista, H. D. Magurudeneiya, *Polym. Chem.*, **2012**, *3*, 1693-1701.
12. R. S. Loewe, P. C. Ewbank, J. Liu, L. Zhai, R. D. McCullough, *Macromolecules*, **2001**, *34*, 4324-4333.
13. A. C. Mayer, M. F. Toney, S. R. Scully, J. Rivnay, C. J.; Brabec, M. Scharber, M. Koppe, M. Heeney, I. McCulloch, M. D. McGehee, *Adv. Funct. Mater.*, **2009**, *1*9, 1173-1179.

CHAPTER VII: DEVICE OPTIMIZATION THROUGH THE USE OF INTERLAYERS

1. Introduction

1.1 Overview

In order to improve hole extraction and collection combined with an enhancement of the power conversion efficiency (PCE) of bulk-heterojunction (BHJ) solar cells, polythiophene electrolytes with different pendant cationic moieties can be used as interlayers between the photoactive and cathode films with the aim to modify the interactions between layers at interface.[1-6]

Cationic conjugated polyelectrolyte (CPE) acts as an electron transporting layer (ETL) and their presence between active layer and an electrode in a solar cell can modify the dipole moment at the interface.[7] The increase of polarity seems to improve the final performance of the device by an easier charge transport and collection with a reduced recombination due to the better charge carriers mobility.[8-10] Moreover, several recent studies report the use of conjugated polyelectrolytes - which combine the presence of a delocalized π–conjugated backbone with pendant ionic groups - as promising cathode interface modifiers.[11,12]

1.2. Aim of the chapter

In order to improve photovoltaic performances and to prepare more green and eco-friendly devices, three polythiophene derivatives were synthetized and investigated as interfacial cationic conjugated polyelectrolyte (CPE) layers for halogen-free bulk heterojunction (BHJ) polymeric solar cells, based on an alcohol-soluble electron-donor polymer (poly[3-(6-diethanolamino)-hexyl thiophene]) and a water-soluble electron-acceptor fullerene derivative (C_{60}-Ser). The insertion of the CPE interlayer between the active layer and the aluminum cathode could lead to the enhancement of power conversion efficiency (PCE) of the final device and optimization of the morphology of the layers.

The structural properties were investigated by spectroscopy techniques (^{1}H-NMR, ^{13}C-NMR, ^{31}P-NMR, FT-IR, UV-Vis), thermogravimetric analysis (TGA), differential scanning calorimetry (DSC), X-ray diffraction (XRD), atomic force microscopy (AFM) and external quantum efficiency (EQE). Finally, the final materials were tested as cathode interlayers in organic solar devices prepared with halogen-free solvents.

This chapter is a readjustment of "Effects of water/alcohol soluble cationic polythiophenes as cathode interlayers for eco-friendly solar cells" D. Quadretti, M. Marinelli, E. Salatelli, F. Pierini, A. Zanelli, M. Lanzi, *Macromolecular Chemistry and Physics*, 2023, 2200422.

The atomic force microscopy (AFM) and external quantum efficiency (EQE) measurements were carried out in collaboration with Prof. Filippo Pierini of Department of Biosystem and Soft Matter – Institute of Fundamental Technological Research, Polish Academy of Science (Warsaw, Poland).

The electrochemical measurements (CV) were carried out in collaboration with National Research Council (CNR) - Institute for Organic Synthesis and Photoreactivity (ISOF), Bologna (BO), Italy.

The synthesis of poly-[3(6-tributylphosphonium-hexyl-1-oxy)thiophene]bromide (PTO6buP^{+}Br^{-}) and the respective synthetic results reported in this chapter were performed by Riccardo Zuppiroli under the supervision of the author, or by the author herself.

2. Results and discussion

2.1. Synthesis

With the aim to prepare a completely eco-friendly photovoltaic device (photoactive blend and interlayers), the electron-donor material (ED) was synthesized through the post-functionalization of regioregular poly[3-(6-bromohexyl)thiophene] (rrPT6Br) with diethanolamine (Scheme 1), giving the corresponding poly[3-(6-diethanolamino)-hexyl thiophene] (PT6N(EtOH)$_2$) as a neutral water-alcohol-soluble polymer.[13] The most commonly ED used in BHJ solar cells is poly-3-hexylthiophene (P3HT) but results to be insoluble in polar solvents.

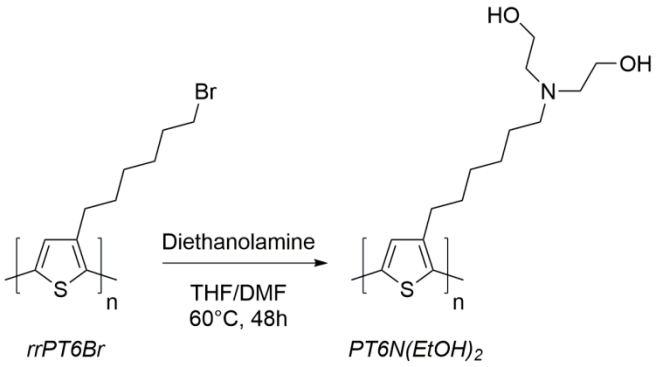

Scheme 1. Synthetic route to obtain PT6N(EtOH)$_2$.

In case of interlayers, the synthetic approach followed was based on polymerization of monomers - in the same conditions - through oxidative reaction with $FeCl_3$ and subsequent post-functionalization with the same substituent (tributylphosphine), as depicted in Scheme 2.

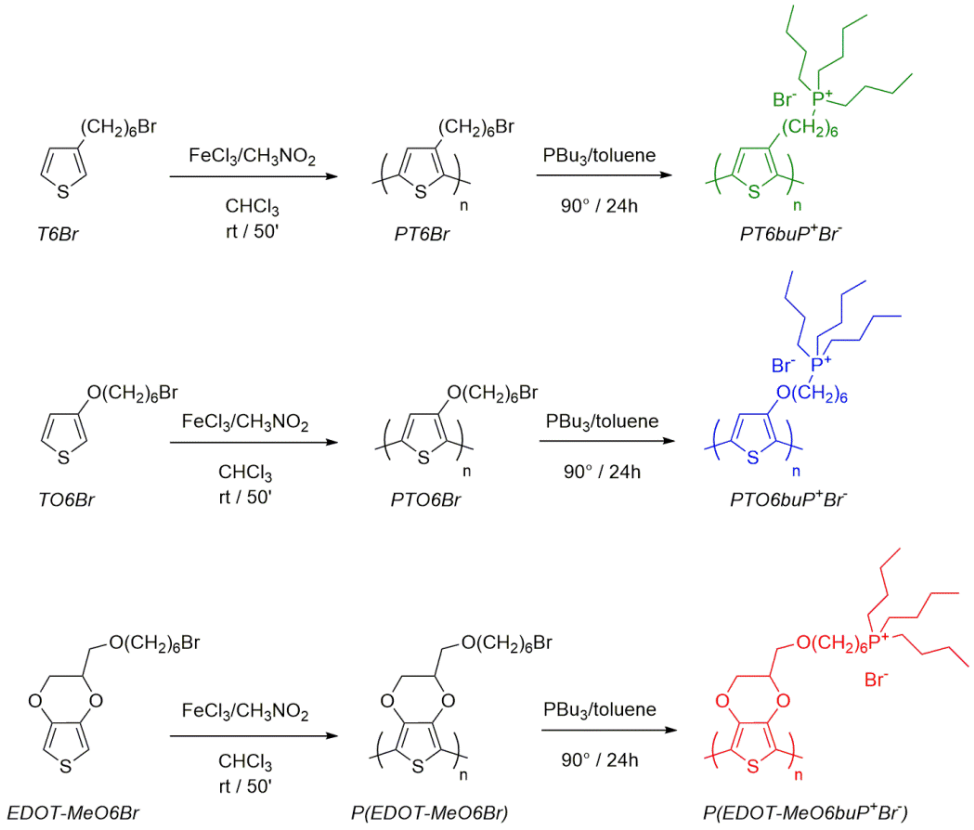

Scheme 2. Synthetic routes to obtain interlayers PT6buP$^+$Br$^-$, PTO6buP$^+$Br$^-$ and P(EDOT-MeO6buP$^+$Br$^-$).

At first, starting from commercially available reagents the monomers 3-(6-bromohexyl)thiophene (T6Br), 3-(6-bromohexyl-1-oxy)thiophene (TO6Br) and 6-bromohexyl-1-oxymethyl-EDOT (EDOT-MeO6Br) were synthetized through several synthetic steps.

In detail, the monomer 3-(6-bromohexyl)thiophene was synthetized by the protection of target alkylic chain (1,6-dibromohexane) with p-methoxyphenol group with subsequent cross-coupling reaction with 3-bromothiophene and finally deprotection, as previously reported in Chapter II.

With regard to the monomer 3-(6-bromohexyl-1-oxy)thiophene, the syntheses involved were mainly the substitution reaction on 1,6-hexandiol to obtain 1-bromo-6-hexanol[14] and the subsequent transetherification reaction with 3-methoxythiophene.

In case of 6-bromohexyl-1-oxymethyl-EDOT, the synthesis involved the use of 1,6-dibromohexane for the transetherification reaction in situ with hydroxymethyl-EDOT in presence of tetrabutylammonium bromide (TBAB).[15]

The synthetized monomers T6Br,[16] TO6Br and EDOT-MeO6Br were then allowed to react with $FeCl_3$ in dry chloroform for 50 minutes under inert conditions, obtaining the corresponding polymers PT6Br, PTO6Br and P(EDOT-MeO6Br). The choice to use a non regiospecific polymerization procedure to obtain CPEs was based on the purpose to preserve their solubility in polar solvents, avoiding clustering or crystallization phenomena.

Finally, polymeric precursors were post-functionalized with tributylphosphine at 90°C for 24 hours leading to the complete post-functionalization of side-chain substituents and giving an optimal solubility of the resulting materials in polar solvents.[17,18]

Table 4. Polymers' characteristics.

	Reaction Yield (%)	***HT (%)*** [a]	***Mn (kDa)***	***PDI***
rrPT6Br	23	95	9.0 [b]	1.3 [b]
PT6N(EtOH)$_2$	35		9.9 [c]	1.3 [c]
PT6Br	56	85	9.8 [b]	1.9 [b]
PT6buP$^+$Br$^-$	97		17.9 [c]	1.9 [c]
PTO6Br	45	68	2.3 [b]	1.8 [b]
PTO6buP$^+$Br$^-$	93		4.1 [c]	1.8 [c]
P(EDOT-MeO6Br)	31	81	4.3 [b]	1.7 [b]
P(EDOT-MeO6buP$^+$Br$^-$)	88		6.9 [c]	1.7 [c]

[a] Determined by ^{1}H-NMR; [b] Determined by GPC chromatography; [c] Calculated from the molecular mass of the corresponding precursors.

The average molecular weights were determined through GPC analysis of the soluble fractions of the synthesized precursor polymers (Table 1). The comparison between rrPT6Br and PT6Br and the other two polymers shows the obtainment of lower molecular weights for the latter, and this can be ascribed to the presence of alkoxy-groups grafted on the thiophene ring. In this case, the electron-donating effect of the oxygen stabilizes the radicals involved in the oxidative polymerization thus favoring the formation of shorter polymeric chains.[19]

2.2. NMR characterization

All the synthesized products and polymeric materials were characterized by NMR spectrometry (^{1}H-NMR, ^{13}C-NMR, and ^{31}P-NMR for interlayers) to confirm their chemical structure.

Taking into account only polymeric precursors and corresponding post-functionalized polymers, it's possible to verify the success of substitution reactions with diethanolamine and tributylphosphine for PT6N(EtOH)$_2$ and CPEs, respectively.

Although different deuterated solvents were used, the comparison between rrPT6Br and PT6N(EtOH)$_2$ spectra (Figure 1) shows the effective substitution of bromide group with diethanolamine due to the disappearance of signal ascribable to the methylenic protons near the halide group.

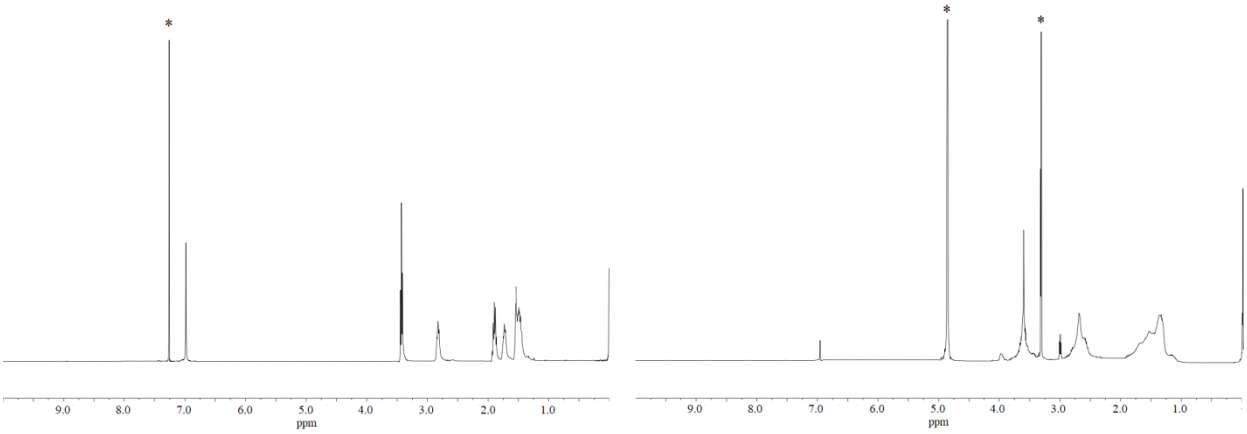

Figure 1. ^{1}H-NMR spectra of PT6Br (left) and PT6N(EtOH)$_2$ (right). Asterisk: solvent resonances ($CDCl_3$ and CD_3OD).

The analysis of ^{1}H-NMR spectra of cationic polythiophenes (Figure 2) shows the total absence of methylenic protons in α position to -Br group evidencing the successful post-functionalization of precursors with tributylphosphine. In particular, the presence of a broad multiplet at 2.36-2.15 ppm, 2.31-1.99 ppm, and 2.24 ppm, for PT6buP^{+}Br^{-}, PTO6buP^{+}Br^{-} and P(EDOT-MeO6buP^{+}Br^{-}), respectively, can be ascribed to the eight methylenic protons near to the phosphine moiety, thus confirming the substitution of bromide group.

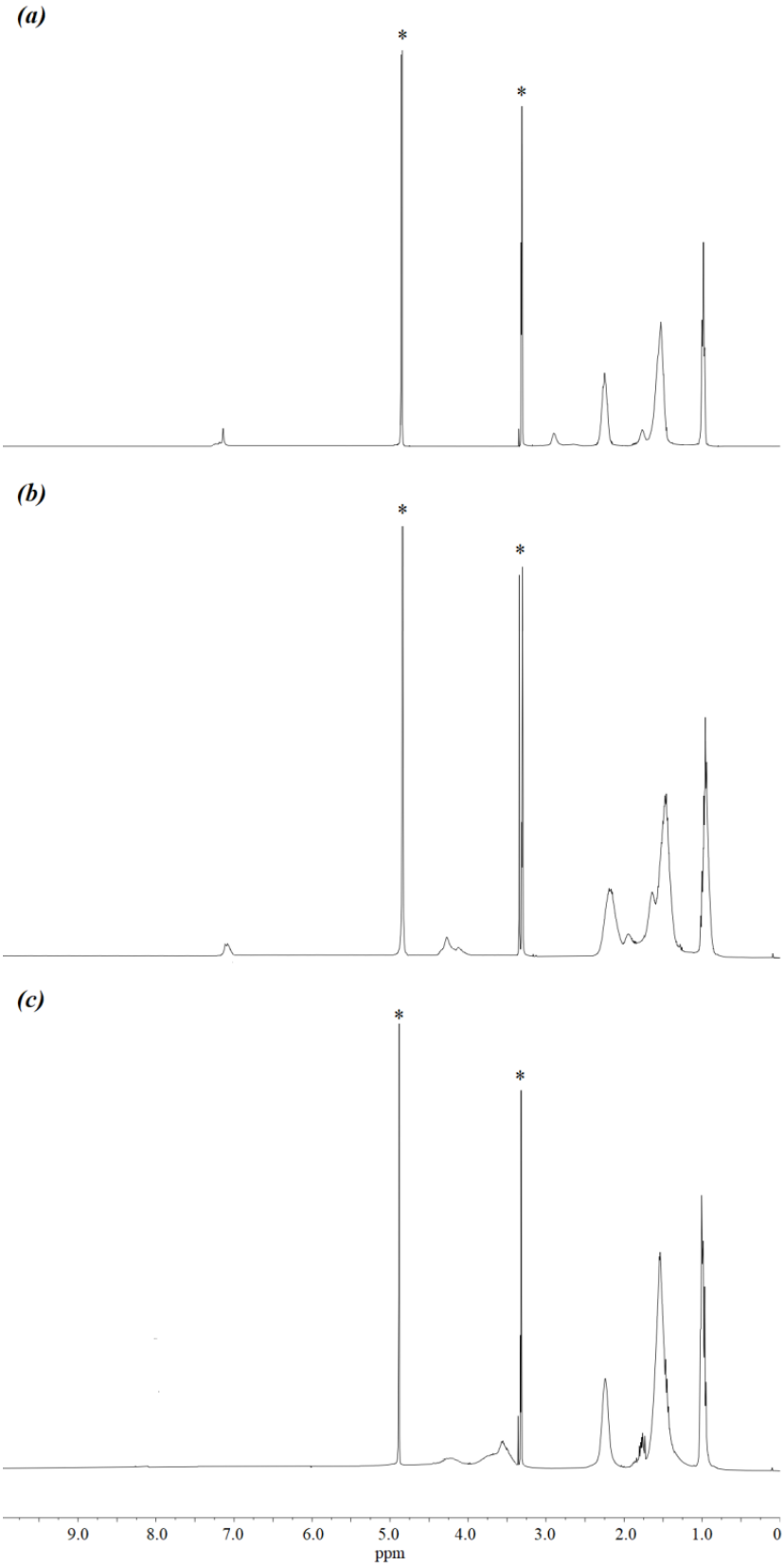

Figure 2. ^{1}H-NMR spectra of PT6buP^{+}Br^{-} (*a*), PTO6buP^{+}Br^{-} (*b*) and P(EDOT-MeO6buP^{+}Br^{-}) (*c*). Asterisk: solvent resonance (CD_3OD).

The occurrence of the post-functionalization of precursors was further verified by ^{31}P-NMR spectroscopy (Figure 3) also evidencing the absence of unreacted tributylphosphine and the complete substitution with phosphonium, as previously verified by ^{1}H-NMR.

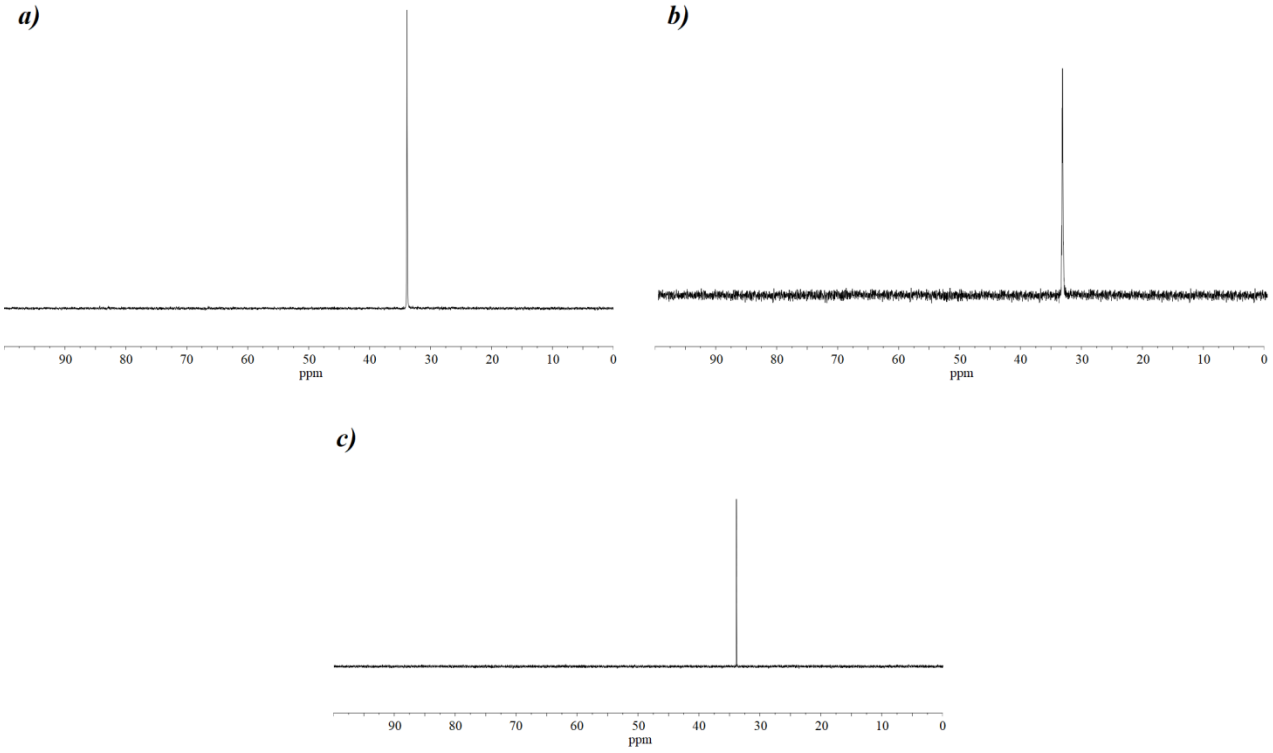

Figure 3. ^{31}P-NMR spectra of PT6buP^{+}Br^{-} (*a*), PTO6buP^{+}Br^{-} (*b*) and P(EDOT-MeO6buP^{+}Br^{-}) (*c*).

2.3. FT-IR characterization

FT-IR spectroscopy further confirms the chemical structure of all synthesized materials. The FT-IR bands of photoactive material PT6N(EtOH)$_2$ with their assignments are shown in Table 2 while IR spectra of interlayers PT6buP^{+}Br^{-}, PTO6buP^{+}Br^{-}, P(EDOT-MeO6buP^{+}Br^{-}) are reported in Figure 4.

Table 2. Main IR absorption bands (cm^{-1}) of rrPT6Br and PT6N(EtOH)$_2$.

rrPT6Br	***PT6N(EtOH)$_2$***	***Assignments***
-	3317	υ -OH
3052	3055	υ C-H β thiophene
2928	2923	υ_{as} -CH_2- side chain
2855	2852	υ_{sym} -CH_2- and –CH_3
1511	1508	υ_{as} -C=C- thiophene
1459	1455	υ_{sym} C=C thiophene
1257	1259	υ C-C thiophene-thiophene
1089	1075	δ –CH thiophene
-	1028	υ C-N (alkyl amine)
832	799	γ C-H thiophene 2, 3, 5-trisubstituted
728	726	rocking -CH_2-
645, 562	-	*υ* C-Br aliphatic

υ = stretching; γ = out of plane bending; δ = in-plane bending.

As already underlined by ^{1}H-NMR, the evidence of the success of reaction to obtain the photoactive material is given by the disappearance of bands at 645 and 562 cm^{-1} combined with the presence of a band ascribable to C-N bond stretching.

Analyzing the IR spectra of PT6buP$^+$Br$^-$, PTO6buP$^+$Br$^-$ and P(EDOT-MeO6buP$^+$Br$^-$) (Figure 4), the presence of bands ascribable to phosphonium group (~1379 cm^{-1}) and the absence of peaks ascribable to -Br terminal group (~ 640 and 560 cm^{-1}) confirm the successful reaction of post-functionalization with the tributylphosphine group.

The broad band at ~ 3400 cm^{-1} (O-H stretching) is due to the high hygroscopicity of synthesized polymers thus confirming their high affinity for polar solvent (water).

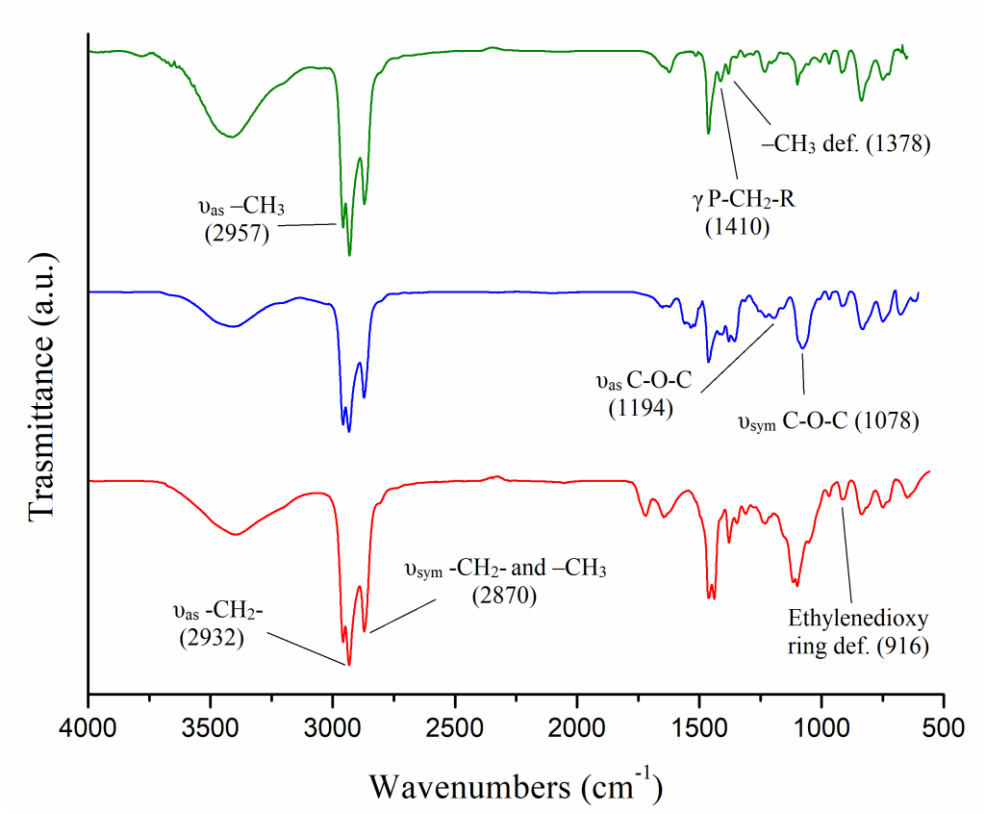

Figure 4. FT-IR spectra of PT6buP$^+$Br$^-$ (green line), PTO6buP$^+$Br$^-$ (blue line) and P(EDOT-MeO6buP$^+$Br$^-$) (red line).

2.4. Thermal properties

The thermal stability of CPEs (PT6buP$^+$Br$^-$, PTO6buP$^+$Br$^-$ and P(EDOT-MeO6buP$^+$Br$^-$)) and photoactive material (PT6N(EtOH)$_2$) were evaluated by TGA analysis under oxidizing atmosphere (air), at a heating scan rate of 10°C min^{-1} and up to 600°C (Figure 5 and Table 3).

In the TGA curves of all cationic interlayers, the three main weight losses can be ascribed to the elimination of phosphonium group (up to 200°C), to the aliphatic side chain scission (280-310 °C) and to the macromolecular backbone combustion (up to 370 °C), respectively. In the case of PT6N(EtOH)$_2$, the first loss of weight (~10%) is ascribable to diethanolamine group in pendant chain. In case of interlayers, the percentage of first loss of weight changes from 20% to 40%. The different behavior is ascribable to the absence or presence of one or more oxygen atoms in polymeric unit, which in oxidant atmosphere would result to be emphasized.

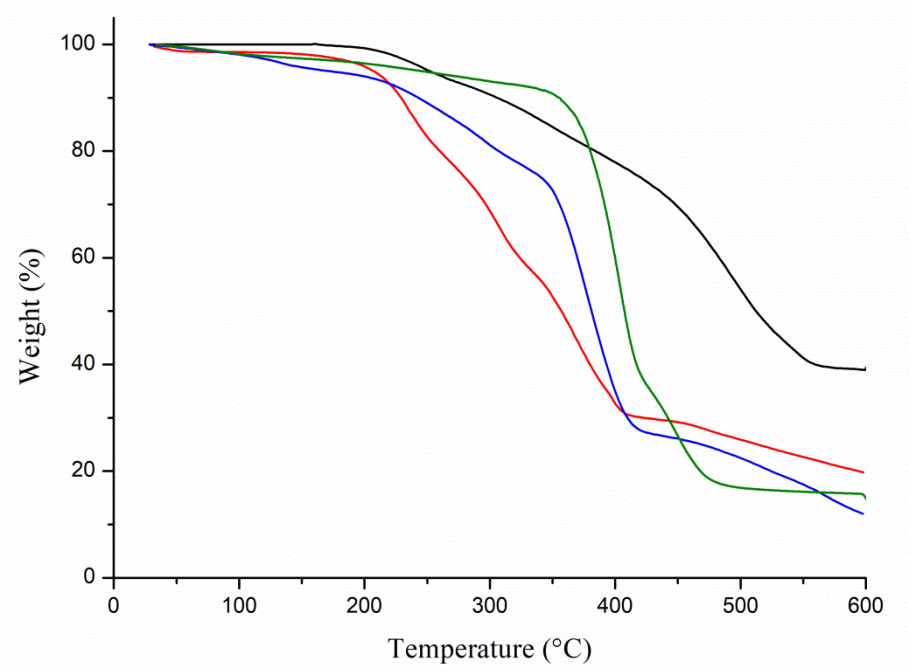

Figure 5. Thermograms of PT6N(EtOH)$_2$ (black line), PT6buP$^+$Br$^-$ (green line), PTO6buP$^+$Br$^-$ (blue line) and P(EDOT-MeO6buP$^+$Br$^-$) (red line).

The presence of oxygen atom(s) determines a decrease of thermal stability (i.e. decomposition temperature) of polymers, as expected. However, the synthesized samples may be considered stable enough to be used as photoactive materials in organic photovoltaic devices since the temperatures at which they begin to degrade are higher than that of use.

Thermal properties of polymers were evaluated by DSC analyses which were carried out under nitrogen atmosphere with a heating ramp of 10°C min^{-1} from -20°C up to 200°C (Table 3 and Figure 6).

Table 3. Decomposition (T_d) and glass-transition (T_g) temperatures of polymers.

	T_d (°C) [a]	$T_{d,max}$ (°C) [b]	T_g (°C) [c]
PT6N(EtOH)$_2$	216	253	70
PT6buP$^+$Br$^-$	373	402	55
PTO6buP$^+$Br$^-$	217	250	35
P(EDOT-MeO6buP$^+$Br$^-$)	207	237	32

[a] Determined by the onset point of the first inflection; [b] calculated from the first derivative of the weight/temperature curve; [c] evaluated by DSC analysis.

All polymeric samples show an endothermic flexure, ascribable to the glass transition temperature (T_g). The absence of melting and crystallization phenomena is due to the amorphous nature of materials: the steric hindrance of tributylphosphonium group linked to the side chains decreases the conformational order of polymers - not regioregular - with a consequent loss of crystallinity of the examined materials.

Moreover, the possibility to form inter- or intra-chain hydrogen bonds when the hydroxylamine substituent is employed increases the T_g value of PT6N(EtOH)$_2$ sample even if any clear endothermic melting peak cannot be found.

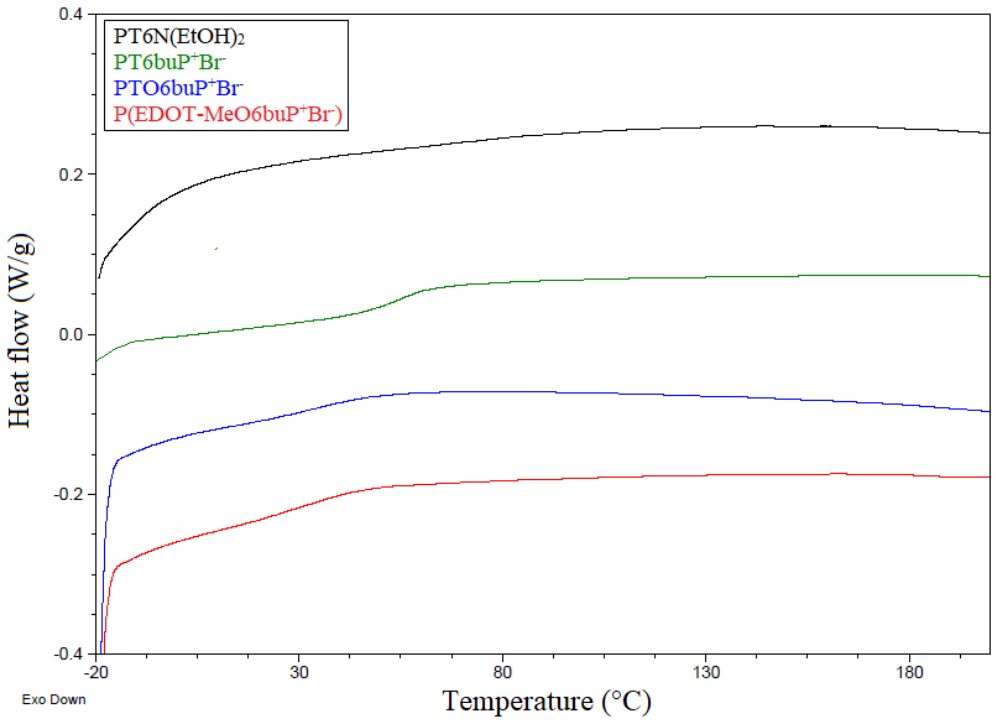

Figure 6. DSC curves of interlayers and photoactive material.

2.5. Optical properties (UV-Vis characterization)

In order to evaluate the optical properties, interlayers and photoactive material were analyzed by UV-Vis spectroscopy in solution of different polar solvents (i.e. alcohols and water) and in solid state (film on quartz slides). The normalized absorption spectra obtained in solution and film are reported in Figure 7 and Figure 8, respectively, and both maximum absorption wavelengths and solubility in different solvents are reported in Table 4.

Table 4. Wavelengths of maximum absorption and solubility of synthetized polymers in several polar solvents.

	Solvent	***λ_{max} solution 10^{-5}M (nm)***	***λ_{max} film (nm)***	***Solubility (mg/mL)***
PT6N(EtOH)$_2$	Methanol	459	551	26
	Ethanol	443	476	
	MeOH/H_2O (1:1)	509	489	<5
	EtOH/H_2O (1:1)	490	487	
PT6buP$^+$Br$^-$	Methanol	425	445	>50
	Ethanol	426	444	
	Water	447	444	35
PTO6buP$^+$Br$^-$	Methanol	518	518	>50
	Ethanol	518	514	37
	Water	510	509	17
P(EDOT-MeO6buP$^+$Br$^-$)	Methanol	347, 428, 470	342, 432, 473	10
	Ethanol	348, 426, 469	337, 429, 471	7
	Water	347, 431, 472	329, 429	5

The analysis of PT6N(EtOH)$_2$ spectra shows that the optical behavior is different in solution and in solid state – the range of absorption increases and there is a bathochromic shift - due to the change in the conformational order of polymeric chains. In this case, the maximum absorption wavelength shifts from a minimum of 443 nm (solution of ethanol) up to a maximum of 551 nm (film from methanol), suggesting that this polymer is able to achieve highly planar conformations with a high electronic delocalization when in the solid state. Enhanced planarizing interactions can also be ascribed to inter- and intrachain hydrogen bonds, thus leading to an extended conjugation length for this polymer. This behavior is a crucial requirement in view of the final application as electron-donor material in the photoactive layer of polymeric solar cells. On the contrary, the comparison of UV-Vis spectra of cationic polymers (CPEs) in solution and in solid state shows only modest shifts of maximum absorption wavelengths.

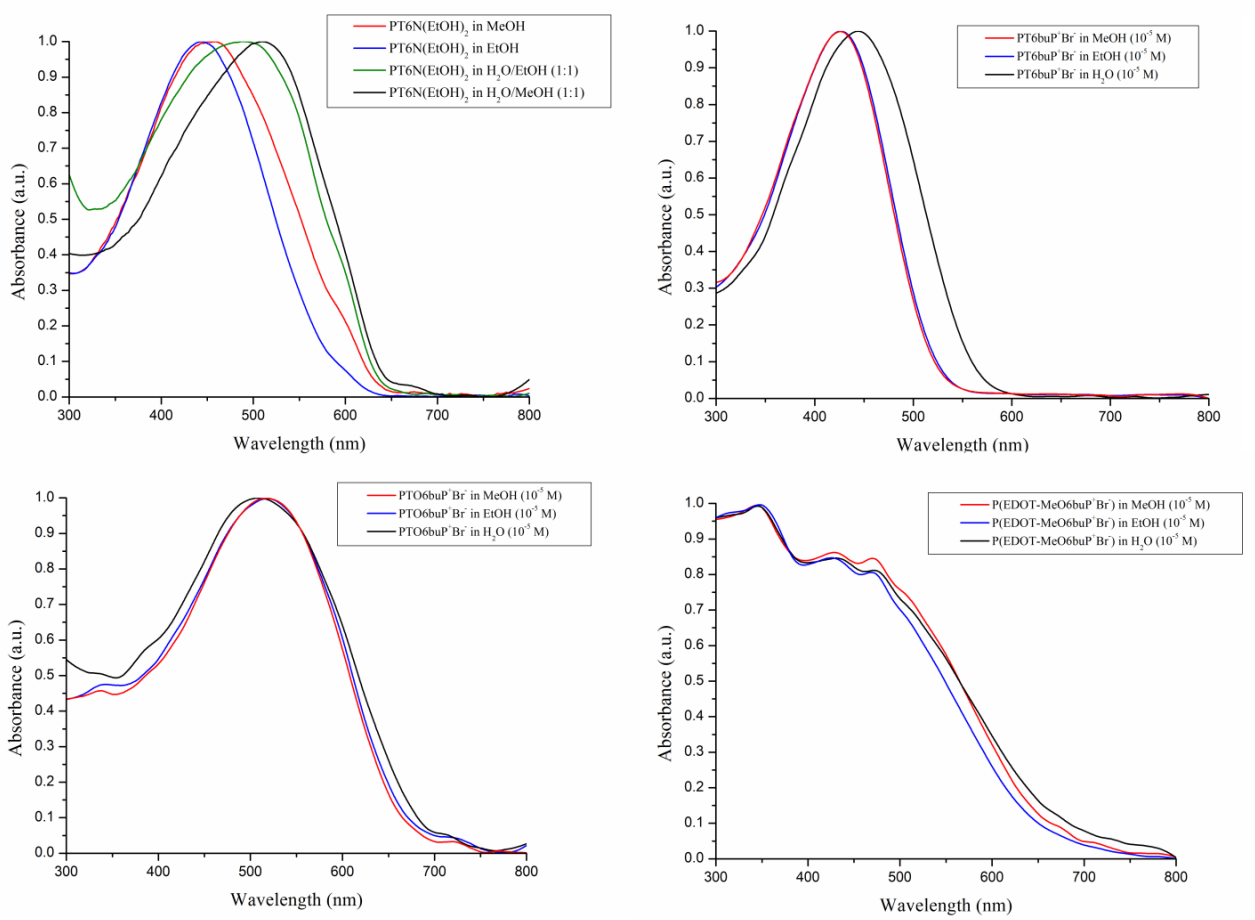

Figure 7. Normalized UV-Vis spectra of polymers in solution of several polar solvents.

The UV-Vis spectral profiles of cationic polymers are almost independent from the solvents employed for their dissolution and subsequent deposition. In view of this, ethanol was used as filming solvent for the preparation of cell interlayers due to its low toxicity and with the aim of obtaining more sustainable and eco-friendly devices. Furthermore, an interesting behavior can be observed for P(EDOT-MeO6buP^{+}Br^{-}) sample, which shows structured profiles with three absorption maxima both in solution and in film spectra, suggesting the coexistence of three main chromophores at different conjugation lengths.

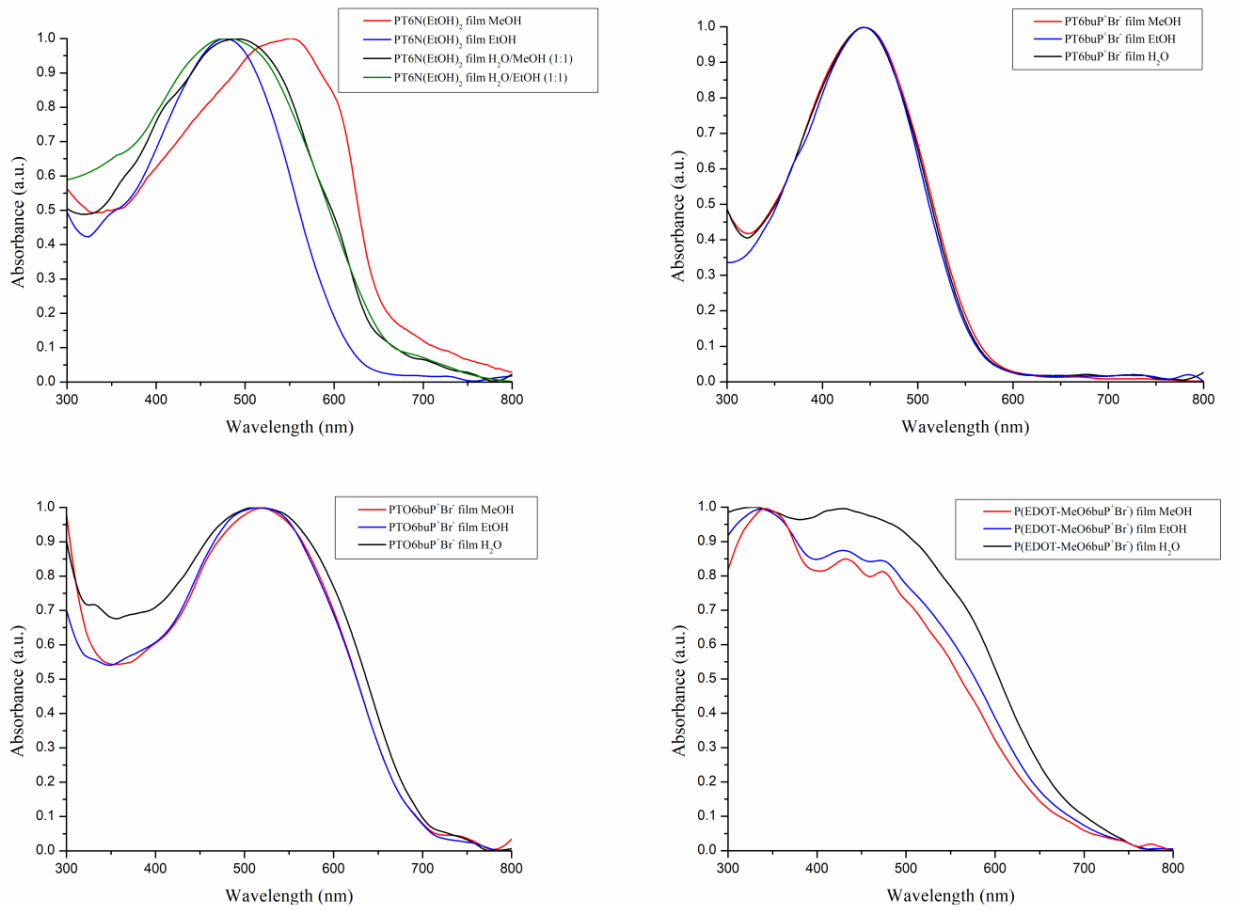

Figure 8. Normalized UV-Vis spectra of polymers drop cast from solution of different polar solvents.

2.6. Electrochemical properties (CV)

The potentials of synthetized ionic interlayers and neutral photoactive layer were evaluated by cyclic voltammetry (CV) and related curves are reported in Figure 9. The electrochemical parameters of materials in thin films - obtained by drop-casting their solution in methanol on Pt electrodes – are summarized in Table 5.

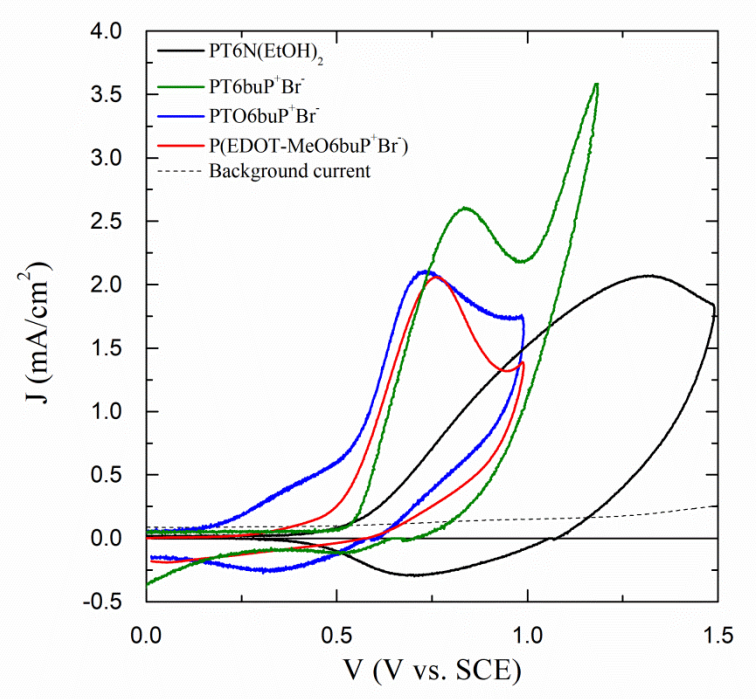

Figure 9. Cyclic voltammograms of photoactive material and interlayers.

In detail, the electrochemical properties of the synthetized polymers are quite similar between them. However, PTO6buP$^+$Br$^-$ and P(EDOT-MeO6buP$^+$Br$^-$) show a lower oxidation potential when compared to the other two polymers (Table 5). This can be ascribed to the electron-donating effect of the oxygen atom(s) directly linked to the thiophenic ring. Moreover, the latter showed also a reduced optical bandgap, which could originate both from the electronic effect of the heteroatom on the polyconjugated backbone and the reduced distortion of the main chain.

Table 5. Electrochemical and optical properties of synthesized polymers in thin film.

	E_{ox} (V) [a]	HOMO (eV)	LUMO (eV) [b]	$E_{g,\,opt}$ (eV) [c]
PT6N(EtOH)$_2$	+0.57	-4.81	-2.93	1.88
PT6buP$^+$Br$^-$	+0.56	-4.80	-2.61	2.19
PTO6buP$^+$Br$^-$	+0.47	-4.71	-2.91	1.80
P(EDOT-MeO6buP$^+$Br$^-$)	+0.50	-4.74	-2.90	1.84

[a] Onset potential of anodic scan; [b] The LUMO energy levels were calculated from the HOMO levels and the optical bandgaps; [c] Optical bandgap in film.

While the energy levels of the highest occupied molecular orbitals (HOMO) of the four polymers were evaluated by CV according to the following equation:

$$\text{HOMO (eV)} = -e\,(E_{ox} + 4.24)$$

the energy level of lowest unoccupied molecular orbital (LUMO) was evaluated indirectly from the values of HOMO and the optical bandgaps (E_g opt) obtained from the UV–Vis spectra of the films, following the equation:

$$LUMO\ (eV) = HOMO + E_g$$

Interestingly, the photoactive polymer and the cationic interlayers exhibited similar energy levels and bandgaps, suggesting comparable degrees of electronic delocalization through the polyconjugated backbone that can help the charge extraction.

The obtained LUMO energy levels values are schematically reported in Figure 10.

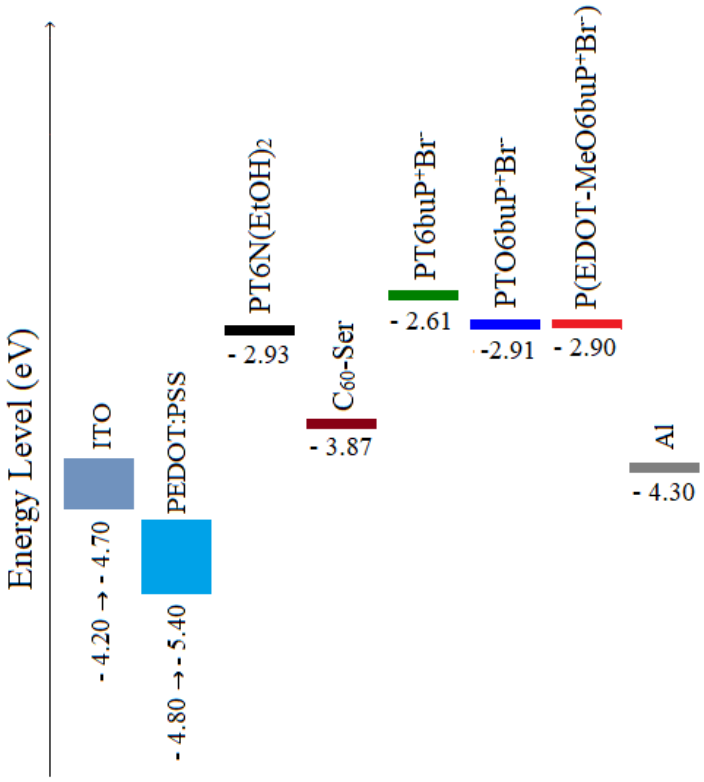

Figure 10. Energy-level alignment of OPVs layers (ITO, PEDOT:PSS and Al)[20] and comparison between PT6N(EtOH)$_2$:C_{60}-Ser and interlayers.

2.7. XRD diffraction

X-ray diffraction (XRD) patterns of polymer films cast on glass slides are shown in Figure 11.

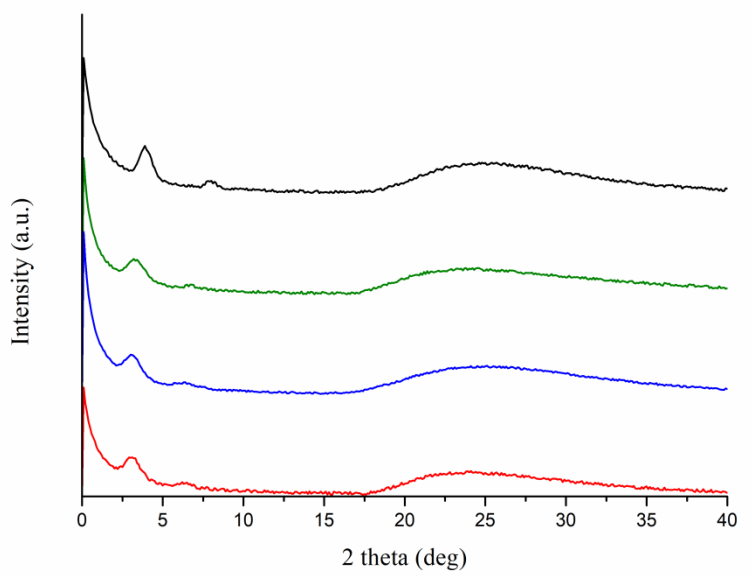

Figure 11. X-ray diffractograms of PT6N(EtOH)$_2$ (black line), PT6buP$^+$Br$^-$ (green line), PTO6buP$^+$Br$^-$ (blue line) and P(EDOT-MeO6buP$^+$Br$^-$) (red line).

All the examined samples show a diffractogram pattern ascribable to an essentially amorphous polymer according to the absence of evident melting/crystallization peaks, as already evidenced in the thermal analysis section.

They only provide for a weak diffraction peak in the 2θ range from 3.11 to 3.93 degrees (Table 6), a second one from 6.29 to 7.95 degrees, and a broad amorphous halo at wider angles.

Table 6. Structural parameters of polymers.

	Low-angle diffractions (degrees)	***High-angle diffractions (degrees)***	***On plane Th chains distances (Å)***	***Planes stacking distances (Å)***
PT6N(EtOH)$_2$	3.93; 7.95	-	22.4	-
PT6buP$^+$Br$^-$	3.31; 6.72	-	26.6	-
PTO6buP$^+$Br$^-$	3.13; 6.33	-	28.2	-
P(EDOT-MeO6buP$^+$Br$^-$)	3.11; 6.29	-	28.4	-

2.8. Photovoltaic properties

Cationic water/alcohol soluble polymers PT6buP$^+$Br$^-$, PTO6buP$^+$Br$^-$, P(EDOT-MeO6buP$^+$Br$^-$) were tested as electron transport interlayers for the building up of halogen-free BHJ solar cells based on a photoactive layer composed by PT6N(EtOH)$_2$ and C_{60}-Ser, a fullerene derivative previously synthetized (Chapter IV).[21] Photovoltaic properties were investigated by adopting the device configuration ITO/PEDOT:PSS/photoactive layer/CPE/Al. PT6N(EtOH)$_2$ was used in a 1:1

weight ratio blend with C_{60}-Ser, while CPEs were filmed from an ethanol solution (2.0 mg/mL). Photovoltaic performance parameters are shown in Table 7, while J/V curves are reported in Figure 12.

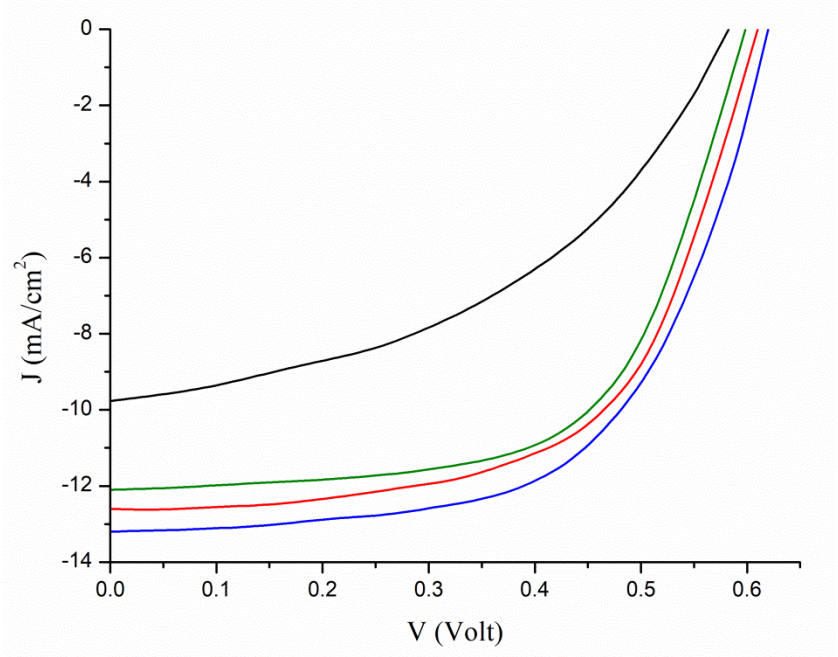

Figure 12. Current density-voltage (J/V) for the best-performing cells tested under AM 1.5 one-sun illumination. PT6N(EtOH)$_2$:C_{60}-Ser without (black line) and with interlayer: PT6buP$^+$Br$^-$ (green line), PTO6buP$^+$Br$^-$ (blue line) and P(EDOT-MeO6buP$^+$Br$^-$) (red line).

Taking as a reference the photovoltaic device composed by the photoactive blend PT6N(EtOH)$_2$:C_{60}-Ser without any cationic interlayer, the photovoltaic parameters obtained underline that devices prepared with CPE interlayers notably increase them, and this is particularly true examining the current density. The effect of CPE interlayers on the interface between the cell active layer and the Al cathode can be ascribed to the interactions between PT6N(EtOH)$_2$ and the cationic polymer, which enhances the electron injection to the Al cathode.[22] Moreover, the enhancement of V_{OC} (Table 7) can be ascribed to the reduction in the electrode (Al) work function owing to the formation of an interfacial dipole between the cathode interlayers and the metal, induced by the presence of the ionic salts in the side chains of the employed cationic polythiophenes. Indeed, at cathodes with an interfacial layer composed of a tetra-alkylphosphonium-bromide polythiophene-derivative, the ohmic contact with the electrons transported from the photoactive layer to the metal electrode is enhanced.[23]

Table 7. Short-circuit current density (J_{SC}), open-circuit voltage (V_{OC}), fill factor (FF) and power conversion efficiency (PCE) of tested photovoltaic devices.

	Interlayer	***J_{sc} (mA/cm^2)***	***V_{oc} (V)***	***FF***	***PCE (%)***
PT6N(EtOH)$_2$:C$_{60}$-Ser	-	9.77	0.58	0.57	3.23
	PT6buP$^+$Br$^-$	12.1	0.60	0.58	4.21
	PTO6buP$^+$Br$^-$	13.2	0.62	0.61	4.99
	P(EDOT-MeO6buP$^+$Br$^-$)	12.6	0.61	0.59	4.54

In order to test the functionality of synthetized materials, the most widely used blend composed by poly(3-hexylthiophene) (P3HT) and $PC_{61}BM$ was used as photoactive layer and tested with interlayers as previously reported obtaining the values reported in Table 8.

Table 8. Short-circuit current density (J_{SC}), open-circuit voltage (V_{OC}), fill factor (FF) and power conversion efficiency (PCE) of tested solar cells.

	Interlayer	***J_{sc} (mA cm^{-2})***	***V_{oc} (V)***	***FF***	***PCE (%)***
P3HT:PC$_{61}$BM	-	10.38	0.59	0.61	3.73
	PT6buP$^+$Br$^-$	10.61	0.60	0.61	3.88
	PTO6buP$^+$Br$^-$	10.88	0.61	0.61	4.05
	P(EDOT-MeO6buP$^+$Br$^-$)	10.73	0.61	0.61	4.00

Although the ED and EA materials and solvent (chlorobenzene) used for the deposition of photoactive layer were very different, the enhancement is also appreciable in this case as shown in J/V curves reported in Figure 13.

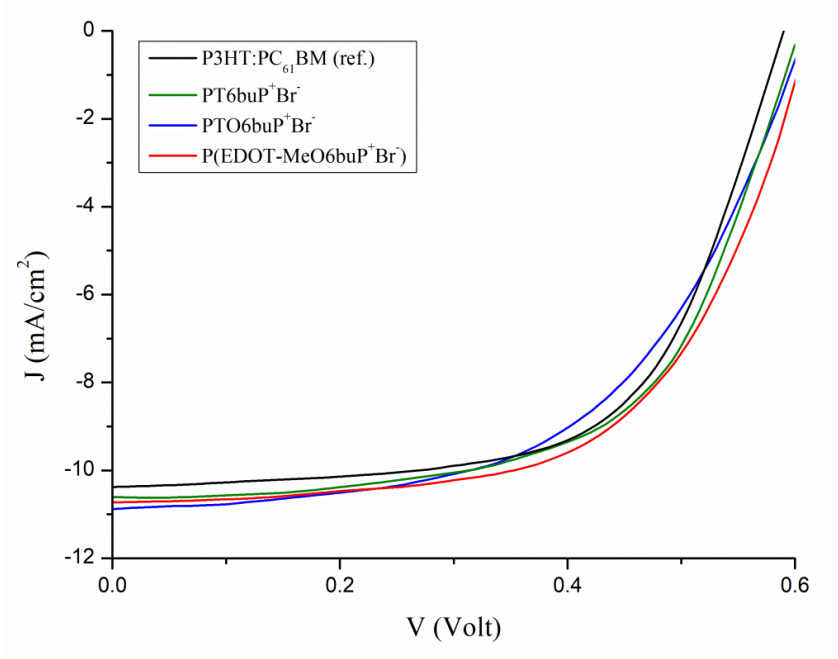

Figure 13. Current density-voltage (J/V) for cells tested under AM 1.5 one-sun illumination.

2.9. EQE measurements

The increment of electron extraction efficiency by the insertion of cathodic layers was further confirmed by the analysis of the EQE spectra reported in Figure 14. The photovoltaic cell without interfacial layer (PT6N(EtOH)$_2$) shows an EQE in the 350-600 nm range of about 40%, while those with CPE reach an EQE of about 50-60% in the 350-650 nm range. In particular, the cell with PTO6buP$^+$Br$^-$ as an interfacial layer has wider absorption and a higher value of quantum efficiency. The obtained results are in good agreement with the improvement in photocurrent reported in Table 7 when interlayers are employed.

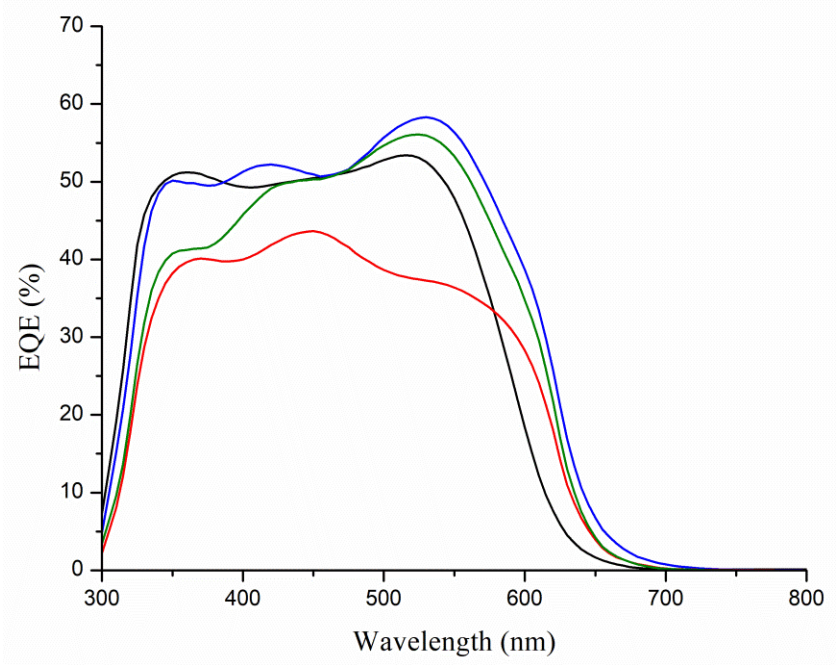

Figure 14. EQE spectra of the tested devices: PT6N(EtOH)$_2$:C$_{60}$-Ser without (black line) and with interlayer: PT6buP$^+$Br$^-$ (green line), PTO6buP$^+$Br$^-$ (blue line) and P(EDOT-MeO6buP$^+$Br$^-$) (red line).

2.10. Morphology characterization

The morphology of the examined solar devices was evaluated by AFM technique in order to investigate the surface nano-topography.

Analyzing the image of the active layer film composed by PT6N(EtOH)$_2$ (Figure 15A) - with surface RMS roughness of 10.2 nm - a phase separation can be observed and it is ascribable to the presence of polymer crystallites, as already evidenced by XRD measurements. The deposition of CPE layers on the active surface decreases the surface roughness leading to RMS values of 7.07, 5.08, and 6.03 nm with PT6buP$^+$Br$^-$, PTO6buP$^+$Br$^-$ and P(EDOT-MeO6buP$^+$Br$^-$), respectively (Figure 15B, C, D). Moreover, the high affinity of the CPE with respect to the underlying active layer and the use of alcohol solvent for deposition leads to complete coverage of the photoactive

film and an improvement of surface, a fundamental requisite to achieve high performance of the organic photovoltaic device.[8]

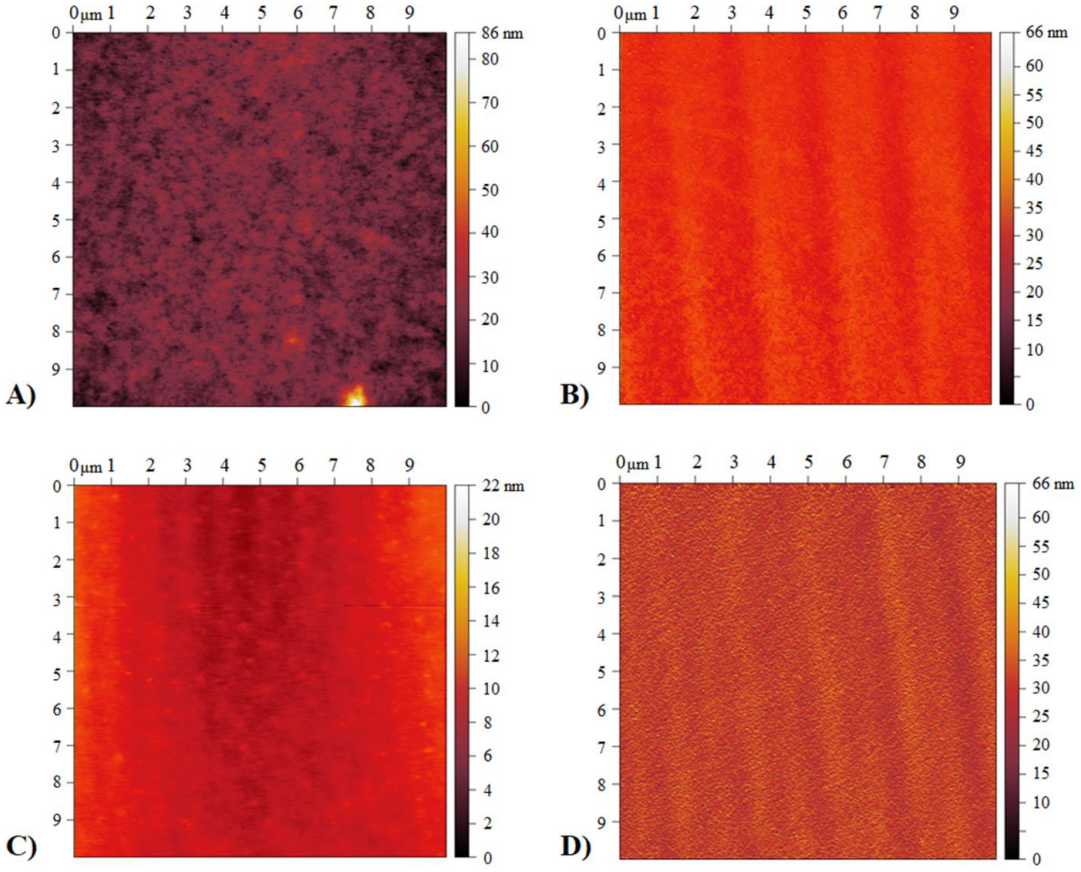

Figure 15. AFM topography images of PT6N(EtOH)$_2$ layer (A) and of PT6N(EtOH)$_2$ after spray-coating of PT6buP$^+$Br$^-$ (B), PTO6buP$^+$Br$^-$ (C), P(EDOT-MeO6buP$^+$Br$^-$) (D) layer.

2.11. Conclusions

A neutral water/alcohol soluble electron-donor material (PT6N(EtOH)$_2$) and three polythiophenes functionalized with a tetra-alkylphosphonium bromide cationic group (PT6buP$^+$Br$^-$, PTO6buP$^+$Br$^-$ and P(EDOT-MeO6buP$^+$Br$^-$)) were successfully synthesized through a simple and effective post-polymerization functionalization reaction on the corresponding ω-alkylbrominated polymeric precursors.

The prepared cationic polythiophenes were then employed as cathode interlayers in BHJ photovoltaic solar cells. The comparison of photovoltaic parameters obtained with the use of two reference devices (PT6N(EtOH)$_2$:C$_{60}$-Ser and P3HT:PC$_{61}$BM) without and then with cathode interlayers showed that the insertion of the CPEs improves photoconversion efficiency. Electrical measurements revealed an increase in charge collection efficiency while the AFM measurements

evidenced that CPEs afforded a complete coverage of the photoactive layers, owing to the high physico-chemical affinity between the two polymeric layers.

The obtained results demonstrate that the incorporation of CPE layer is a powerful, convenient and promising methodology for the development of highly efficient polymeric solar cells processable without the use of toxic or harmful solvents (chlorinates and aromatics).

3. Experimental section

3.1. Materials

Tributylphosphine (97%), 1,6-hexandiol (99%), tetrahydrofuran (THF, >99.9%), toluene (C_7H_8, >99.9%), diethyl ether (Et_2O, >99.5%), ethyl acetate (EtOAc, >99.5%), hydroxymethyl EDOT, 3-methoxythiophene (98%) and chloroform ($CHCl_3$, 99.0-99.4%) were purchased from Sigma Aldrich Chemical Co. (USA). Petroleum ether (Etp, >90%) was purchased from Sigma Aldrich (Israel). N,N-Dimethylformamide (≥99.8%) and sodium hydroxide (NaOH, ≥98%), were purchased from Sigma Aldrich (Germany). Hexane (≥99%) and dichloromethane (≥99.9%) were purchased from Sigma Aldrich (France). Nitromethane (CH_3NO_2, ≥98.5%), Tetrabutylammonium bromide (TBAB, ≥99%), hydrobromic acid (HBr, 48%), hydrochloric acid (HCl, ≥37%) and ferric chloride ($FeCl_3$, ≥98%) were purchased from Fluka (Switzerland). Diethanolamine (DEA, 99%) was purchased from Aldrich. 1,6-Dibromohexane (B6B, >97%) was purchased from TCI (Tokyo). P-Toluensulfonic acid monohydrate was purchased from Carlo Erba (Italy). Sodium sulfate (Na_2SO_4, anhydrous) and sodium bicarbonate ($NaHCO_3$, puriss.) were purchased from Riedel-deHaën (Poland). Methanol (MeOH, >99.8%) was purchased from Honeywell (Germany). In order to remove the stabilizer, diethyl ether and THF were freshly distilled before the use. Otherwise noted, all other materials were used as received. All manipulations involving air/moisture-sensitive reagents were performed under argon atmosphere.

3.2. Synthesis of non-ionic electron-donor material poly[3-(6-diethanolamino)-hexylthiophene] [PT6N(EtOH)$_2$]

In a three neck flask, 100 mg (0.408 mmol) of rrPT6Br were dissolved in a solution of 20.0 mL of anhydrous THF. Subsequently, 5.00 mL of DMF and 50.0 mg (4.76 mmol) of diethanolamine were added to the system. The mixture was allowed to react for 48h at 60°C under inert atmosphere. After cooling down to room temperature, the crude product was added slowly into 300 mL of distilled water and the precipitate was filtered on a glass microfiber membrane obtaining 68.0 mg (0.252 mmol) of PT6N(EtOH)$_2$ as a dark purplish solid (yield 62%).

^{1}H-NMR (CD_3OD, ppm): δ 6.96 (s, 1H, Th *H*4), 3.60 (m, 4H, C*H*$_2$OH), 2.99 (t, 2H, ThC*H*$_2$), 2.69 (bs, 4H, C*H*$_2$CH$_2$OH), 2.60 (bm, 2H, C*H*$_2$N), 1.84-1.64 (bs, ThCH$_2$C*H*$_2$), 1.63-1.47 (bm, 2H, C*H*$_2$CH$_2$N), 1.45-1.21 (bm, 4H, aliphatic C*H*$_2$).

^{13}C-NMR ($CDCl_3$, ppm): δ 136.12 (Th *C*3), 132.39 (Th *C*5), 127.97 (Th *C*2), 124.22 (Th *C*4), 73.52 (*C*H$_2$OH), 64.31 (N*C*H$_2$CH$_2$OH), 57.50 (*C*H$_2$N), 33.13, 32.12, 30.76, 30.09, 23.73 (aliphatic *C*H$_2$).

FT-IR (Ge, cm^{-1}): 3317, 3055, 2923, 2852, 1508, 1455, 1259, 1075, 1028, 799, 726.

3.3. Synthesis of monomers

3.3.1. Synthesis of 3-(6-bromohexyl-1-oxy)thiophene (TO6Br)

In a round bottom flask equipped with a cooling system, 1.19 g (6.57 mmol) of 6-bromo-1-hexanol (B6OH) and 83.3 mg (0.438 mmol) of p-toluensulfonic acid monohydrate (pTSA) were dissolved in 15.0 mL of anhydrous toluene. Subsequently, 0.45 mL (4.38 mmol) of 3-methoxythiophene were added to the system under inert atmosphere. The mixture was allowed to react under reflux for 22h.

After cooling down the system to room temperature, the solvent was removed under reduced pressure and the crude product was recovered with 60.0 mL of CH_2Cl_2. The organic phase was then extracted with 50.0 mL of saturated solution of $NaHCO_3$, washed with water (2 × 80.0 mL) up to neutrality and dried under vacuum. The obtained oily residue was purified by silica gel column chromatography (Hexane/EtOAc 85:15) to give 0.679 g (2.58 mmol) of TO6Br (yield 59%).

^{1}H-NMR ($CDCl_3$, ppm): δ 7.17 (dd, 1H, Th *H*2), 6.75 (dd, 1H, Th *H*5), 6.23 (dd, 1H, Th *H*4), 3.95 (t, 2H, ThOCH_2), 3.42 (t, 2H, CH_2Br), 1.89 (m, 2H, CH_2CH$_2$Br), 1.79 (m, 2H, ThOCH$_2$CH_2), 1.50 (m, 4H, aliphatic CH_2).

^{13}C-NMR ($CDCl_3$, ppm): δ 158.50 (Th *C*3), 125.26 (Th *C*5), 120.15 (Th *C*4), 97.72 (Th *C*2), 70.62 (ThO*C*H$_2$), 34.45 (*C*H$_2$Br), 33.33 (*C*H$_2$CH$_2$Br), 29.75 (ThOCH$_2$*C*H$_2$), 28.58, 25.97 (aliphatic *C*H$_2$).

FT-IR (KBr, cm^{-1}): 3117, 3069, 2937, 2861, 1541, 1459, 1234, 1177, 1071, 730, 682, 627, 560.

3.3.2. Synthesis of 6-bromohexyl-1-oxymethyl-EDOT (EDOT-MeO6Br)

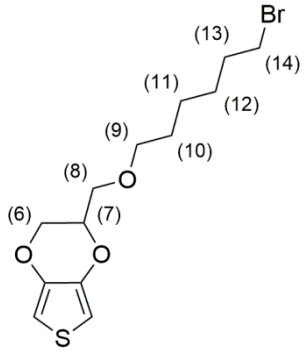

250 mg (1.45 mmol) of hydroxymethyl-EDOT, 5.06 g of 1,6-dibromohexane (20.8 mmol) and 140 mg (0.434 mmol) of tetrabutylammonium bromide (TBAB) were dissolved in 6.30 mL of dichloromethane (DCM) in a three neck flask. The solution was stirred for 5 minutes, under inert atmosphere, and 6.20 mL of a solution of NaOH (50% wt) were subsequently added to the system. The mixture was allowed to react under stirring at room temperature for 2h and then the crude product was extracted with CH_2Cl_2 (2 × 50 mL). The organic phase was then washed with distilled

water (6 × 100 mL) up to neutrality, dried over Na_2SO_4, filtered and concentrated under reduced pressure.

The obtained residue was purified by silica gel column chromatography (DCM) to give 423 mg of a white crystal solid (yield 87%).

^{1}H-NMR ($CDCl_3$, ppm): δ 6.32 (dd, 2H, Th *H*2 and *H*5), 4.29 (m, 1H, H7), 4.24 (dd, 1H, H6), 4.05 (dd, 1H, H6), 3.67 (dd, 1H, H8), 3.61 (dd, 1H, H8), 3.49 (t, 2H, H9), 3.42 (t, 2H, H14), 1.88 (m, 2H, H13), 1.60 (m, 2H, aliphatic H10), 1.47 (m, 2H, H13), 1.37 (m, 2H, H11).

^{13}C-NMR ($CDCl_3$, ppm): δ 141.92 (Th *C*3 and *C*4), 100.03 (Th *C*2), 99.92 (Th *C*5), 72.98 (*C*7), 72.13 (*C*8), 69.50 (*C*9), 66.56 (*C*6), 34.17 (*C*14), 33.01, 29.68, 28.26, 25.59 (aliphatic *C*H_2).

FT-IR (KBr, cm^{-1}): 3113, 2935, 2859, 1484, 1428, 1308, 1247, 1126, 1021, 912, 858, 759, 644, 560.

3.4. Synthesis of cationic polythiophene interlayers

3.4.1. General procedure for oxidative polymerization with $FeCl_3$

In a three-neck flask, the monomer was dissolved in anhydrous chloroform under inert atmosphere, and a solution of $FeCl_3$ in CH_3NO_2 was added dropwise to the system (10 minutes) and the mixture was allowed to react under a flux of argon for 40 minutes at room temperature. Afterward, THF was added, and the system stirred for further 50 minutes.

The mixture was poured into 300 mL of MeOH/HCl (5% v/v), and the precipitated product was recovered by filtration on a PTFE membrane (0.45 μm pore size). The obtained solid was then dissolved in $CHCl_3$, washed with HCl 2% up to exhaustive extraction of the iron (III) ion (negative NH_4SCN test), and several times with water up to neutrality. The organic phase was dried over Na_2SO_4, filtered, and the solvent was removed under reduced pressure.

In the case of P(EDOT-MeO6Br) the darkish solid was recovered in $CHCl_3$ (5 mg/mL), added to a solution of NH_4OH (1:1), and heated until reflux conditions for 2 h. The organic phase was washed several times with distilled water until neutrality, dried with Na_2SO_4, filtered, and concentrated under reduced pressure.

3.4.1.1. Poly[3-(6-bromo-hexyl)thiophene] (PT6Br)

Starting from 450 mg (1.82 mmol) of 3-(6-bromohexyl)-thiophene (T6Br) in 25.0 mL of anhydrous $CHCl_3$, the addition of 1.18 g (7.28 mmol) of $FeCl_3$ in 7.50 mL of CH_3NO_2 gave 250 mg (1.02 mmol) of PT6Br as a reddish solid (yield 56%).

^{1}H-NMR ($CDCl_3$, ppm): δ 6.98 (s, 1H, Th *H*4), 3.43 (bt, 2H, C*H*$_2$Br), 2.82, 2.58 (bt, 2H, ThC*H*$_2$), 1.96-1.80 (m, 2H, C*H*$_2$CH$_2$Br), 1.80-1.64 (m, 2H, ThCH$_2$C*H*$_2$), 1.60-1.36 (m, 4H, (C*H*$_2$)$_2$).

^{13}C-NMR ($CDCl_3$, ppm): δ 143.71, 143.01, 141.03, 140.28 (Th *C*3), 136.94, 135.88, 134.61, 134.77 (Th *C*5), 131.32, 130.85, 130.23, 129.85 (Th *C*2), 129.04, 128.65, 128.32, 127.63 (Th *C*4), 34.55 (CH_2Br), 33.81 (CH_2CH_2Br), 30.94 (ThCH_2), 29.96, 29.15, 28.53 (aliphatic CH_2).

FT-IR (Ge, cm^{-1}): 3055, 2929, 2854, 1509, 1457, 1259, 1090, 827, 727, 645, 562.

3.4.1.2. Poly[3-(6-bromo-hexyl-1-oxy)thiophene] (PTO6Br)

Starting from 300 mg (1.14 mmol) of 3-(6-bromohexyl-1-oxy)thiophene (TO6Br) in 25.0 mL of anhydrous $CHCl_3$, the addition of 755 mg (4.65 mmol) of $FeCl_3$ in 4.73 mL of CH_3NO_2 gave 133 mg (0.509 mmol) of a reddish solid (yield 45%).

^{1}H-NMR ($CDCl_3$, ppm): δ 7.03-6.70 (b, 1H, Th *H*4), 4.16, 3.93 (2bm, 2H, ThOCH_2), 3.42 (bm, 2H, CH_2Br), 2.12-1.74 (bm, 4H, ThOCH$_2$CH_2 and CH_2CH$_2$Br), 1.73-1.27 (bm, 4H, aliphatic CH_2).

^{13}C-NMR ($CDCl_3$, ppm): δ 154.82 (Th *C*3), 136.32 (Th *C*5), 107.99 (Th *C*4), 106.72 (Th *C*2), 68.00, 67.78 (ThOCH_2), 32.67 (CH_2Br), 29.85 (ThOCH$_2$$CH_2$), 30.04, 28.14, 24.16, 23.04 (aliphatic CH_2).

FT-IR (Ge, cm^{-1}): 3079, 2937, 2860, 1520, 1456, 1222, 1191, 1071, 829, 734, 645, 562.

3.4.1.3. Poly(6-bromohexyl-1-oxymethyl-EDOT) [P(EDOT-MeO6Br)]

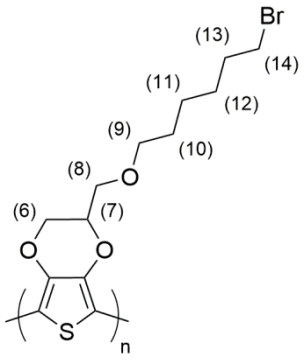

Starting from 262 mg (0.782 mmol) of 6-bromohexyl-1-oxymethyl-EDOT (EDOT-MeO6Br) in 13.0 mL of anhydrous $CHCl_3$, the addition of 517 mg (3.13 mmol) of $FeCl_3$ in 2.36 mL of CH_3NO_2 gave 80.0 mg (0.240 mmol) of a dark purple solid (yield 31%).

^{1}H-NMR ($CDCl_3$, ppm): δ 4.76-3.93 (bm, 3H, H7 and H6), 3-92-3.62 (b, 2H, H8), 3.49 (bs, 2H, H9), 3.41 (bs, 2H, H14), 1.85 (bs, 2H, H13), 1.59 (bs, 2H, H10), 1.50-1.24 (bm, 4H, H11 and H12).

^{13}C-NMR ($CDCl_3$, ppm): 143.87 (Th *C*3+*C*4), 121.70 (Th *C*2+*C*5), 82.70 (*C*7), 81.89 (*C*8), 77.57 (*C*9), 72.18 (*C*6), 34.22 (*C*14), 32.99, 29.74, 28.28, 25.57 (aliphatic CH_2).

FT-IR (Ge, cm^{-1}): 2935, 2862, 1460, 1438, 1305, 1240, 1225, 1117, 1057, 913, 841, 751, 643, 561.

3.4.2. General procedure for the post-functionalization with tributylphosphine

The brominated polymeric precursor was dissolved in toluene in a three-neck flask and then tributylphosphine was added to the system under stirring and in an inert atmosphere. After reacting at 90°C for 24 h, the supernatant was removed, and the film formed on the flask surface was recovered with methanol. The solvent was evaporated under reduced pressure, and the product was washed several times with diethyl ether and dried under vacuum to give the final cationic polymer.

3.4.2.1. Poly[3-(6-tributylphosponium-hexyl)thiophene]bromide (PT6buP$^+$Br$^-$)

Starting from 360 mg (1.47 mmol) of PT6Br in 20.0 mL of toluene, the addition of 3.60 mL (14.6 mmol) of tributylphosphine gave 636 mg (1.42 mmol) of PT6buP$^+$Br$^-$ as a dark red solid (yield 97%).

^{1}H-NMR (CD_3OD, ppm): δ 7.14 (s, 1H, Th *H*4), 2.90, 2.64 (bs, 2H, ThC*H*$_2$), 2.25 (bs, 8H, C*H*$_2$P$^+$C*H*$_2$), 1.85-1.71 (bm, 2H, ThCH$_2$C*H*$_2$), 1.70-1.43 (bm, 18H, (C*H*$_2$)$_n$) 0.98 (bt, 9H, C*H*$_3$).

^{13}C-NMR (CD_3OD, ppm): δ 141.62 (Th *C*3), 134.92 (Th *C*5), 131.67 (Th *C*2), 130.28 (Th *C*4), 31.49, 30.18, 29.74, 25.10, 24.94, 24.50, 22.49 (aliphatic *C*H$_2$), 19.54 (*C*H$_2$P$^+$), 19.08 (P$^+$*C*H$_2$), 13.88 (*C*H$_3$).

^{31}P-NMR (CD_3OD, ppm): δ 33.86.

FT-IR (Ge, cm^{-1}): 3053, 2957, 2929, 2870, 1513, 1463, 1410, 1378, 1232, 1099, 833, 723.

3.4.2.2. Poly[3-(6-tributylphosphonium-hexyl-1-oxy)thiophene]bromide (PTO6buP$^+$Br$^-$)

Starting from 120 mg (0.458 mmol) of PTO6Br in 8.00 mL of toluene, the addition of 1.14 mL of tributylphosphine gave 198 mg (0.428 mmol) of PTO6BuP$^+$Br$^-$ as a dark-red solid (yield 93%).

^{1}H-NMR (CD_3OD, ppm): δ 7.08 (b, 1H, Th *H*4), 4.24-4.05 (2bm, 2H, ThOC*H*$_2$), 2.31-1.99 (bm, 8H, C*H*$_2$P$^+$), 1.98-1.82 (bm, 2H, ThOCH$_2$C*H*$_2$), 1.70-1.29 (bm, 18H, (C*H*$_2$)$_2$CH$_2$P$^+$), 1.01-0.82 (bm, 9H, C*H*$_3$).

^{13}C-NMR (CD_3OD, ppm): δ 140.76 (Th *C*3), 133.45 (Th *C*5), 129.82 (Th *C*2), 127.96 (Th *C*4), 66.90 (ThO*C*H$_2$), 28.16, 27.52, 25.27, 25.12, 24.91, 24.62 (aliphatic *C*H$_2$), 19.49 (*C*H$_2$P$^+$), 18.89 ($^+$P*C*H$_2$), 13.90 (*C*H$_3$).

^{31}P-NMR (400 MHz, ppm): δ 33.88.

FT-IR (Ge, cm^{-1}): 3028, 2957, 2932, 2871, 1536, 1463, 1407, 1379, 1229, 1194, 1078, 831, 727.

3.4.2.3. Poly(6-tributylphosphinehexyl-1-oxymethyl-EDOT)bromide [P(EDOT-MeO6buP$^+$Br$^-$)]

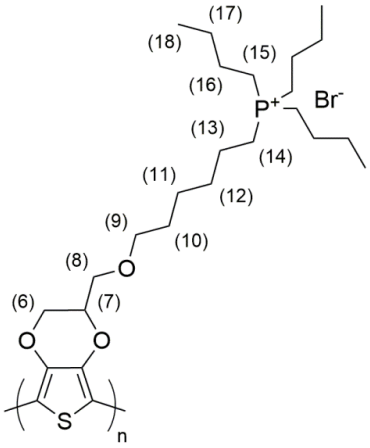

Starting from 100 mg (0.300 mmol) of P(EDOT-MeO6Br) in 11.0 mL of toluene, the addition of 750 μL of tributylphosphine gave 142 mg (0.266 mmol) of a red cherry solid (yield 88%).

^{1}H-NMR (CD_3OD, ppm): δ 4.36-4.02 (b, 2H, H7 and H6), 3.95-3.65 (bm, 2H, H8), 3.64-3.36 (b, 2H, H9), 2.24 (bs, 8H, H14 and H15), 1.90-1.72 (bm, 2H, H10), 1.70-1.33 (bm, 18H, aliphatic C*H*$_2$), 0.98 (m, 9H, H18).

^{13}C-NMR (CD_3OD, ppm): 137.82 (Th *C*3+*C*4), 115.57 (Th *C*2+*C*5), 72.80 (*C*7), 70.29 (*C*8), 64.98 (*C*9), 60.76 (*C*6), 31.63, 30.51, 28.10, 27.45, 25.07, 22.46 (aliphatic *C*H$_2$), 19.48 (*C*14), 19.04 (*C*15), 13.90 (*C*18).

^{31}P-NMR (CD_3OD, ppm): δ 33.90.

FT-IR (Ge, cm^{-1}): 2957, 2932, 2870, 1462, 1439, 1379, 1311, 1231, 1226, 1115, 1052, 916, 835, 749.

3.5. NMR spectra

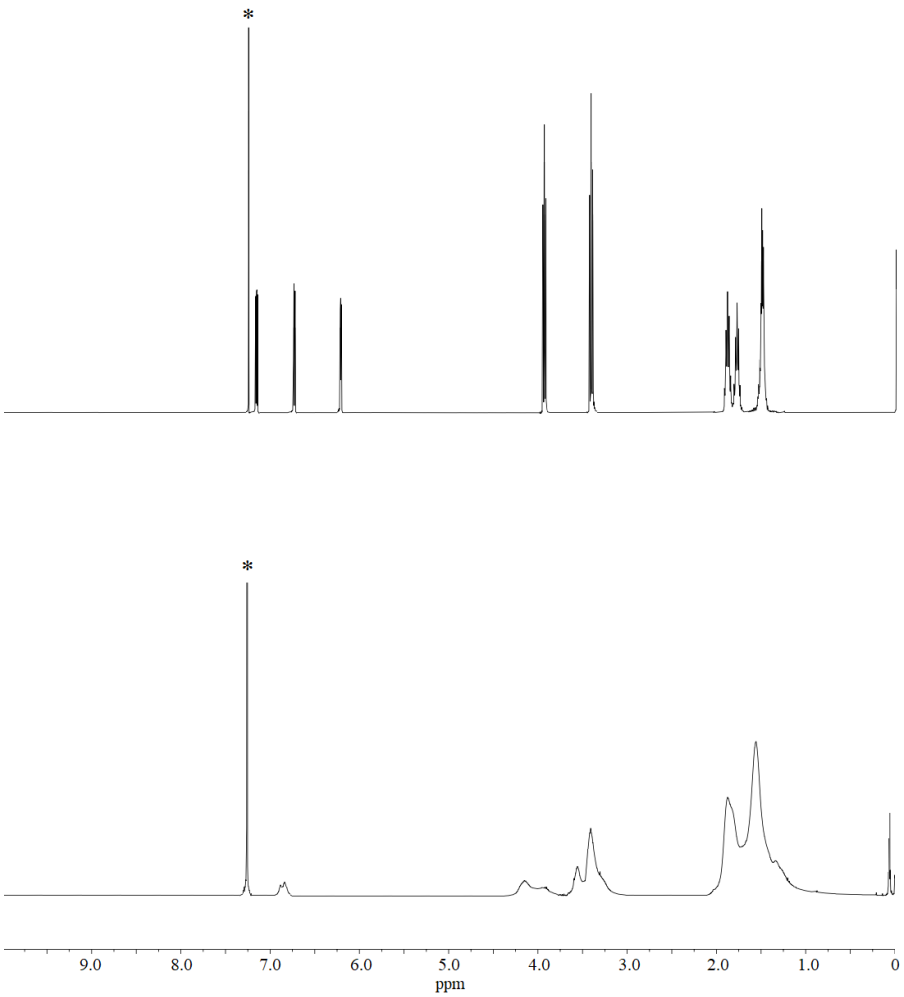

Figure 16. ^{1}H-NMR spectra of TO6Br (top) and PTO6Br (bottom). Asterisk: solvent resonance ($CDCl_3$).

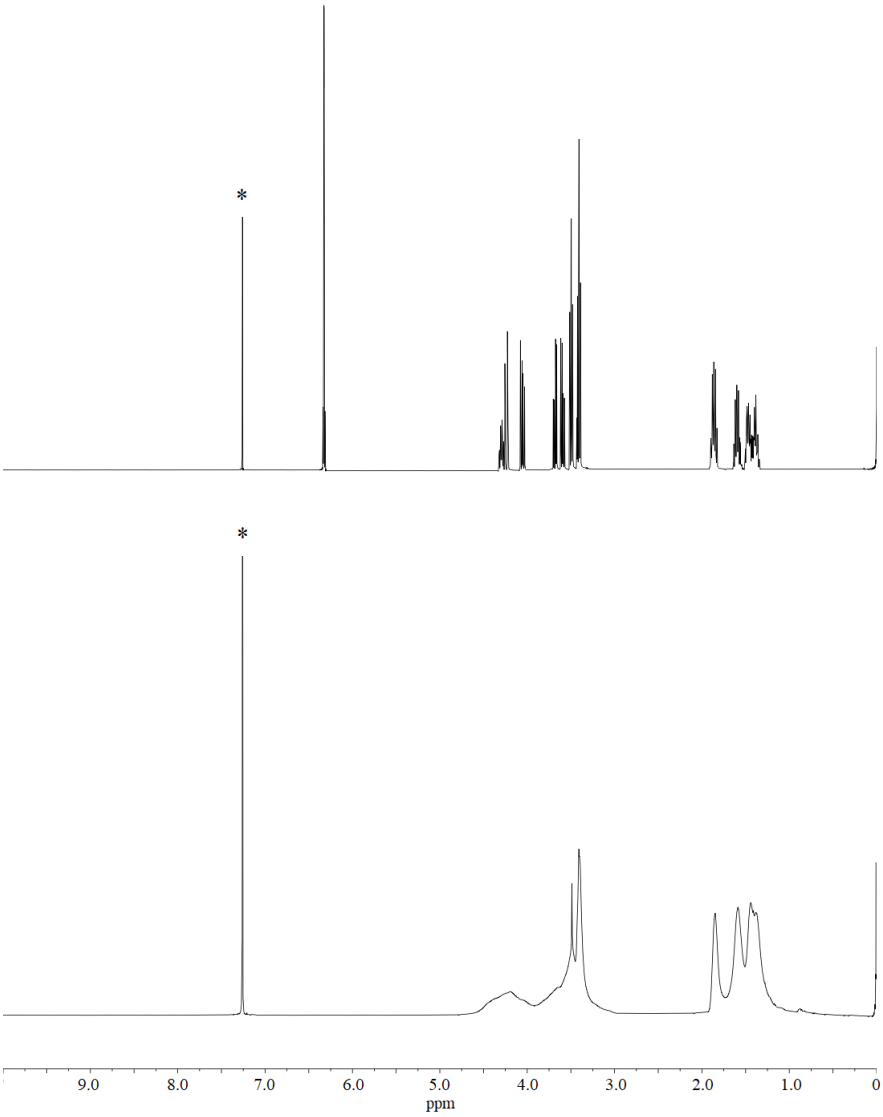

Figure 17. ^{1}H-NMR spectra of EDOT-MeO6Br (left) and P(EDOT-MeO6Br) (right). Asterisk: solvent resonance ($CDCl_3$).

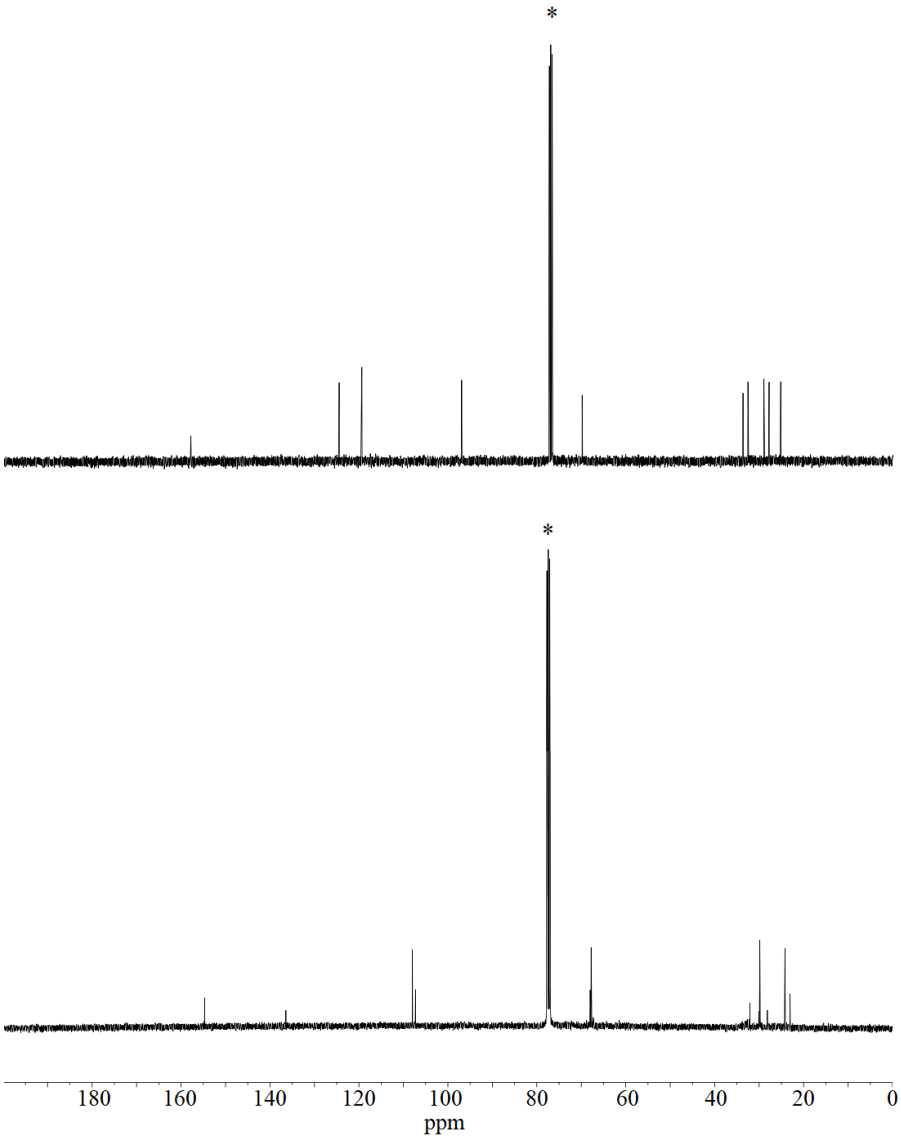

Figure 18. ^{13}C-NMR spectra of TO6Br (top) and PTO6Br (bottom). Asterisk: solvent resonance ($CDCl_3$).

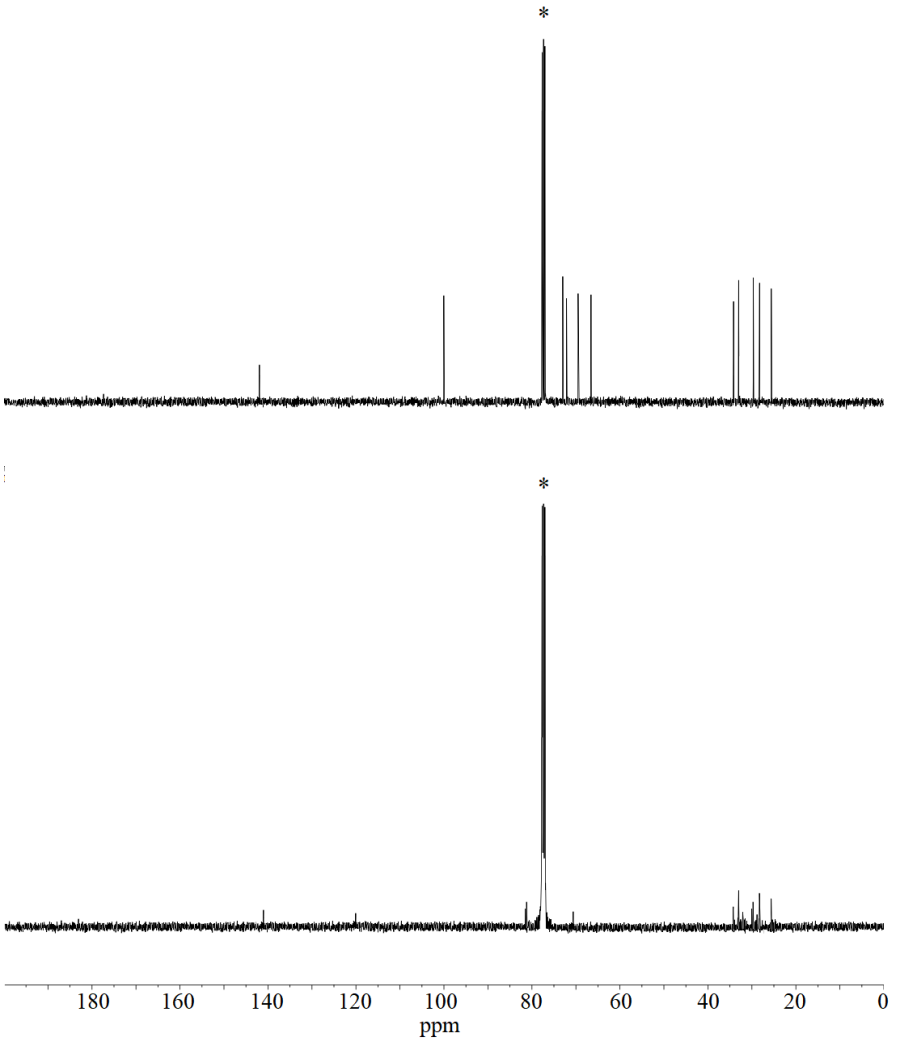

Figure 19. ^{13}C-NMR spectra of EDOT-MeO6Br (top) and P(EDOT-MeO6Br) (bottom). Asterisk: solvent resonance ($CDCl_3$).

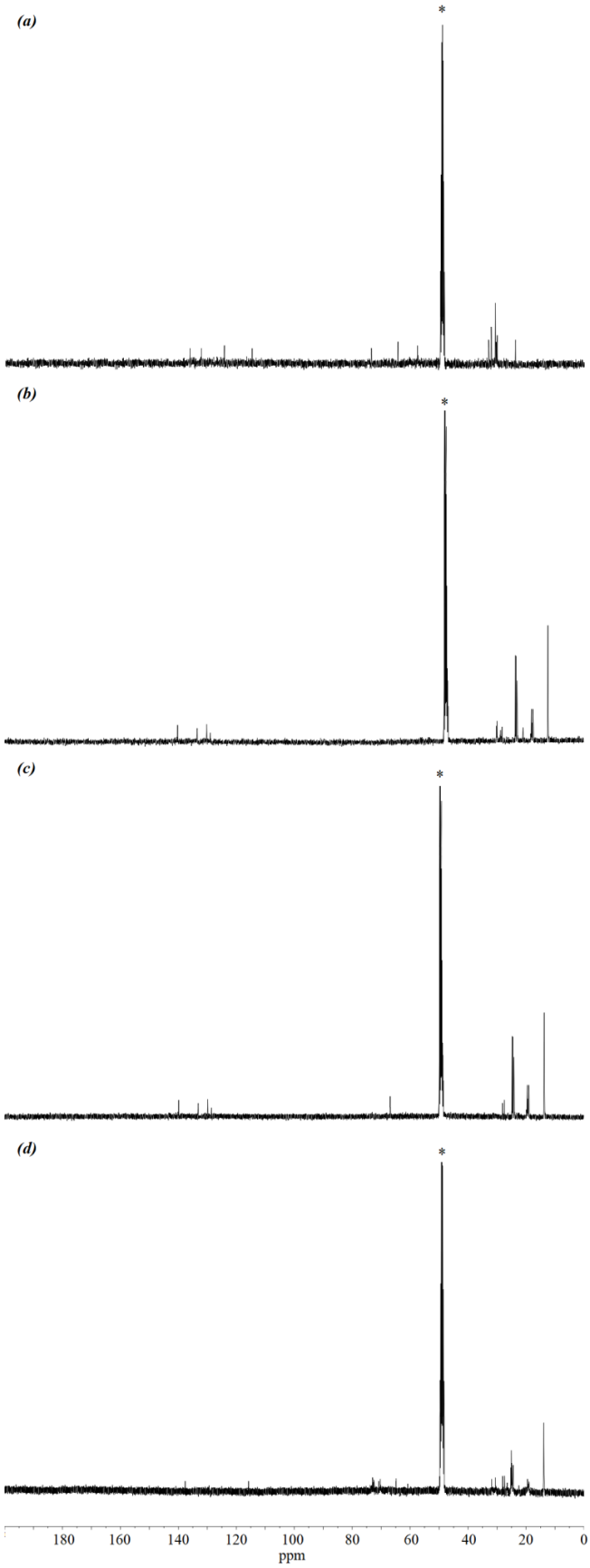

Figure 20. ^{13}C-NMR spectra of PT6N(EtOH)$_2$ (*a*), PT6buP$^+$Br$^-$ (*b*), PTO6buP$^+$Br$^-$ (*c*) and P(EDOT-MeO6buP$^+$Br$^-$) (*d*). Asterisk: solvent resonance (CD_3OD).

3.6. FT-IR assignments

Table 11. Main IR absorption bands (cm^{-1}) of PTO6buP$^+$Br$^-$ and precursors.

B6OH	***TO6Br***	***PTO6Br***	***PTO6buP$^+$Br$^-$***	***Assignments***
3339	-	-	-	υ –OH
-	3117	-	-	υ C–H (aromatic α H)
-	3069	3079	3028	υ C–H (aromatic β H)
-	-	-	2957	υ_{as} –CH_3 (phosphonium group)
2932	2937	2937	2932	υ_{as} -CH_2- (side chain and phosphonium group)
2859	2861	2860	2871	υ_{sym} -CH_2- and –CH_3
-	1541	1520	1536	υ_{as} C=C thiophene ring
-	1459	1456	1463	υ_{sym} C=C thiophene ring
-	-	-	1407	γ P-CH_2-R
-	-	-	1379	-CH_3 deformation (phosphonium group)
-	1234	1222	1229	Vibration thiophene ring
-	1177	1191	1194	υ_{as} C-O-C ether
-	1071	1071	1078	υ_{sym} C-O-C ether
1053	-	-	-	Primary alchohol
-	-	829	831	γ C-H thiophene 2,3,5-trisubstituted
728	730	734	727	Rocking -CH_2
-	682	-	-	γ C-H thiophene 3 monosubstituted
644, 561	627, 560	645, 562	-	υ -C-Br aliphatic

Table 10. Main IR absorption bands (cm^{-1}) of P(EDOT-MeO6buP$^+$Br$^-$) and precursors.

EDOT-MeO6Br	***P(EDOT-MeO6Br)***	***P(EDOT-MeO6buP$^+$Br$^-$)***	***Assignments***
3113	-	-	υ C–H (aromatic α H)
-	-	2957	υ_{as} –CH_3 (phosphonium group)
2935	2935	2932	υ_{as} -CH_2- (side chain and phosphonium group)
2859	2862	2870	υ_{sym} -CH_2- and –CH_3
1484	1460	1462	υ_{as} -C=C- thiophene
1428	1438	1439	υ_{sym} -C=C- thiophene
-	-	1379	–CH_3 deformation (phosphonium group)
1308	1305	1311	υ C-C thiophene ring
1247	1240	1231	Vibration thiophene ring
1219	1225	1226	υ C-O-C ethylenedioxy group
1126	1117	1115	υ_{as} C-O-C ether
1021	1057	1052	υ_{sym} C-O-C ether
912	913	916	Ethylenedioxy ring deformation[21]
858	841	835	γ C-H thiophene 3,4-bisubstituted
759	751	749	Rocking -CH_2-
644, 560	643, 561	-	*υ* C-Br aliphatic

υ = stretching; γ = out of plane bending; δ = in-plane bending.

3.7. Methods

NMR spectra (^{1}H-NMR, ^{13}C-NMR, and ^{31}P-NMR) were recorded on a Varian Mercury Plus 400 spectrometer using TMS as a reference.

IR spectra were taken on KBr or Ge disks using a Perkin Elmer Spectrum One spectrophotometer.

UV-Vis spectra were recorded on a Perkin Elmer Lambda 19 spectrophotometer using either around 10^{-5} M polymer solutions in spectroquality solvents in Suprasil quartz cuvettes (1 × 1 cm) or films on quartz slides.

The molecular weight of precursor polymers was determined by gel permeation chromatography (GPC) using THF solutions on a HPLC Lab Flow 2000 apparatus equipped with a Rheodyne 7725i injector, a Phenomenex MXL 5 μm mixed bed column, and an RI K-2301 KNAUER detector. The calibration curve was recorded using monodisperse polystyrene standards.

Thermogravimetric analyses were recorded on NETZSCH TG 209 F1 Libra operating in air flux, which was used to determine sample decomposition temperatures by heating from 30°C to 600°C with a ramp of 10°C min^{-1}.

A TA Instruments Q2000 differential scanning calorimeter (DSC) was used for the thermal analysis by varying the temperature from -20 to 200°C with a heating and cooling ramp of 10°C min^{-1} in a nitrogen atmosphere.

Cyclic voltammetry (CV) analyses were performed in a three compartments glass cell under Ar pressure and at room temperature by using a AMEL 5000 Electrochemical System. Polymers were deposited by drop casting from methanol solutions on Pt electrode (1 mm diameter). Auxiliary electrode was Pt wire spiral and reference electrode was aqueous saturated calomel electrode (SCE). Supporting electrolyte used was a solution of $(C_4H_9)_4NClO_4$ (0.1 mol/L) while the solvent was chosen in order to avoid the dissolution of film (acetonitrile/toluene, 25:75). SCE absolute potential is 4.24 eV.

X-ray diffraction data were recorded at room temperature by using a CuKα (λ = 1.5406 Å) radiation source (Philips PW 1050) and a Bragg-Brentano diffractometer (Philips PW 1710) equipped with a graphite monochromator in the diffracted beam. The 2θ range between 2.0 and 90.0° was scanned by 881 steps of 0.1° with a counting time of 15 s for each step. The XRD characterization was carried out on polymer films on glass slides deposited by doctor blading (100 nm average thickness) after an annealing procedure (heating at 120°C for 30 min under vacuum).

The sample surface topography was evaluated with an atomic force microscope (AFM, Ntegra, NT-MDT) equipped with a silicon cantilever (HA_NC, NT-MDT, tip radius of 10 nm, and spring constant of 12 N/m). Measurements were performed in a semi-contact mode with a resonance

frequency of around 150 kHz; the scanning rate was 0.5 Hz, while the size of the scanned sample was 10 μm × 10 μm per image.

3.7.1. Solar cells

Photovoltaic devices were prepared by the following procedure: the ITO glass substrate (2 × 2 cm, surface resistance 21 Ω/sq) was etched on one side using a 10% wt aqueous solution of HCl heated at 60°C for 10 min, in order to obtain an area of 1.5 × 1.0 cm covered by indium tin oxide. The glass was then cleaned with distilled water and 2-propanol and dried with a nitrogen flow with the resulting final resistance of the ITO glass of 12 Ω/sq. Poly(3,4-ethylenedioxythiophene):polystyrene sulfonic acid (PEDOT:PSS, 2.8 wt% dispersion in water, viscosity 20 cps) was diluted 1:1 v/v with 2-propanol, sonicated for 15 min using an ultrasonic bath (Elmasonic S 30H), filtered on a Gooch G2, and the resulting solution (viscosity 12 cps) deposited over the previously treated ITO glass with the doctor blading technique using a Sheen Instrument Model S265674, leaving only a small (0.5 × 1.0 cm) area uncovered at the opposite side of the previously etched area.

The PEDOT:PSS film was heated in a Buchi GKR-50 glass oven at 120°C for 90 min under vacuum (10^{-3} mmHg). A solution made by mixing 2.5 mg of PT6N$(EtOH)_2$ and 2.5 mg of C_{60}-Ser in 0.5 mL of methanol was sonicated and deposited by doctor blading on the slide in order to cover the PEDOT:PSS layer. Subsequently, the sample was annealed in the glass oven under vacuum (10^{-3} mmHg) at 120°C for 30 minutes. A solution of 1.0 mg of CPE in 0.5 mL of ethanol was deposited on the photoactive layer by spray coating (Gohelper Mini Kit Airbrush, nozzle diameter 0.3 mm) and annealed at 120°C for 15 minutes. Finally, a 50 nm-thick Al electrode was deposited over the polymeric layer through a shadow mask using an Edwards 6306A coating system operating at 10^{-6} mmHg. The active area of the cell was 1 × 1 cm^2. The current-voltage characteristics were measured in air using a Keithley 2401 source meter under the illumination of an Abet Technologies LS150 Xenon Arc Lamp Source AM 1.5 Solar Simulator (100 mW/cm^2) calibrated with an ILT 1400-BL photometer. The structure of the final devices was: ITO (80 nm)/PEDOT:PSS (100 nm)/active layer (150 nm)/interlayer (20 nm)/Al (50 nm). The solar cell spectral response was measured using a 7-SC Spec III Modularized Solar Cell Spectral Test System (SevenStar Optics, Beijing, PRC). The layer thickness was measured using a FTPAdvances FTPadv-2 Film Thickness Probe (Sentech GmbH, Germany) equipped with the FTPExpert software.

References

1. J. H. Seo, A. Gutacker, Y. Sun, H. Wu, F. Huang, Y. Cao, U. Scherf, A. J. Heeger, and G. C. Bazan, *J. Am. Chem. Soc*., **2011**, *133*, 8416-8419.
2. C. Duan, K. Zhang, C. Zhong, F. Huang, Y. Cao, *Chem. Soc. Rev*., **2013**, *42*, 9071-9104.
3. H.-L. Yip, A. K.-Y. Jen, *Energy Environ. Sci.*, **2012**, *5*, 5994-6011.
4. J. Luo, H. B. Wu, C. He, A. Y. Li, W. Yang, Y. Cao, *Appl. Phys. Lett*., **2009**, *95*, 043301.
5. H. Zeng, X. Zhu, Y. Liang, X. Guo, *Polymers*, **2015**, *7*, 333-372.
6. Y. Zhao, Z. Y. Xie, C. J. Qin, Y. Qu, Y. H. Geng, L. X. Wang, *Sol. Energy Mater. Sol. Cells*, **2009**, *93*, 604-608.
7. H. Wu, F. Huang, Y. Mo, W. Yang, D. Wang, J. Peng, Y. Cao, *Adv. Mater*., **2004**, *16*, 1826-1830.
8. J. Kesters, S. Govaerts, G. Pirotte, J. Drijkoningen, M. Chevrier, N. Van den Brande, X. Liu, M. Fahlman, B. Van Mele, L. Lutsen, D. Vanderzande, J. Manca, S. Clément, E. Von Hauff, W. Maes, *ACS Appl. Mater. Interfaces*, **2016**, *8*, 6309–6314.
9. B.H. Lee, I.H. Jung, H.Y. Woo, H.-K. Shim, G. Kim, K. Lee, *Adv. Funct. Mater*., **2014**, *24*, 1100–1108.
10. Z. He, C. Zhong, X. Huang, W. Wong, H. Wu, L. Chen, S. Su, Y. Cao, *Adv. Mater.*, **2011**, *23*, 4636-4643.
11. J. E. Houston, S. Richeter, S. Clément, R. C. Evans, *Polym. Int*., **2017**, *66*, 1333-1348.
12. S. Bishnoi, R. Datt, S. Arya, S. Gupta, R. Gupta, W. C. Tsoi, S. N. Sharma, S. P. Patole, V. Gupta, *Adv. Mater. Interfaces*, **2022**, *9*, 2101693.
13. C. Xie, L. Chen, Y. Chen, *J. Phys. Chem. C*, **2013**, *117*, 47, 24804-24814.
14. J. Chang, S. Zhang, Y. Jiang, L. Xu, J. Yu, W. Zhou, X. Sun, *ChemMedChem*, **2013**, *8*, 976-984.
15. C.-J. Lee, H. Wang, M. Young, S. Li, F. Cheng, H. Cong, G. Cheng, *Acta Biomaterialia*, **2018**, *75*, 161-170.
16. M. Lanzi, E. Salatelli, M. Marinelli, F. Pierini, *Macromol. Chem. Phys.*, **2020**, *221*, 1900433.
17. S. Hladysh, A. Murmiliuk, J. Vohlídal, D. Havlíček, V. Sedlařík, M. Štěpánek, J. Zedník, *Eur. Polym. J.*, **2018**, *100*, 200-208.
18. S. Hladysh, D. Bondarev, J. Vohlídal, D. Vrbata, J. Zedník, *Eur. Polym. J.*, **2016**, 83, 367-376.
19. J. Roncali, *Chemical Reviews*, **1992**, *92*, 4, 711-738.
20. S. A. Rutledge, A. S. Helmy, *J. Appl. Phys*. **2013**, *114*, 133708.
21. M. Lanzi, D. Quadretti, M. Marinelli, Y. Ziai, E. Salatelli, F. Pierini, *Polymers*, **2021**, *13*, 1640.

22. L. Zhang, C. He, J. Chen, P. Yuan, L. Huang, C. Zhang, W. Cai, Z. Liu, Y. Cao, *Macromolecules*, **2010**, *43*, 9771-9778.
23. S. I. Na, S. H. Oh, S. S. Kim, D. Y. Kim, *Org. Electron.*, **2009,** *10*, 496-500.